DEVELOPMENT OF APPARATUS TO STUDY THE STRAIN RATE SENSITIVITY FACTOR IN COPPER SINGLE CRYSTALS BY INCREMENTAL TRANSIENT CREEP EXPERIMENTS

by

H. Reginald Hardy, Jr

Submitted in partial fulfilment of the requirements
for the degree of Master of Science

Department of Physics
Faculty of Pure and Applied Science,
The University of Ottawa
Ottawa, Canada,
1962

ABSTRACT

The strain rate sensitivity factor is one of the important parameters associated with Basinski's approach to the study of strain hardening in plastically deformed metals. This thesis describes the design and construction of an apparatus to study the strain rate sensitivity factor in single crystal wire specimens of copper by incremental creep experiments.

A number of initial experiments were carried out over a wide range of stress, strain rate and temperature in order to evaluate the performance of the apparatus and to gain initial information on the variation of the strain rate sensitivity factor with these parameters. In particular the strain rate sensitivity factor was studied as a function of applied stress, temperature and impurity concentration for single crystals of pure copper and copper-silver alloys up to 0.3 at.% concentration.

ACKNOWLEDGEMENTS

The author wishes to express his gratitude to Dr. Z.S. Basinski of the National Research Council for suggesting the problem and for his constant interest throughout the project. He would also like to thank Dr. D.K.C. MacDonald, the former head of the Physics Department for his encouragement during the Masters program.

The many useful suggestions from the staff and other graduate students of the Physics Department have been most useful. In particular the frequent discussions and assistance of Dr. G. Lamarche were greatly appreciated. Mr. N. Goodchild's assistance in the design and construction of the apparatus was also appreciated, as was the assistance of Mr. H. Pett (Physics Department Summer Assistant - 1960) in carrying out many of the experiments.

A number of persons outside the department provided assistance or facilities. In particular Mr. J. Perry, Metal Forming Section, Mines Branch; Dr. C. Mitchell, X-Ray Laboratory, Mines Branch; Dr. W. Henry, Applied Chemistry Division, National Research Council; and Mr. W. Fisher, Solid State Physics Section, National Research Council.

The members of the authors Division (Fuels and Mining Practice) of the Mines Branch have been of great assistance. In particular the authors Section Head, Dr. W.M. Gray who provided constant encourage-

ment throughout the project. Mr. L. Nadon was responsible for construction of many of the precision parts of the apparatus and Mr. C. Vary assisted in preparing the many graphs and diagrams.

The author would like to thank Mr. A. Ignatieff, Chief of the Fuels and Mining Practice Division of the Mines Branch for his faith and assistance in originally establishing this research program.

The assistance given by Dr. E. Smith of the Physical Metallurgy Division, Mines Branch in reviewing and final editing of the thesis is gratefully acknowledged.

Finally the author would like to acknowledge the many hours of assistance given by his wife Margaret, in preparing this thesis.

TABLE OF CONTENTS

ABSTRACT iii

ACKNOWLEDGEMENTS iv

LIST OF FIGURES ix

LIST OF PLATES xiii

LIST OF TABLES xv

CHAPTER I. Introduction 1

1. Hardening in Metal Single Crystals 1
   1.1. Basinski's Approach to the Study of Strain Hardening 4
   1.2. Scope of the Present Work 6

CHAPTER II. Design, Construction and Calibration of Apparatus for the Measurement of Transient Creep 56

1. Discussion of Previously Used Apparatus 56

2. Design and Construction of the Present Apparatus 59
   2.1. The Loading System 60
      2.1.1. The Mounting Frame 63
      2.1.2. The Chalmer's Beam 64
      2.1.3. The Specimen Yoke 74
      2.1.4. The Load Application System 77
   2.2. The Strain Measurement System 84
      2.2.1. The Optical Section 89
      2.2.2. The Servo Balancing and Recording Section 92
   2.3. The Temperature Control and Measurement System 109
      2.3.1. The Fixed Temperature Bath 109
      2.3.2 The Nitrogen Vapour Cryostat 113

CHAPTER II. Design, Construction and Calibration of Apparatus for the Measurement of Transient Creep (Cont'd)

2.4. The Anti-Vibration Mounting System 116
2.5. A Study of the Operation of the Creep Apparatus 118
2.5.1. Operating Characteristics 119
2.5.2. Effect of Rate of Loading 120
2.5.3. Typical Experimental Curves 123
2.6. Brief Description of a Typical Creep Experiment 125

CHAPTER III. Preparation of Test Specimens 127

1. Easy Glide and the Problem of Specimen Orientation 127
2. Materials 129
3. Preparation of Alloy Ingots 131
4. Preparation of Polycrystal Wire Samples 133
5. Preparation of Single Crystal Wires 135
5.1. The Single Crystal Mould 135
5.2. Initial Preparation 137
5.3. The Furnace Tube 138
5.4. The Out-Gasing Procedure 138
5.5. Design of the Crystal Growing Furnace 140
5.6. Crystal Growing Procedure 151
5.7. Cutting of Test and X-Ray Specimens 152
6. Measurement of Single Crystal Orientations 156
7. Cleaning and Mounting of Finished Test Specimens 159
8. Checking Homogeneity and Impurity Concentration of Alloys 164

CHAPTER IV. Results and Conclusions 170

1. Introduction 170
2. Analysis of Experimental Data 170
3. Experimental Results 174
3.1. Consistancy of Results 175
3.2. Effect of the Magnitude of the Secondary Load 175
3.3. Effect of the Sign of the Secondary Load..... 176

CHAPTER IV. Results and Conclusions (Cont'd)

3.4. Comparison of Results from Transient Creep, constant strain rate, and Stress Relaxation Experiments 176
3.5. Variation of K_2 with Stress 177
3.6. Variation of K_3 with Temperature 191
3.7. Variation of K_3 with Nominal Alloy Concentration and Residual Resistance Ratio 193
3.8. Variation of σ_E and Extent of Easy Glide Region with Resistance Ratio 196
4. Conclusions 198

REFERENCES 200a

VITA 200d

APPENDIX I - Mechanics of Crystal Deformation 200e

APPENDIX II - Tables of Experimental Data 200g

LIST OF FIGURES

Figure 1. Typical Stress-Strain Curve for a Plastically Deformed Metal 2

Figure 2.* Diagram Illustrating the Change of Flow Stress as a Result of a Unit Strain Rate Change in Stage I and II 7

Figure 16.* Block Diagram Illustrating the General Form of the Creep Apparatus 61

Figure 17. Diagram Illustrating the Theory of the Chalmer's Beam System 65

Figure 18. Diagram Illustrating the Design of the Specimen Yoke and its Relationship to Other Parts of the Loading System 75

Figure 19. Design of the Load Application System 78

Figure 20. Detailed Design of Secondary Loading System 82

Figure 21. Outline of the Strain Measurement System 87

Figure 22. Design of the Optic Section of the Strain Measurement System 90

Figure 23. Block Diagram of Zero Balancing and Recording System of the Strain Measurement System 93

Figure 24. Electronic Circuits of the Balancing and Recording Section of the Strain Measurement System 95

---

* Discontinuity in figure and page numbers at this point.

LIST OF FIGURES (Cont'd)

Figure 25. Mechanical Arrangement of Servo Balancing System and Recorder Pen Drive 103

Figure 26. Mechanical Arrangement of Recorder Sensitivity Control 106

Figure 27. Constant Temperature Bath Arrangement and Details of Temperature Measurement System 111

Figure 28. Design of the Nitrogen Vapour Cryostat System 114

Figure 29. Arrangement of Anti-Vibration Mounting System 117

Figure 30. Applied Load Versus Time for a Typical Incremental Loading 122

Figure 30A. Typical Experimental Curves 124

Figure 30B. Illustration Showing Region of Orientation Triangle Where Unperturbed Easy Glide is Most Probable 128

Figure 31. Design of Split Graphite Mould for Growing Single Crystal Wires 139

Figure 32. Design of Furnace Tube 139

Figure 33. Design of the Out-Gas Furnace and the Associated Vacuum System 141

Figure 34. Design of the Crystal Growing Furnace and the System for Lowering the Sample Through it 143

Figure 35. Variation of Temperature as a Function of Time, at a Constant Current for Crystal Growing Furnace 149

Figure 36. Variation of Temperature for Different Positions Within the Furnace and for Different Maximum Currents 150

LIST OF FIGURES (Cont'd)

Figure 37. Arrangement of Cutting and Labelling Samples 153

Figure 38. Diagram Illustrating the Basic Operation of the Acid Saw 154

Figure 39. Orientation of High Purity and Alloy Copper Single Crystal Specimens 158

Figure 40. Impurity Concentration for Copper-Silver Alloys Determined From Residual Resistance Ratio Measurements and Spectrographic Analysis 166

Figure 41. Impurity Concentration for Copper-Gold Alloys Determined From Residual Resistance Ratio Measurements and Spectrographic Analysis 167

Figure 41A. Typical Transient Creep Curves for an Incremental Loading Experiments 171

Figure 41B. Graphical Method of Obtaining the Required Data from the Transient Creep Curves 171

Figure 42. Variation of the Hardening Coefficient (Θ), and Strain Rate Sensitivity (K_3) with Resolved Shear Stress, for (a) Specimen 14H-2 178

Figure 43. (b) Specimen 14F-2 180

Figure 44. (c) Specimen 13C-1 181

Figure 45. (d) Specimen 13C-2 182

Figure 46. (e) Specimen 14E-1 183

Figure 47. (f) Specimen 14G-1 184

Figure 48. Stress-Strain Curve for Specimen 13C-1 186

Figure 49. Stress-Strain Curve for Specimen 13C-2 187

LIST OF FIGURES (Cont'd)

Figure 50. Variation of Strain Rate Sensitivity (K_3) with Resolved Shear Stress for Specimen 6(A)B-1 189

Figure 51. Variation of Strain Rate Sensitivity (K_3) with Resolved Shear Stress for Specimen 7B-1 190

Figure 52. Variation of Strain Rate Sensitivity (K_3) with Temperature for Specimen 14G-1 192

Figure 53. Variation of Average Strain Rate Sensitivity (K_3) with Residual Resistance Ratio and Nominal Alloy Concentration 195

Figure 54. Variation of Initial Stress for Easy Glide (τ_E) with Residual Resistance Ratio 197

LIST OF PLATES

Plate I.	A Side View of the Completed Creep Apparatus	62
Plate II.	'Chalmer's Beams': (a) Rough Blank Mounted on Machining Block and (b) Completed Beams, One With Mounting Attachments	70
Plate III.	Photographs of 'Chalmer's Beam' With Attachments, in Position on the Mounting Frame	72
Plate IV.	Photograph Showing Details of the Load Application System	79
Plate V.	Photograph Showing a Rear, Side View of the Strain Measuring System	88
Plate VI.	Photograph of the Type CS-9 Semiconductor, Photo-conductive Cell Used in the Strain Measurement System	97
Plate VII.	Photographs of the Servo Balancing and Recording System Showing the Mechanical Arrangement	104
Plate VIII.	Photograph Showing Construction and Assembly of Split Graphite Moulds for Growing Single Crystal Wires	136
Plate IX.	Front View of the Out-Gas Furnace and the Associated Vacuum System	144
Plate X.	Photograph of the Completed Crystal Growing System	144
Plate XI.	Close-Up of Single Crystal Furnace	146
Plate XII.	Photograph of Acid Saw for Cutting Crystal Wires	155
Plate XIII.	Plastic 'V-Block' Saddle Used to Clean Single Crystal Test Specimens	161

LIST OF PLATES (Cont'd)

Plate XIV. Specimen Mounting Unit Dismantled, Showing Component Parts 163

Plate XV. Specimen Mounting Unit Assembled, Ready for Soldering-On of End Grips 163

LIST OF TABLES

Table I.	Data for Machining of 'Chalmer's Beams' for Single Crystals of Various Orientations and for Polycrystals	69
Table II.	Fixed Temperature Baths	110
Table III.	The Effect of Different Rates of Loading on the Loading Parameters T_1, T_2 and $L_{osc.}$	123
Table IV.	Weight Percentages of Impurities in High Purity Copper Used to Prepare Test Specimens	130
Table V.	Details of Alloy Constitution	131
Table VI.	Operating Characteristics of Crystal Growing Furnace	151
Table VII.	Orientation Angles (λ and χ) for Single Crystal Specimens	159
Table VIII.	Relationship of the Average Strain Rate Sensitivity (K_3) and Initial Stress for Easy Glide (τ_E) to Nominal Impurity Concentration and Residual Resistance Ratio for Copper and Copper-Silver Alloy Single Crystals	194
Table IX.	Experimental Data for Specimen 14P(1)-1 (Pure Copper Polycrystal)	200g
Table X.	Experimental Data for Specimen 14H-1 (Pure Copper Single Crystal)	201
Table XI.	Experimental Data for Specimen 14H-2 (Pure Copper Single Crystal)	202
Table XII.	Experimental Data for Specimen 14F-2 (Pure Copper Single Crystal)	204

LIST OF TABLES (Cont'd)

Table XIII.	Experimental Data for Specimen 13C-1 (Pure Copper Single Crystal)	205
Table XIV.	Experimental Data for Specimen 13C-2 (Pure Copper Single Crystal)	208
Table XV.	Experimental Data for Specimen 14E-1 (Pure Copper Single Crystal)	210
Table XVI.	Experimental Data for Specimen 14G-1 (Pure Copper Single Crystal)	212
Table XVII.	Experimental Data for Specimen 6(A)B-1 (Copper Alloy Single Crystal, 0.1 at.% Ag.)	214
Table XVIII.	Experimental Data for Specimen 7B-1 (Copper Alloy Single Crystal, 0.3 at.% Ag.)	216

CHAPTER I

INTRODUCTION

1. Hardening in Metal Single Crystals

When a metal single crystal is deformed at a constant temperature and a constant strain rate, the relationship between the measured resolved shear stress (flow stress), and the applied resolved shear strain is in general of the form shown graphically in Figure 1. This curve is known as the stress-strain curve, and the slope at any point $\theta = \frac{d\tau_R}{de}$ is known as the strain hardening coefficient. According to Seeger (1956) the stress strain curve consists of the following regions: OA, the elastic region; AB, a transition region in which the behaviour is partly elastic and partly plastic in nature; BC, stage I of plastic deformation known as the easy glide region; CD, a second transition region; DE, stage II of plastic deformation known as the linear hardening region; and EF, stage III of plastic deformation. The three stages of plastic deformation may be classified by their strain hardening coefficients; stage I is characterized by a low value, stage II by a much larger value, usually a factor five to ten times larger than in stage I, and stage III by a value which decreases with increasing strain.

The plastic deformation of crystals has been studied for many years, but for the most part this work was purely emperical, or based

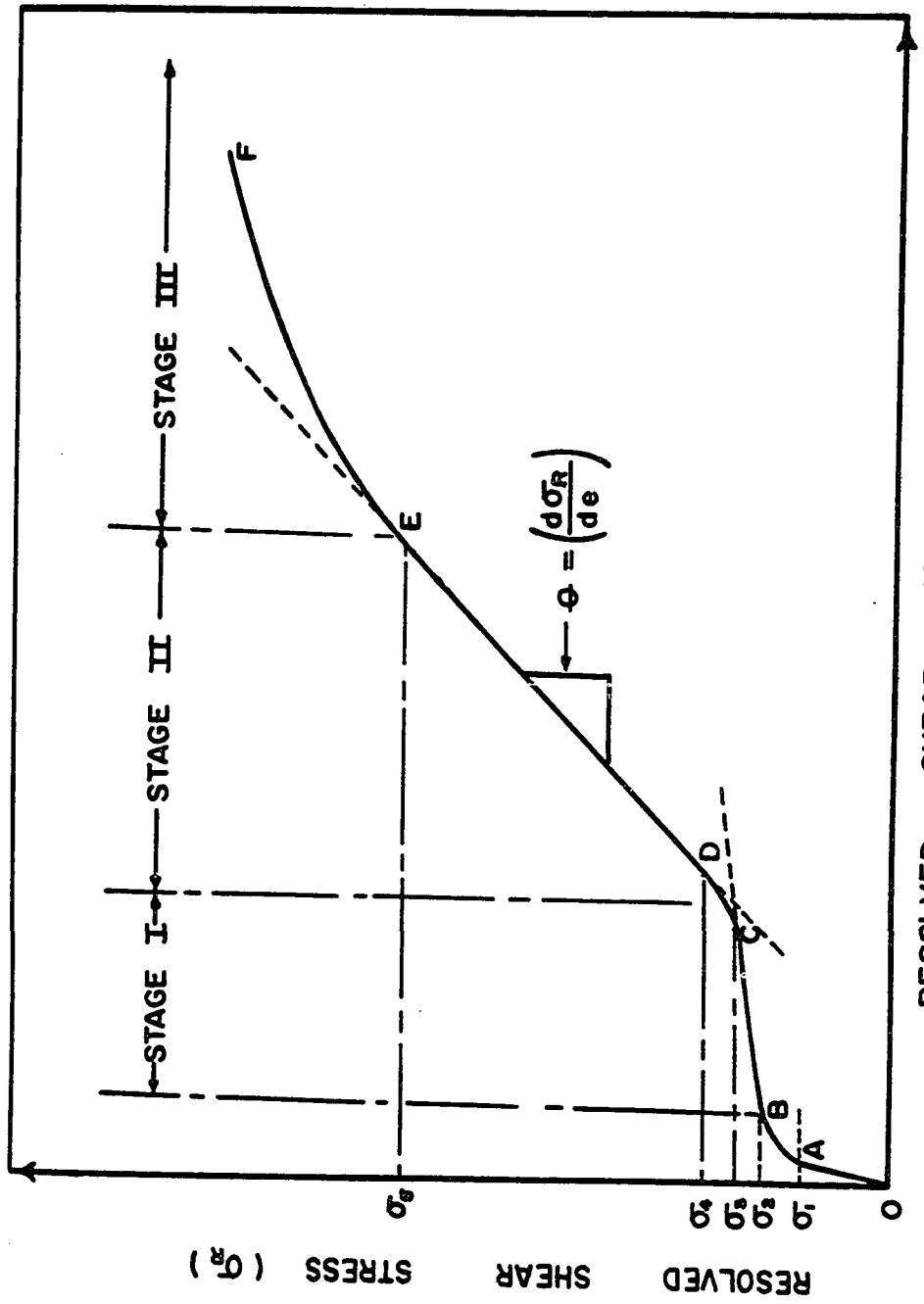

FIGURE 1 -- TYPICAL STRESS-STRAIN CURVE FOR A PLASTICALLY DEFORMED METAL.

on the principles of crystal geometry. Schmid and Boas (1935) in their text on plasticity of crystals cover this field in great detail and include a very comprehensive bibliography on the subject up to 1935. Another classic work in the field is the paper by Andrade and Roscoe (1935) on glide in metal single crystals. The basic geometry of crystal deformation discussed in these two works is still valid.

The increase in strength (increase in the flow stress) of metals with plastic deformation is known as strain or work hardening. Over the past ten years considerable attention has been given to the study of strain hardening in terms of dislocation theory.* Theoretical work has been carried out on this problem by Friedel (1955), Mott (1952, 1953), Seeger (1956, 1957), and Seeger et al (1957). This recent work has been based to a great extent on the original ideas of Taylor (1934) who produced the first detailed theory of strain hardening. Basically, these theories assume that for the most part strain hardening is due to the long-range elastic interactions between parallel dislocations accumulating in the lattice during deformation.

However it has been suggested by Mott (see Cottrell and Stokes 1955) that "the important elastic forces on a glide dislocation are those from its immediate neighbours rather than the long-range stresses from

---

* Details of dislocation theory may be found in such texts as Cottrell (1953) and Read (1953).

piled up groups, for then the elastic forces and the forest forces acting on the dislocation can both be ascribed to the same thing, the presence of nearby dislocations". Basinski (1959) further states that if the constancy of the flow stress ratio observed by Cottrell and Stokes (1955), and others is to be explained then "the important elastic forces must be restricted to those dislocations which can act as short-range obstacles, i.e. the dislocations threading the glide plane".

1.1 Basinski's Approach to the Study of Strain Hardening

Basinski's (1959) approach to the study of strain hardening has been to consider that the motion of glide dislocations are impeded by obstacles within the crystal lattice, to design experiments to determine what particular obstacles are active in the different stages of deformation, and to gain information on the form and magnitude of the forces associated with the different dislocation-obstacle interactions, as well as the activation distance or range of the obstacle. Rather then assuming a definite form for any dislocation-obstacle interaction he has developed a general expression from which the activation energy required to overcome the obstacles, the form of the interaction force versus distance curve, the maximum force and the activation distance may be calculated from experimentally determined quantities.

Starting with the Wyatt Creep Theory (Wyatt (1953)) Basinski has developed the following expression for the activation energy:

$$U = kT\left\{\frac{\left(\frac{1+K_2}{K_1 K_2}\right)}{K_4}\right\} \quad . \qquad (1)$$

The factors K_1, K_2, K_3 and K_4 are given as follows:

$$K_1 = \left(\frac{\sigma_T/\mu_T}{\sigma_0/\mu_0}\right)_{\dot{e}} \quad , \qquad (2)$$

$$K_2 = \left(\partial \frac{\sigma_T/\mu_T}{\sigma_0/\mu_0} \Big/ \partial T\right)_{\dot{e}} \quad , \qquad (3)$$

$$K_3 = \frac{1}{T}\left(\frac{\partial \ln \sigma}{\partial \ln \dot{e}}\right)_T \quad , \qquad (4)$$

and

$$K_4 = \left(1 - T\frac{\partial \ln \mu}{\partial T}\right) \quad , \qquad (5)$$

where σ, μ and $\dot{e}$ represent flow stress, elastic modulus and strain rate, σ_T and μ_T, and σ_0 and μ_0 are the flow stress and elastic modulus at a temperature T and absolute zero respectively, k is the Boltzman constant, and $(\ )_{\dot{e}}$ and $(\ )_T$ indicate that the particular bracketed quantity was determined for a constant strain rate, or constant temperature respectively. Factors K_1, K_2 and K_3 may be evaluated from the results of mechanical tests, and factor K_4 may be determined from the work of Overton and Gaffney (1955) using the equation of Foreman (1955).

Basinski (1959) has studied the variation of the factors K_1 and K_3 (strain rate sensitivity) as a function of temperature and stress for single crystals of pure copper, aluminum and silver in stage II deformation

where he considers the obstacles to be the forest dislocations.

1.3 Scope of the Present Work

This thesis is mainly concerned with the development of apparatus and procedures for the measurement of the strain rate sensitivity factor, $K_3 = \frac{1}{T}\left(\frac{\partial \ln \sigma}{\partial \ln \dot{\epsilon}}\right)_T$ for plastic deformation in the easy glide region. Basically this factor may be determined by a number of methods including constant strain rate experiments, transient creep experiments, and stress relaxation experiments.

Basinski's studies to date have mainly concentrated on behaviour in the linear hardening region and for this work he has found constant strain rate experiments most convenient. This experimental procedure involves carrying out constant strain rate experiments in which abrupt changes in the strain rate are introduced and the corresponding change in flow stress observed. Figure 2 illustrates such a condition, a change in strain rate from $\dot{\epsilon}_1$ to $\dot{\epsilon}_2$ in the linear hardening region resulting in a change in the flow stress of τ_{II}. When a similar experiment is conducted in the easy glide region the resulting change in flow stress τ_I is considerably smaller and as a result accurate determinations of K_3 are difficult.

Under such conditions incremental transient creep experiments similar to those described by Wyatt (1953) and Conrad (1958) present a considerable advantage. This method involves carrying out transient

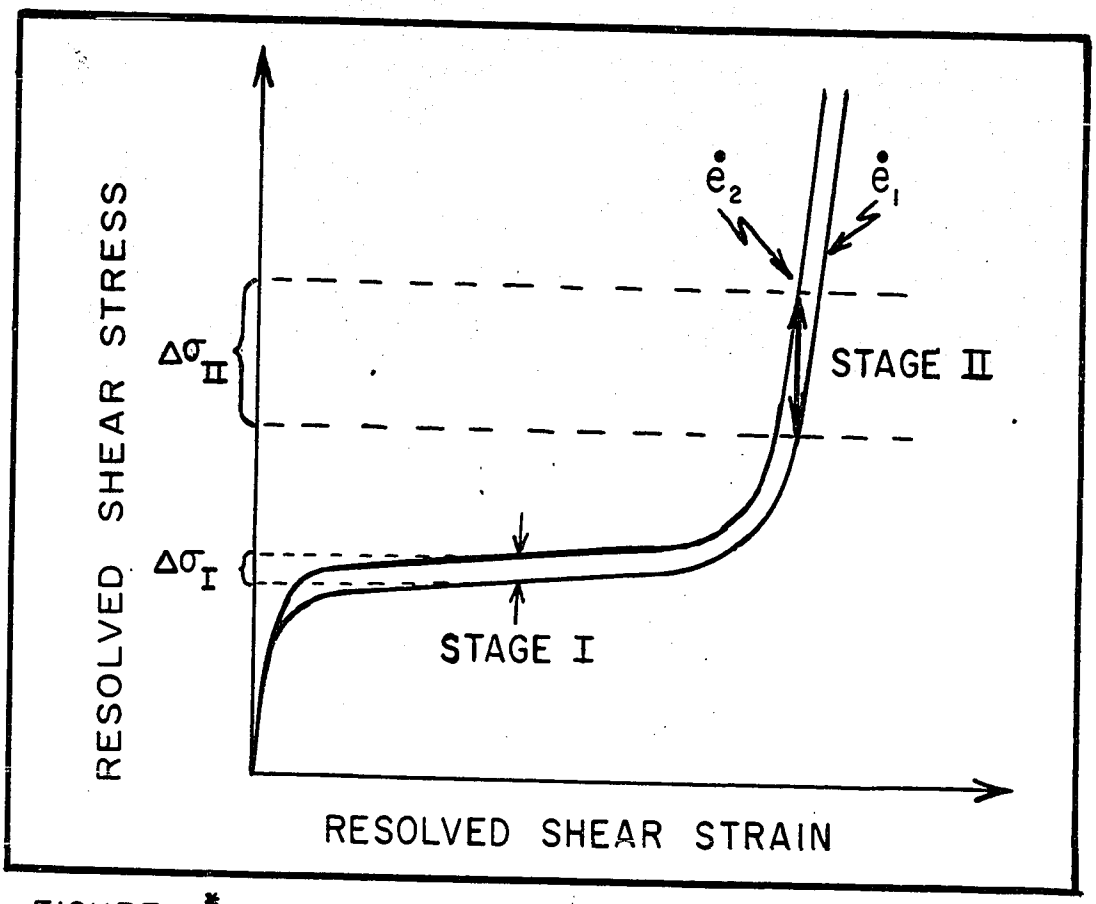

FIGURE 2* -DIAGRAM ILLUSTRATING THE CHANGE OF FLOW STRESS AS A RESULT OF A UNIT STRAIN RATE CHANGE IN STAGE I & II

* Figure numbers are discontinuous at this point. The next figure number will be 16.

creep experiments in which abrupt changes in the applied stress are made and the resulting variation in the strain versus time curves observed. Provided the strain recording system is sensitive enough, and capable of following the rapid strain rate changes which follow changes in the applied stress, then the method is capable of measuring much smaller effects far more accurately than the constant strain rate method. A further advantage of this method lies in the fact that the extent of the easy glide region in many specimens is rather limited and as a result it is desirable to make only small changes in the applied stress in order to maintain the specimen well within the easy glide region. This method has been employed in this thesis for the determination of the strain rate sensitivity factors for pure copper and copper-silver alloy single crystals at temperatures from 300° to 78°K.

---

* Page numbers are discontinuous at this point. The next page number will be 56.

CHAPTER II

DESIGN, CONSTRUCTION, AND CALIBRATION OF THE APPARATUS FOR THE MEASUREMENT OF TRANSIENT CREEP

1. Discussion of Previously Used Apparatus

The study of the phenomena of creep has been undertaken for a number of years, and during that time a number of different types of apparatus have been developed for observing it experimentally in the laboratory. Andrade and Chalmers (1932) have described an apparatus for measuring creep on which the majority of later ones have been patterned. Basically this apparatus was designed to perform the following functions. (a) to apply a constant stress to the test specimen, which was in the form of a fine wire, and (b) to measure the variation of length of the wire as a function of time.

The part of the apparatus which applied the stress to the specimen was of such a design that the stress remained constant although the cross sectional area of the specimen decreased with elongation. To accomplish this, the load was applied to the specimen via a specially contoured beam, now known as the 'Chalmer's Beam System'. This system maintained the tensile stress to within 1% for extensions up to 30%. In the Andrade and Chalmers apparatus the creep strain was recorded

---

a Page and figure numbers are discontinuous at this point.

photographically by a light beam falling on a drum holding sensitive paper, which was rotated by a synchronous motor. The apparatus was capable of measuring strains of 5×10^{-5}. These workers conducted experiments in the temperature range of 273°K to 373°K. These temperatures were obtained with baths of ice water and thermostatically controlled oil.

Wyatt (1953) developed a creep machine using pneumatic loading and continuous strain recording. The pneumatic loading feature resulted in a machine with a small inertia, the mass of the moving parts being only 0.6 K_g. As a result this machine was suitable for investigating the initial part of the creep curve (transient creep) where the strain rates changed rapidly and where the effects of inertia might destort the true creep curve. Wyatt states that the load could be measured to $\pm$ 0.1% of the maximum capacity of the machine which was 22.5 K_g. The error in constancy of the applied tensile stress with specimen elongation was quoted as being approximately $\pm$ 0.5%. Wyatt also states that there was in inherent error of $\pm$ 15 gm. in the applied load due to friction and other factors. This would introduce a large error when small stresses were required. The specimen extension in Wyatt's apparatus was recorded by projecting a graticule attached to the specimen loading frame onto the lens of a rotating drum camera. With this apparatus the strain could be measured to a sensitivity of 2×10^{-5}.

Wyatt carried out experiments at a number of different temperatures between 77°K and 413°K. These temperatures were obtained using different constant temperature baths and thermostaticly controlled oil.

A recent paper by Conrad (1958) describes a machine for measuring creep of copper single crystals. The loading was accomplished using a modified form of the Chalmer's beam system. The loading technique appeared to be extremely crude and consisted of adding known amounts of lead shot to a loading pan. The strain was measured with a clip-on-type resistence strain gauge transducer mounted externally to the specimen. The output of the transducer was recorded electronically and a sensitivity of 2.7×10^{-5} strain is quoted. The low temperatures used by Conrad in his experiments were obtained using a nitrogen vapour spray unit (probably similar to the nitrogen vapour cryostat described later in this thesis). Temperatures were maintained constant to $\pm$ 1°K and were uniform to 1.5°K over the 10 cm. gauge length of the specimen.

There have been many papers, too numerous to mention, published recently describing apparatus for the measurement of steady-state creep. Here the standard Chalmer's beam loading system is normally employed, and creep strains since they are slow, are observed using a sensitive cathetometer.

The creep machine developed at the University of Ottawa has been

a combination of many of the features of the machines just described. However since the research problem was of a different nature than that for which these machines were designed, a number of special features were added. The loading system used incorporates a Chalmer's beam, but it was constructed to be of low mass in order to reduce the effect of inertia at rapidly changing strain rates. The loads were applied manually up to the initiation of easy glide, but after that they were applied automatically at a fixed rate. The creep strains were recorded electronically, and since the strain transducer employed only an optical coupling to the specimen it did not modify the true behaviour of the specimen.

Due to the fact that many of the component parts of the apparatus were not available commercially the majority of the apparatus was constructed in the Physics Department work shops. It is suggested that further modification in the design of the apparatus could be introduced to simplify its construction and operation.

2. Design and Construction of the Present Apparatus

Most of the apparatus constructed to measure creep described in the literature to date has been designed to measure steady-state creep or the gross features of transient creep. In contrast the apparatus described in this thesis was designed to be (a) extremely sensitive, strains of 5×10^{-6} being easily observable on a specimen with a 10 cm. gauge length,

(b) capable of recording very rapid strain rates, up to 10 sec^{-1}, (c) capable of maintaining the resolved shear stress on the glide plane to within 1% over a range of crystal extension up to 15%, and (d) capable of making very rapid and accurate changes in the applied load, facilities were provided for increasing or decreasing the applied load by approximately 3 to 17 grams in a time interval of less than 0.3 sec without producing impact stresses in the specimen.

Basically the apparatus consists of three major systems, which will be described in detail in the following sections. These are the loading system, the strain measuring system, and the temperature controlling and measuring system. Figure 16 shows a block diagram illustrating the general form of the apparatus. Plate I shows a side view of the completed apparatus.

2.1. The Loading System

To gain the high accuracy required in the loading system, and as well to have a relatively simple and inexpensive unit the Chalmer's beam system was used. However, special care was taken to construct the beams with the lowest possible mass, and to provide them with a low friction bearing. The crystal specimen (within the specimen yoke) is held between a bottom fixed 'ring-joint', and a top 'ring-joint' which is connected through a pull-rod and loading tape to the front contour of the Chalmer's beam.

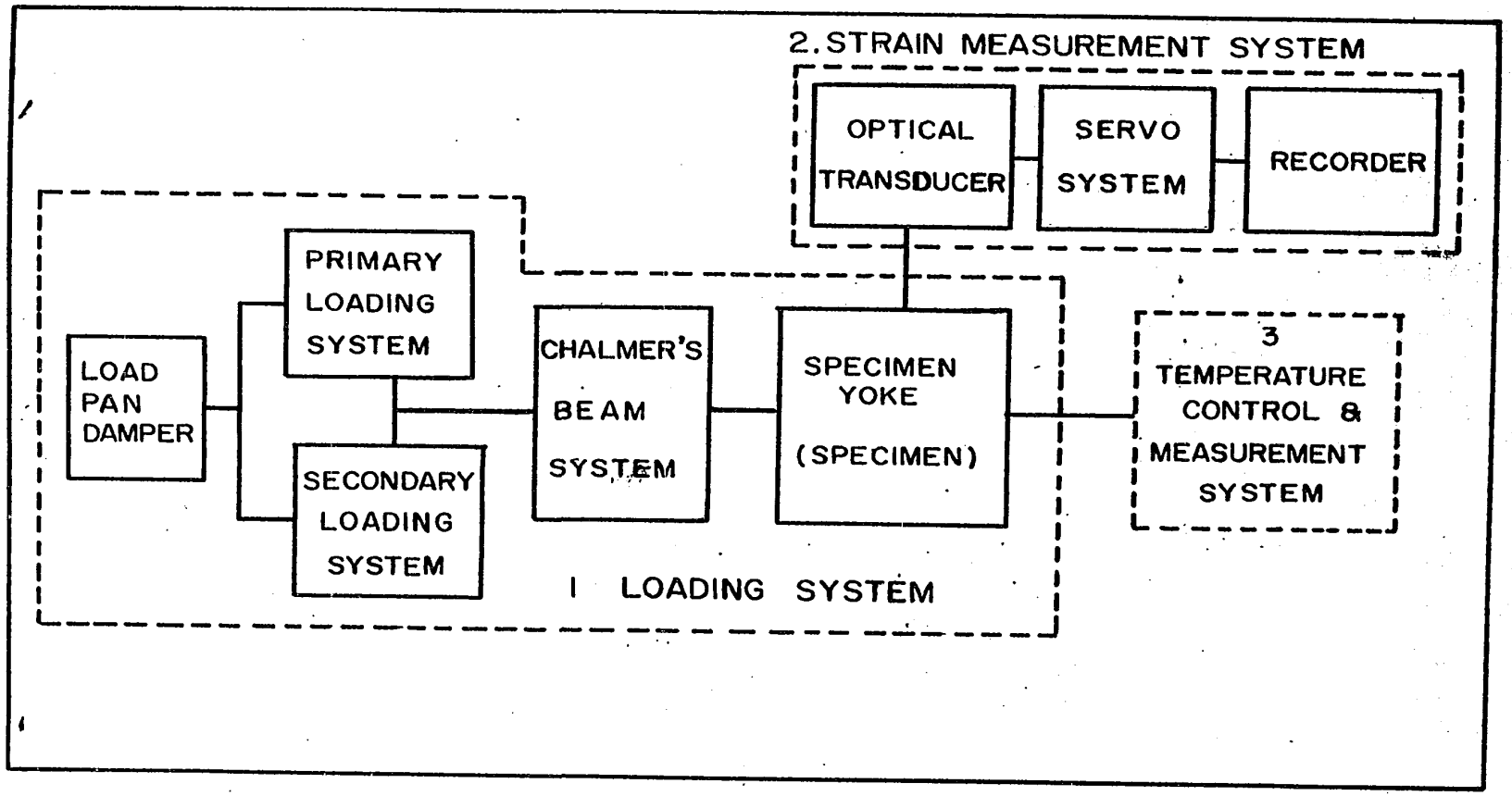

FIGURE 16 — BLOCK DIAGRAM ILLUSTRATING THE GENERAL FORM OF THE CREEP APPARATUS

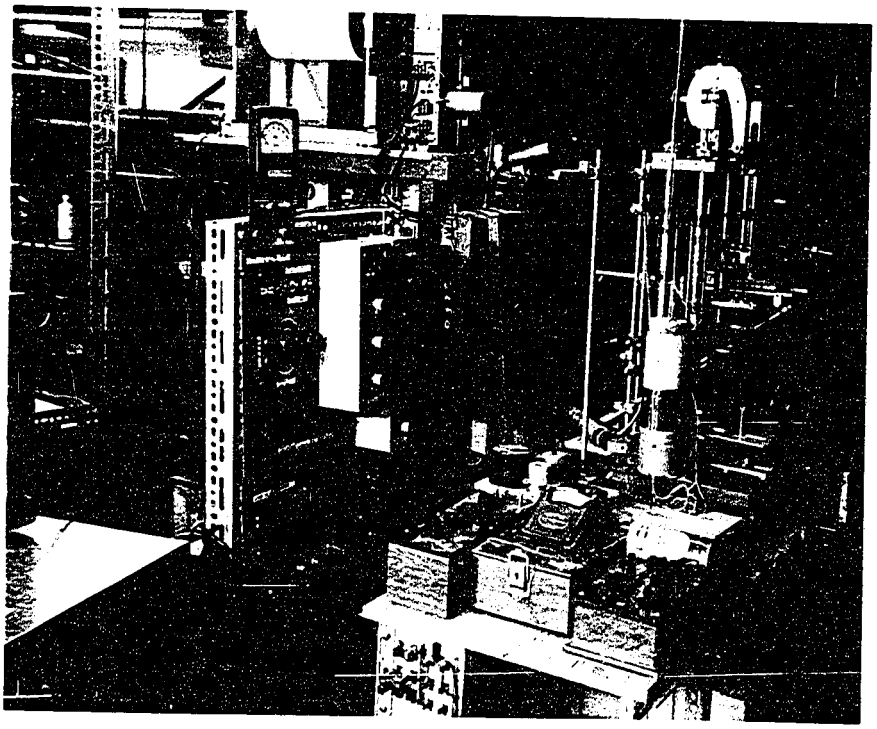

PLATE I

A Side View of the Completed Creep Apparatus.

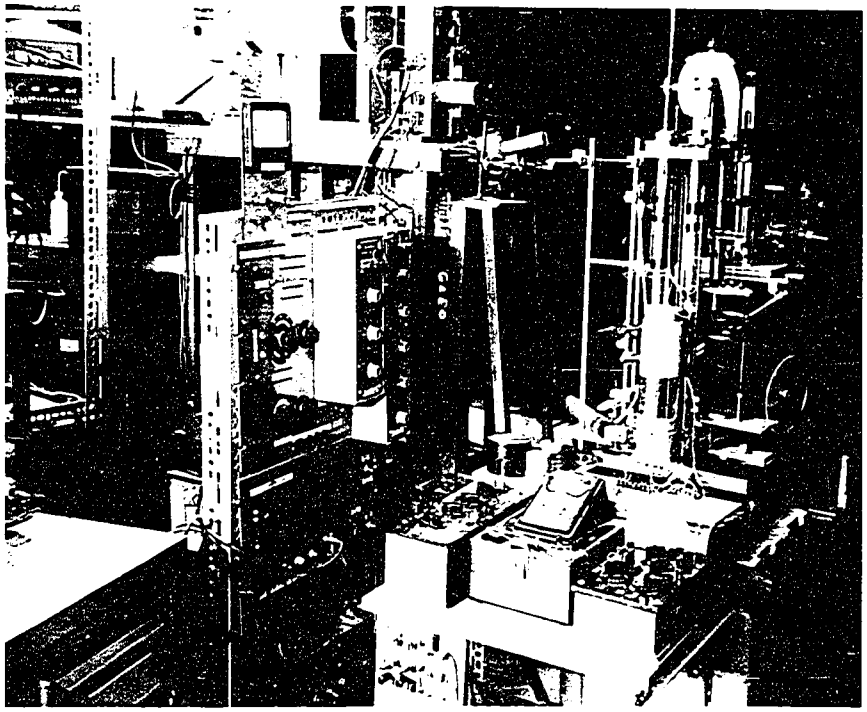

Side view of the Compl[illegible] Creep Apparatus.

The beam itself is pivoted on a steel/agate bearing, and loads are applied to a loading pan suspended from a second tape attached to the rear contour of the beam. Applying dead loads in the form of weights to the loading pan thus increases the tensile stress on the test specimen. The loading system consists basically of four major units namely: the mounting frame, the Chalmer's beam, the specimen yoke, and the load application system.

2.1.1. The Mounting Frame

The Chalmer's beam system and specimen yoke were mounted on a heavy steel plate (8" x 5-1/4" x 3/4" thick) which was supported on top of four steel posts (20" long x 1-1/4" diameter) attached to a steel bottom plate (13" x 13" x 1" thick). The bottom plate itself was set on adjustable levelling screws, which rested on sockets attached to two steel U- beams, which were themselves tied to a concrete block pillar which formed part of the anti-vibration mounting system to be described later (see Section 2.4.).

Some parts of the loading system, in particular the load pan arrester and incremental load applicator were not attached to this frame, but were tied to a separate frame which was bolted to the floor in order to reduce the effect of vibration on the apparatus. The construction of the mounting frame is shown clearly in Plate I.

2.1.2. The Chalmer's Beam

As mentioned earlier in this chapter Andrade and Chalmers have described in an early paper (Andrade and Chalmers (1932) a device for maintaining a constant tensile stress, independent of deformation, on a polycrystaline wire specimen during plastic flow. This device has become known as the 'Chalmer's beam system' and has been employed in many modified forms since that time. Figure 17 illustrates the basic theory of the beam system. The beam, which consists of a plate pivoted at P, is constructed with a special front and rear contour. Flexible tapes are fastened at F_1 and F_2 and are allowed to hang down along the contours. Equating moments on either side of the beam gives,

$$P_a R_2(\theta) = P_c R_1(\theta) \quad , \qquad (6)$$

where P_a is the load applied to the beam, P_c is the load applied to the specimen, and $R_1(\theta)$* and $R_2(\theta)$ are the lengths of the front and rear level arms, which are themselves some function of the angular rotation (θ) of the beam. Normally $R_1(\theta)=R_1$ (a constant), and the contour is thus a radius about the pivot point P.

For convience let $P_c = P_a$ when the beam is horizontal ($\theta=0$), and therefore $R_2(\theta)=R_1$. For all other positions of the beam however

* $R_1(\theta)$ indicates that R_1 is a function of θ.

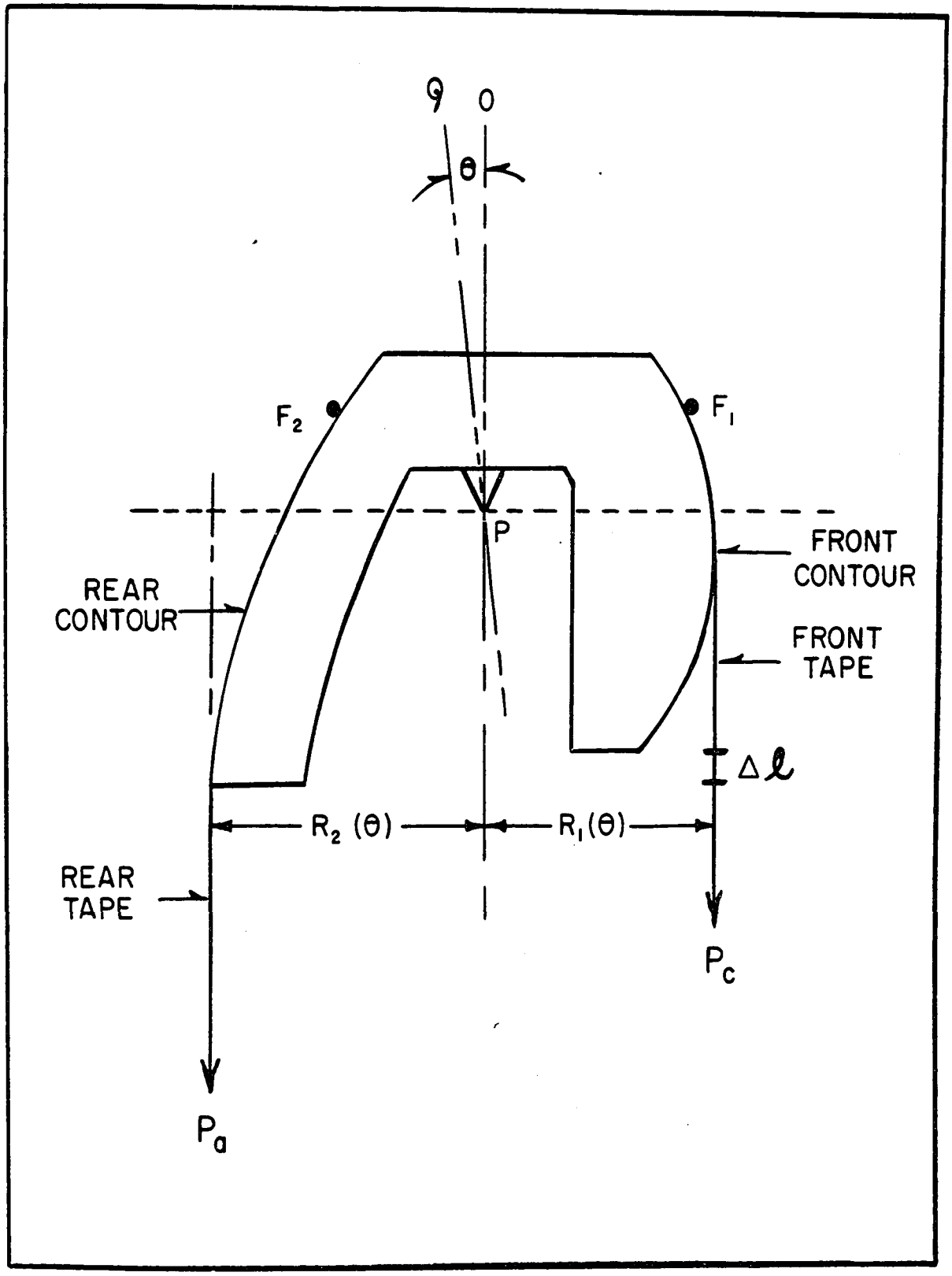

FIGURE 17 - DIAGRAM ILLUSTRATING THE THEORY OF THE CHALMERS BEAM SYSTEM.

R_2 must decrease with increasing θ therefore,

$$R_2(\theta) = \beta(\theta) R_1 \quad . \tag{7}$$

Since the front contour is a radius, and Δl the elongation of the specimen, then Δl is related to the rotation $\Delta\theta$ of the beam by $\Delta l = R_1 \Delta\theta$. Therefore equation (38) may be written as,

$$R_2(\Delta l) = \beta(\Delta l) R_1 \quad . \tag{8}$$

As mentioned previously these beams were originally designed to maintain the tensile stress constant in polycrystaline wire specimens where the cross-sectional area decreased with extension. A beam of this type was designed for the creep apparatus and in this case $R_2(\theta)$ is a decreasing function for increasing θ. In this case the change in the cross-sectional area of the specimen related to the change in the length by the relationship

$$\frac{A_2}{A_1} = \frac{l_1}{l_1 + \Delta l} \quad , \tag{9}$$

where l_1 is the original length, Δl the extension, and A_1 and A_2 are the cross-sectional areas before and after extension. This relationship is based on the assumption that during extension the volume of the specimen remains constant. Now to maintain the tensile stress constant during deformation will require that the length of the lever arm R_2 decrease in the

same manner as the cross-sectional area decreases, therefore,

$$\beta(\Delta l) = \frac{l_1}{l_1 + \Delta l} \,. \qquad (10)$$

In the case of single crystal specimens it is the resolved shear stress in the glide direction, on the glide plane, which must be held constant during crystal extension. It has been shown previously (Andrade and Roscoe (1937)) that this resolved shear stress increases with specimen extension as follows,

$$\sigma = \sigma_0 \left(\frac{1 - \left(\frac{l^2 \sin^2 \lambda}{(l + \Delta l)^2} \right)}{1 - \sin^2 \lambda} \right)^{1/2} , \qquad (11)$$

where σ is the resolved shear stress after an elongation Δl, σ_0 is the initial resolved shear stress, l is the initial specimen length and λ is the initial angle between the tensile axis and the glide direction. If the resolved shear stress is to remain constant during deformation it will be necessary for the length of the lever arm R_2 to decrease in the same manner as the resolved shear stress would normally increase. Therefore,

$$\beta(\Delta l) = \left(\frac{1 - \left(\frac{l^2 \sin^2 \lambda}{(l + \Delta l)^2} \right)}{1 - \sin^2 \lambda} \right)^{1/2} . \qquad (12)$$

For polycrystalline specimens the form of the factor $\beta(\Delta l)$ depends only on the original length of the specimen, however for single crystal specimens $\beta(\Delta l)$ also depends on λ, one of the crystal orientation angles. It

was determined that in order to cover the orientation range from λ = 33° to 50° with a maximum deviation of less than 1% in the resolved shear stress a set of eight beams designed for the orientations 33°, 35°, 37°, 39°, 41°, 44°, 47°, and 50° would be required. For convenience each beam was designed to allow 12% extension, with an overlap into the range of the next beam after 5% extension. Table 1 lists the values of R_2 for different specimen extensions (and the resulting beam rotation) for the different initial values of λ listed above, as well as the values for the polycrystal case.

The beams were first cut roughly from a sheet of 1/4 inch thick 24-S aluminum as shown in Plate II. They were drilled with a set of locating holes and mounted on a special machining block (see Plate II) which allowed the beams to be firmly clamped during the machining operation. This machining block was set in a dividing head and the contours were 'roughly' cut using a vertical milling machine. After making the calculated cuts at each half degree interval the space between cuts were carefully evened out using a hand file while checking the contour continuously with a dial gauge. The finished beams were checked against the design figures and were found to be accurate to at least $\pm$ 0.0002". The completely machined beams weighed approximately 150 grams without the attachments. Some of the completed beams are shown in Plate II includ-

TABLE I

Data for Machining of 'Chalwers Beams' for Single Crystal Specimens of Various Orientations and Polycrystal Specimens

Beam Rotation (θ)	Equivalent Specimen Elongation ($\Delta\ell$)	Values of R_2 (1) - Inches								
		Single Crystal Data								Polycrystal Data
		Initial Angle Between Glide Direction and Tensile Axis								
Degrees	Inches	33°	35°	37°	39°	41°	44°	47°	50°	
0	0.0000	2.5000	2.5000	2.5000	2.5000	2.5000	2.5000	2.5000	2.5000	2.5000
0.5	0.0218	2.4943	2.4933	2.4923	2.4910	2.4898	2.4875	2.4843	2.4808	2.4862
1.0	0.0438	2.4885	2.4868	2.4845	2.4823	2.4795	2.4750	2.4690	2.4620	2.4725
1.5	0.0655	2.4830	2.4803	2.4773	2.4738	2.4700	2.4630	2.4545	2.4443	2.4591
2.0	0.0873	2.4776	2.4740	2.4700	2.4658	2.4605	2.4515	2.4405	2.4273	2.4458
2.5	0.1090	2.4725	2.4680	2.4630	2.4578	2.4513	2.4405	2.4268	2.4108	2.4326
3.0	0.1310	2.4673	2.4620	2.4560	2.4498	2.4423	2.4295	2.4135	2.3945	2.4195
3.5	0.1528	2.4623	2.4563	2.4495	2.4420	2.4335	2.4188	2.4008	2.3793	2.4066
4.0	0.1745	2.4575	2.4508	2.4430	2.4348	2.4250	2.4085	2.3885	2.3645	2.3939
4.5	0.1963	2.4525	2.4450	2.4368	2.4273	2.4168	2.3985	2.3765	2.3500	2.3813
5.0	0.2183	2.4478	2.4395	2.4305	2.4203	2.4085	2.3888	2.3648	2.3360	2.3687
5.5	0.2400	2.4433	2.4343	2.4243	2.4133	2.4008	2.3793	2.3535	2.3228	2.3564
6.0	0.2618	2.4385	2.4290	2.4185	2.4068	2.3930	2.3703	2.3425	2.3098	2.3441
6.5	0.2838	2.4343	2.4240	2.4125	2.3998	2.3858	2.3613	2.3318	2.2970	2.3319
7.0	0.3055	2.4300	2.4190	2.4070	2.3935	2.3785	2.3525	2.3215	2.2848	2.3200
7.5	0.3273	2.4258	2.4143	2.4013	2.3873	2.3713	2.3440	2.3115	2.2730	2.3081
8.0	0.3490	2.4215	2.4093	2.3960	2.3810	2.3643	2.3358	2.3018	2.2618	2.2964
8.5	0.3710	2.4175	2.4048	2.3905	2.3750	2.3575	2.3278	2.2920	2.2505	2.2847
9.0	0.3928	2.4133	2.4003	2.3853	2.3693	2.3510	2.3198	2.2828	2.2398	2.2732
9.5	0.4145	2.4095	2.3958	2.3805	2.3635	2.8445	2.3123	2.2740	2.2293	2.2619
10.0	0.4363	2.4058	2.3915	2.3755	2.3578	2.3383	2.3045	2.2653	2.2190	2.2506
10.5	0.4583	2.4020	2.3870	2.3705	2.3523	2.3318	2.2973	2.2565	2.2090	
11.0	0.4800	2.3983	2.3828	2.3658	2.3470	2.3260	2.2903	2.2483	2.1995	
11.5	0.5018	2.3948	2.3788	2.3610	2.3418	2.3200	2.2833	2.2403	2.1903	
12.0	0.5235	2.3913	2.3748	2.3565	2.3365	2.3143	2.2765	2.2323	2.1813	
15.0	0.6545	2.3713	2.3520	2.3310	2.3078	2.2823	2.2390	2.1888	2.1313	
20.0	0.8728	2.3423	2.3193	2.2943	2.2670	2.2368	2.1863	2.1285	2.0630	
25.0	1.0908	2.3183	2.2920	2.2638	2.2328	2.1993	2.1433	2.0798	2.0085	
30.0	1.3090	2.2975	2.2688	2.2378	2.2043	2.1678	2.1075	2.0390	1.9640	

(1) The values of R_2 are based on the assumption that $R_1 = 2.5$ inches.
(2) This angle is the orientation angle λ.

(a) Rough Blank Mounted on Machini :g Block.

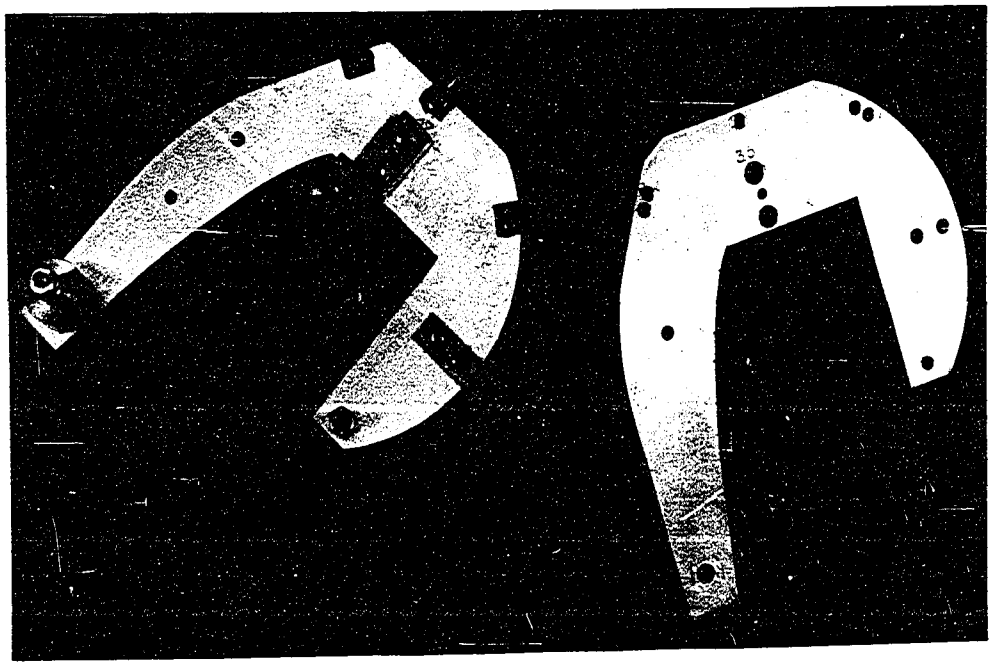

(b) Completed Beams, One With Mounting Attachments.

PLATE II

'Chalmer's Beam.'

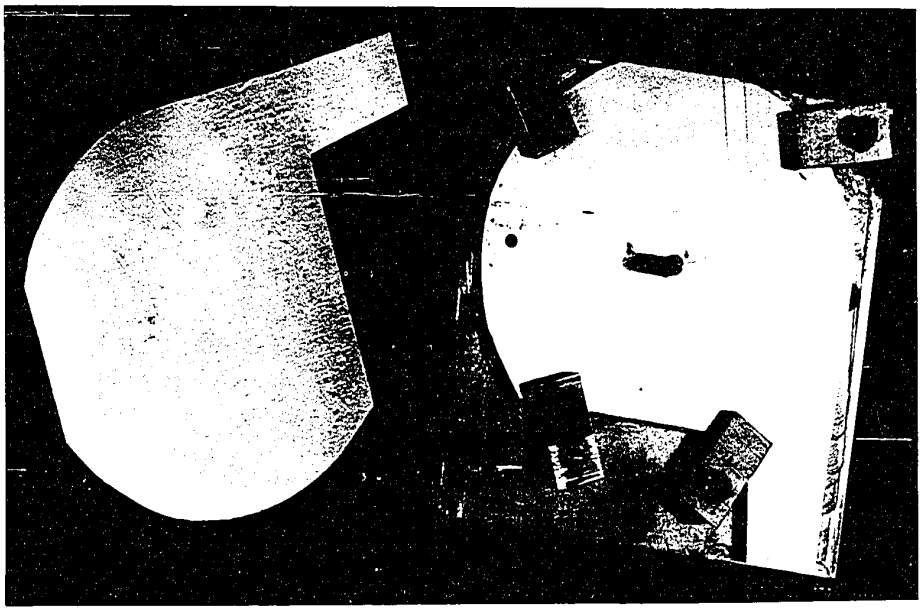

(a) Rough Blank Mounted on Machining Block.

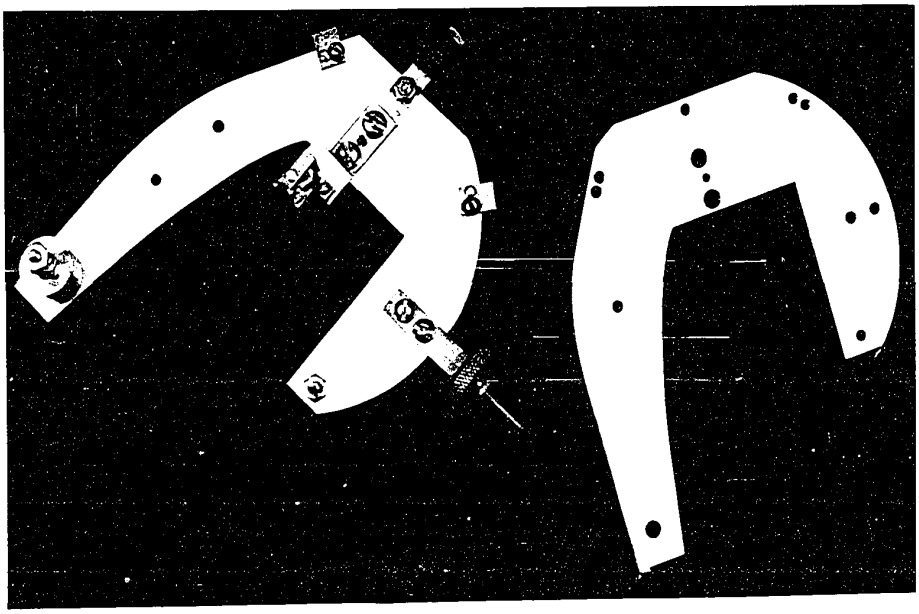

(b) Completed Beams, One with Mounting Attachments.

PLATE II

Chalmers Beam

ing one fitted with its mounting attachments. Only one set of these attachments were made and these were fastened temporarily to the particular beam in use.

These attachments consisted of a steel knife edge (the top half of the beam balance bearing), an adjustable mirror (part of the strain measuring system which will be described later), a tape clamp at the top of the front and rear beam contour, and a set of course and fine adjustments for positioning the centre of gravity (C.G.) of the beam both horizontally and vertically. Plate III shows a front and side view of the beam located in position on the mounting frame.

The beam bearing* consists of a steel knife edge approximately 40 mm long attached to the beam, and on an agate bearing attached to the bearing support on the mounting frame. The agate bearing was ground optically flat in the centre part where it came in contact with the steel knife edge. The complete bearing was designed for a maximum load of $3K_g$ with a minimum of friction.

The adjustments for the centre of gravity (C.G.) of the beam are extremely important. If the weights applied to the loading pan (plus the weight of the pan, loading tapes etc.) are to be an accurate measure of the total applied load then there must be no restoring torque (due to gravity)

* The bearings were supplied and mounted by the George Westphal Co. of Canada, Ltd., Toronto, Ontario.

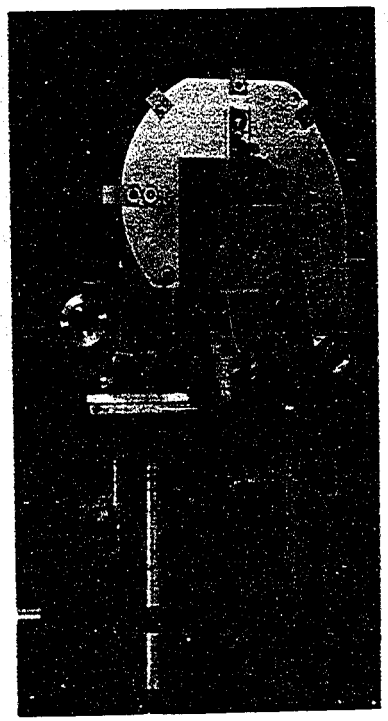

(a) Side View.

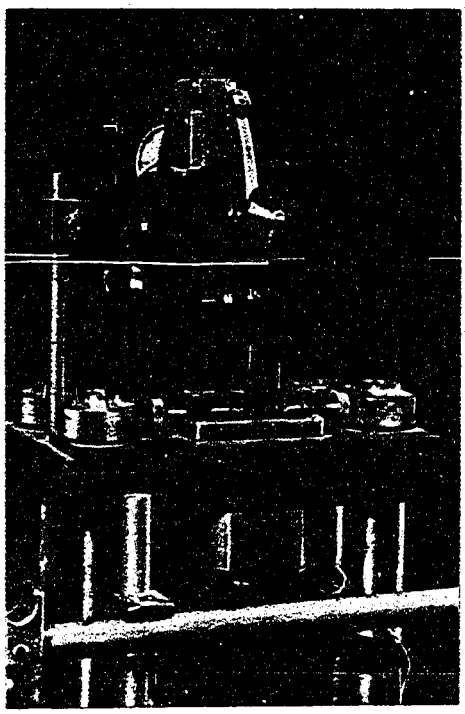

(b) Front View.

PLATE III

Photographs of 'Chalmer's Beam' with Attachments, in Position on the Mounting Frame.

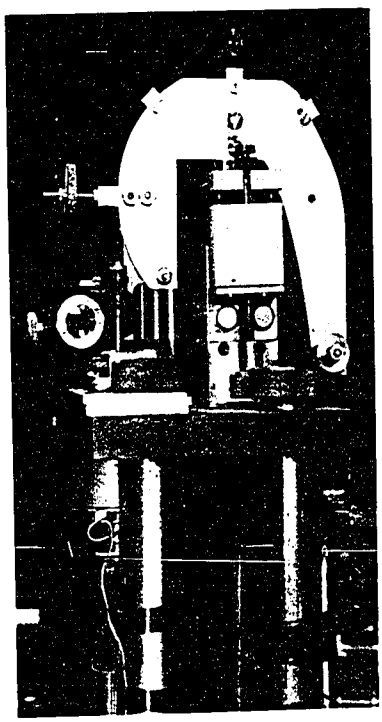

(a) Side View.

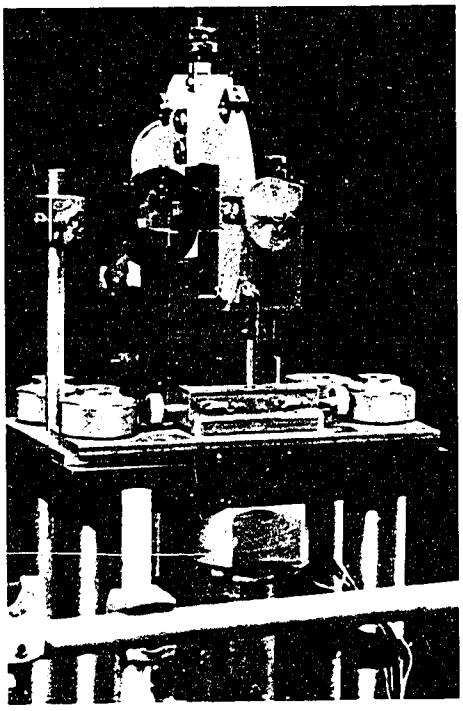

(b) Front View.

PLATE III

Photographs of 'Chalmer's Beam' with Attachments, in Position on the Mounting Frame.

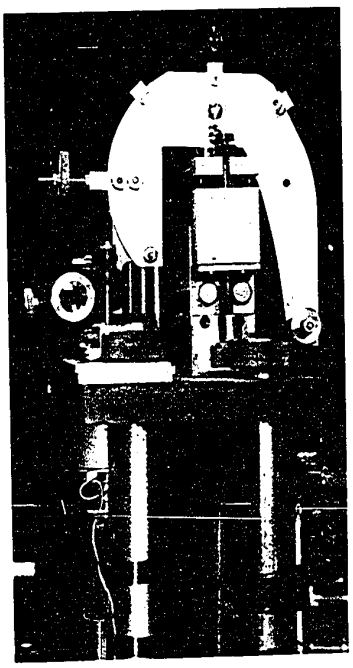

(a) Side View.

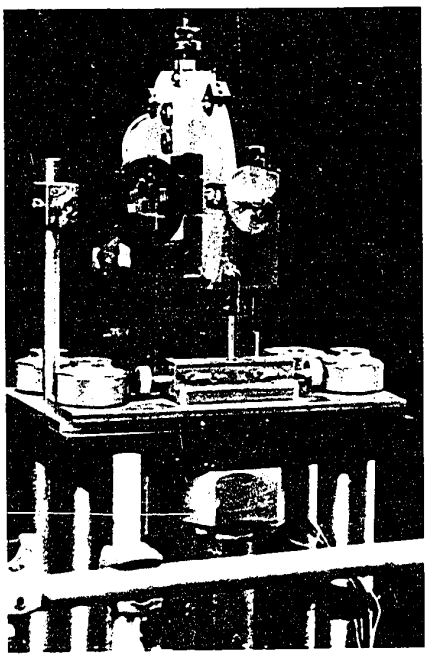

(b) Front View.

PLATE III

Photographs of 'Chalmer's Beam' with Attachments, in Position on the Mounting Frame.

on the beam itself. The absence of a restoring torque is possible only when the C.G. of the beam and its attachments lie at the balance point of the beam. To adjust the C.G. of the beam to this point a set of course and fine adjustments are provided. To balance the beam the loading pan and loading tapes are first removed. The two course adjustments which lie below the level of the knife edge at the front and back of the beam were adjusted so that the C.G. lies vertically slightly below the knife edge and horizontally approximately at the knife edge. The fine horizontal adjustment was next set so that the beam was balanced horizontally. The beam should now oscillate freely. The vertical position of the centre of gravity was then adjusted upwards by raising the vertical fine adjustment until the beam just ceased to oscillate freely. It was necessary then to further adjust the fine horizontal balance weight in order to obtain perfect horizontal balance. With careful manipulation of the two fine adjustments a point will be reached where the beam will be practically free of restoring torques and will sit almost undisturbed at any angular position. The beam is now said to be balanced or 'dead'. A rough check on the behaviour of the polycrystal beam after balancing showed it to be sensitive to loads of less than 10 mg and to exhibit a restoring torque of approximately 200 mg.* Since the smallest incremental loads used will probably be of the order of 5 gm this means a maximum error of 4% due to the restoring torque on the

* The adjustment of the C.G. of the beam was extremely delicate and this value represents the minimum restoring torque which could be obtained.

beam and a negligible effect due to bearing friction.

The steel tapes connected from the beam to the specimen pull-rod and the loading pan were cut 0.15" wide from 0.001" thick steel shim stock. These were attached to the beam by the two tape clamps at the top of the front and rear beam contours. The tape clamps consisted of a flat plate approximately 1/4" long x 1/8" x 1/16" and two #4:40 set screws in a U-clamp. Tightening up the set screws caused the tape to be held rigidly between the plate and the beam contour. No slippage has been observed with this arrangement with loads as high as 2 kg on the tapes. Since the tapes used have an extremely low mass per unit length their effect on the C.G. of the beam is very small and may be neglected.

In order to prevent the beam rotating accidently a beam arresting device which hold the beam steady in the horizontal position was attached to the side of the beam-bearing platform.

2.1.3. The Specimen Yoke

The main function of the specimen yoke is to provide a support for the lower end of the test specimen. Figure 18 illustrates the design of the specimen yoke. The lower section of the yoke is constructed from a length of hard brass rod approximately 6" long and 3/4" in diameter. This rod was drilled-out over most of its length to an I.D. of 1/2" and the front and rear of the tube opened-up over all but a short section at the

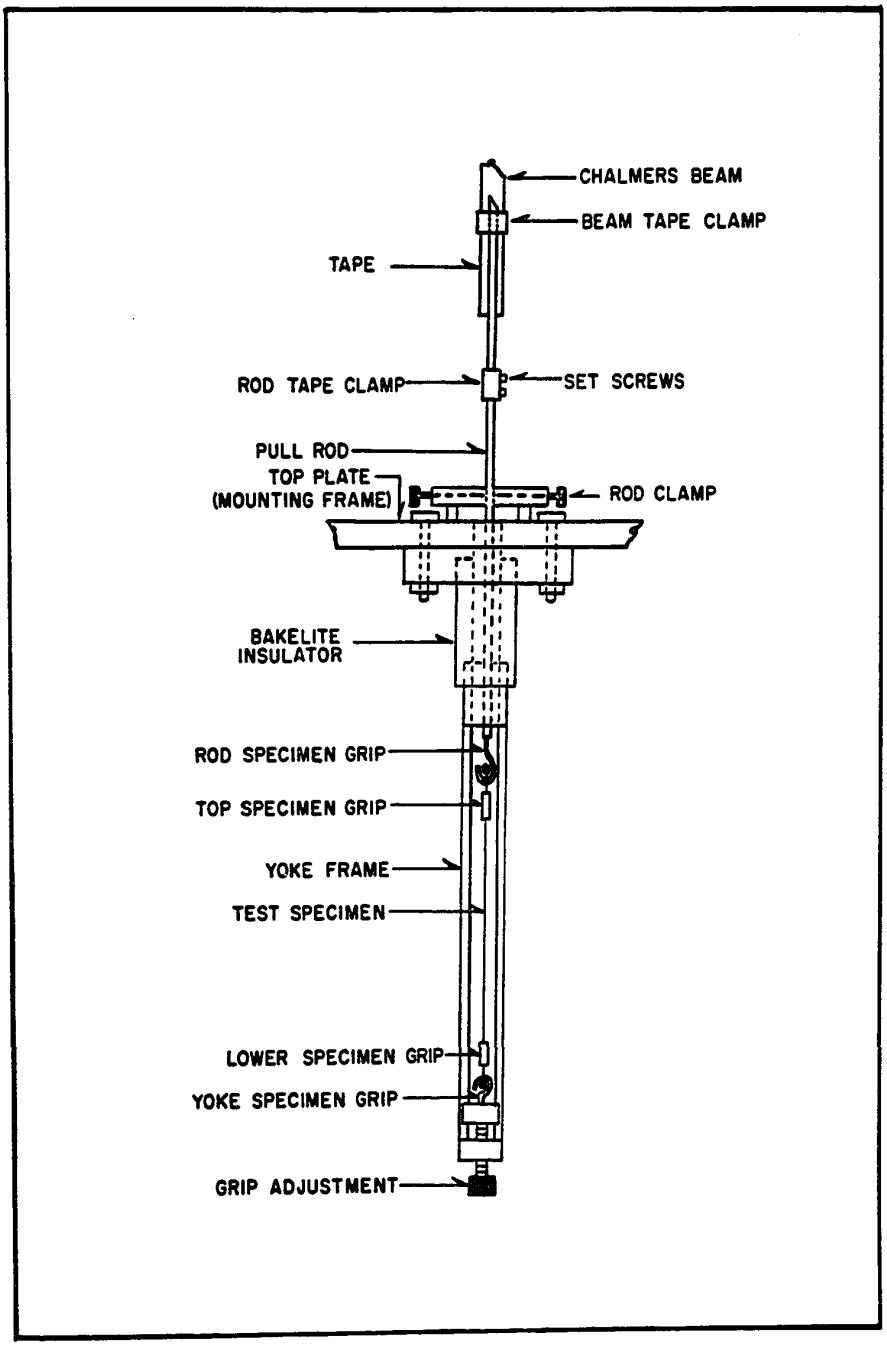

FIGURE 18 - DIAGRAM ILLUSTRATING THE DESIGN OF THE SPECIMEN YOKE AND ITS RELATIONSHIP TO OTHER PARTS OF THE LOADING SYSTEM.

top and the bottom. The bottom end was drilled and tapped to take an adjustable carriage which contains the lower specimen grip. The upper end of the brass tube was press-fitted into a piece of bakelite tube, which itself was press-fitted into a brass flange which bolts to the lower surface of the top plate of the mounting frame. This bakelite insert serves as a thermal insulator between the leading frame and the lower part of the yoke which is subjected to temperatures down to approximately 80°K.

The yoke is also provided with a mounting strip for attaching two thermocouples for the measurement of specimen temperature. Further details on this are given in the section dealing with temperature control and measurement.

In operation a tensile stress is applied to the specimen via the specimen loading tape and specimen pull-rod. The specimen pull-rod is constructed from a length of 1/8" diameter brass rod which projects through the top plate of the mounting frame into the specimen yoke. The upper end of the rod was silver soldered into a larger brass rod which forms a clamp for attachment to the loading tape. The lower end of the rod was silver soldered into the upper specimen grip. To prevent damage to the specimen during the adjustment of the beam system and when inserting a new test specimen a specimen rod clamp was located above the yoke on upper surface of the top plate of the mounting frame. Figure 18 illustrates

the relationship of the test specimen to the yoke, specimen pull-rod, and loading tape.

2.1.4. The Load Application System

As described previously the test specimen is loaded using a Chalmer's beam system. Weights applied to a loading pan suspended from one side of the beam result in the application of a tensile load to the specimen which is held between a fixed lower grip and an upper grip attached through the specimen pull-rod to the other side of the Chalmer's beam. There are two types of loading employed during a test, namely: a primary loading where relatively large loads are applied manually, and a secondary loading where relatively small loads are applied automatically at a fixed rate. Primary loading is employed in order to determine the approximate load required to give an observable strain rate under a particular set of temperature and strain conditions, and also in order to provide large extensions of the test specimen when required. Secondary loading is employed where incremental and decremental loading studies are being made. Considerable experimental study was required to develop the fine loading system and to determine its optimum operating conditions. A brief outline of these studies will be given in section 2.5 of this chapter. Figure 19 illustrates the details of the load application system finally developed and its method of attachment to the Chalmer's beam. Plate IV shows a photograph of the

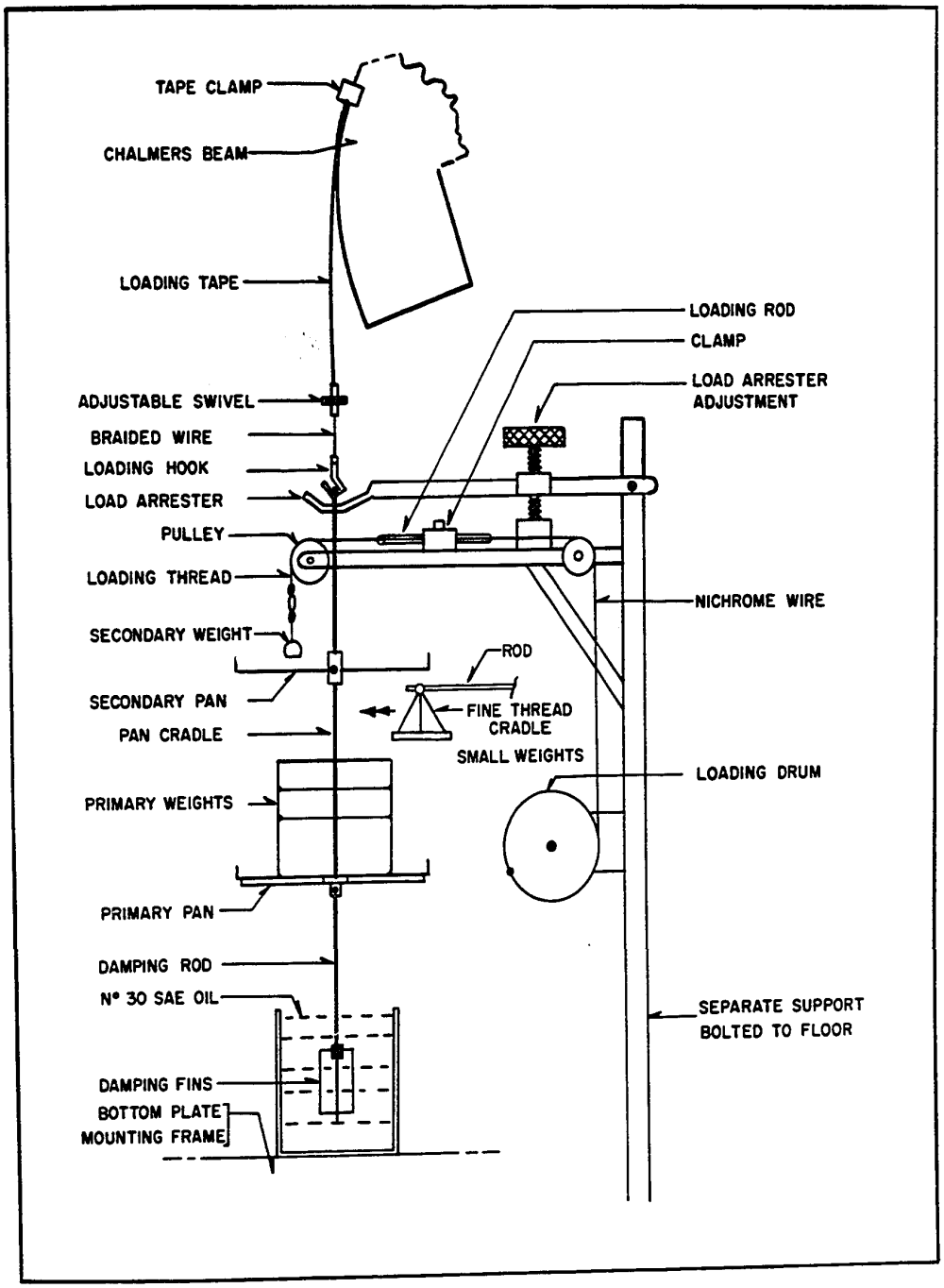

FIGURE 19 - DESIGN OF THE LOAD APPLICATION SYSTEM

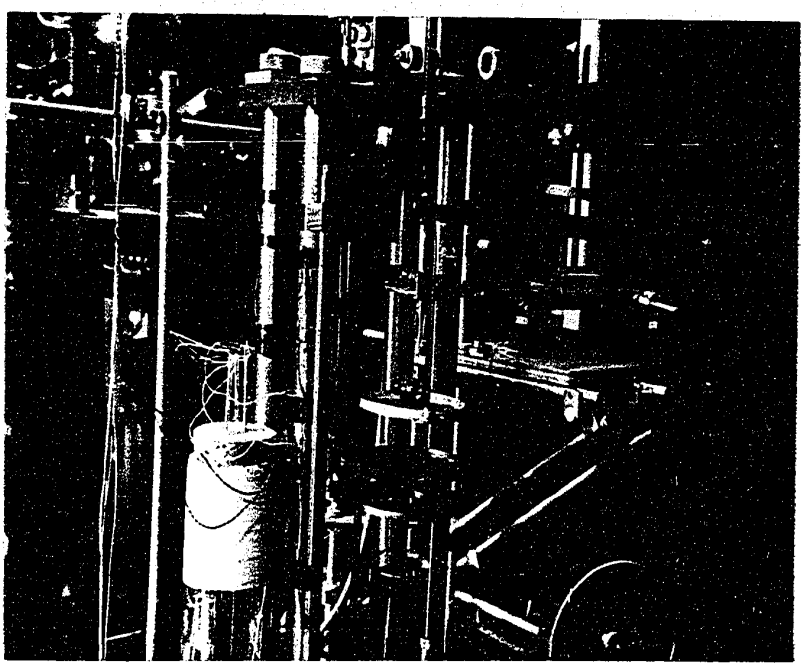

PL .TE I/

Photograph Showin ; Details of the Load Application System.

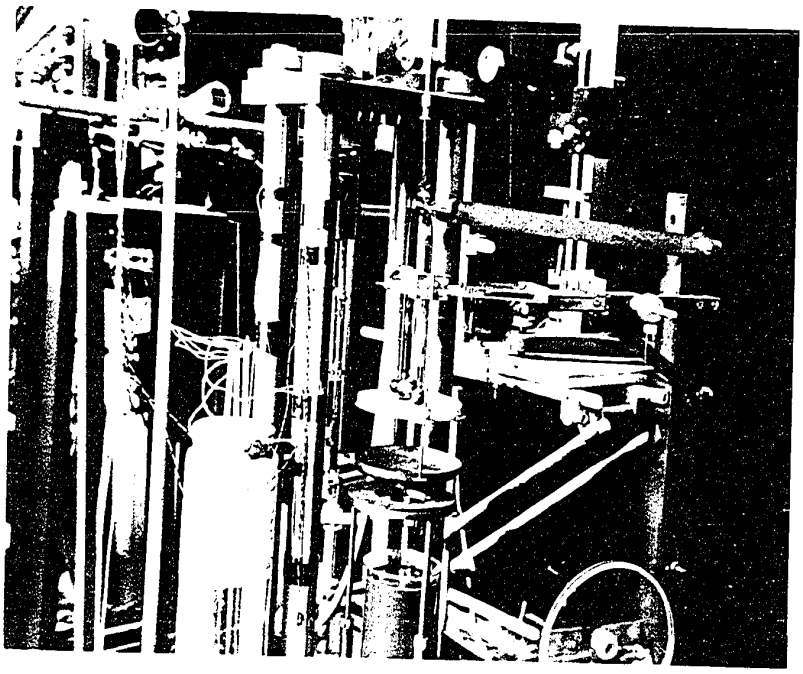

completed system.

The primary and secondary loads are applied to separate loading pans attached to the pan cradle which transfers this load through a coupling arrangement consisting of a loading hook, a length of flexible braided wire and an adjustable swivel to the loading tape tied to the rear contour of the Chalmer's beam. This coupling arrangement allows the loading cradle to be self-aligning, and makes it possible to adjust the pan cradle so that the secondary loading system, which is suspended between the two arms of the cradle, is free of the cradle at all times.

Directly below the bottom loading pan (primary) is attached the damping rod which carries a set of fins on its lower end. These fins are fully immersed in a bath of #30 SAE oil. This arrangement forms the pan damper which assists in preventing oscillations developing in the loading system due to its large damping coefficient in the horizontal plane. The damping system also has a small vertical damping coefficient which prevents impact stressed being produced in the specimen when the secondary loads are applied rapidly.

So that all or part of the applied load may be removed from the loading tape during changes in temperature, adjustment of the test specimen etc. a load arrester arrangement was provided. This is in the form of an adjustable lever arm with an attached forked lift at one end. When

the lever is raised by the attached adjusting screw, the forked end lifts the upper end of the loading pan cradle off the loading hook and thus removes the load from the beam system.

The primary weights, which vary from 10 to 500 gms are applied manually. The large weights (100 gms and up) are applied only after first partially arresting the loading pan cradle. The smaller weights are normally applied without arresting the cradle by slowly lowering the weights by a thread cradle attached to each weight. This method appears to prevent any impact effects due to jaring of the pan or accidental contact with the operators fingers.

The secondary weights, which vary from approximately 1 to 16 gms. are employed when rapid loading or unloading at a controlled rate is required during incremental and decremental loading experiments. The secondary weights consist of small steel spheres (ball bearings) with a slightly flattened bottom surface to prevent rolling once the weight has come in contact with the loading pan. These weights are lowered mechanically at a fixed rate by a system illustrated in detail in Figure 20. This system was designed so that four separate weights could be raised or lowered independently. The operation of the system is best described by reference to Figure 20. When the motor turns counterclockwise the winding drum unwinds the attached loading wire, which is attached by a clip

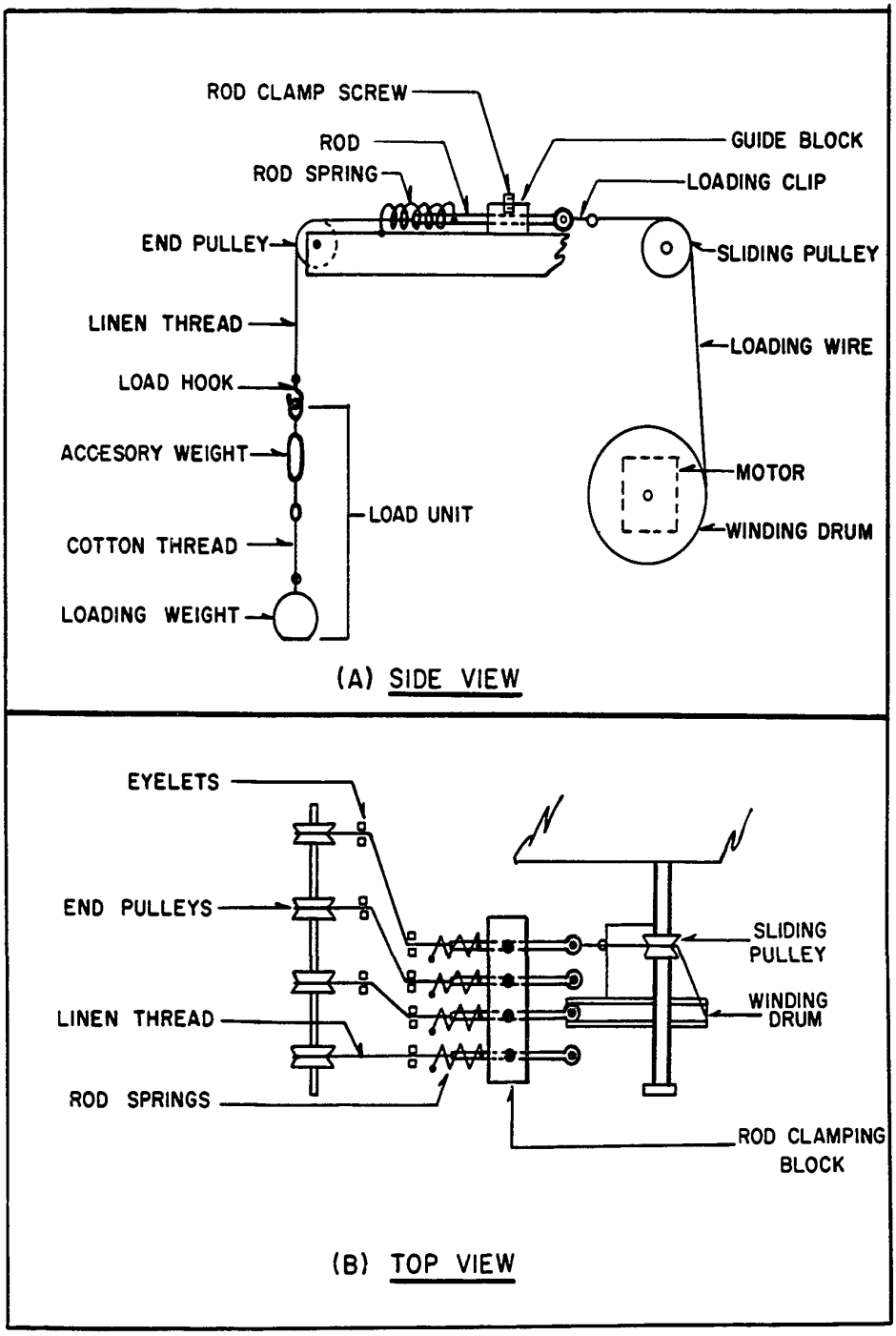

FIGURE 20 - DETAILED DESIGN OF SECONDARY LOADING SYSTEM

to the guide rod, and provided the rod clamp screw is released, this will allow the spring to pull the rod forward at a rate determined by the rate of unwinding of the drum. A fine linen thread tied to the front end of the rod passes through a series of metal eyelets and over the front pulley, and the weight attached to a hook at the lower end of this thread is lowered. To remove the weights the motor direction is reversed, and when the load has been lifted off the pan, the rod clamp screw is tightened to hold the rod fixed in this position. The four separate weights may be lowered in sequence by attaching the lowering clip to each rod in turn and lowering the weight as required.

The load units themselves consist of two parts, the loading weight which is formed from a small steel ball bearing and an accessory weight to which the loading weight is attached by a short length of very fine cotton thread. The purpose of this accessory weight, which itself is not allowed to come in contact with the loading pan, is to insure that all tension is removed from the cotton thread supporting the loading weight when this weight comes in contact with the loading pan. As a result, the value of the applied load was very accurately reproducable within approximately $\pm$ 30 mg. The loading units were made easily removable and a number were made up with loading weights of approximately 3.7, 8.6, and 16.7 gm.

A number of experiments were conducted with this loading system

to determine the optimum rate for applying or removing the loads (described in detail later in the thesis). It was finally decided to use a drop rate of approximately 6.3 mm/sec which insured that the loads were fully applied within 0.3 sec and fully removed within 0.4 sec. No impact loading was observed, and the maximum time for stabilization* of the loading system was 1.4 sec.

2.2. The Strain Measurement System

A number of types of extensometers (devices for measuring extension) have been developed for the measurement of small strains. Amongst these are systems incorporating electrical devices, whose outputs may be easily recorded (such as linear differential transformers, resistance strain gauges, and capacitance type gauges), as well as numerous optical systems.

In this particular application the electrical extensometers were all rejected since they tend to induce undesirable loading of the specimen. A number of optical methods have been used in the past but these either employed manual observation, which would not be fast enough for transient creep studies, or photographic recording, which was not considered convenient. The system finally developed incorporated an optical extensometer,

* Slight elastic oscillations were found to be produced by the rapid application of the secondary loads, these oscillations were normally damped out very rapidly.

the output of which was measured and recorded electronically. In this way the extensometer itself caused no loading of the test specimen.

The system for measuring and recording the output of the optical extensometer is normally referred to as a 'photoelectric followup servo system'. Considerable detail of a theoretical and practical nature is available on the general design and operation of such systems (see Porter (1950), and Thaler and Brown (1953)), unfortunately advantage was not taken of this literature until late in the project and as a result the development of the servo system was more or less empirical. A recent paper by Bowman and Macurdy (1959) describes an excellent (although more involved) system which they have used for recording the motion of the beams of high-precision balances. Their system is generally the same as the one described in this thesis but contains extra circuits to allow the observation of a very rapidly moving light beam. Unfortunately this paper was not published at the time when the creep apparatus was being developed.

The system was designed to fulfill the following requirements; (a) to be isolated from any physical contact with the test specimen itself; (b) to be extremely sensitive and highly stable over the test period and; (c) to be capable of responding to very rapid changes in strain rate. The apparatus to be described has been found to fulfill these requirements extremely well.

The strain measurement system is as follows: a shaped light spot is reflected from the surface of a mirror which is attached to the Chalmer's beam at the beam balance, point in such a way that the reflecting surface lies in a plane which passes through the balance point. The position of the reflected spot is detected by a split photoconductive cell, remote from the beam, which positions itself by an associated servo system, so that the reflected spot always falls evenly on both halves of the cell. This is called the balance position. The motion of the photoconductive cell (photocell) required to keep the photocell in the balance position is plotted on an attached recorder as a function of time. Since the degree of rotation of the Chalmer's beam is directly proportional to the elongation of the specimen it was possible to calibrate the recorder directly in terms of specimen strain. The apparatus was constructed so that on high sensitivity an inch on the recorder chart paper corresponded to a strain of 10^{-4} or 0.01% on a specimen with a 10 cm. gauge length. Figure 21 shows an outline of the strain measurement system. Plate V shows a rear view of the strain measuring system. On top of the mounting frame at the right hand side of the photograph can be seen the Chalmer's beam. The extensometer mirror is located on the far side of the beam. In the top left hand corner is the recorder and the vertical screw system which carries the photoconductive cell. In the lower left hand corner can be seen the electronics associated with the servo posit-

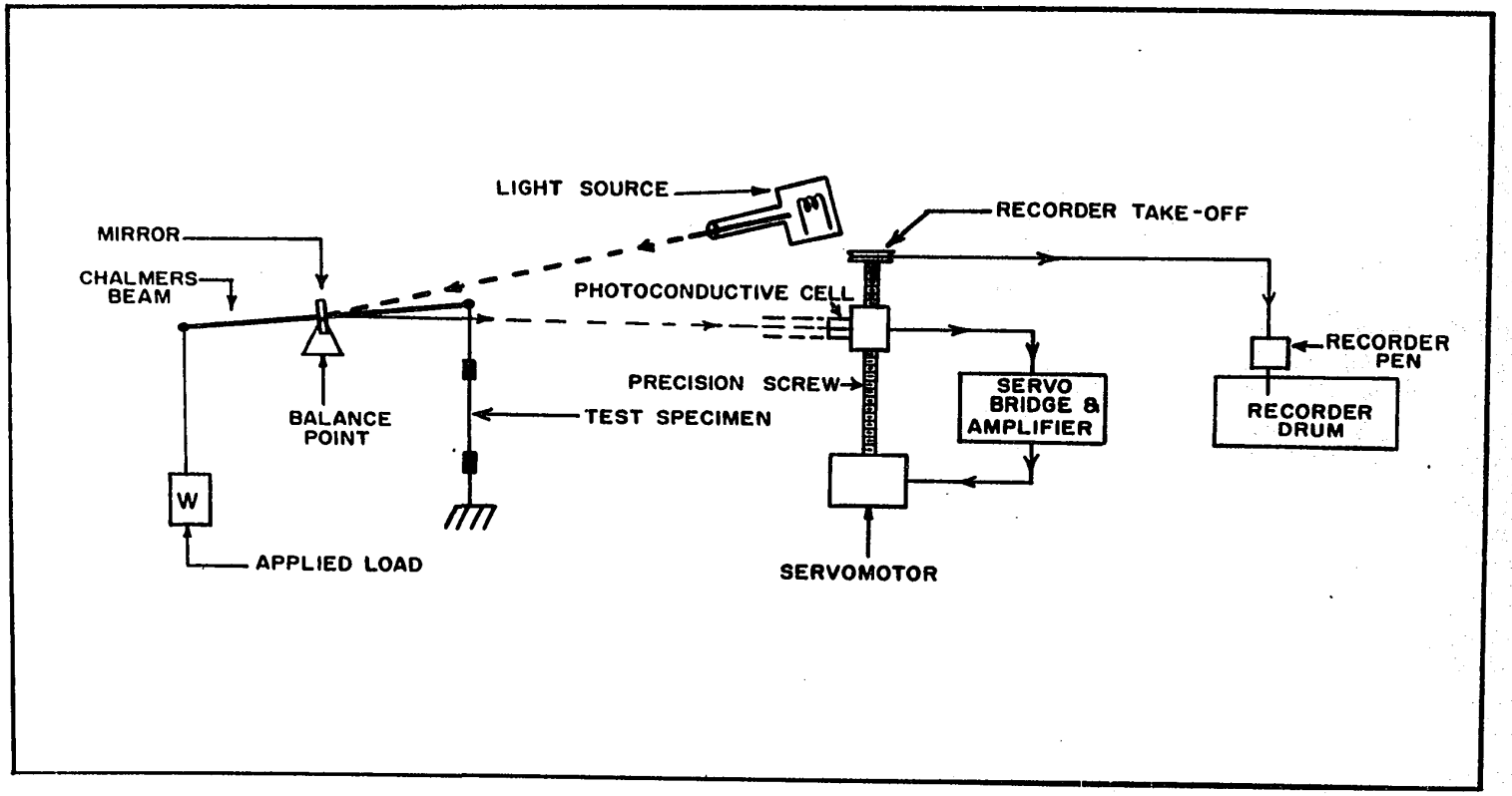

FIGURE 21 - OUTLINE OF THE STRAIN MEASUREMENT SYSTEM

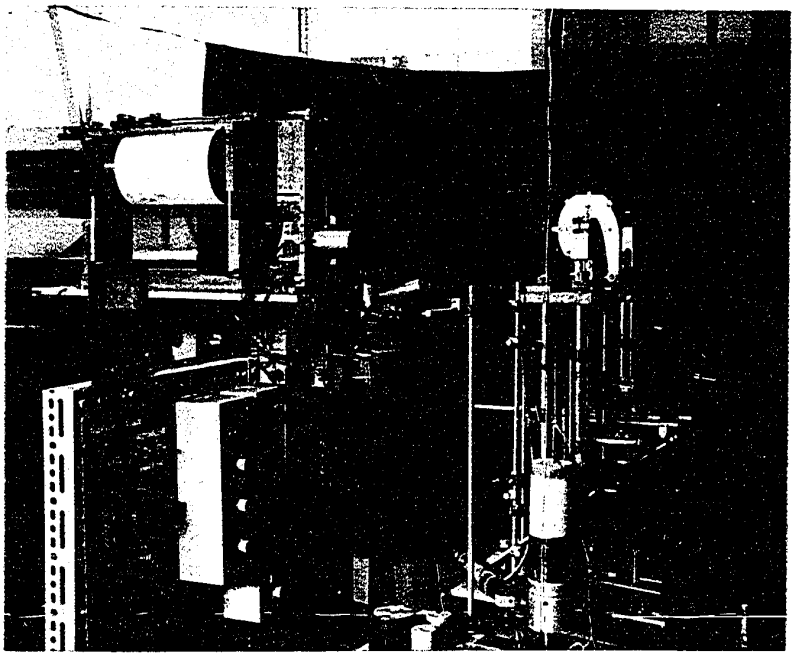

PLATE V

Photograph Showing a Rear Side View of the Strain Measuring System.

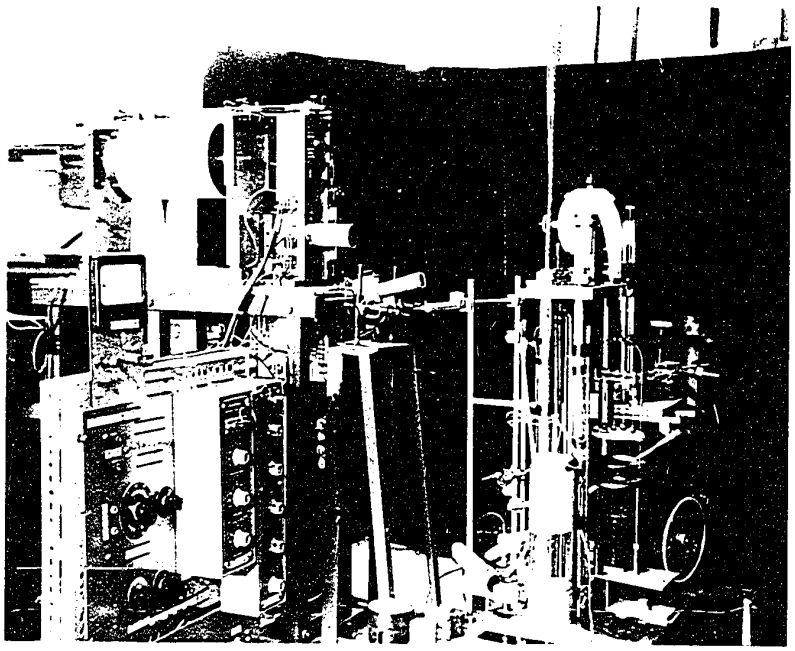

ioning system.

2.2.1. **The Optical Section**

The optical section consists of three parts as illustrated in Figure 22. These are the optical transducer, the light source and spot shaper,, and the position detector.

The optical transducer is merely a small front surface mirror attached to the Chalmer's beam at its pivot point. Since the front contour of the beam is a radius about the pivot point then the degree of rotation of the beam and hence the rotation of the mirror is directly proportional to the specimen elongation. The insert in Figure 22 shows the geometric arrangement. A light beam originating at P is normally reflected along OS_1. When the beam rotates through an angle of β radians, due to the specimen elongation, then the light beam will be reflected along OS_2, where the angle S_1OS_2 is α radians. From the geometry of the system it may be shown that $\alpha = 2\beta$.

Now $$\beta = \frac{\Delta l}{R_1}, \qquad (13)$$

where β is the angle of rotation of the beam (and mirror) in radians, Δl is the specimen elongation, and R_1 is the radius of the front beam contour.

Also $$\Delta S = \alpha d = 2d\beta, \qquad (14)$$

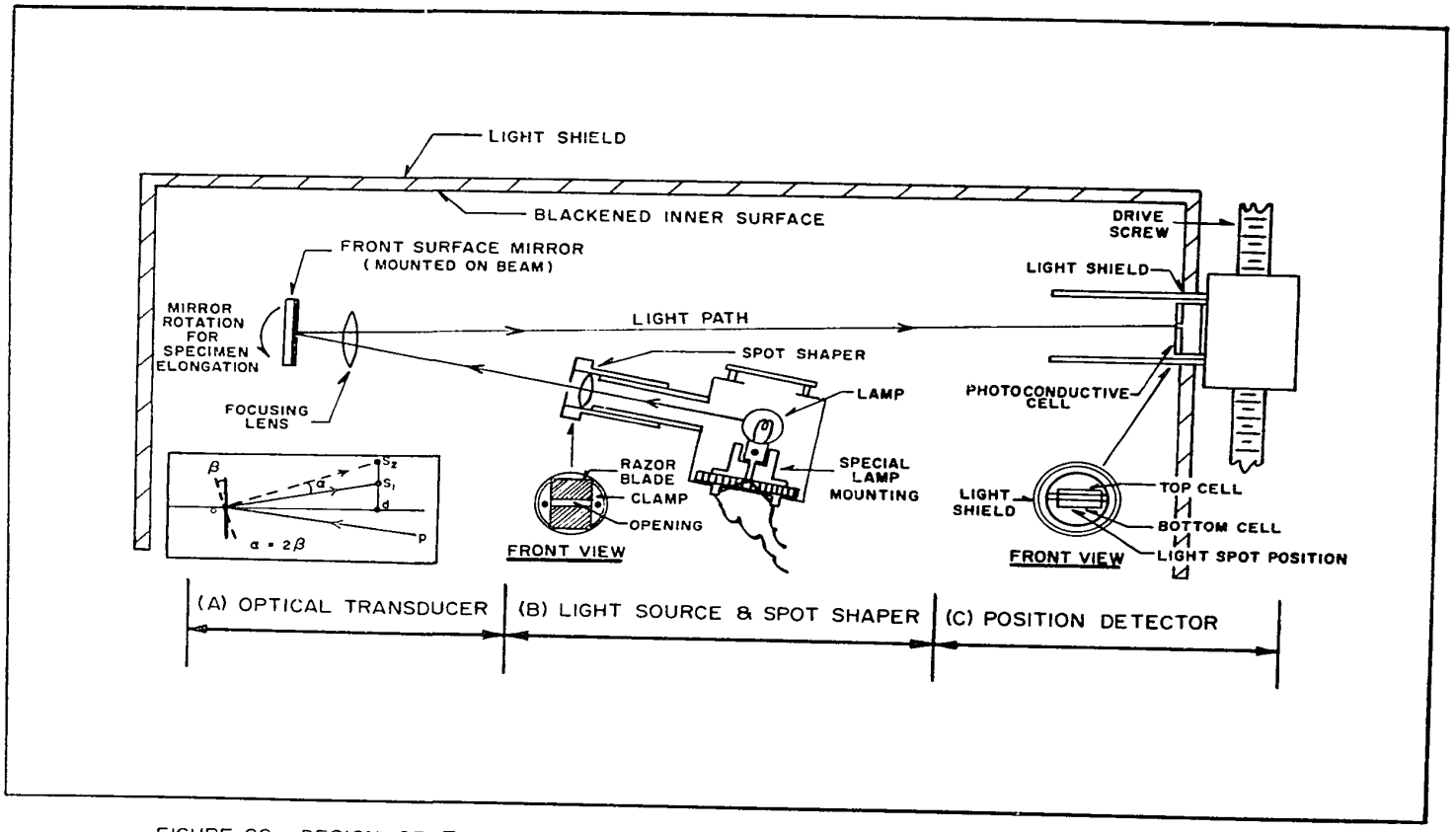

FIGURE 22 - DESIGN OF THE OPTIC SECTION OF THE STRAIN MEASUREMENT SYSTEM.

where ΔS is the scale deflection $(S_2 - S_1)$ at a distance d from the mirror (distance from mirror to photocell). Now the sensitivity of the transducer k_t is defined as,

$$k_t = \frac{\Delta S}{\Delta \ell} \quad , \tag{15}$$

and substituting equations (13) and (14) into (15) gives:

$$k_t = \frac{2d}{R_1} \tag{16}$$

In this apparatus $R_1 = 2.5$ inches and $d = 27.9$ inches, this gives a calculated value for k_t of 22.2. A series of tests were carried out on the transducer and it was found to be extremely linear, and to have a sensitivity factor of 22.1.

The light source and spot shaper was constructed from a Tinsley type 4745 galvanometer projector. The normal body and lens arrangement of the projector was retained but a special lamp mounting arrangement was added so that a higher wattage bulb could be used, and as well, a spot shaper was added to the front of the projector. The special lamp mounting allowed connections to be permanently soldered to the bulb to eliminate the problem of the bulb instability due to poor base connections, which are often found when using high powered bulbs with a spring type socket. A Westinghous #1134 bulb, rated at 6-8 volts, was used and this

was operated from a six volt storage battery. The battery source prevented any modulation of the light which might develop from using an AC lamp supply.

The spot shaper consisted of a brass cap which was fitted over the projector lens tube. The end of this cap contained an adjustable slit-opening formed from a set of razor blade edges. This arrangement produced a well defined rectangular light spot which was sharply focused on the surface of the photocell by a lens placed approximately one inch in front of the transducer mirror. It was found that a slit opening of 1/16" x 3/4", which resulted in a spot 1/8" wide extending fully across the surface of the photocell, gave the optimum sensitivity and stability.

The position of the reflected light spot was detected by a split photocell mounted at the end of a horizontal light shield tube. This photocell forms part of a servo balancing system which adjusts the vertical position of the photocell so that both halves of the cell receive the same degree of illumination.

The complete optic section was enclosed on all sides and on top by a light shield to reduce the effect of room illumination, this shield consisted of a tentest box whose interior was painted dead black.

2.2.2. The Servo Balancing and Recording Section

Figure 23 show a block diagram of the servo balancing and recording

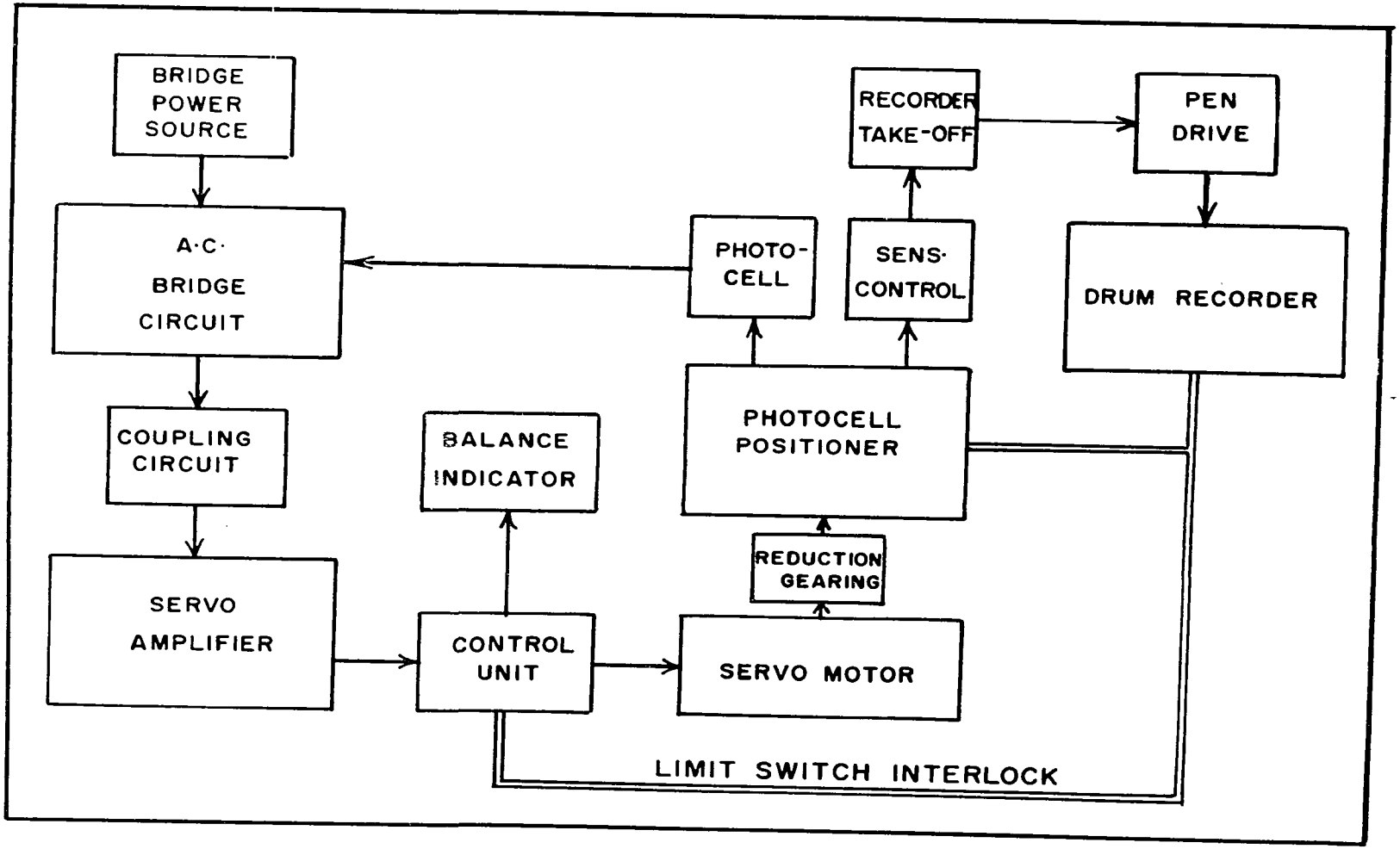

FIGURE 23 - BLOCK DIAGRAM OF SERVO-BALANCING AND RECORDING SECTION OF THE STRAIN MEASUREMENT SYSTEM.

section. The split photoconductive cell consists of two resistances which are extremely light sensitive and these form two arms of an AC Wheatstone bridge. The other two arms are located in the bridge unit itself. When light from the optical transducer falls equally on both halves of the photocell the bridge is balanced. If (due to specimen elongation) the light beam shifts, then the light will fall unequally on the two halves of the photocell causing an unbalance in the bridge circuit. The unbalance voltage produced at the output of the bridge is amplified by a servo amplifier and the output of the amplifier energizes the servo motor, and drives the photocell positioner. This repositions the photocell to a new position then the bridge is again balanced. During the measurement of creep this balancing process takes place continuously. The photocell positioner is also mechanically coupl d to the pen drive on the drum recorder through a quick change gear box which functions as a sensitivity control for the recorder.

The electronic circuit of the balancing and recording section is shown in Figure 24. It consists of the photoconductive cell, the AC bridge circuit, the coupling unit, the servo amplifier, the control unit, and the servo motor.

The photoconductive cell used in the apparatus was a type CS-9, semiconductor photoconductive cell manufactured by Canadian Semiconductors Reg'd, Montreal. The two light sensitive sections of the cell are

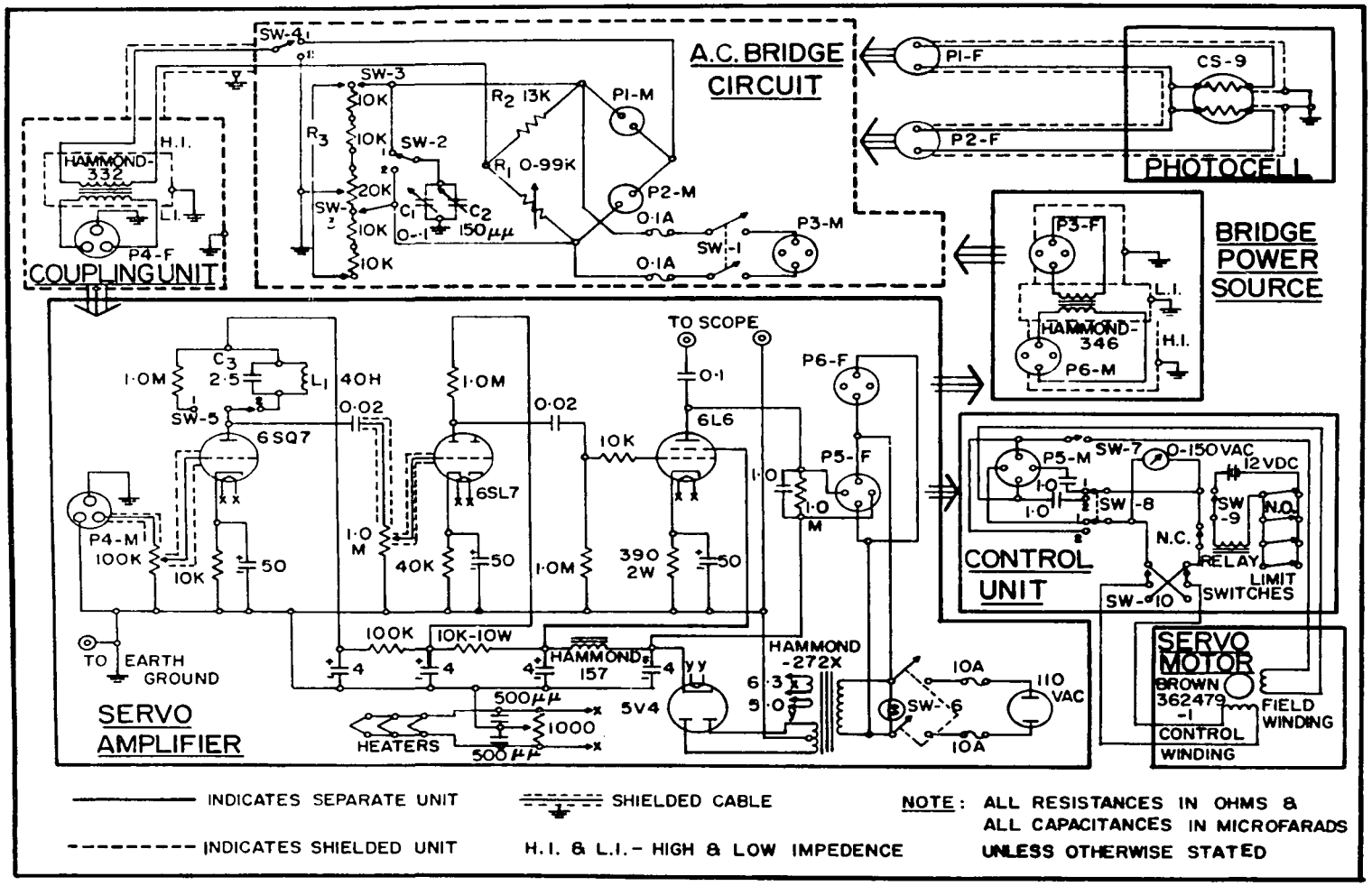

FIGURE 24 - ELECTRONIC CIRCUITS OF THE BALANCING AND RECORDING SECTION OF THE STRAIN MEASUREMENT SYSTEM.

in the form of a grid network separated by the photosensitive material. These grids are moulded in clear plastic on the end surface of an octal tube base and the electrical connections are made to the cell grids via the socket pins. Plate VI shows a photograph of one of these cells.

According to the manufacturer these cells may operate at voltages up to 120 AC or DC. They have a dark resistance of up to 2000 megohms and a resistence of as low as 2000 ohms when illuminated with 50 foot candles. Each section of the particular cell used in the apparatus was found to have a dark resistance of approximately five megohms, when in position under the light shield with normal room light outside the shield, and a resistance of approximately 50,000 ohms under full illumination with a rectangular shaped light spot of the optimum size.

Considerable investigation (which will not be presented in this thesis) was conducted to determine the optimum operating voltage, light spot shape and dimensions, and light intensity for the best sensitivity and stability. In the final form of the apparatus each section of the cell was operated at approximately 40 volts AC. It was found that a rectangular spot approximately 1/8" x 1-1/4" (with the length of the spot parallel to the grids of the photocell) gave the best results. In general it was found that the more intense the light the greater the sensitivity. The upper limit being determined by the noise level of the cell which was found to increase

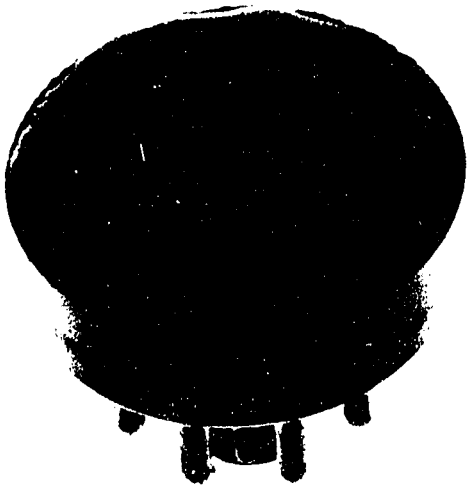

PLATE VI

Photograph of the Type CS-9 Semi-conductor, Photoconductive Cell Used in the Strain Measurement System.

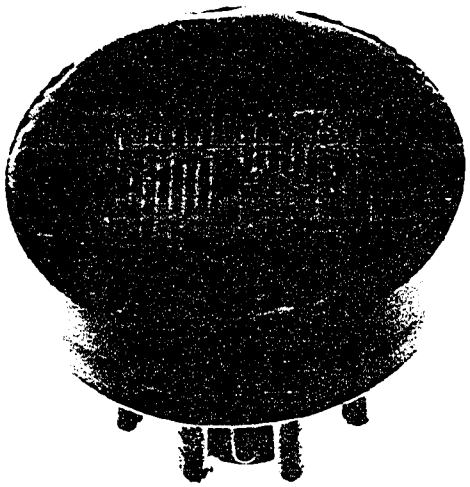

PLATE II

Photograph of the Type Cs-9 Semi-conductor, Photoconductive Cell Used in the Strain Measurement System.

with increasing illumination.

An AC Wheatstone bridge (see Laws (1938) and Owen (1950)) was constructed with the split photoconductive cell forming two external arms (see Figure 24). The two internal bridge arms consisted of a fixed arm (R_2), and a balancing arm (R_1) in the form of a decade resistance box. The balancing arm was adjusted to obtain the initial condition of the bridge. A simple Wagner-Earthing system (see Owen (1950) and Wolff (1959)) consisting of C_1, C_2 and R_3 was also included in the bridge circuit in an effort to eliminate the stray capacitances. The switch SW-4 makes it possible to observe the degree of either the general bridge balance (position 1) or the Wagner-earthing system balance (position 2). In operation the bridge is first roughly balanced using R_1 (SW-4 in position 1), then the Wagner-earth is balanced (SW-4 in position 2), by adjusting R_3, and C_1 and C_2. Switch SW-3 is provided so that the variable capacitor (C_1 and C_2) may be applied to either side of the bridge as required. Finally the bridge balance is readjusted and the Wagner-earth balance is checked and adjusted if necessary.

Power is supplied to the bridge circuit from the 110 volt AC lines through a good quality, shielded, step-down transformer which was mounted some distance (approximately four feet) from the high-gain circuits to prevent stray pick-up. It was found that an applied bridge voltage of approxi-

mately 80 volts gave excellent results.

The bridge unbalance voltage was coupled to the servo amplifier by a coupling unit consisting of a highly shielded transformer. This transformer assists in matching the low impedence output of the bridge into the amplifier. The bridge and coupling unit were located on one large rack panel, but were separately shielded from each other and from outside fields by enclosures constructed of #16 gauge sheet steel.

The unbalance signal obtained from the bridge was amplified by a three stage amplifier, consisting of a tuned voltage amplifier driving an untuned voltage amplifier which in turn drives an untuned power amplifier. The 60 c/s output of the servo amplifier drives the control winding of an AC servo motor. The field winding of the motor is driven directly from the 115 V, 60 c/s mains.

The servo amplifier used (see Figure 24) was a modification of the standard Leeds and Northrup balancing amplifier with the input filter and chopper circuits omitted. In particular the following modifications were made; (a) the first stage was converted to a tuned amplifier with its resonant frequency at 60 c/s, in order to reject 60 c/s harmonics, (b) the overall amplification of the circuit was reduced by eliminating the third voltage amplifier stage (second half of 6SL7 tube), (c) the power supply ripple voltage, as observed on the plate of the 6L6, was greatly

reduced by replacing the first filter resistor by a filter choke, (d) a hum balancing system was added to the 6.3 volt heater circuit in order to balance the heaters with respect to ground, (e) particular care was taken in the mounting of transformers and signal leads in the high grain circuits to prevent 60 c/s pick up, and (f) particular care was taken to ensure that a good ground was obtained and that no ground loops existed.

These modifications mentioned all assisted in raising the overall signal-to-noise ratio of the measurement system. One of the most important modifications was the addition of the tuned amplifier input stage. Initial experiments had shown that the photoconductive cells used in the apparatus tended to increase the harmonic content of the bridge unbalance voltage, preventing a perfect balance. Large percentages of 120 and 180 c/s were observed at the servo motor and this appeared to make the motor sluggish and erratic.

A parallel tuned circuit consisting of C_3 and L_1, with a resonant frequency of approximately 60 c/s was placed in the plate circuit of the amplifier input tube (6SQ7). With all modifications completed the amplifier was checked and found to have a maximum gain of approximately 54 db at 60 c/s with a harmonic suppression of 10/1 at 120 c/s.

An oscilloscope output was provided at the plate of the output tube (6L6) so that the output signal of the amplifier could be carefully

observed when initially balancing the bridge circuits.

A control unit, located at the recorder, was connected between the output of the servo amplifier and the servo motor (see Figure 24). This unit serves a number of purposes, namely: (a) switch SW-7 provides an on-off control for the servo motor, (b) switch SW-8 connects the servo motor as either a servo motor (for normal balancing operation) or as a normal motor (for positioning of the photocell carriage), (c) switch SW-10 is a reversing switch to control the direction of rotation of the motor, (d) switch SW-9 and four microswitch type limit switches (located at the top and bottom of the photocell drive screw, and at either end of the pen drive track respectively) in series with a relay and a 12 volt battery form a circuit which automatically shuts-off the power to the servo motor field coil, preventing damage to the precision mechanical parts, in case of an overload. Also connected to the control unit is a 0-150 volt AC meter which indicates the output level of the servo amplifier and serves as a balance indicator.

The servo motor used was a Brown-Honeywell type 362479-1 with the following operating characteristics: torque (at maximum power output) - 20 inch-ounces, stall torque - 28-inch ounces, speed (at maximum power output) 97 rpm. This motor was further geared down by a ratio of 5/1 with an antibacklash reduction gearing unit located between

the servo motor and the photocell positioner. This provided more available torque and as a result a faster and more positive balancing action.

The servo motor, through the set of reduction gears, drives a screw which positions the photocell carriage. The mechanical arrangement for this is illustrated in Figure 25. Plate VII shows two views of the completed servo balancing and recording system. The photocell carriage consists of a block of magnesium, 2" x 1-3/4" x 1-1/2" with a central vertical brass insert, precision threaded for the 5/8:11 precision-cut drive screw. The front of the carriage is machined to take an octal tube socket, in which the photocell is mounted, and a light-shield tube. Magnesium was used as much as possible for all parts associated with the photocell carriage to reduce to a minimum any loading on the precision screw.

The screw itself was carefully lathe-cut from tool steel and fitted to the threaded insert in the photocell carriage. This was necessary since it is important that any backlash in the mechanical parts of the balancing system be kept to a minimum. All moving mechanical parts from the servo motor to the recorder pen drive were fastened together with shaft pins since set-screws were found to give erratic results.

Three special spring devices were also incorporated to reduce backlash and play in the balancing system. These are (see Figure 25) the

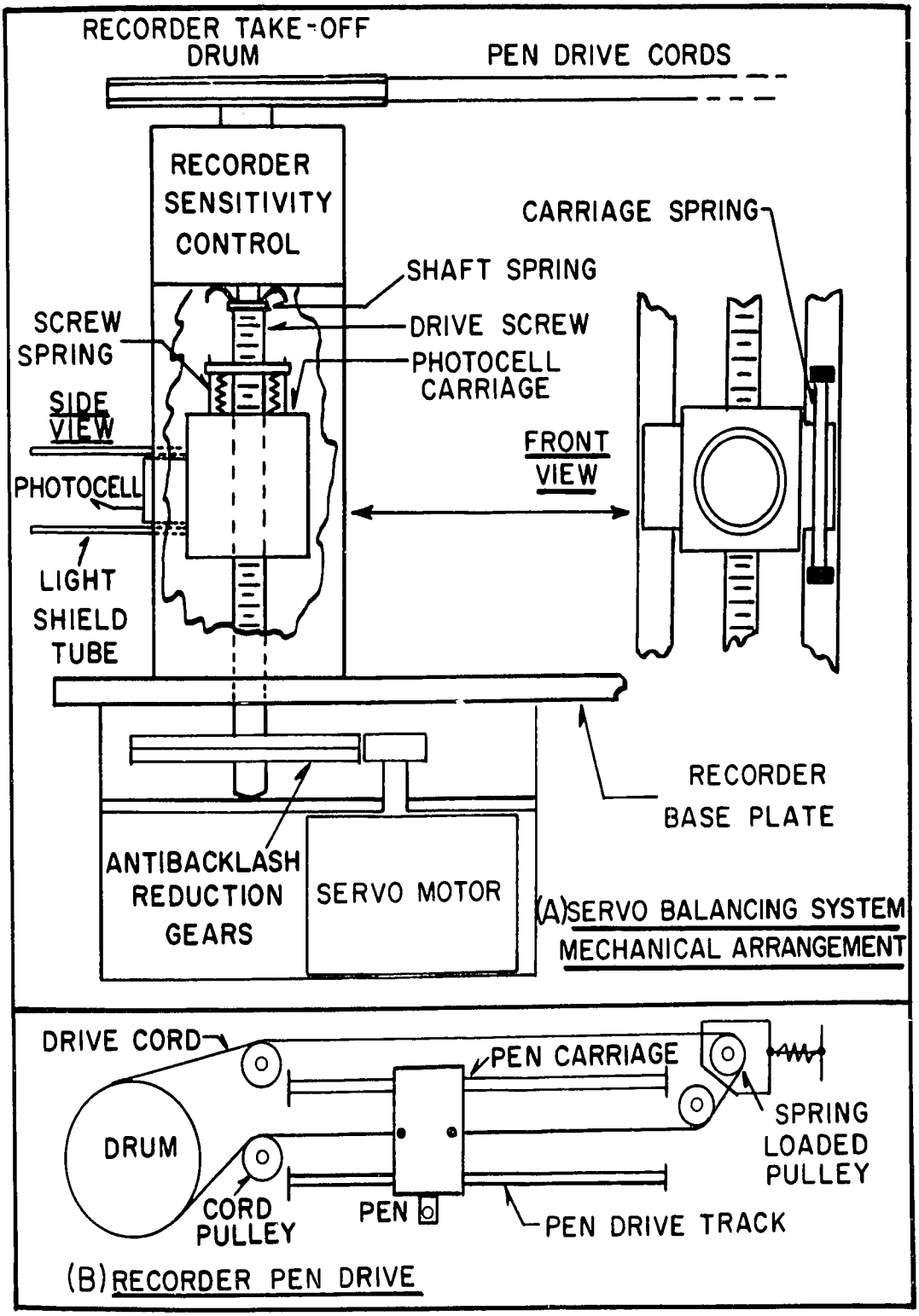

FIGURE 25 - MECHANICAL ARRANGEMENT OF SERVO BALANCING SYSTEM AND RECORDER PEN DRIVE.

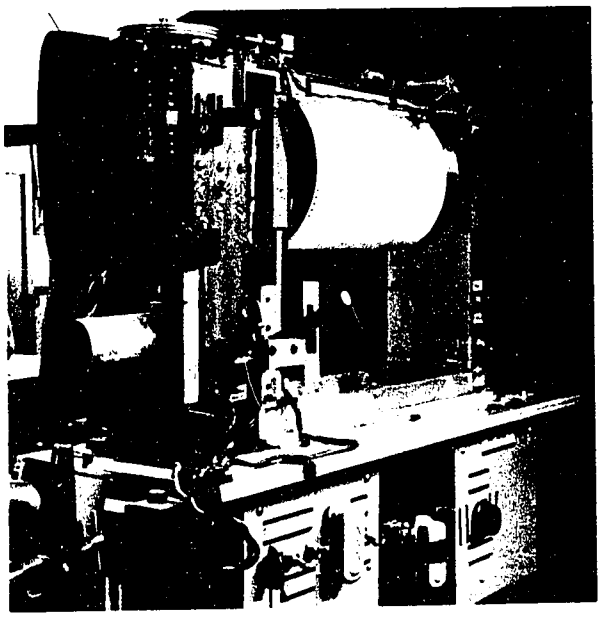

(a) Right Hand Side of Apparatus.

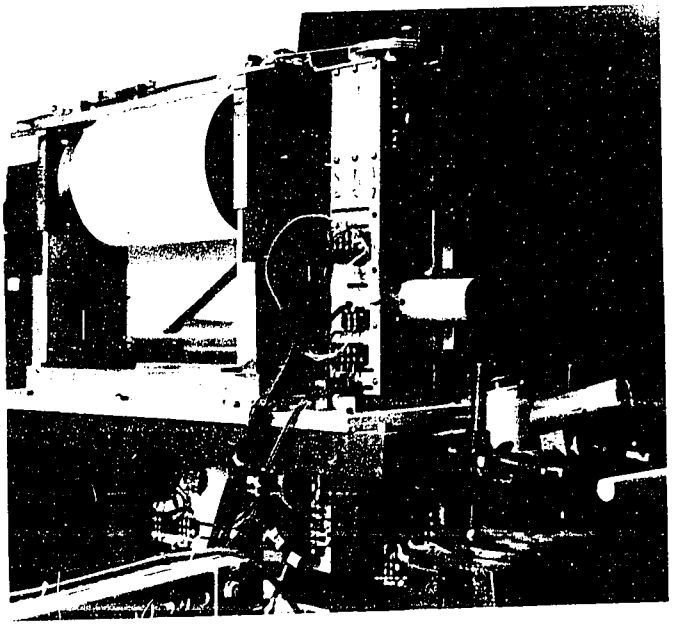

(b) Left Hand Side of Apparatus.

PLATE VII

Photographs of the Servo Balancing and Recording System Showing the Mechanical Arrangement.

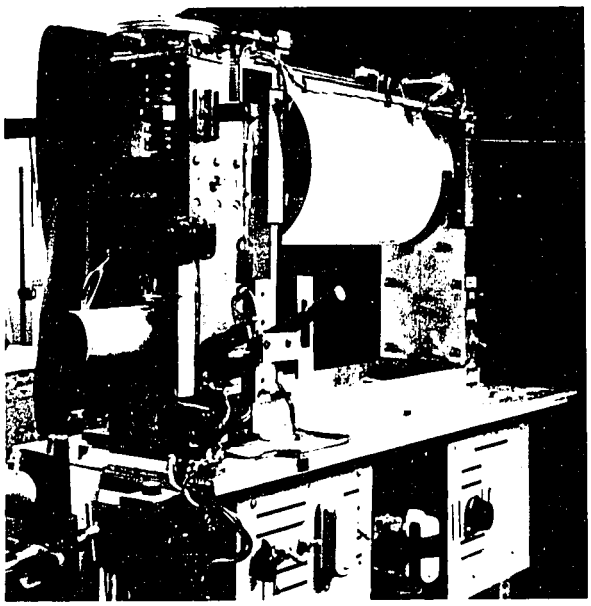

(a) Right Hand Side of Apparatus.

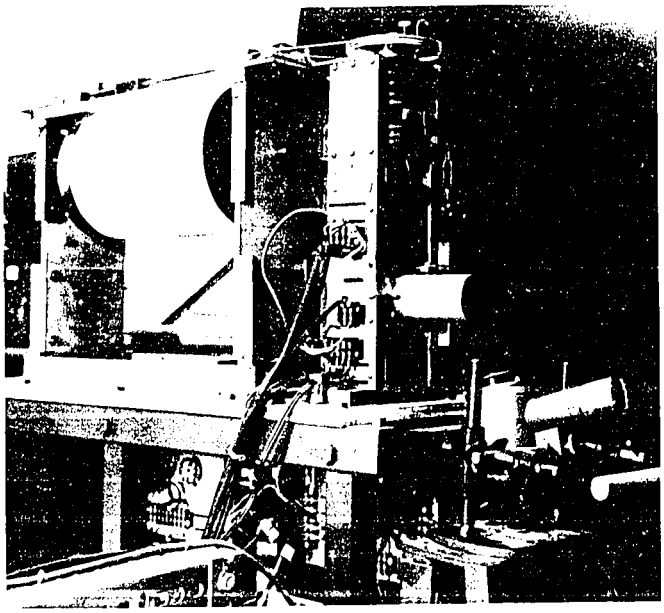

(b) Left Hand Side of Apparatus.

PLATE VII

Photographs of the Servo Balancing and Recording System Showing the Mechanical Arrangement.

shaft spring, the screw spring, and the carriage spring. The shaft spring was in the form of a split spring cup washer which prevented vertical play in the drive screw. The screw spring was designed to keep a compressive stress on the drive screw threads independent of whether the carriage was moving up or down. Finally the carriage spring was designed to prevent the carriage from rotating in the horizontal plane, since this would cause a shift in the balance position if the light spot was not perfectly uniform. The addition of these three devices was found to almost completely eliminate backlash in the system. The maximum backlash was determined experimentally to be equivalent to a strain of 0.5×10^{-5}.

The drive screw, besides positioning the photocell carriage, also operates the recorder pen drive via a sensitivity control in the form of a two-ratio quick-change gear box. The gear box was designed to provide a neutral position for readjusting the pen carriage as well as two sensitivity ratios, 1/1 and 1/10. The design of the gearing and clutch arrangement is illustrated in Figure 26. Plate VII shows the layout of the sensitivity control in the final apparatus. Basically the gear box consists of two gear paths, a direct and a reduction one, which may be selected by a clutch arrangement. Referring to Figure 25 and 26, the photocell drive screw is connected to the input shaft of the sensitivity control, and the

shaft spring, the screw spring, and the carriage spring. The shaft spring was in the form of a split spring cup washer which prevented vertical play in the drive screw. The screw spring was designed to keep a compressive stress on the drive screw threads independent of whether the carriage was moving up or down. Finally the carriage spring was designed to prevent the carriage from rotating in the horizontal plane, since this would cause a shift in the balance position if the light spot was not perfectly uniform. The addition of these three devices was found to almost completely eliminate backlash in the system. The maximum backlash was determined experimentally to be equivalent to a strain of 0.5×10^{-5}.

The drive screw, besides positioning the photocell carriage, also operates the recorder pen drive via a sensitivity control in the form of a two-ratio quick-change gear box. The gear box was designed to provide a neutral position for readjusting the pen carriage as well as two sensitivity ratios, 1/1 and 1/10. The design of the gearing and clutch arrangement is illustrated in Figure 26. Plate VII shows the layout of the sensitivity control in the final apparatus. Basically the gear box consists of two gear paths, a direct and a reduction one, which may be selected by a clutch arrangement. Referring to Figure 25 and 26, the photocell drive screw is connected to the input shaft of the sensitivity control, and the

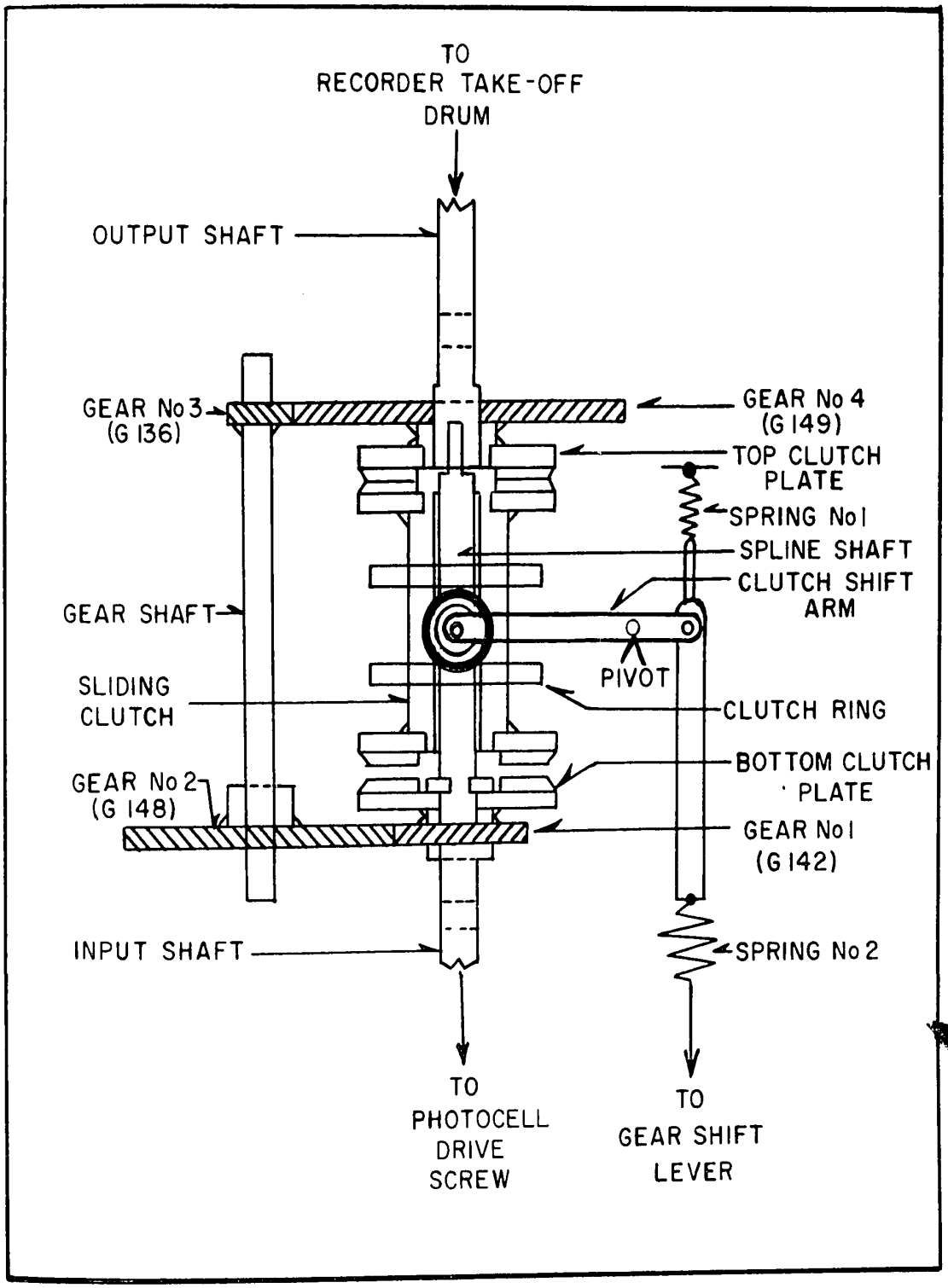

FIGURE 26 - MECHANICAL ARRANGEMENT OF RECORDER SENSITIVITY CONTROL

upper part of this shaft is splined into a double sliding clutch. With the sliding clutch in the upper contact position (as shown in Figure 26) the input shaft motion is transferred directly to the top clutch plate and to the output shaft, which drives the pen drive drum. This is the 1/1 sensitivity position, which results in one inch of the chart paper being equivalent to a strain of 10^{-4}. With the sliding clutch in the lower contact position the input shaft motion is coupled via the bottom clutch plate through the gear train (1, 2, 3, 4) and hence to the output shaft. This gear train introduces a gear reduction of ten. This is the 1/10 sensitivity position, which results in one inch of the chart paper being equivalent to a strain of 10^{-3}. If the sliding clutch is positioned between the upper and lower clutch plates (not touching either) it is in the neutral position which is used for adjusting the pen position or isolating the servo balance system from the recorder. The gears used were standard brass gears manufactured by the Boston Gear Company.

The clutch was switched into its three positions through a mechanical linkage system. The sliding clutch contains a set of two rings between which a forked clutch shift arm rides on two ball bearing races. Coupled to this horizontal shift arm is a vertical linkage which is connected to a shifting lever and positioning plate on the base of the recorder frame. Spring #1 holds the sliding clutch firmly against the bottom clutch plate

when the system is in the 1/10 sensitivity position. When it is in the 1/1 sensitivity position spring #2 is in tension and this holds the sliding clutch firmly against the top clutch plate.

Considerable difficulty was encountered in obtaining the correct clutch plate facing materials. Initially gasket rubber was tried, but although it prevented actual clutch slippage it resulted in a highly elastic coupling. This rubber clutch facing was later replaced with a combination of one face thin gasket cork, and the other #100 emery paper. This combination gave a positive coupling within a rotation equivalent to 0.5×10^{-5} strain on the recorder.

Figure 25B shows the arrangement of the recorder pen drive. The drive cord finally selected was bronze woven radio dial cable. It combines a high degree of flexibility with a minimum of elasticity. The slack was taken out of the pen drive arrangement by a spring-loaded pulley which insured positive pen positioning.

Considerable effort was spent in obtaining a suitable marking device. Pencil lead, ink pens and ball point pens were tried. A high quality ball point pen refill (Paper-Mate, Detergent Type) was finally selected and this has proven very successful. The pen itself was mounted on a short arm which pivots from the pen carriage. This arm was loaded with a dead weight of approximately 30 grams to ensure that the pen gives a heavy

tracing on the graph paper.

The graph paper, in the form of a single sheet (20" x 10-1/2") was attached by masking tape to a large brass drum which was turned at a constant fixed rate by a slow speed synchronous motor. The motor speed is such that 1.8 inches of chart paper is equivalent to one minute. This speed was found in general to be most suitable, although a quick change gear arrangement with three speeds would provide greater flexibility.

2.3. The Temperature Control and Measurement System

The creep apparatus described in this thesis was designed to be capable of operating over the temperature range 80 - 300°K. Two simple methods have been used to obtain temperatures throughout this range, namely; the use of constant temperature baths, and the nitrogen vapour cryostat. The former will be described first along with details of the temperature measurement system, which is common to both methods.

2.3.1. The Fixed Temperature Bath

A number of fixed temperature baths have been used in the past to obtain constant low temperatures. Table II lists a number of these baths along with their temperature.

TABLE II

Fixed Temperature Baths

Type of Bath	Fixed Point	Temperature °K
Ice-water	M.P.	273
Ice-calcium chloride	-	225
Acetone-CO_2 (solid)	-	200
Ethyl Alcohol* - CO_2 (solid)	Sub. P.	196
Ethyl Alcohol - (solid-liquid)	F.P.	158
Liquid Oxygen	B.P.	90.2
Liquid Nitrogen	B.P.	78

M.P. - Melting point; F.P. - Freezing point; Sub. P. Sublimation point

In this technique the particular bath contained in a dewar is brought in contact with either the specimen (and specimen yoke) directly, or with a copper shield which in some experiments completely encloses the specimen and yoke. This arrangement is illustrated in Figure 27. The bath was tall enough so that the yoke was immersed up to bakelite insulator. The open space around the top of the dewar was loosely pluged with cotton wool to reduce the effect of room temperature.

* The bath provides a convenient temperature point, but it has been found difficult to prepare and as a result it was not used in the following experiment.

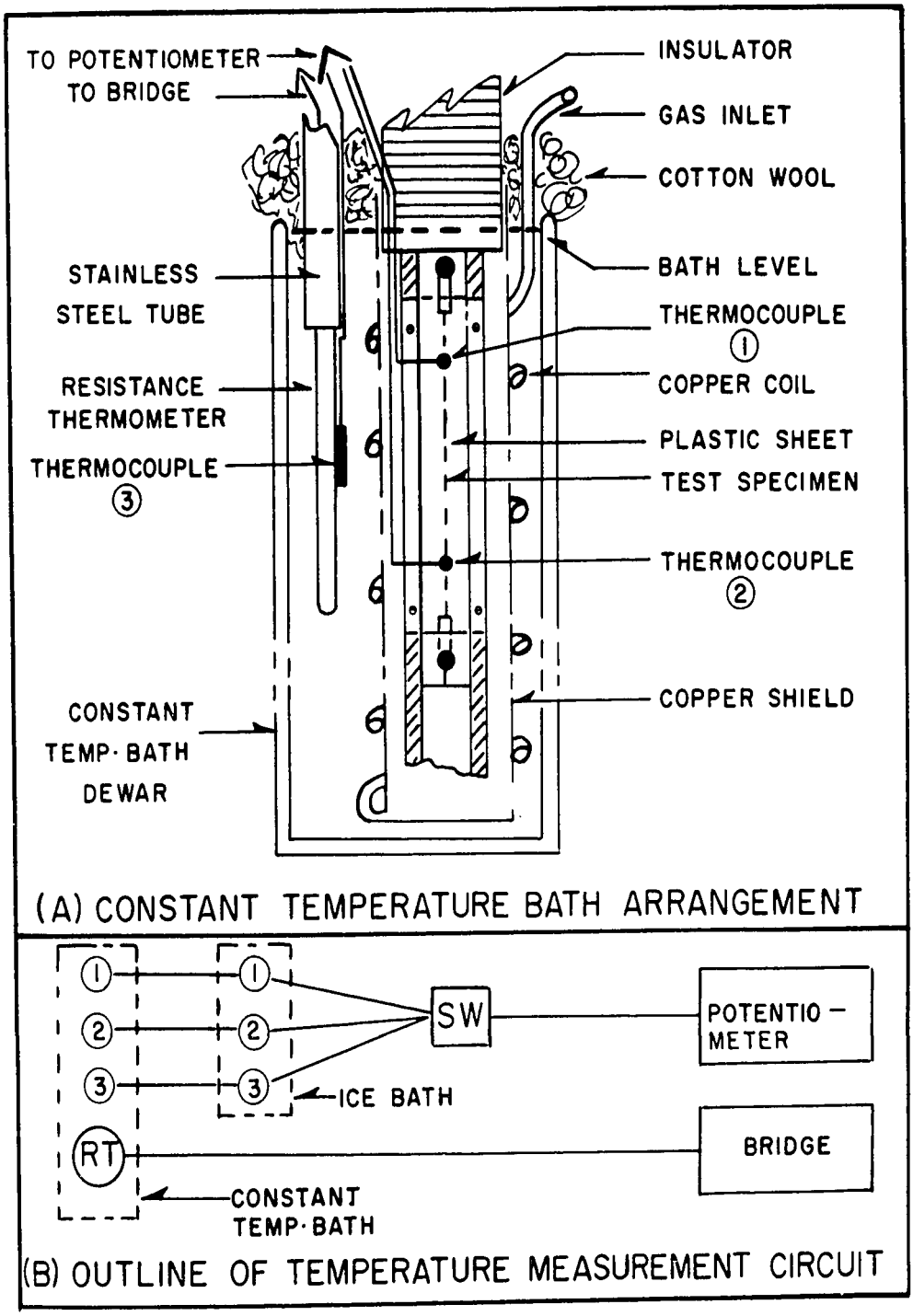

FIGURE 27- CONSTANT TEMPERATURE BATH ARRANGEMENT AND DETAILS OF TEMPERATURE MEASUREMENT SYSTEM.

The temperature was measured at a number of locations. Two copper-constantan thermocouples (1 and 2) project from a plastic strip screwed to the cut-out rear section of the specimen yoke. The tips of the thermocouples were positioned within 0.2 cm. from the surface of the test specimen at a distance of 1.0 cm. from either end of the specimen. When using the copper yoke shield these two thermocouples indicate the temperature near the surface of the test specimen, and also the temperature gradient along an 8.0 cm. gauge length. A third thermocouple (3) was located outside the shield to measure the bath temperature itself. Each of the three thermocouples were connected in series with a companion thermocouple located in an ice bath, which serves as an accurate temperature reference point. The particular thermocouple to be observed was selected by a set of copper knife switches, and its output voltage was measured using a standard Leeds and Northrup portable potentiometer. All three thermocouples were initially calibrated against a resistance thermometer which is also suspended in the bath dewar (see Figure 27). The resistance thermometer was observed with a standard DC Wheatstone bridge. With these calibrated thermocouples the temperatures may be read to a sensitivity of $\pm$ 1/2°K and an accuracy of with 1°K at liquid nitrogen (78°K).

Reasonable stability has been obtained using a number of these baths with the exception of the acetone - CO_2 (solid) mixture which appeared

to exhibit large temperature fluctuations over a period of time. In those cases where it was not convenient for the bath ingredients to come in direct contact with the specimen and specimen yoke, and where as a result the copper yoke shield was used, difficulty was found in obtaining rapid temperature equilibrium at the specimen. The time required for the specimen to attain the bath temperature, with a low temperature gradient along its length, was speeded up considerably by circulating helium gas (or argon gas at bath temperatures above liquid nitrogen) up through the yoke shield. Temperature gradients of less than 0.01°K/ cm. were observed in a liquid nitrogen bath using the yoke shield, and with only a very slight flow of helium gas.

2.3.2. The Nitrogen Vapour Cryostat

Another simple method of attaining low temperatures is by the use of a nitrogen vapour cryostat. In this technique liquid nitrogen is boiled in a dewar by an immersed electric heater (50 ohms, 10 watt wire wound resistor). This boiling produces a vapour pressure which forces the cold vapour through an insulated rubber tube to a coil of copper tubing wound about a copper yoke shield. This cools the shield and eventually the enclosed yoke and specimen. A second electric heater is attached to the lower end of this shield for raising its temperature if necessary. Figure 28 illustrates the nitrogen vapour cryostat and the associated system.

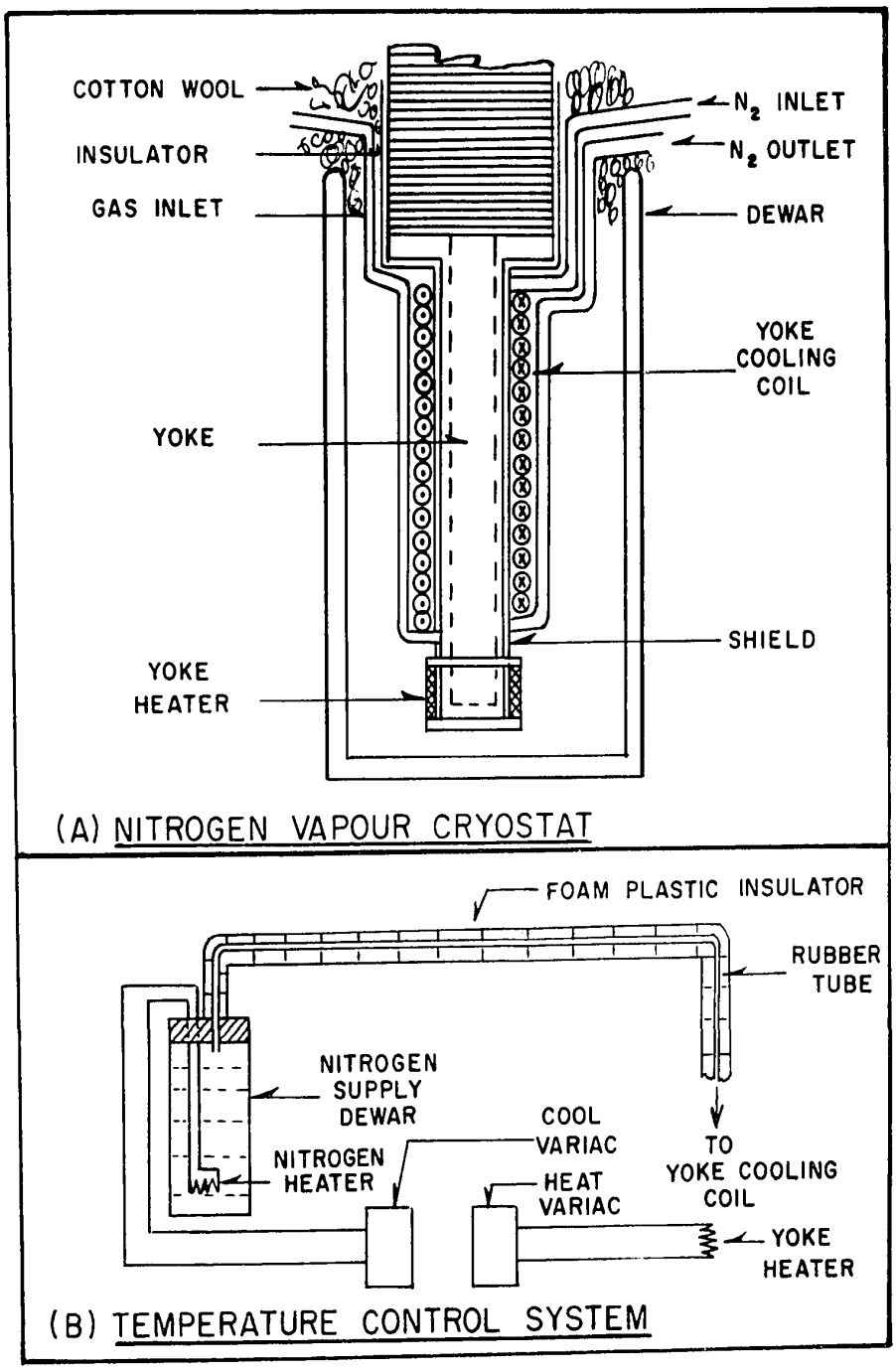

FIGURE 28 - DESIGN OF THE NITROGEN VAPOUR CRYOSTAT SYSTEM.

A number of experiments have been conducted using this apparatus. For each particular experimental arrangement (length of rubber tube, quality of insulation etc) there is an equilibrium temperature corresponding to each value of power supplied to the nitrogen bath heater. It is only necessary then to set the current to the nitrogen heater to a predetermined value and wait for equilibrium to be attained. Unfortunately this method suffers from a number of disadvantages, first the time to get from one equilibrium temperature to another (say 50 degrees lower) is normally of the order of 40 to 60 minutes which is rather long for certain purposes. Secondly it is normally convenient to boil nitrogen from the large transportation dewers, which are in direct contact with the floor, and it has been found that after the rubber connecting tube becomes frozen it allows many of the floor vibrations to be transmitted directly to the creep machine inhibiting its operation. This second disadvantage has been partly eliminated by mounting a smaller dewar directly on the antivibration frame of the apparatus. This arrangement appears to function relatively free of vibration but it must be frequently refilled with liquid nitrogen on a long run, at the lower temperatures.

When using the nitrogen vapour cryostat the specimen temperature is measured (as in the case of the fixed bath method) by the two yoke thermocouples (1 and 2). Similarily, in order to reduce temperature gradients,

helium or argon gas was circulated inside the yoke shield through a separate gas inlet tube at the bottom of the shield.

2.4. The Anti-Vibration Mounting System

After the apparatus was completed and initial tests were run it was found that building vibrations caused excessive impact loading of the test specimen and erratic behaviour in the balancing system, due to the fact that these vibrations were being transmitted to the mounting frame of the apparatus. To eliminate this problem required a complete remounting of the creep machine. Three separate mounting units were required as illustrated in Figure 29.

Mounting unit #1 supported the specimen loading frame and light source. It was constructed of six concrete blocks (approximately 50 lbs each) cemented together, two blocks wide by three high. These concrete blocks rested on four isomould stacks one at each corner. The isomould stacks consisted of five sheets of isomould rubber 1-1/4" x 1-1/4" x 1/4" interspaced with sheets of aluminum 1-1/4" x 1-1/4" x 1/16". This arrangement rested on a steel plate 16" x 16" x 1/2" which in turn rested on a stack of three sheets of tentest 16" x 16" x 1/2". The isomould stacks themselves were designed to bear 50 psi each.

Mounting unit #2 was rigid, welded, angle iron frame bolted directly to the floor. This unit supported the incremental loading system and

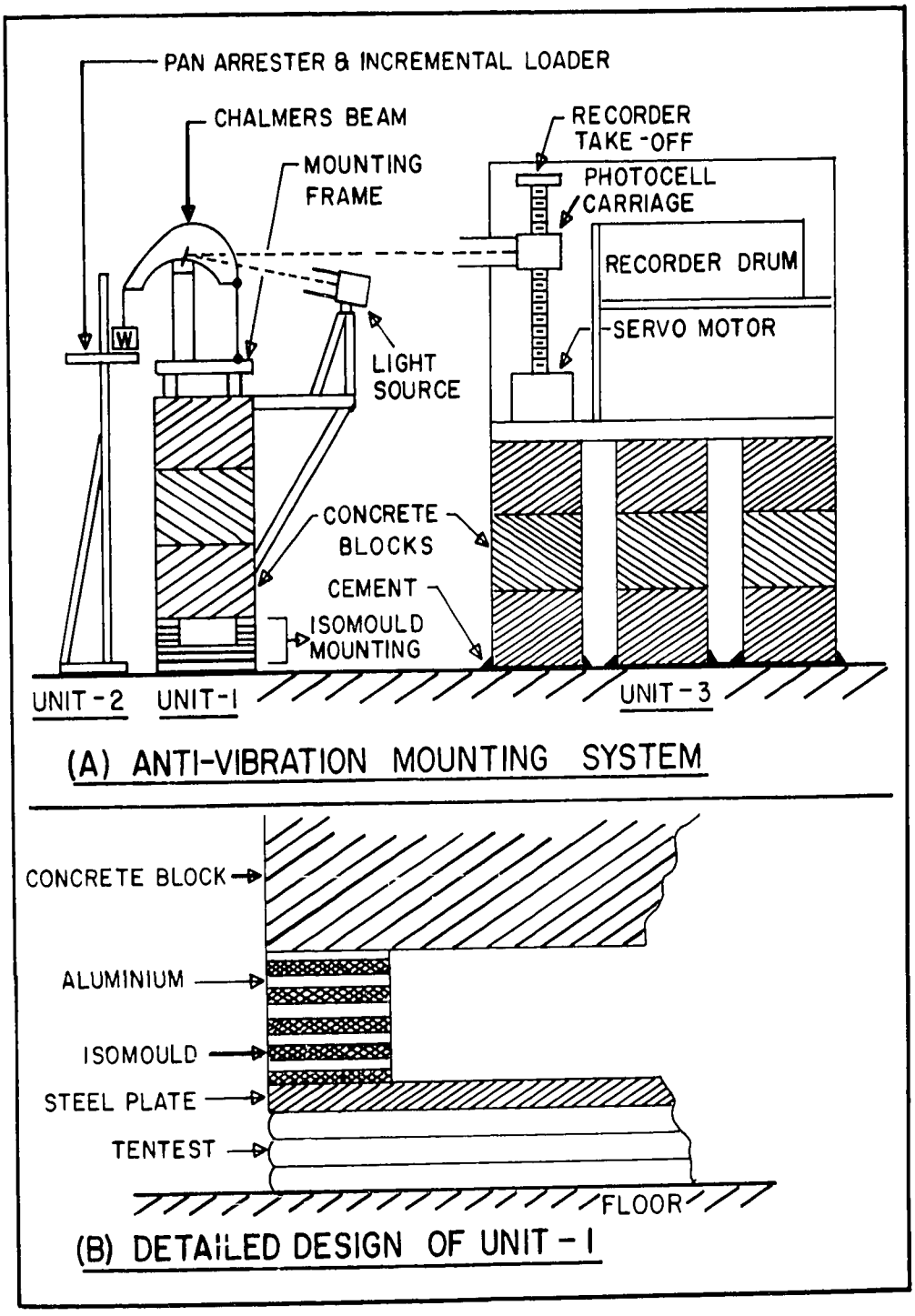

FIGURE 29 - ARRANGEMENT OF ANTI-VIBRATION MOUNTING SYSTEM

the loading pan arrester.

Mounting unit #3, which supported the servo balancing and recording system, consisted of three concrete block pillars, two blocks wide by three high. These were cemented together and the bottom ones were cemented to the floor. A frame to support the balancing and recording system was constructed from angle iron and fastened to the concrete blocks by a set of bolts cemented into them.

When the anti-vibration system was completed it was found to eliminate all but the very heavy floor vibrations, which are apparently produced by heavy trucks and busses operating on the nearby streets. As a result experiments could be carried out at all times with exception of peak traffic hours when large numbers of busses pass very close to the building.

2.5. A Study of the Operation of the Creep Apparatus

The behaviour of the completed apparatus was investigated to determine its typical operating characteristics. The data was obtained after a two month program of testing and modification of the original apparatus. The details of these studies will not be given, but the operating characteristics of the final apparatus will be listed. The effect of the rate of incremental loading was investigated in detail, these tests will be briefly described.

2.5.1. Operating Characteristics

(a) Sensitivity - The strain measurement system was capable of indicating strains, as small 0.5×10^{-5} in a specimen with a 10 cm. gauge length. Two sensitivity ranges were provided, the 1/1 range, where one inch on the recorder chart corresponded to a strain of 10^{-4}, and a 1/10 range, where one inch on the recorder chart corresponded to a strain of 10^{-3}.

(b) Linearity - The maximum non-linearity of the strain measuring and recording system was less then 5%.

(c) Stability - The short term instability at the lowest strain rates was less then 0.5×10^{-5} strain units. The long term instability (over periods of hours) was less then 2×10^{-5} strain units per hour.

(d) Reproducibility - By introducing an electrical unbalance in the strain measuring circuit it was possible to measure the reproducibility of the system. A maximum error of 1×10^{-5} strain units was observed.

(e) Response Time - The maximum time for full scale deflection of the recorder pen (10^{-3} strain units) was found to be 3 seconds.

(f) Elastic Distortion of Apparatus - The elastic distortion of the combined Chalmer's beam, specimen loading tape and pull rod, specimen grips, and specimen yoke was found to range from 0.8 to 1.1×10^{-5} strain units per ten gram increase in load, at room temperature. The

higher value being obtained for the case where the initial specimen load was the weight of the loading pan only approximately 150 grams, the lower value was for an initial load of approximately 650 grams.

2.5.2. Effect of Rate of Loading

The rate at which the incremental loads were added or removed was considered to be of particular importance, and as a result, a series of tests were carried out to study the problem. Basically these experiments consisted of applying different sized loads at various rates to the secondary load pan, and observing the variation of load with time using an electric load cell placed between the loading pan yoke and the Chalmer's beam.

A miniature proving-ring-type load cell was constructed to observe the small load changes (maximum load applied 28.5 gms). This load cell consisted of a 3/8" length of German silver tubing, with an 0.800" O.D. and a wall thickness of 0.008". A set of specimen grips were fastened with machine screws to opposite sides of the ring for mounting purposes.

Four Philips type PR-9814 resistance strain gauges were attached to the ring with Philips type PR 9244/00 quick setting cement. The strain gauges were mounted around the circumference of the ring, two inside and two outside, and were wired in the form of a complete four arm bridge

circuit. After allowing one hour for the cement to set, the cell was cycled ten times from zero to 200 gms. After this cycling the zero point was found to remain stable.

During the tests the load cell was connected to a Brush BL-320 universal bridge and amplifier* and the variation of load were recorded on a Brush BL-202 recorder* at a chart speed of 25 mm./sec. The sensitivity of the measuring system was approximately five grams per scale division.

The loads in the form of steel ball bearings were lowered by a fine thread which was unwound from a drum by an adjustable speed motor. Loading rates ranging from 2 to 50 mm./sec were tried using a 28.5 gm load. Figure 30 illustrates a typical incremental loading curve and illustrates its important features. The incremental load ΔL was lowered at a rate R and was fully applied at the point B in a time T_1. Over the next period of time T_2 a decaying elastic oscillation of maximum magnitude T osc. took place which completely died-out by the point C. It is interesting to note that there was no impact loading observed when the pan damping arrangement (described previously) was used. Apparently this damping arrangement has a sufficiently large vertical viscous component to prevent impact loading. On removal of the pan damper, impact effects were observed.

---

* Supplied by the Physics Section, Physical Metallurgy Division, Mines Branch, Department of Mines and Technical Surveys, Ottawa.

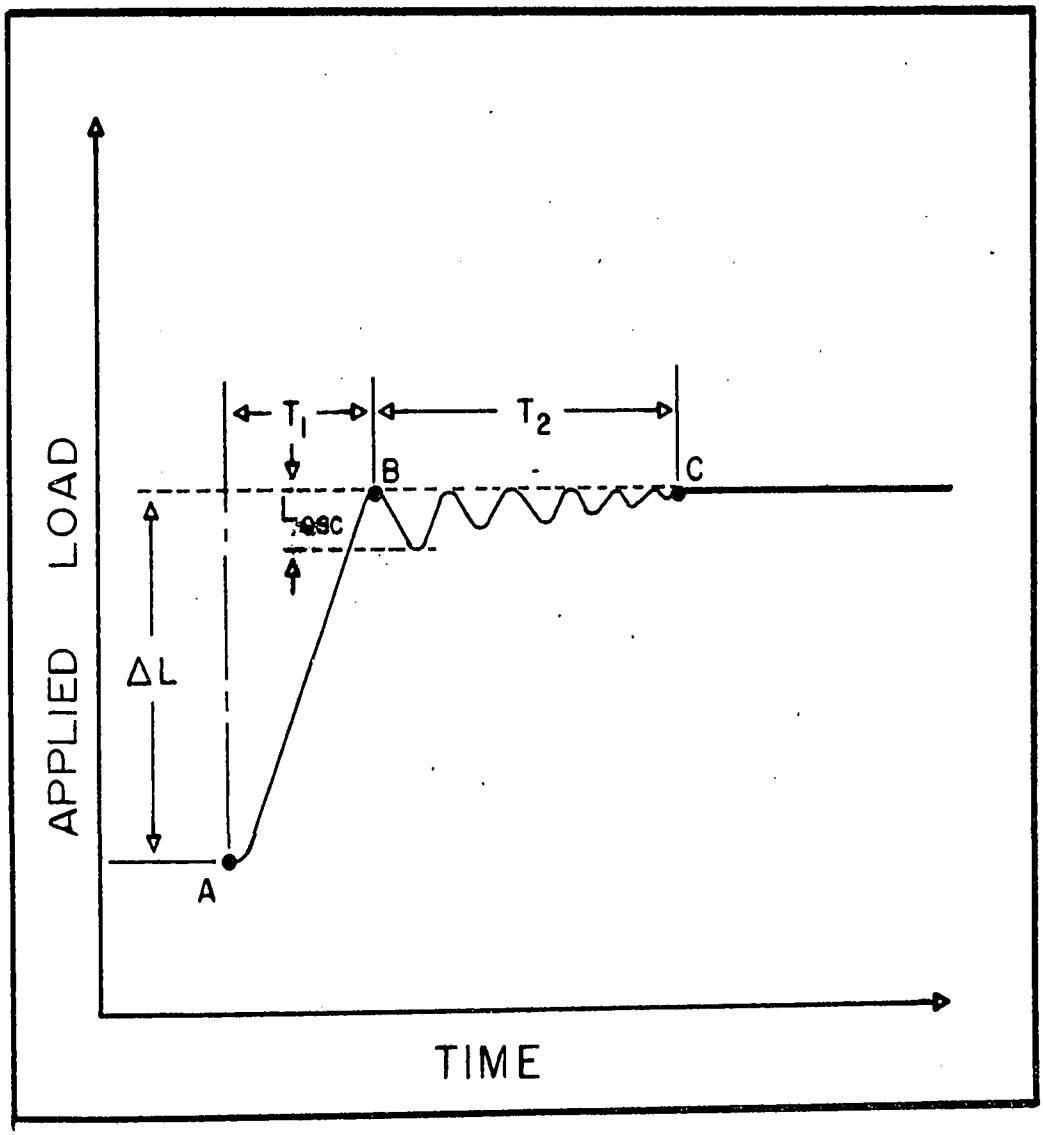

FIGURE 30 – APPLIED LOAD VERSUS TIME FOR A TYPICAL INCREMENTAL LOADING

Table III shows the results for a number of experiments. Considering all factors it was decided to use a standard loading rate of 6.3 mm./sec.

TABLE III

The Effect of Different Rate of Loading on the Loading Parameters T_1, T_2 and Losc.

R* mm/sec.	L gms.	T_1 sec.	L osc. gms.	T_2 sec.
2	28.5	1.2	< 5	< 1.0
6.3	8.6	0.3	< 5	< 1.4
13	28.5	0.2	5	1.6
23	28.5	0.05	10	2.1
36	28.5	0.025	16	3.6
45	28.5	< 0.025	15	> 4.0

* The different factors are defined earlier in the text.

2.5.3 Typical Experimental Curves

Figure 30A illustrates actual sections of incremental transient creep curves recorded by the apparatus. The respective sensitivity and chart speed are indicated on each curve. The upper curve illustrates the behaviour of a specimen (14G-1) undergoing easy glide at a temperature of 78°K. The initial section of the curve (AB) represents an applied load of 520 grams (resolved shear stress 650 gm/mm^2). Load changes were made at points B, C, and D of + 3.72, - 3.72, and + 3.72 grams respectively. The corresponding strain rate change at point B is approxi-

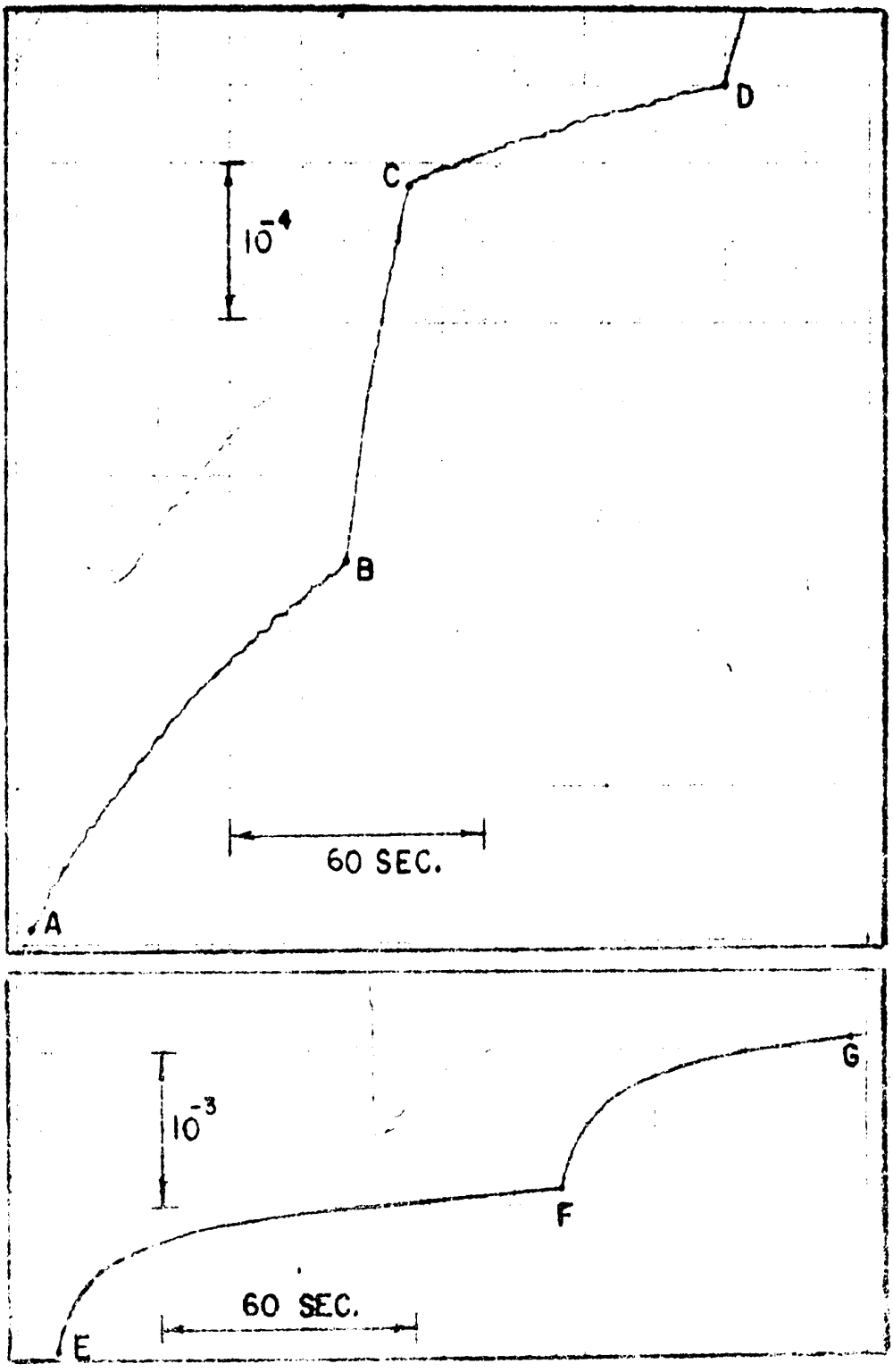

FIGURE 30A – TYPICAL EXPERIMENTAL CURVES

mately 2 x 10^{-6}/ sec to 10^{-5}/ sec. The high sensitivity, stability, and freedom from transient phenomena of the apparatus is obvious from this curve.

The lower curve illustrates the behaviour of a specimen (14E-1) undergoing easy glide at a temperature of 300°K. The initial section of the curve (EF) represents an applied load of 500 grams (resolved shear stress approximately 630 gm/ mm^2). A load change of 10 grams was made at point F. This curve was recorded at a sensitivity of 1/10 that of the upper curve. It should be noted that at this sensitivity there is a complete absence of instability, the curves appearing as perfectly smooth lines.

The behaviour illustrated by these curves are typical and indicate that the apparatus is suitable for carrying out the proposed experimental studies.

2.6. Brief Description of a Typical Creep Experiment

The steps followed in a typical creep experiment are listed below.

(1) All electronic circuits are allowed to warm up at least 24 hours before a test. Under normal conditions the electronic circuits remain on permanently.

(2) The Chalmer's beam is levelled, the loading pan arrested, the specimen pull-rod clamped and the specimen inserted into the specimen grips. An empty dewar is usually placed around the specimen yoke to isolate the specimen from the effects of room temperature fluctuations.

(3) The light spot lamp is turned on, and transducer mirror (mounted on the Chalmer's beam) is adjusted to reflect the light spot onto the center of the photocell, which has been lowered to its bottom position.

(4) The cover is placed over the optical system. By alternately adjusting the bridge section, and Wagner earthing section, a good balance may be obtained. An oscilloscope attached to the output of the servo amplifier serves as a balance indicator. With half the maximum amplifier gain a good balance results in a maximum unbalance voltage of about 10-15 volts on the control winding of the servo motor.

(5) The light cover is temporary removed, the specimen pull-rod unclamped, and the cover replaced. The chart pen is zeroed with the sensitivity control in its neutral position, and the sensitivity control is then set to the 1/1 sensitivity position.

(6) With no additional loads on the primary loading pan, the load pan arrester is gently released (this applies a load of approximately 150 grams to the specimen), and the pen deflection noted on the recorder. Small loads (10 and 20 gms) are manually applied to the primary loading pan until a substantial transient creep curve is observed. The load required to produce the first creep is recorded.

(7) Once the load has been increased to the point where creep takes place, a series of incremental loadings and unloadings are performed using the incremental loading system. The primary load is increased and the incremental loadings repeated. In this way a number of transient creep curves are obtained for a series of increasing applied loads.

(8) A number of the experiments involved alternate deformation at room and liquid nitrogen temperature. In these cases the procedure is as follows; first a series of incremental loadings are made at a particular applied load, at room temperature. The load is increased to a higher value and a second series of incremental loadings made at the same temperature. The specimen is then immersed in liquid nitrogen. It is necessary to increase the applied load at the lower temperature to initiate creep, and then a series of incremental loadings are performed. The primary load is reduced to the earlier room temperature value, the liquid nitrogen is removed, and the specimen allowed to warm up to room temperature. Once there, the tests are continued following a similar cycle.

(9) After sufficient experiments are carried out the recorder charts are analyzed and the strain rate sensitivity (K_3) and the work hardening coefficient (Θ) are determined following the procedure outlined in the following chapter.

CHAPTER III

PREPARATION OF TEST SPECIMENS

1. Easy Glide and the Problem of Specimen Orientation

Garstone et al (1956) and Seeger (1956) have shown that the presence and extent of easy glide in single crystals of the face-centered cubic metals appear to be dependent on the crystallographic orientation of the test specimen. Their experiments indicate that there exists only a small region of the orientation triangle where the easy glide is unperturbed (independent of orientation). Garstone et al (1956) after experimental studies on aluminium and copper state that "the occurrence of easy glide depended markedly on the orientation of the crystal, -------- in particular, crystals near the (100) and (111) poles and on the (100) - (111) boundary gave no region of easy glide and showed marked strain hardening (stage II) from the beginning of the deformation". Accordingly Figure 30B illustrates the region of the orientation triangle where unperturbed easy glide is most probable.

After a review of the literature it was decided that it would be difficult to grow single crystals with preferred orientations restricted to the region associated with unperturbed easy glide. It was decided therefore to grow a sufficiently large number of crystals and to select from this group those which were most suitable.

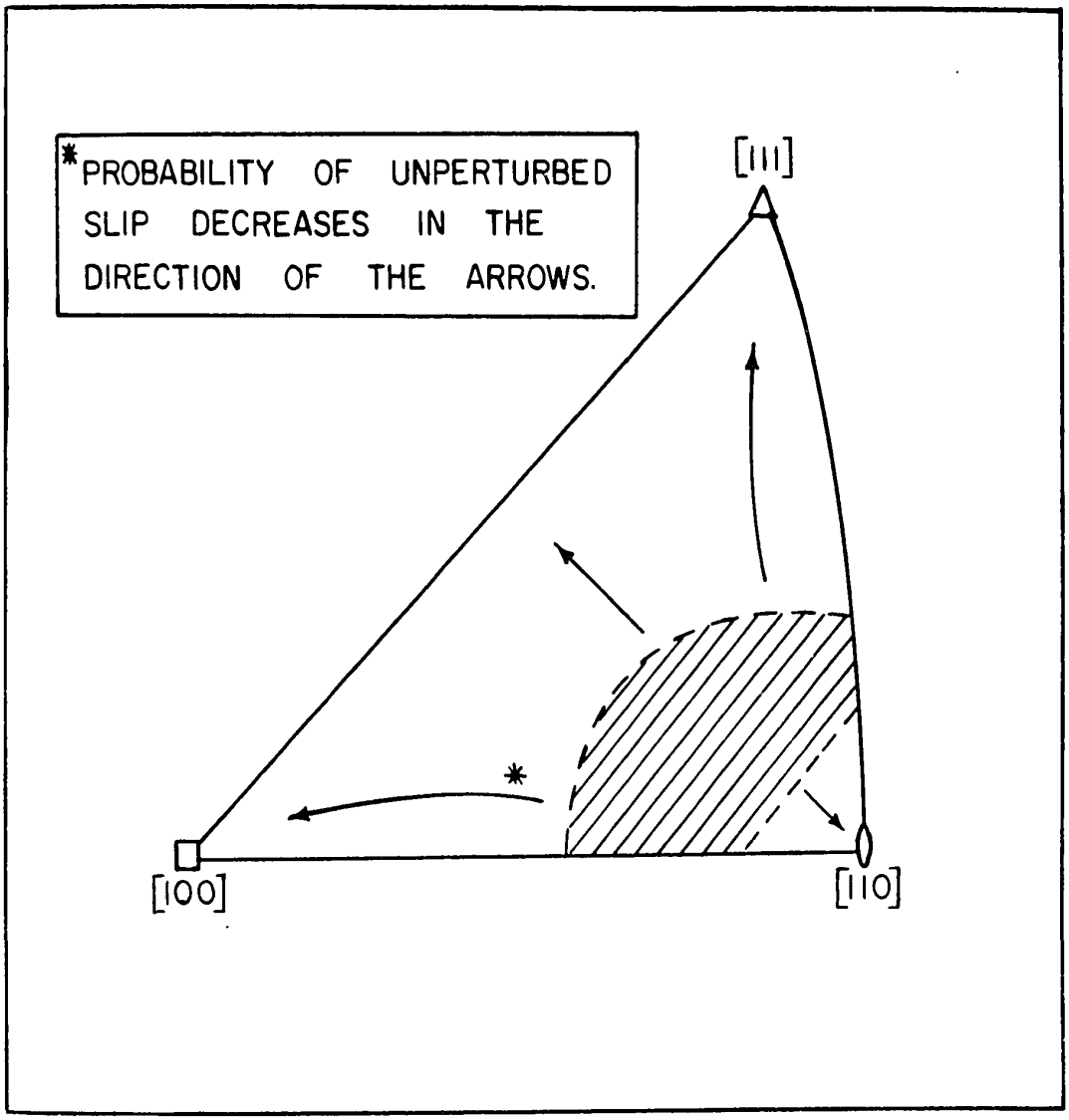

FIGURE 30B-ILLUSTRATION SHOWING REGION OF ORIENTATION TRIANGLE WHERE UNPERTURBED EASY GLIDE IS MOST PROBABLE.

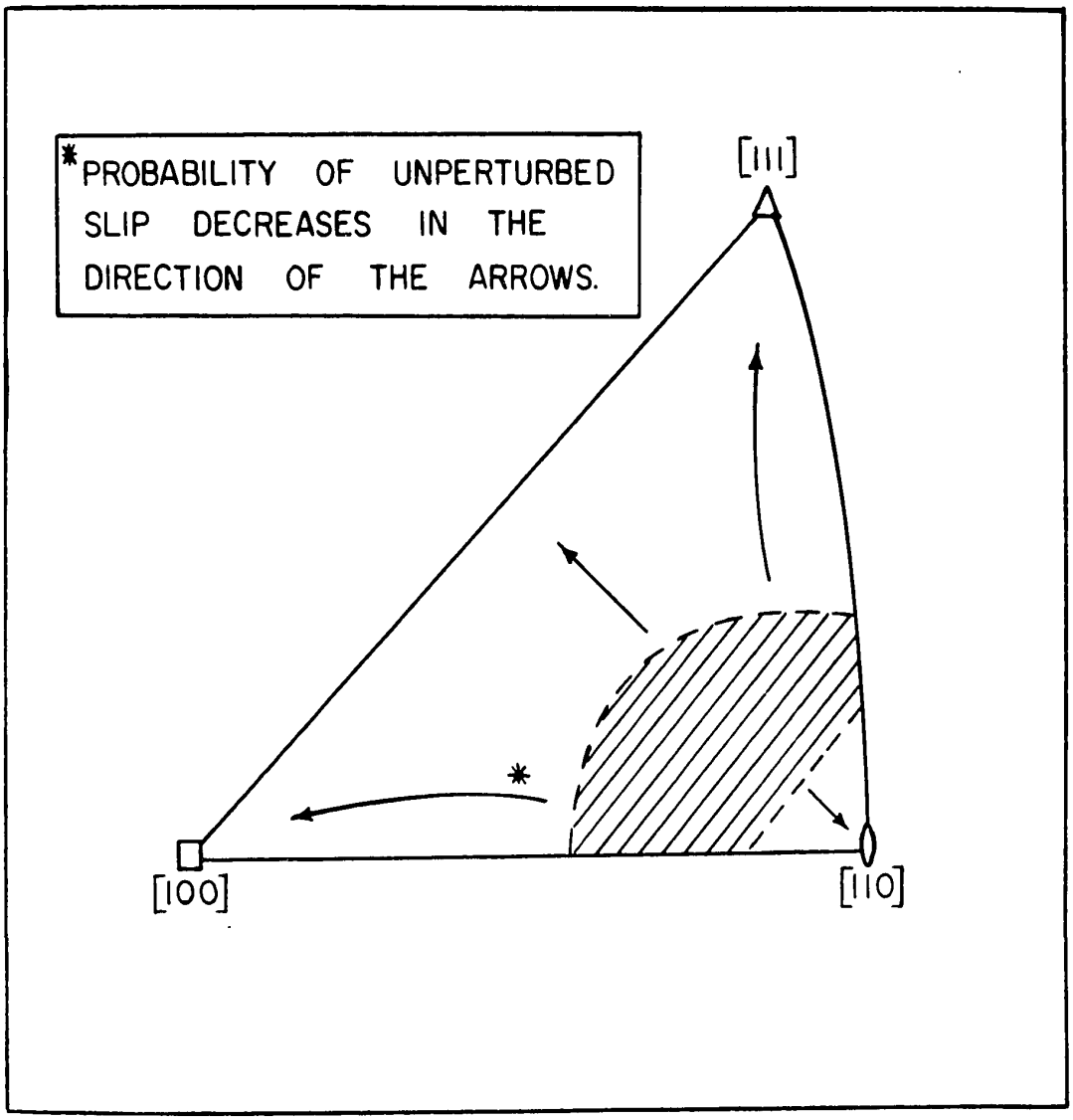

FIGURE 30B-ILLUSTRATION SHOWING REGION OF ORIENTATION TRIANGLE WHERE UNPERTURBED EASY GLIDE IS MOST PROBABLE.

2. Materials

Three lots of high purity, oxygen free copper, labelled A-1, A-2 and A-3, were obtained from the American Smelting and Refining Company (ASRC). The spectrographic analysis of all three lots of this copper quoted by the company is given in Table IV.

A partial, independent, spectrographic analysis* was carried out on lot A-1 of the ASRC material as received, and the results are also listed in Table IV. Although both analysis indicate very low impurity concentrations there is considerable difference in the two analyses. It is suggested that the one supplied by the company is the more reliable, since accurate standards for pure copper were not available at Ottawa. A check was made on the amount of dissolved oxygen and hydrogen in the ASCR copper** and this data is included in Table IV. A piece of high purity (99.999%) copper was also obtained from A.D. MacKay Inc., labelled M, but this was found to obtain at least 0.026 wt. % of oxygen and could thus not be used for preparation of low impurity alloys.

High purity gold and silver were obtained in the form of drawn wire 1/100 inch in diameter from A.D. MacKay Inc. The purity of both metals was listed as 99.95% by the supplier.

---

* Spectrographic Laboratory reports 58-388 and 59-22, Mines Branch Department of Mines and Technical Surveys, Ottawa, November 1958 and February 1959.

** Determined from vacuum fusion gas analysis, Mines Branch, Department of Mines and Technical Surveys, Ottawa, December, 1958.

TABLE IV

Weight Percentage of Impurities in High Purity Copper Used to Prepare Test Specimens

Type of Analysis	Elements	Weight Percentage	
		A.S.R.C. Analysis	Ottawa Analysis
Spectrographic Analysis	Fe	0.00007	0.006
	Sb	0.0001	-
	Pb	0.0001	0.005
	Sn	0.0001	-
	Ni	0.0001	-
	Bi	0.00001	-
	Ag	0.00003	-
	As	0.0002	-
	Cr	0.00005	-
	Si	0.00001	0.005
	Te	0.0002	-
Vacuum Fusion Gas Analysis	H_2	-	0.00005
	O_2	-	0.00005-0.0003

Considerable experimental work, using the constant strain rate method, has been reported recently by Garstone and Honeycombe (1956) on copper-gold and copper-silver alloy single crystals. It was considered advantageous to use similar alloys in the present work. The two alloys were prepared in a series of concentrations ranging from 0.05 to 1.0 atomic percent. (Due to a lack of time it was not possible to carry out deformation experiments on the copper-gold alloys, however details of their alloy concentration and residual resistance ratio

have been included for possible future use). The weights of solute and solvent required for the different alloys are listed in Table V.

TABLE V

Details of Alloy Constitution

Sample Number	Alloy	Solvent Lot Number	Impurity at.%	Weights Grams		Remarks
				Solvent	Solute	
1	Cu-Au	A-1	0.05	26.270	0.0440	-
2	Cu-Au	A-1	0.10	26.920	0.0848	Spoiled
2A	Cu-Au	A-1	0.10	33.137	0.1058	-
3	Cu-Au	A-2	0.30	34.028	0.3085	-
4	Cu-Au	A-2	0.70	33.553	0.7224	-
5	Cu-Ag	A-1	0.05	26.290	0.0240	-
6	Cu-Ag	A-1	0.10	25.723	0.0240	Spoiled
6A	Cu-Ag	A-1	0.10	32.532	0.0589	-
7	Cu-Ag	A-1	0.30	31.570	0.1680	-
8	Cu-Ag	A-2	0.70	33.456	0.3940	-
9	Cu-Au	A-2	1.00	33.053	1.0340	-
10	Cu-Ag	M	1.00	33.820	0.5663	-
11	Cu-Au	-	3.00	27.000	2.5933	Not Prepared
12	Cu-Ag	-	3.00	27.000	1.4187	Not Prepared
13	Pure	A-1	0.00	-	-	-
14	Pure	A-3	0.00	-	-	-

3. Preparation of Alloy Ingots

All alloy samples were prepared using a chill-casting vacuum induction furnace* (for details see Craw and Henry (1956)). Chill casting

* Metallurgical Chemistry Section, Division of Applied Chemistry, National Research Council, Ottawa, Canada.

prevents segregation and using this technique homogeneous ingots may be prepared. The use of induction heating provides two advantages, namely; that the constituents of a melt may be brought to the melting point in a short time (order of two or three minutes) which is of particular importance if one of the constituents is volatile, and also that rapid stirring is induced in the melt which further assures the formation of a homogeneous ingot.

Basically the procedure was as follows: the weighed solvent and solute for a particular alloy were first cleaned, the copper (in the form of a length of rod approximately 1.25" long by 0.25" diameter) was etched in 50/50 dilute nitric acid for one to two minutes, washed in distilled water, rinsed in ethyl alcohol, rinsed in ether and finally placed on a clean kleenex and dryed completely using a hair dryer. Throughout this thesis this procedure will be referred to as the 'standard cleaning procedure'. The solute in the form of short lengths of wire (0.01 inch in diameter) was cleaned in a similar manner. The solvent and solute metals were then placed in a silica melting crucible which was first cleaned following the standard procedure. The crucible was placed inside the induction heating coil, and the furnace sealed and pumped down to approximately 5×10^{-5} mm hg. (this requires approximately one hour). With the vacuum system still operating the induction heater was turned on and the constituents

brought to the melting point (approximately two to three minutes). The crucible was then tilted and the molten material chill-cast into a water cooled, split copper mould.

The furnace was then opened and the ingot removed from the mould. The top and bottom sections of the ingot were often found to be irregular in shape and were cut-off using a jewelers saw. These end pieces were sent for spectrographic analysis. The remaining center piece of the casting (approximately 1-1/4" long by 3/8" diameter) was machined on a lathe into a cylinder approximately 1" long by 5/16" diameter.

4. Preparation of Polycrystal Wire Samples

The machined ingots were cleaned using the standard procedure (described previously) to remove any surface impurities introduced during the machining. They were then swagged* into rods (approximately 6" long by 1/8" in diameter). After this degree of deformation the rods were again cleaned (using the standard procedure), placed in 5 mm I.D. pyrex tubes, and alternatively evacuated (approximately .01 mm. hg) and flushed with argon three or four times. Finally the tubes were evacuated to .01 mm. hg, filled to 1/2 atmosphere with argon, and sealed off. The sealed tubes were annealed for 24 hours at 500°C and then air quenched. The

* Metal Forming Section, Mines Branch, Department of Mines and Technical Surveys, Ottawa.

annealed rods were then drawn* to a diameter of 0.04 inches for preparation of single crystal test specimens. A number of pieces of pure copper were further drawn to a diameter of 0.02 inches for the preparation of polycrystal test specimens.

After the drawing process the wire must be cleaned. Previous studies by Henry (1959) have shown that the drawing operation used * does not add more then one part per million metallic impurity to the wire. However the lubricants used in the drawing process are difficult to remove and a strict procedure must be followed if proper cleaning of the wire is to be accomplished. The procedure developed was a modification of that used by Henry (1959) and is as follows: the wire was first cut in 14" lengths (size required to fit single crystal mould). These lengths were soaked in benzene for 15 minutes then wiped with kleenex tissue. Alternate soaking in benzene and wiping with fresh dry kleenex was continued until no grease appeared on the dry kleenex wiper. The wire was then rinsed in ether, rinsed in distilled water, and then given the standard cleaning. All wires of each alloy were then placed in a pyrex tube, pumped down to 0.01 mm hg, flushed with argon, evacuated and flushed four times, finally pumped down to 0.01 mm hg, and 1/2 atmosphere of argon added, this procedure will be referred to as argon flushing. The tube was then

* Metal Forming Section, Mines Branch, Department of Mines and Technical Surveys, Ottawa.

sealed-off. The wires were annealed for 24 hours at 500°C then air quenched to room temperature.

5. Preparation of Single Crystal Wires

Single crystal wires were prepared from the annealed polycrystalline wire. The preparation of metal single crystals is at present somewhat of an art and therefore considerable detail will be given in this thesis on the particular method used.

5.1. The Single Crystal Mould

For preparation of single crystals the polycrystal wire must be placed in a split graphite mould, as shown in Figure 31. This mould consists of two lengths of 5/16" diameter high purity spectrographic graphite rod milled to form two halves of a cylindrical split mould. A 0.01" deep groove was then milled down the center of the flat inside surface of each half to within 1/4" of the bottom. The two halves were then held together while a 0.037" diameter drill was run down the center, using the milling grooves for alignment. The result is a split mould with a inside diameter of approximately 0.037" and an inside length of 11.75". The mould is held together during the crystal growing operation by a set of five tight fitting graphite rings also illustrated in Figure 31. Plate VIII shows two such moulds, one assembled and the other dismantled. The tightness of fit of the wire in the mould determines to a large extent the success of the

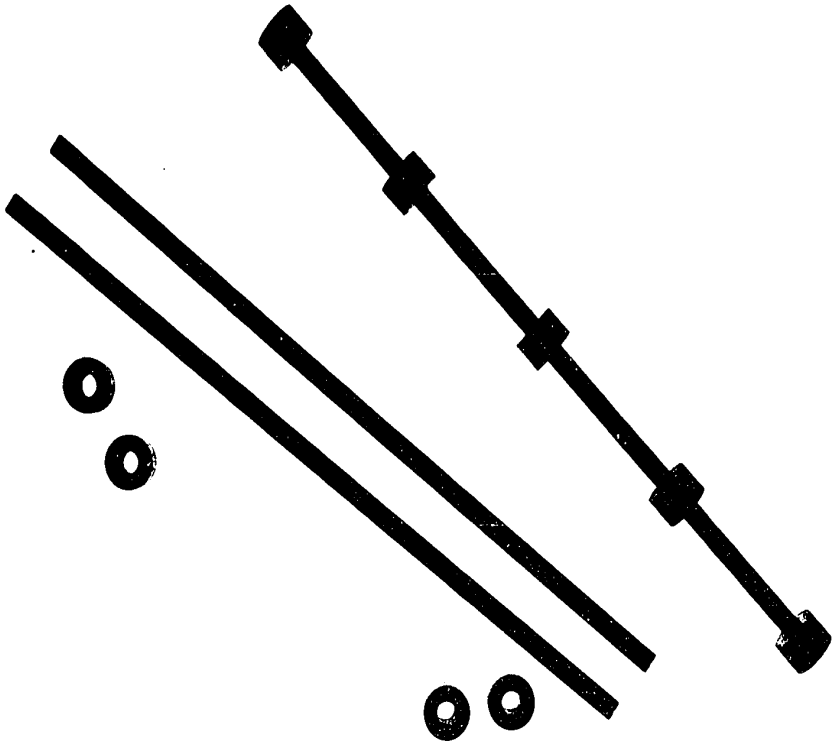

PL TE VIII

Photograph Showing Construction and Assembly of Split Graphite Moulds for Growing Single Crystal Wires.

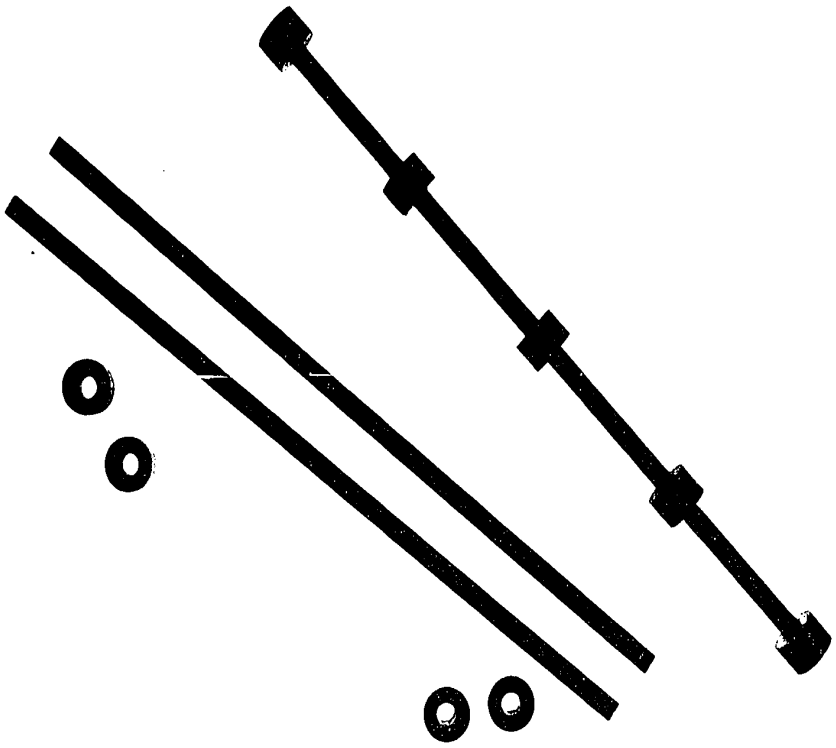

PL T E VIII

Photograph Showing Construction and Assembly of Split Graphite Moulds for Growing Single Crystal Wires.

crystal growth. With too loose a fit the result will be many short pieces of single crystal rather then a continuous wire, with too tight a fit the mould will be open at the sides and molten metal will tend to flow out during melting. A number of experiments were conducted to study this behaviour and it was finally decided that for best success the polycrystal wires should be inserted in the open mould and that the wires should be oversize to the extent that when the two halves of the mould are assembled a space of approximately 0.005" exists between the inner faces of the mould. This provides for complete filling of the mould after melting, and as a result single crystal wires the full length of the mould were grown with only a very slight outflow of copper along the inner mould faces.

5.2. Initial Preparation

After annealing the polycrystal wires were elongated approximately 5% by pulling one end with a pair of pliers while the other end was clamped in a vice. This straightens the wire so that it will easily fit into the single crystal mould. The ends of the wire are deformed during this process and these deformed regions were cut-off with a pair of sharp cutting pliers and then rounded-off with fine emory paper. To obtain the correct fit the polycrystal wires were etched down in size using 50/50 nitric acid, contained in a vertical test tube slightly longer then the wire (approximately 16 inches). After each period of etching (approximately 1 minute) the wires

were washed in distilled water and rinsed in ethel alcohol (each of which was contained in a long vertical test tube). The wire was then tried in the mould and if the fit was not satisfactory the process was repeated. When the fit was successful the graphite rings were slipped over the mould.

5.3. The Furnace Tube

Once the mould was loaded it was lowered into the furnace tube, which was a quartz test tube (approximately 29" long by 3/4" inside diameter) with a quartz ground-glass joint and valve arrangement to allow the tube to be evacuated and sealed off after the mould was inserted. Figure 32 shows the details of this furnace tube.

5.4. The Out-Gasing Procedure

The furnace tube, containing the mould, was placed in a special out-gasing furnace (with a heated area about 18" long) with only the ground glass joint protruding from the top of the furnace. The tube was pumped down to 0.01 mm. hg and then leaving the vacuum system connected, the temperature of the out-gasing furnace was allowed to rise to an equilibrium temperature of approximately 550°C over a period of one hour. To prevent the vacuum grease in the ground-glass joint from melting an electric fan was used to cool the joint. The vacuum system was allowed to pump for another 1/2 hour, after which time the furnace tube was argon flushed (as described previously), 40 cm. hg of argon added, and then isolated from

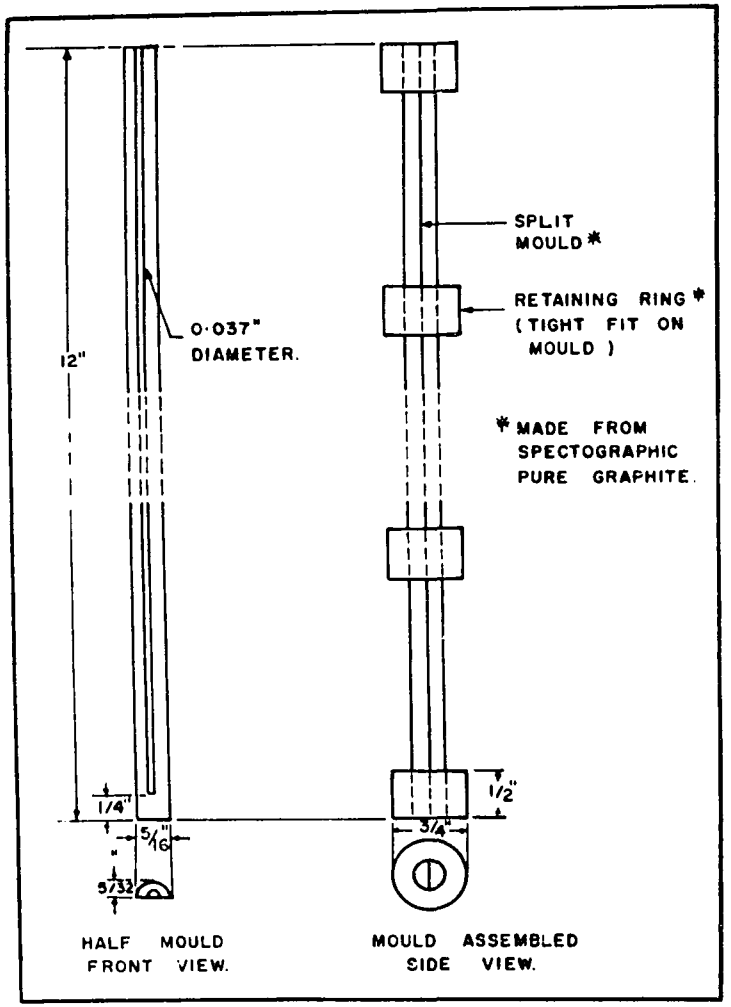

FIGURE 31 - DESIGN OF SPLIT GRAPHITE MOULD FOR GROWING SINGLE CRYSTAL WIRES

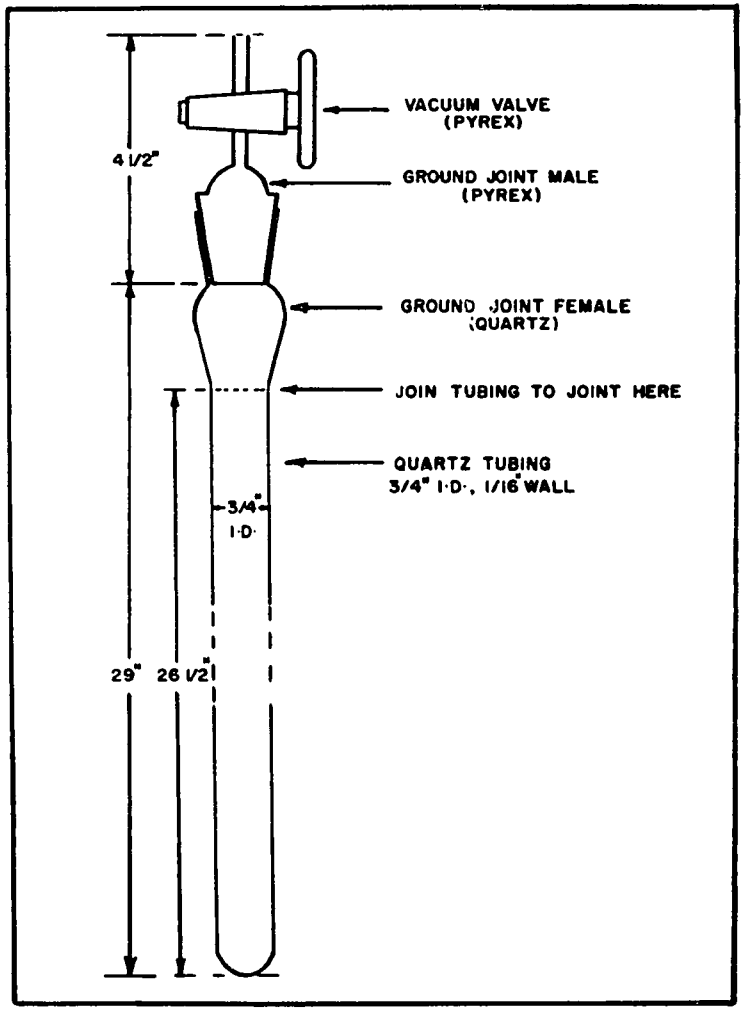

FIGURE 32 - DESIGN OF FURNACE TUBE

the vacuum system. Details of the out-gas furnace and the associated vacuum system are shown in Figure 33. Plate IX shows the completed unit.

5.5. Design of the Crystal Growing Furnace

Single crystals were prepared by passing the polycrystal sample (held in the graphite mould within the furnace tube) through a sharp temperature gradient vertical furnace at a rate of four to ten cms. per hour. The method used is a modification of that due to Andrade and Roscoe (1937). Their work, along with a recent paper by Goss (1953) indicate that the thermal conductivities of the solid and molten metal, the rate of growth, and the degree of stressed growth (vertical or horizontal growth) all effect the quality and orientation of the single crystal.

There appears to be considerable information available on the growth of single crystals of such metals as bismuth, cadimum, indium lead, and zinc but very little is available on the growth of small diameter copper single crystals. According to Basinski (1959) there appears to be no preferred orientation for copper single crystals grown from the melt.

As there appeared little chance of an accurate theoretical determination of the optimum rate of growth, and temperature gradient required for the growth of copper single crystals the system was designed with the optimum characteristics determined by Andrade and Roscoe (1937) for

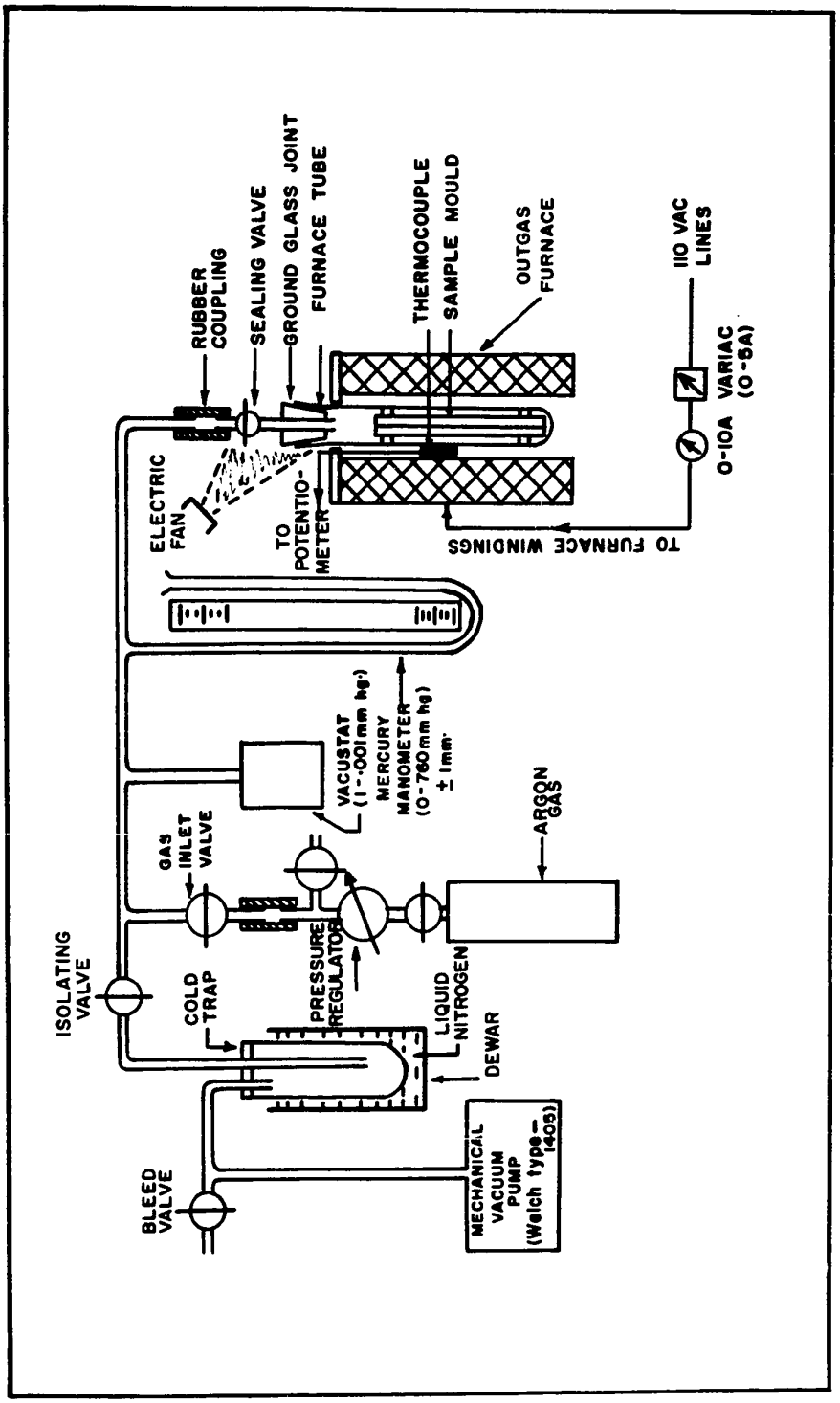

FIGURE 33 - DESIGN OF OUT-GAS FURNACE AND THE ASSOCIATED VACUUM SYSTEM.

cadimum. These were a temperature gradient in the furnace at the point of solidification of 17 to 25°C/ cm. and a velocity of growth of 3 to 5 cm./hr. Figure 34 illustrates the design of the furnace and the system for lowering the sample through it. Plate X shows a view of the completed unit.

Figure 34B illustrates the construction of the furnace itself. A helix of chromel-A formed from a length of wire 26-1/2 feet long (#20 B and S, 0.635 ohms/ft.) was wound on the center 8" of a 12" long Norton corrugated type furnace core. The helix was spread out more at the center of the furnace core in order to prevent over-heating in this region. The winding was fastened to the core with Sternson #30 high temperature cement and allowed to set for six hours. The furnace core with its attached heater was then set in an aluminium can, 10" in diameter and 8" long, with 1/4" thick transite end pieces. This allowed the 2" sections of the core not covered by the heater winding to project out either end. The space between the furnace core and the aluminium can was filled with powdered asbestos. The electrical leads were brought out by way of two steel machine screws through the bottom transite plate. A chromel-alumel thermocouple was suspended within the furnace core to give a rough indication of the temperature.

The furnace was mounted on an angle iron rack as illustrated in

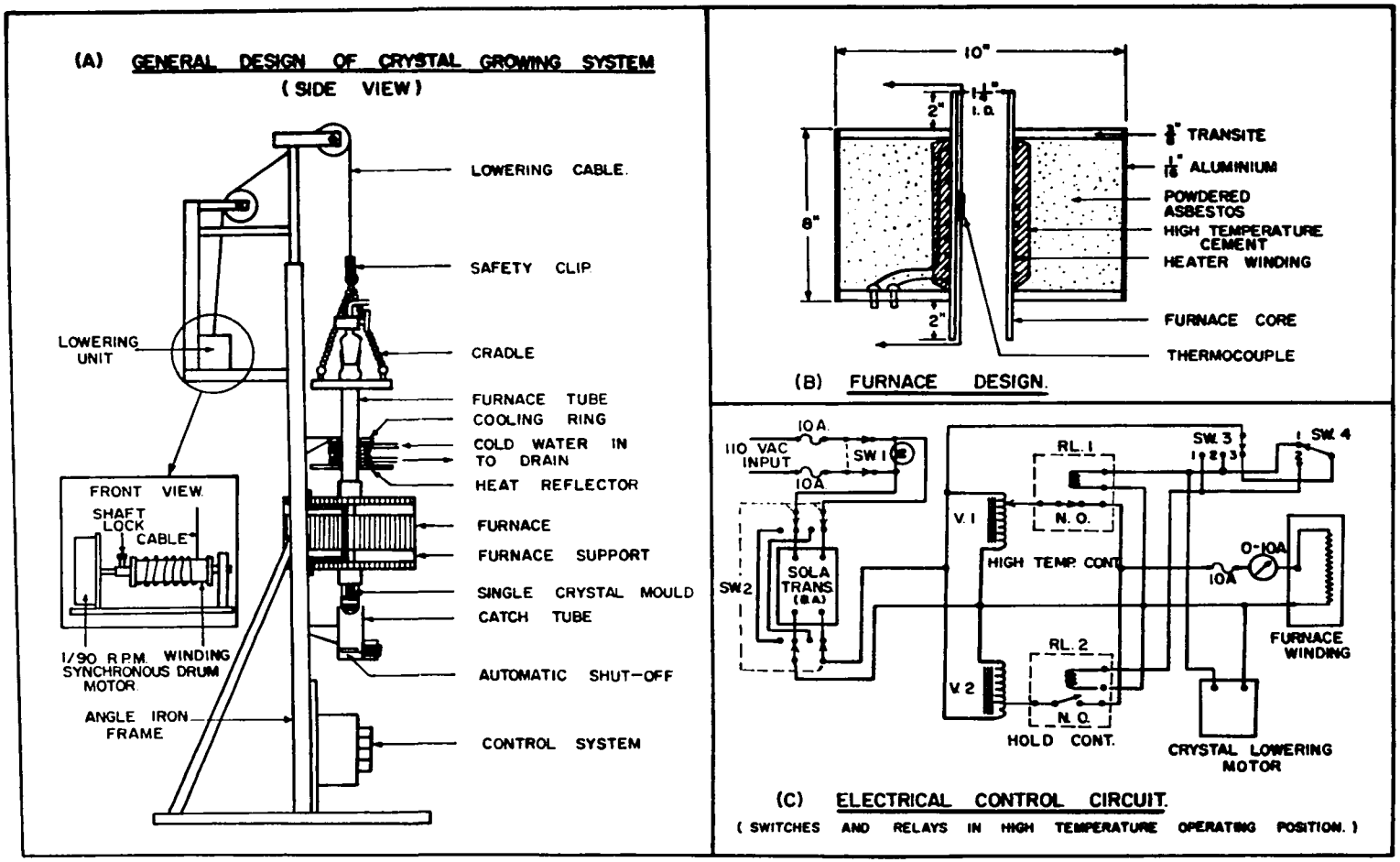

FIGURE 34 - DESIGN OF THE CRYSTAL GROWING FURNACE AND THE SYSTEM FOR LOWERING THE SAMPLE THROUGH IT

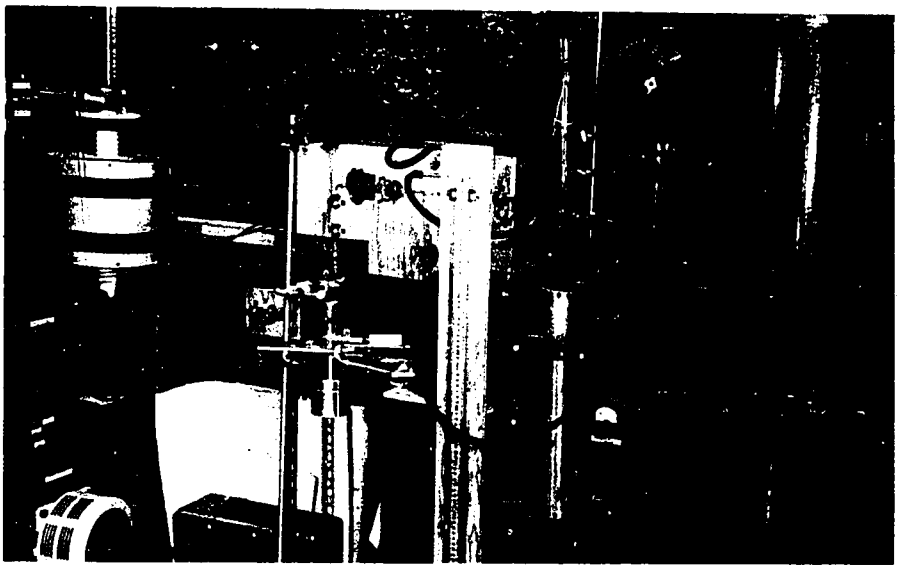

PLATE IX

Front View of the Out-Gas Furnace and the Associated Vacuum System. (The Crystal Growing Furnace can be seen to the left of the Photograph).

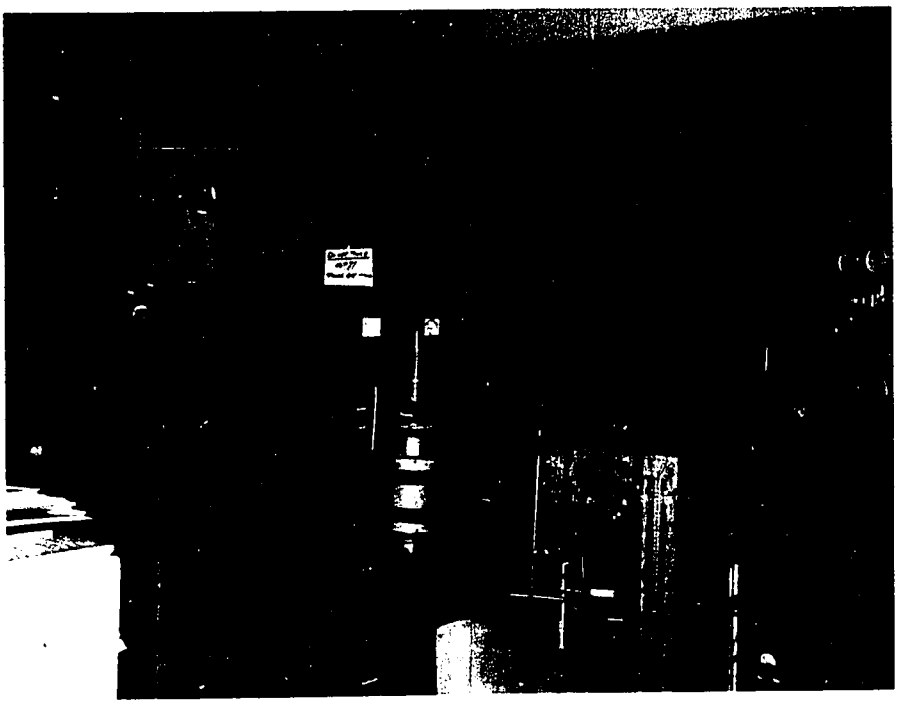

PLATE X

Photograph of the Completed Crystal Growing System.

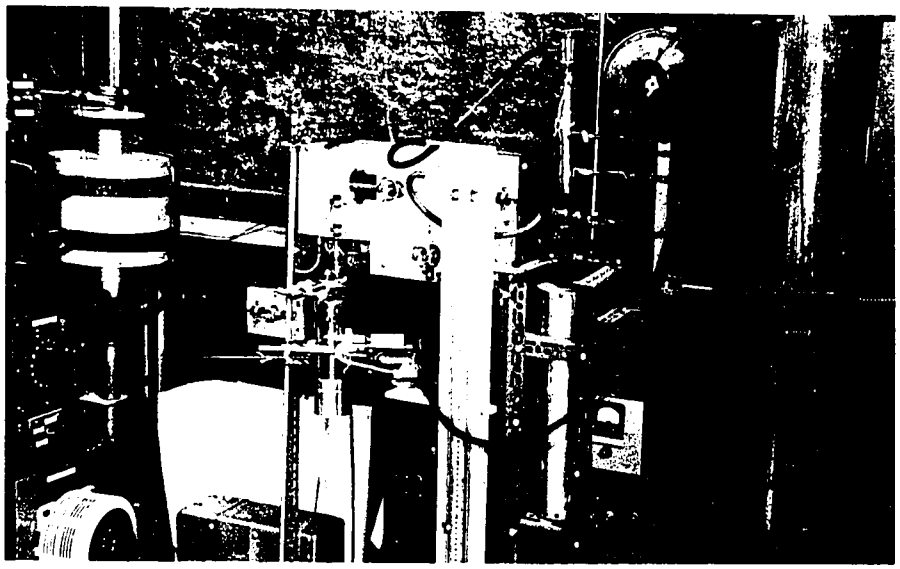

PLATE IX

Front View of the Out-Gas Fu ace and the Associated Vacuum System. The Crystal Growing Furnace can be seen o the left of the Photograph).

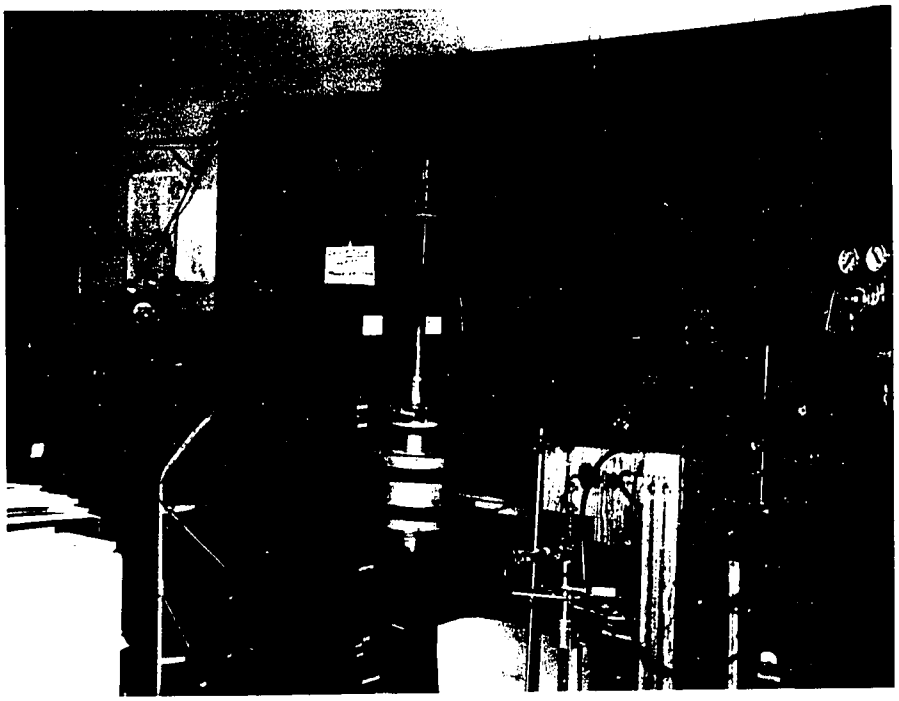

PLATE X

Photograph of the Completed Crystal Growing System.

Figure 34A. The furnace tube (containing the single crystal mould etc) was lowered through the furnace by a cradle and cable arrangement. The cable (#30 nichrome wire) was slowly unwound from a drum driven by a Haydon, 1/90 RPM, sychronous motor. A system of adjustable pulleys allowed the furnace tube to be aligned coaxially with the furnace core. The furnace tube passed through a water cooled coil and heat reflector located immediately above the top opening of the furnace. This was found necessary to prevent the vacuum grease in the furnace tube ground-joint from melting. Plate XI shows a close-up of the furnace, and the cooling ring and heat reflector. The furnace tube is also visible partly inserted in the furnace.

Figure 34C shows the electrical control circuit for the crystal growing system. Under high temperature operating conditions power is supplied from the mains through a Sola voltage regulating transformer to an 8 amp variac (V.1.). The output of this variac is applied to the furnace winding through a mercury type relay (RL.1) and a 0-10 amp meter. This variac allows the maximum temperature of the furnace to be adjusted to the required value. When the lower section of furnace tube, containing the crystal mould passes through the furnace, the bottom end enters the catch tube and depresses a microswitch (SW4) mounted inside. This causes switch SW4 to shift from position 1 to 2, cutting-out

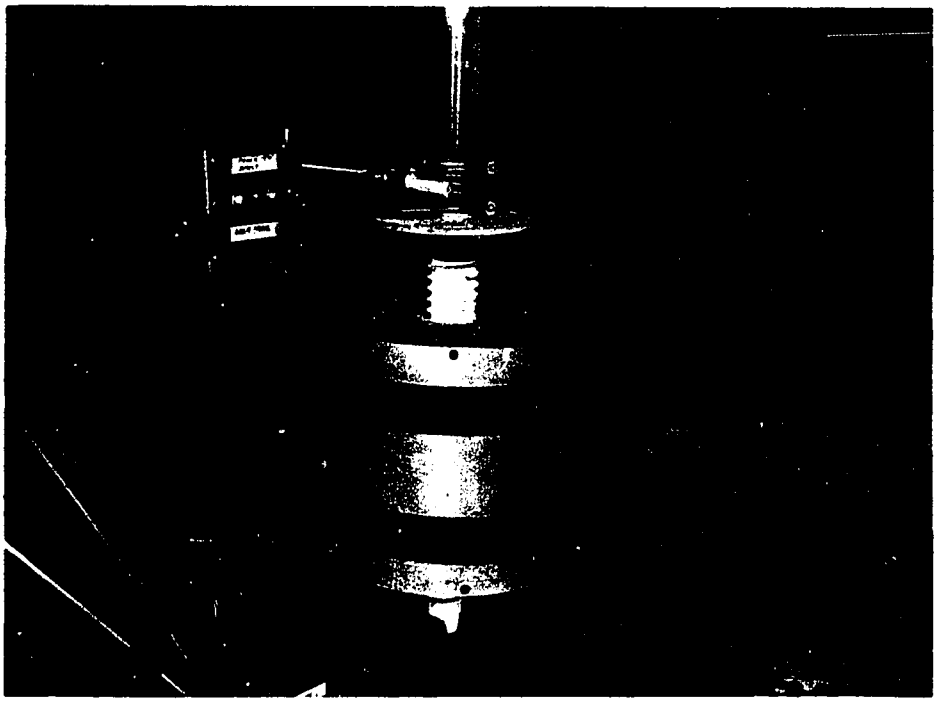

PLATE XI

Close-Up of Single Crystal Furnace.

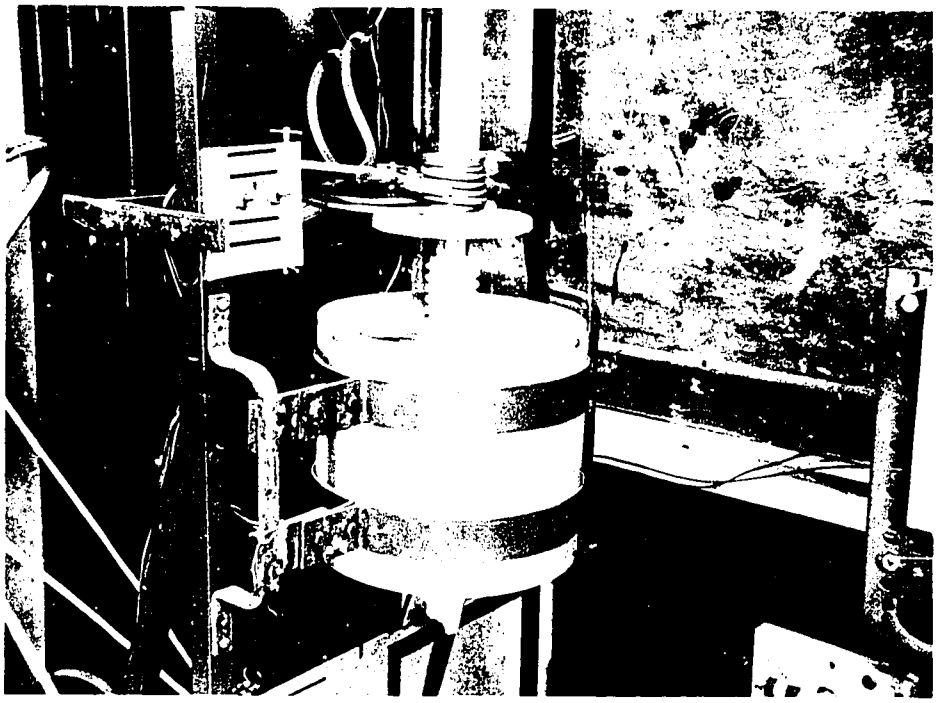

variac V.1, stopping the lowering motor, and connecting variac V.2 to the furnace winding. The output of variac V.2 is adjusted so that the furnace temperature on stand-by operation never goes below 600-700°C. With switch SW.3 in position 1 the furnace is in standby condition, and in position 2 it is in the high temperature condition without the facility for automatic switching to the standby condition. For single runs the automatic switching is used, but when a series of runs are to be made on a continuous basis, it is desireable to keep the furnace operating at the high temperature continuously since a number of hours are required to attain equilibrium at the high temperature.

It is very important that the furnace temperature not be allowed to fall too low between single crystal runs, and that the furnace not be operated at the high temperature any longer then necessary. This is due to the fact that the furnace was required to operate at a temperature very near the limit of the chromel-A wire used in the heating element and secondly the thermal shock of cooling and heating between the maximum temperature and that of the room could cause mechanical failure of the furnace core. A standard procedure was developed for bringing the temperature of the furnace up to the maximum temperature. This consisted of increasing the furnace current from 3 amps (standby) to a maximum current (I max) in steps of 1.5 amps. The current was left for 1/2 hour at each of the intermediate points. It was found that the maximum current must be applied for

a number of hours before a temperature equilibrium is reached. Figure 35 shows the variation of temperature at a constant current of 6.6 amps over a period of approximately eight hours, after the furnace had been at this current for six hours previous. Over the final seven hour period the temperature increase was linear with time at a rate of approximately 1.3°C/hour. The temperature was measured by an exposed thermocouple located at the maximum temperature position in the furnace. During the test an empty furnace tube was inserted in the furnace, such that it projected out both ends, to simulate conditions during actual operations.

The following procedure was followed on all successive occasions:

(a) When not in use furnace was left at a current of 3.0 amps (600-700°C).

(b) Heating up consisted of raising the current in steps of 1.5 amps up to I max, leaving the current for a period of 1/2 hour at each of the intermediate steps.

(c) To achieve thermal equilibrium the current was left at I max. for 6 hours before crystal growth started.

(d) Cooling down consisted of reversing steps (b), adjusting the current down to 3.0 amps.

Figure 36 shows a series of graphs, for different maximum currents, of temperature versus distance for the completed furnace. In all

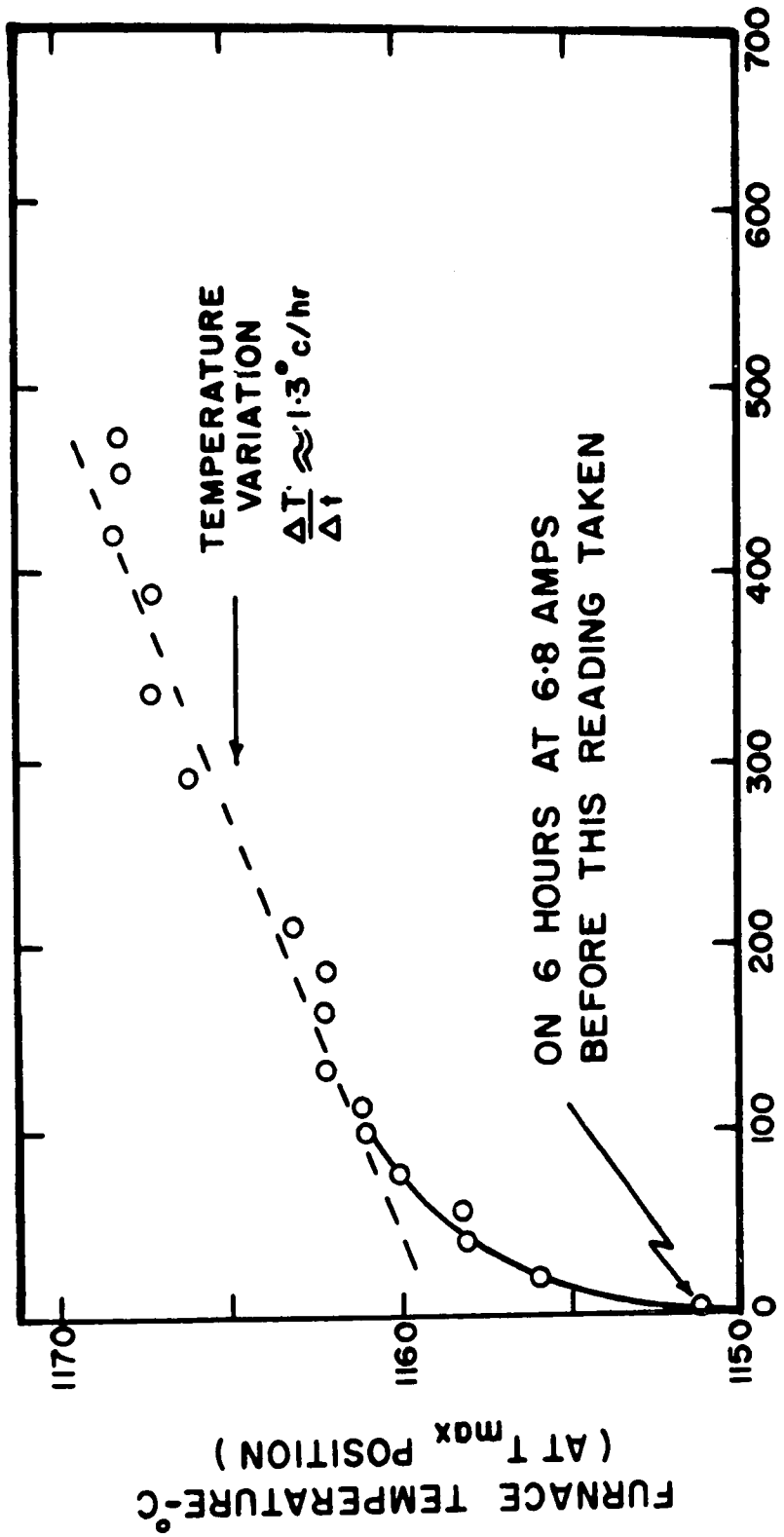

FIGURE 35 - VARIATION OF TEMPERATURE AS A FUNCTION OF TIME AT A CONSTANT CURRENT, FOR CRYSTAL GROWING FURNACE.

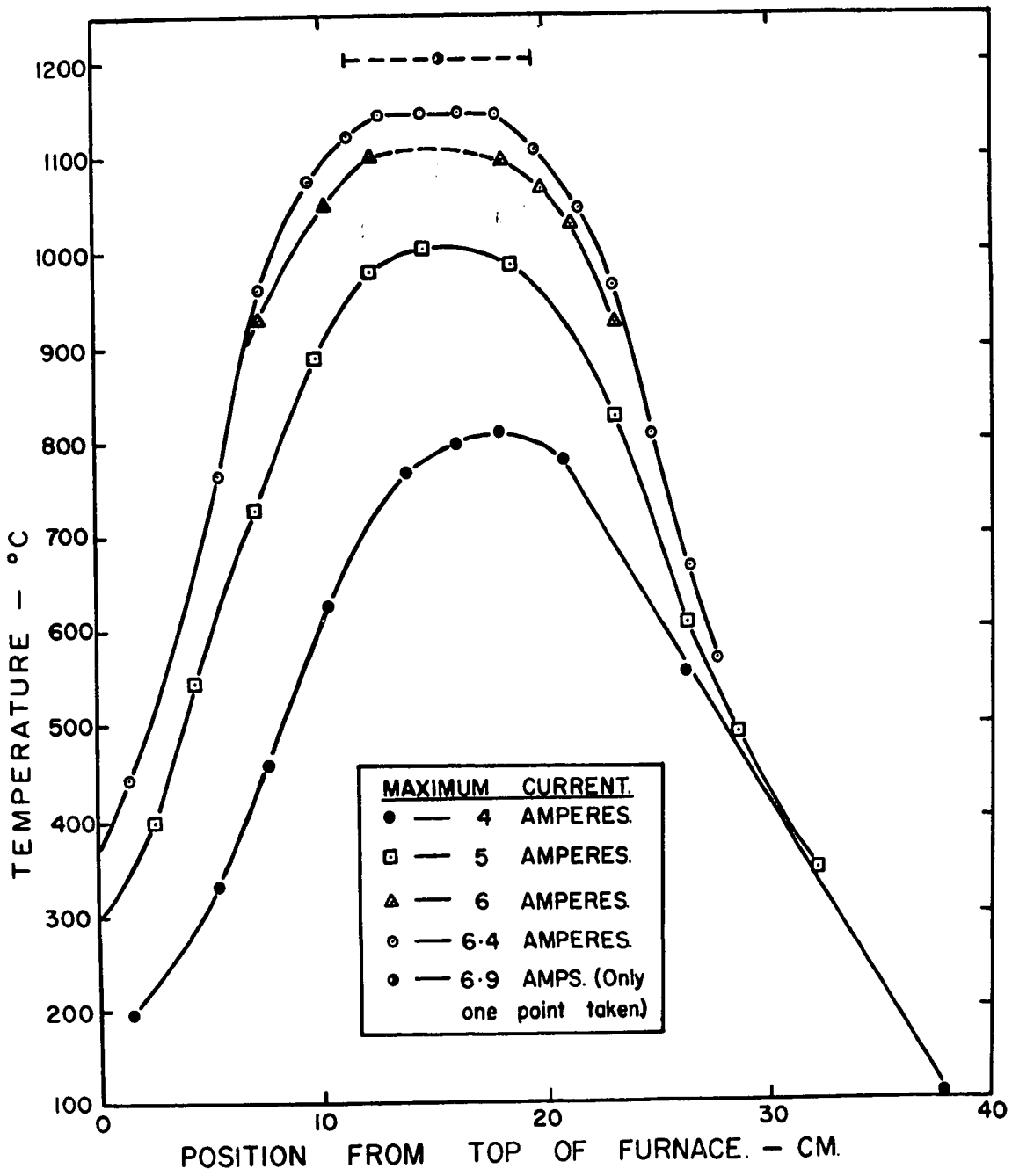

FIGURE 36 - VARIATION OF TEMPERATURE FOR DIFFERENT POSITIONS WITHIN THE FURNACE AND FOR DIFFERENT MAXIMUM CURRENTS.

cases the temperature was measured by a chromel-alumel thermocouple embedded in a 5/16" diameter graphite rod (the same as was used for the single crystal moulds) and located within one of the standard furnace tubes. This whole arrangement was allowed to slowly pass (10 cm/ hour) through the furnace, and the temperature measured at different positions. Table VI lists values of maximum current (I max.), the resulting maximum temperature (T max.), the temperature gradient (G), and the length of furnace with temperature over the melting point of copper (Y).

TABLE VI

Operating Characteristics of Crystal Growing Furnace

I max.	T max.	G	Y
amps	°C	°C/ cm.	cm.
6.0	1110	8	6
6.4	1150	25	10
6.9*	1200	40-50**	-

* Only one reading taken.
** Estimated from general shape of other curves.

5.6. Crystal Growing Procedure

Once the mould and furnace tube were out-gased and filled with

argon (as described earlier) the furnace tube was placed in the dropping cradle and allowed to pass through the furnace at a rate of approximately 4-10 cm./hr. This requires a time of approximately 10-4 hours. The furnace tube was then raised quickly through the furnace, removed from the cradle, and allowed to cool to room temperature. After it was completely cooled the tube was opened and the mould removed. It was necessary to exercise great care when opening the mould, since the copper sometimes had a tendency to stick to both sections of the mould. The crystal was carefully slid out of the open end of the half mould into a thin bore (5 mm.) glass tube which was then corked at both ends. These tubes were labelled as to sample number with attached adhesive tape tags and stored horizontally in a corragated rack to prevent rolling.

5.7. Cutting of Test and X-Ray Specimens

After a number of samples had been prepared, test specimens (approximately 1-1/4" long) and x-ray specimens (approximately 1/4" long) were cut from the single crystal wires and stored in glass tubes. The arrangement of cutting and labelling the samples is illustrated in Figure 37. The crystals were cut using a special acid saw designed to reduce to a minimum any bending of the crystal during the cutting operation. Figure 38 illustrates the basic operation of the acid saw and Plate XII shows a photograph of the completed unit. The cutting process is based

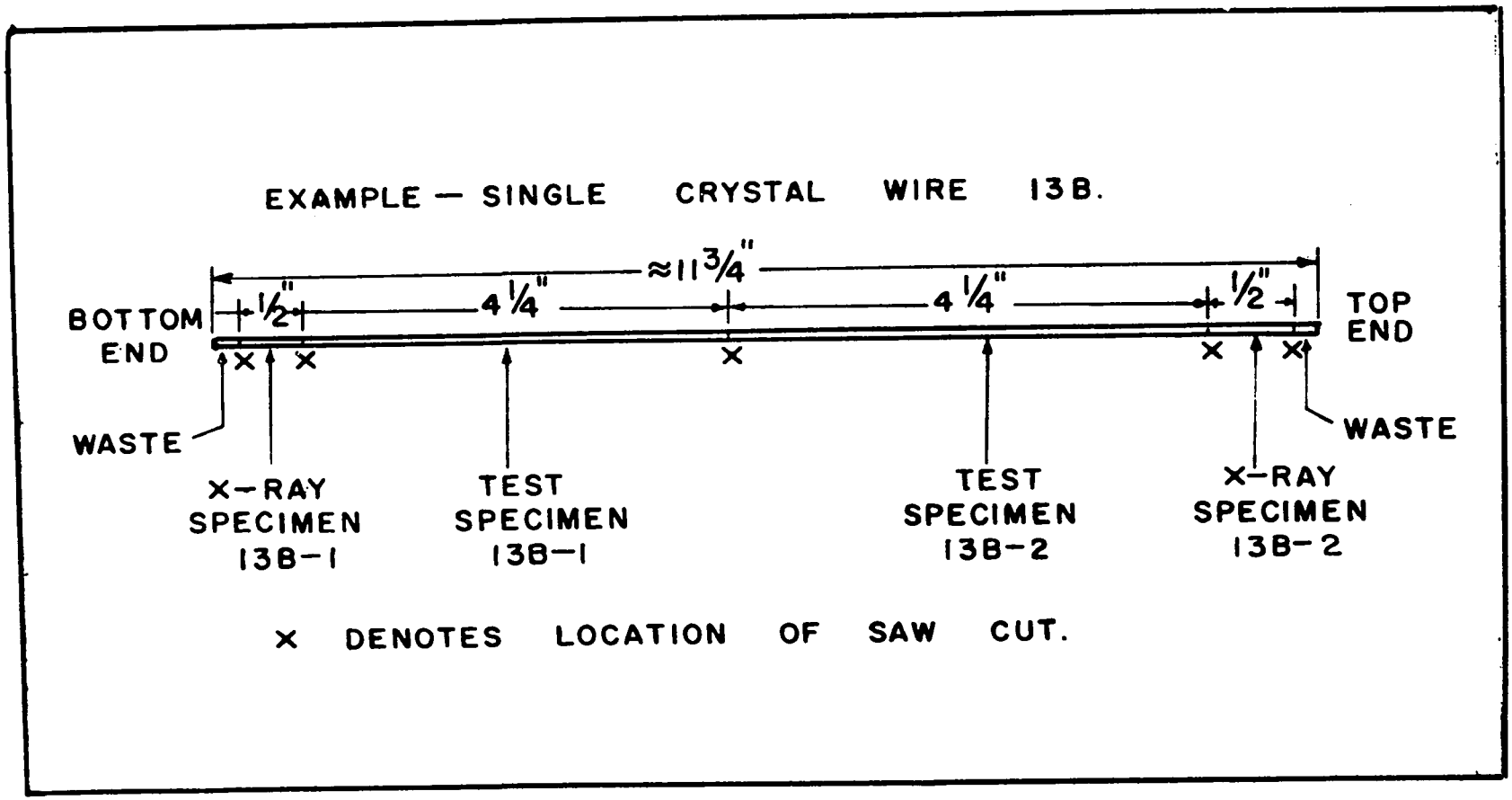

FIGURE 37 - ARRANGEMENT OF CUTTING AND LABELLING SAMPLES

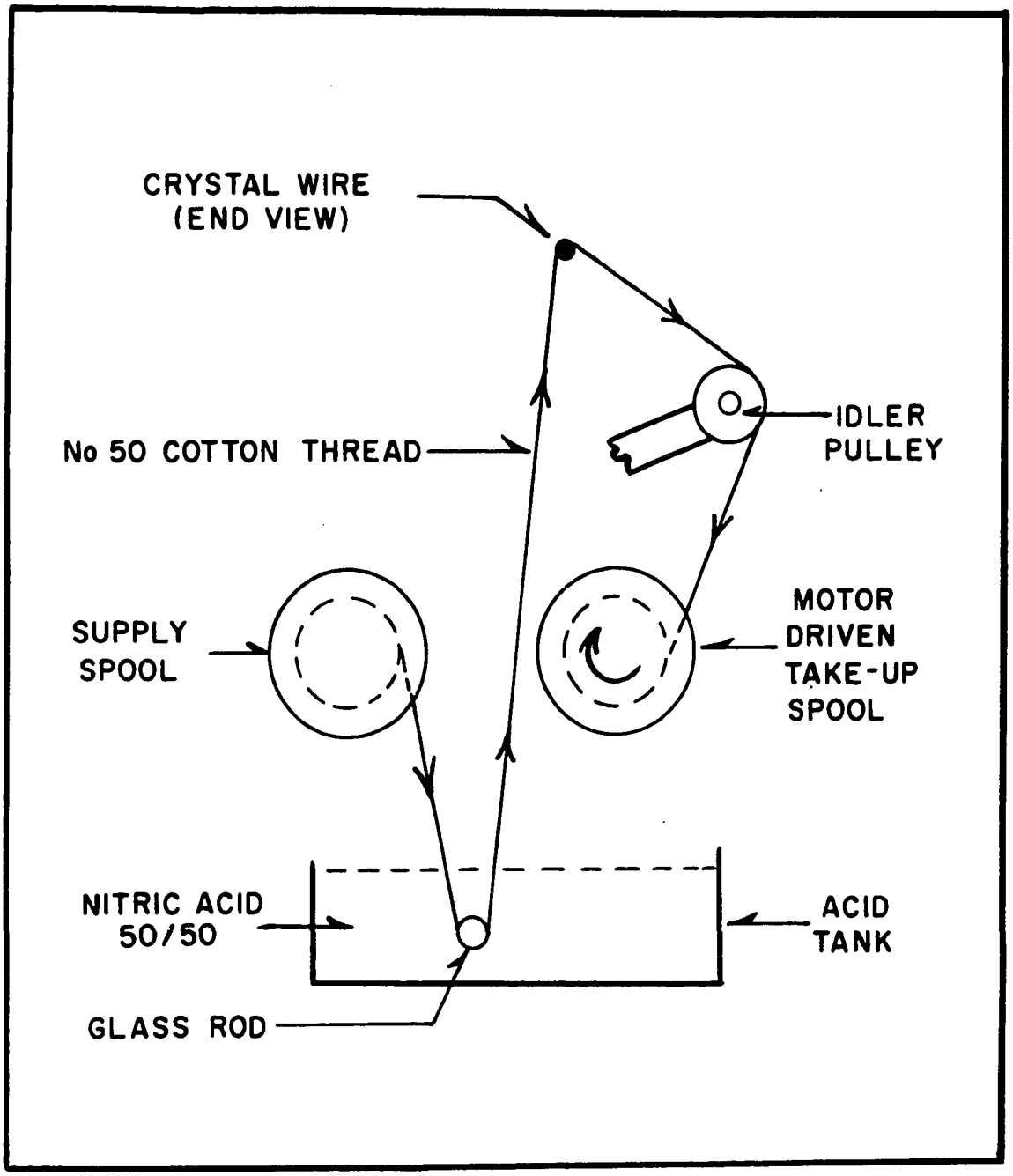

FIGURE 38- DIAGRAM ILLUSTRATING THE BASIC OPERATION OF THE ACID SAW.

PLATE XII

Photograph of Acid Saw for Cutting Single Crystal Wires.

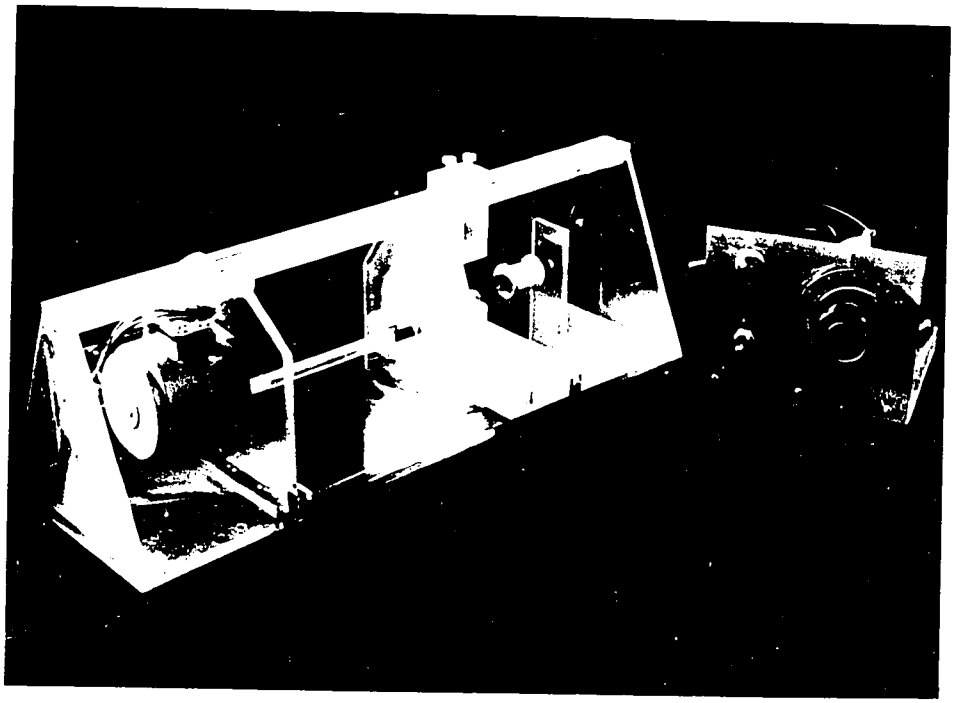

on the action of an acid soaked thread travelling across the crystal at a relatively slow rate. Most acid saws for this purpose use a continuous loop of thread, but in the case of fine wire crystals the tension in the loop necessary to turn it was found sufficient to cause bending of the crystal. It was therefore decided to use the arrangement illustrated in Figure 38. Here thread is unwound from a supply spool, passed through an acid tank, over the crystal and then wound on a take-up spool which is driven by an electric motor. With this arrangement very little tension is developed in the tread, only that required to unwind the supply spool. Number 50 cotton thread was used with an 80/20 concentrated nitric acid cutting solution and a linear thread speed of approximately 12 in./min.

6. Measurement of Single Crystal Orientations

The orientations of the single crystal wires with respect to the wire axis (tensile axis) were determined using x-rays and a rotating crystal camera*. Standard techniques for determining the orientation of single crystals are available in other publications (see for example Barrett (1943), Buerger (1942) and Schmid and Boas (1950)), in particular the method and analysis described by Schmid and Boas (1950) was employed. Only a few comments will be made on the technique as applied specifically to fine single crystal wires.

* X-ray Laboratory, Metal Physics Section, Mines Branch, Department of Mines and Technical Surveys, Ottawa, Canada.

The small x-ray specimen (approximately 1/4" long), previously cut from the single crystal wire, was carefully removed from the glass storage tube using tweezers and placed in a beaker of 50/50 nitric acid for 2 minutes. Tap water was gently flushed into the beaker for 1 minute, the specimen was then removed and allowed to dry on a filter paper. The specimen was mounted in plasticine on the goniometer of the x-ray camera, and standard procedure applied from then on. Great care was required in cleaning and mounting of the crystals to prevent bending, which, if it occurred would seriously complicate the analysis of the x-ray photograph.

In all cases cobalt K_α radiation was used (λ = 1.79 Å) on Ilford Industrial G-type film, with an exposure time of 45 minutes, and with the crystal rotating at 1 rpm. In most cases no filter was employed so that the K_β reflections were also visible on the film, but to a much lesser degree. An exposure was made with a polycrystal copper specimen using an iron filter, to eliminate the K_β reflections, and this was used to index the spots on the other single crystal photographs.

Table VII lists the different specimens prepared, the rate of crystal growth and the orientation angles of their tensile axes. Figure 39 shows these orientations plotted in the standard triangle of the steriographic projection.

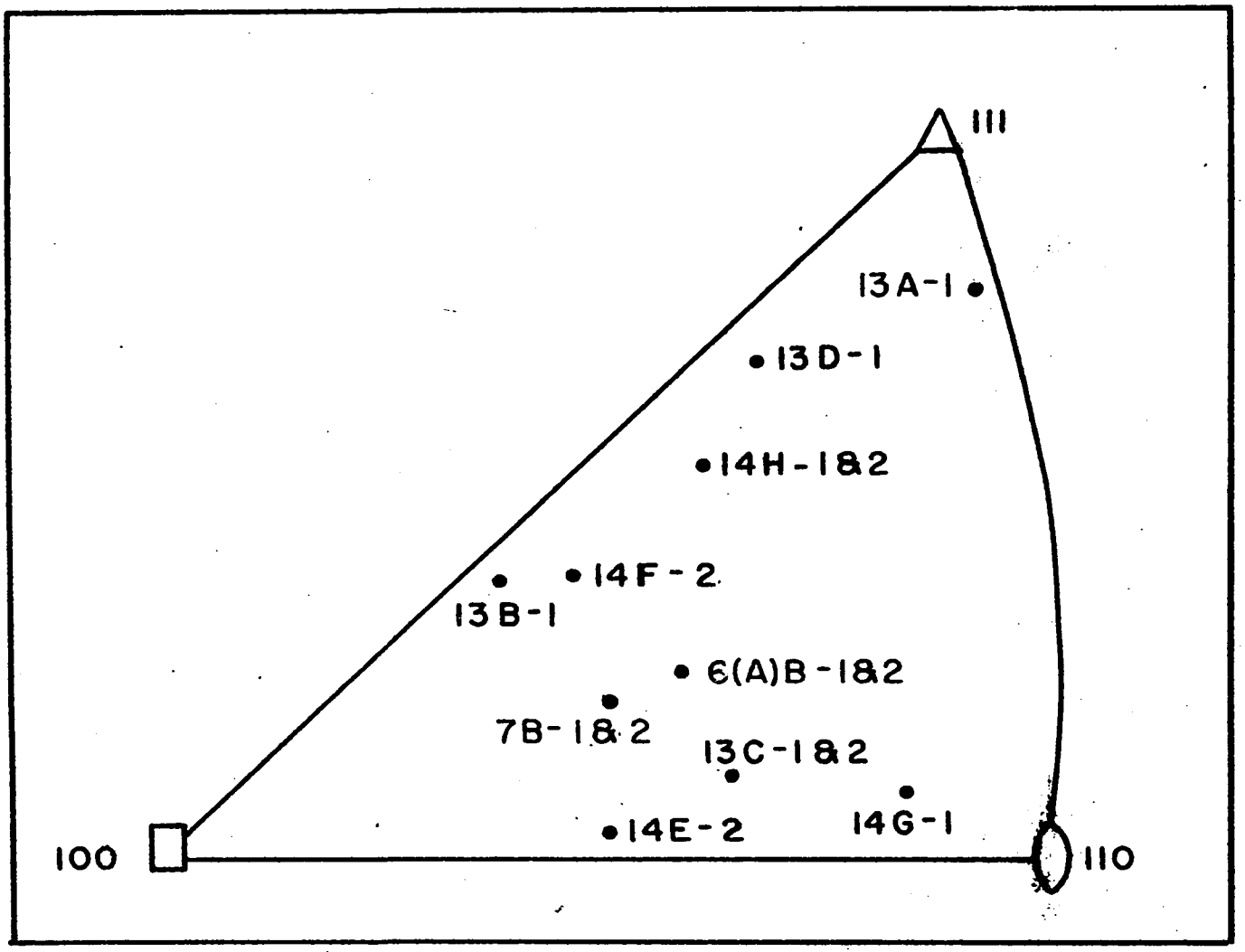

FIGURE 39 — ORIENTATION OF HIGH PURITY & ALLOY COPPER SINGLE CRYSTAL SPECIMENS

TABLE VII

Orientation Angles (λ and χ) for Single Crystal Specimens

Specimen Number	Type	R	λ	χ
		cm./hr	degrees	degrees
13A-1	Pure Cu	10	40	27
13B-1	" "	-	33	32
13C-1	" "	4	48	47
13C-2	" "	4	48	47
13D-1	" "	4	33	27
14E-2	" "	4	48	48
14F-2	" "	4	34	35
14G-1	" "	4	54	51
14H-1	" "	4	35	31
14H-2	" "	4	35	31
6(A)B-1	Cu-Ag	10	43	42
6(A)B-2	Alloy	10	43	42
7B - 1	" "	10	43	43
7B - 2	" "	10	43	43

R - rate of crystal growth.
λ - angle between tensile axis and the glide direction.
χ - angles between tensile axis and the glide plane.

7. Cleaning and Mounting of Finished Test Specimens

The test specimens previously cut to length, were stored in glass tubes until they were ready for testing. At that time the particular specimen was withdrawn by removing the plugs from both ends of the storage tube and gently pushing the crystal out onto a plastic 'V-block' saddle,

shown in Plate XIII. While located in the saddle the crystal was given the standard cleaning (as described previously) by dipping the saddle in dishes of the necessary fluids and finally drying with an electric hair dryer. The specimen was then placed in a pyrex tube, argon flushed, and annealed for 24 hours at 500°C in 1/2 atmosphere of argon. After the annealing, the specimen was allowed to slowly cool to room temperature.

A specimen mounting unit was constructed for the purpose of attaching the specimen and grips, and for supporting the specimen while it was being mounted in the creep apparatus. Plate XIV is a photograph of this unit dismantled showing the mounting frame, the brass 'V-block', the mounting jig and some specimen end-grips. The purpose of the mounting frame was to clamp the mounting jig in a fixed position, and to support and adjust the position of the specimen (which itself is supported on the brass 'V-block') relative to the mounting jig. The mounting jig consists of two chucks in which the specimen end-grips are clamped, and which may be adjusted in the horizontal plane. The mounting jig was designed to be removed from the mounting frame, and to fit into position in the yoke of the creep apparatus to allow a relatively strain-free transfer of the specimen. The end-grips consist of short lengths of brass rod drilled in one end to accommodate the test specimen (approximately 0.005" I.D. oversize) with a steel ring silver soldered into the other end for attachment to the creep

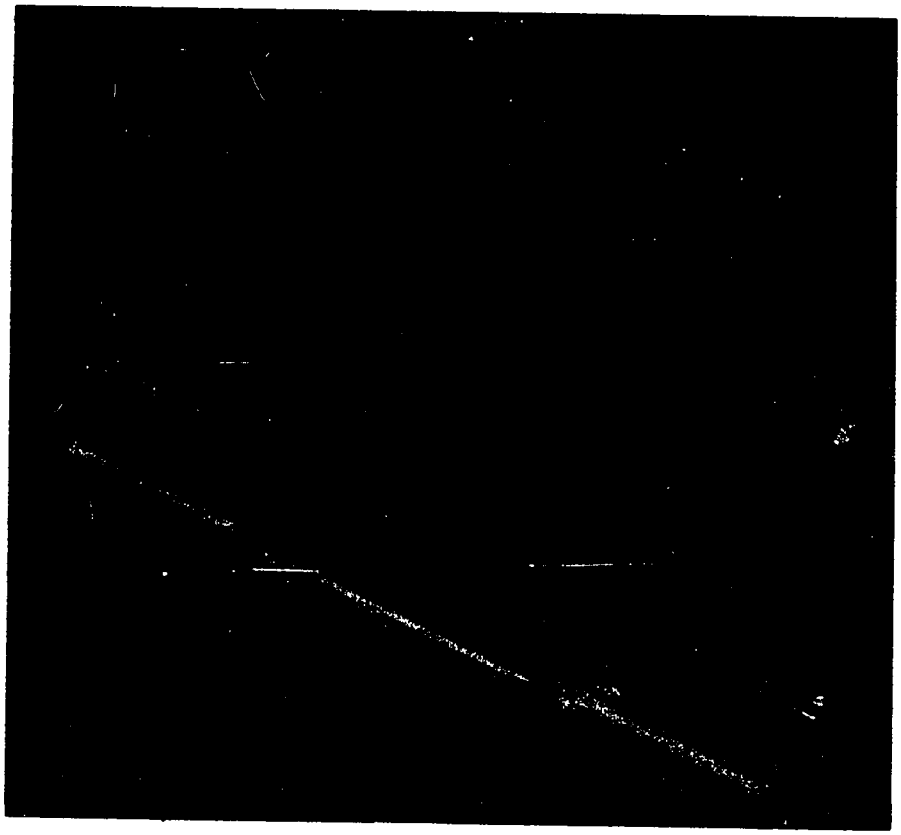

PLATE XIII

Plastic 'V-Block' Saddle Used to Clean Single Crystal Test Specimens.

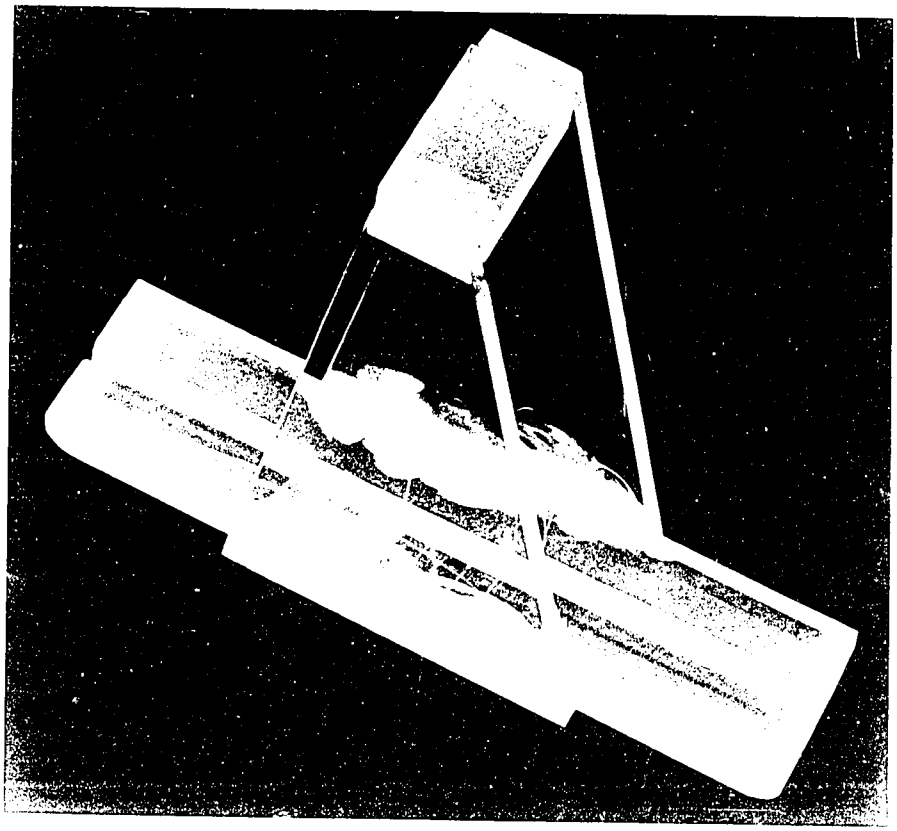

apparatus.

To mount the specimen it was first slid from the plastic saddle into the brass 'V-block', the 'V-block' was placed in position on the mounting frame, the mounting jig clamped in position and the end-grips clamped into the jig chucks. The specimen was carefully aligned by adjusting the vertical position of the 'V-block' and the end grips placed over the ends of the specimen leaving an exposed gauge length of approximately 10.4 cms. The chucks were then clamped in position. Plate XV shows the mounting unit at this stage. The end grips were attached to the specimen by first gently heating the ring-end of the grips with a fine oxyo-acetelene flame to the melting point of solder, great care being taken to ensure the flame does not contact the crystal. Then fine diameter resin flux solder (Ersin-60/40 type) was allowed to flow around the end of the grip and specimen. Finally the grip was heated gently (at the ring end) until the solder flowed well into the space between the specimen and the grip, leaving a surplus at the end of the grip of approximately 2 mm. This resulted in a final specimen gage length of 10 cms.

The mounting jig was removed from the mounting frame by first carfully lowering and removing the 'V-block', then unclamping the jig itself. The jig was placed in position in the yoke of the creep apparatus and the upper and lower end-grips engaged with the set of loading hooks on

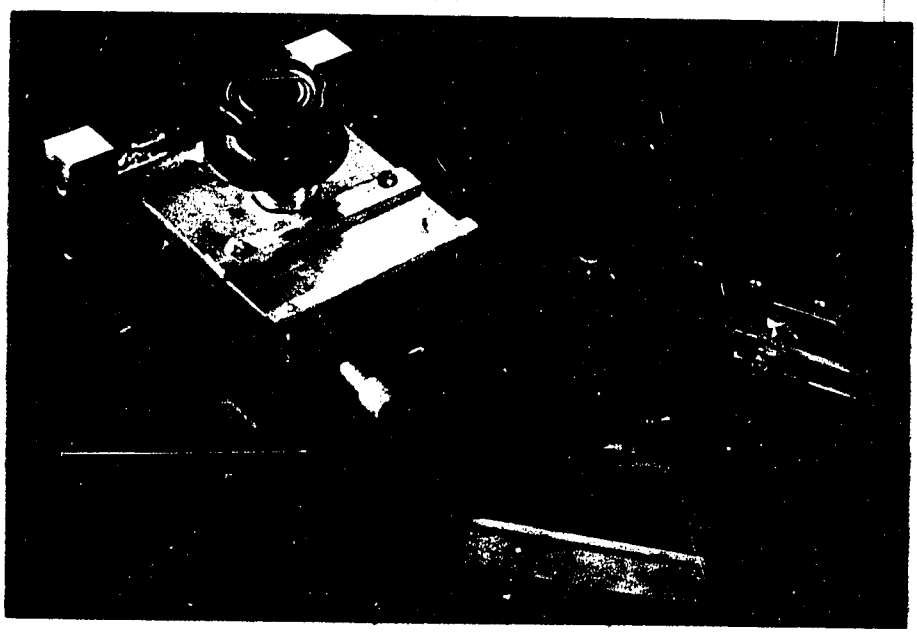

PLATE XIV

Specimen Mounting Unit Dismantled, Showing Component Parts.

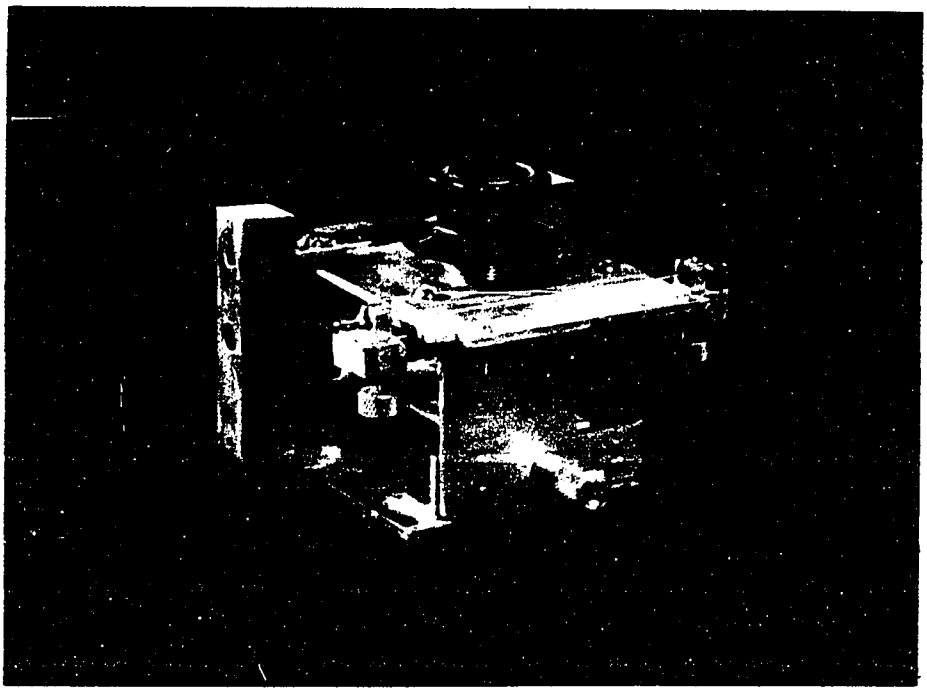

PLATE XV

Specimen Mounting Jig Assembled, Ready for Soldering-On of End Grips.

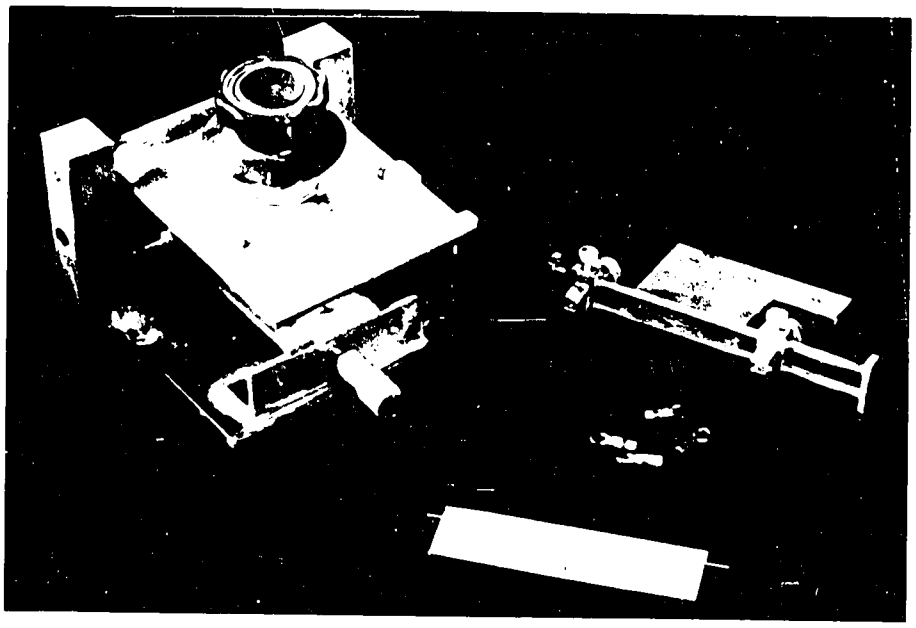

PLATE XIV

Specimen Mounting Unit Dismantled, Showing Component Parts.

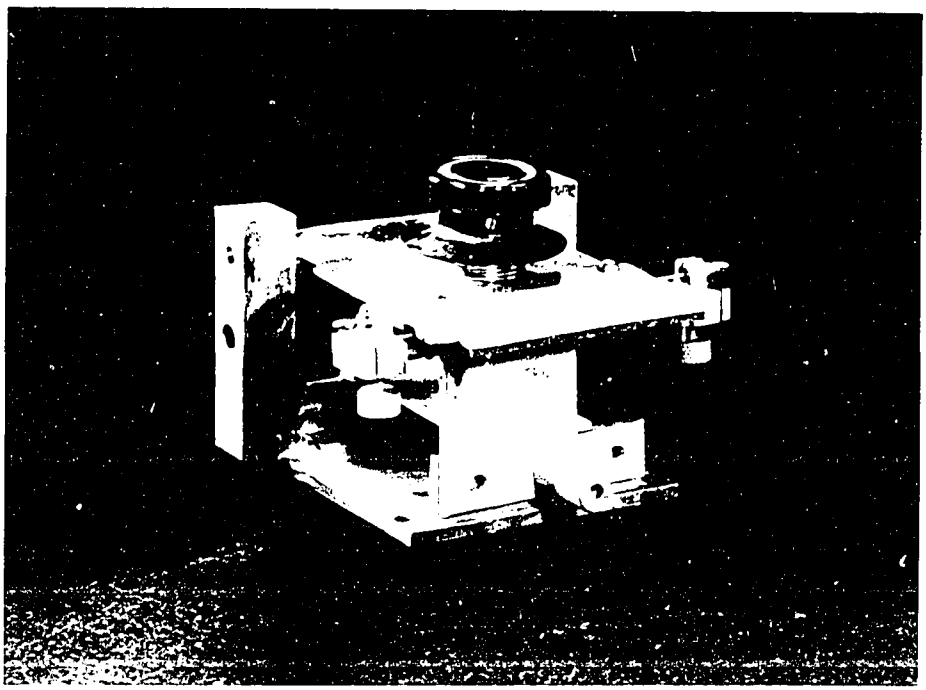

PLATE XV

Specimen Mounting Jig Assembled, Ready for Soldering On of End Grips

the creep apparatus. To release the specimen the end grips were first released from the chucks and then the chucks themselves were brought together. The jig was then withdrawn leaving the specimen ready for testing.

8. Checking Homogeneity and Impurity Concentration of Alloys

Although the alloys were carefully prepared it was considered necessary to check on their homogeneity, and impurity concentration, at various stages of specimen preparation. After the alloy ingots were prepared, the irregular pieces were removed from the top and bottom of each for spectrographic analysis. As mentioned previously, due to the lack of good copper spectrographic standards, the spectrographic data must be considered only relative. However this should still allow a determination the homogeneity of the solute in the ingot to be made. The average deviation between the analysis of the top and bottom samples was less then 8%, six of the alloys showing no deviation at all. It was felt therefore, considering the accuracy of the spectrographic analysis, that the alloy ingots were homogeneous.

After the ingots had been drawn into wire it was decided to make an accurate determination of the impurity concentration using the residual resistance ratio method. In this technique the resistance of a specimen in the form of a thin tape (approximately 1/1000" x 1/8" x 2" long)

rolled from the alloy wire and annealed for 24 hours at 500°C in argon was measured at room temperature (R_{RT}) and at liquid helium temperature ($R_{4.2}$) using an apparatus standard in this laboratory. The impurity concentration in solid solution in the alloy is given by a function of the ratio $R_{4.2}/R_{RT}$. Pure copper should exhibit a low value, in the range of 10^{-3}, a value of 1.57×10^{-3} was found for Sample 14. Figure 40 and 41 show the resistance ratio function* $\frac{R_{4.2}/R_{RT}}{1-(R_{4.2}/R_{RT})}$ plotted against the percent atomic concentration of silver and gold impurity which were put in the original alloy ingot melts. Also shown on these graphs is the impurity concentration obtained from a spectrographic analysis. The deviations of the spectrographic data is obvious. The results for the copper-gold alloys fit a straight line extremely well, in the case of the copper-silver alloys the fit is not as good but the deviation is less then 15%. These results indicate that the alloys still have the required impurity concentration, and the curves should now provide a scale by which the impurity concentration of the alloy single crystals may be determined.

When single crystals are grown from the melt there tends to be an impurity gradient between the melted and the unmelted material. The impurity concentration of the melted zone rises and 'sweeps' a percentage

* This function is necessary to obtain a linear plot, since $R_{4.2}/R_{RT}$ deviates from linearity at the higher values of impurity ($> 0.$ at.%).

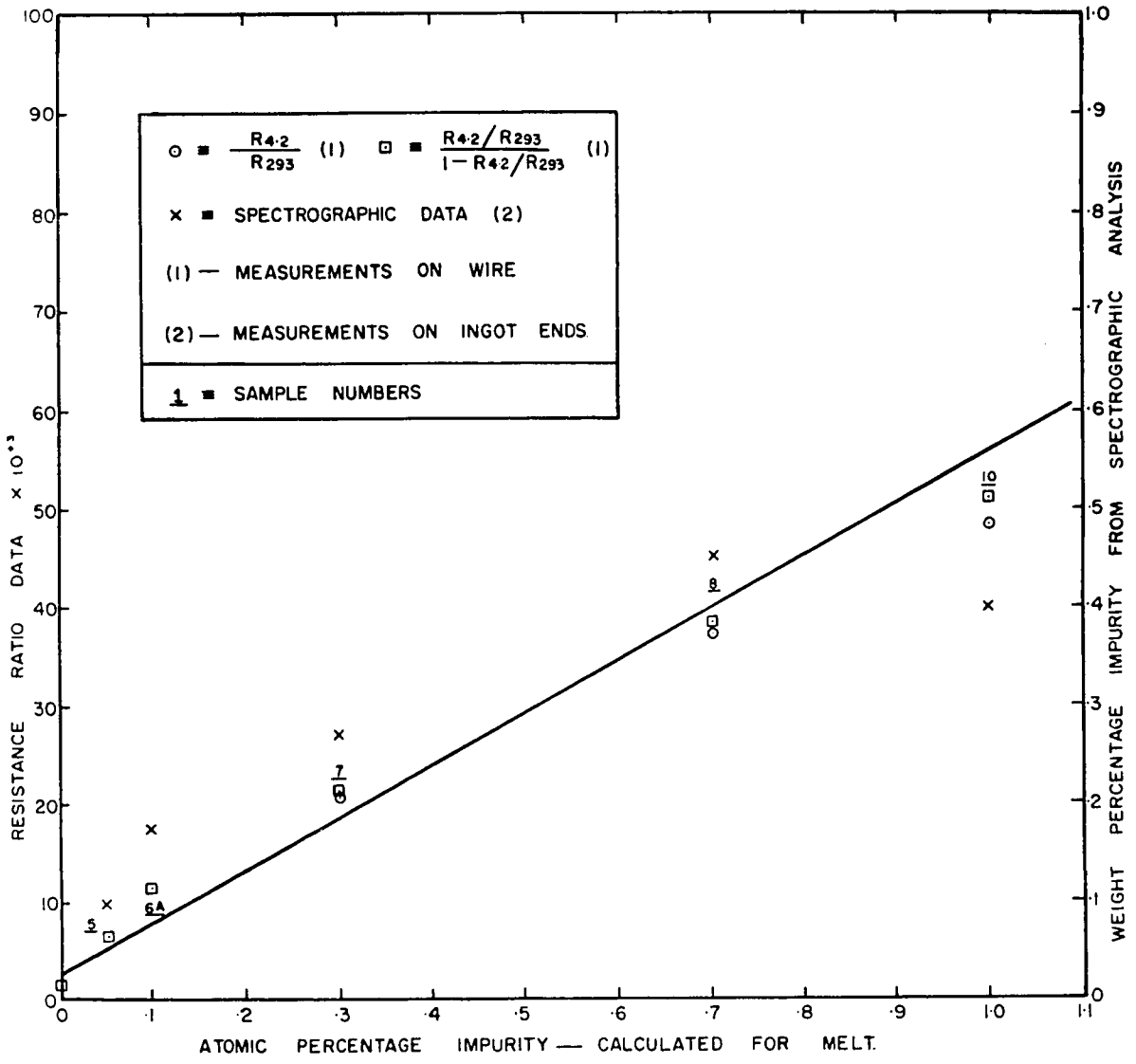

FIGURE 40 - IMPURITY CONCENTRATION FOR COPPER - SILVER ALLOYS DETERMINED FROM RESIDUAL RESISTANCE RATIO MEASUREMENTS AND SPECTROGRAPHIC ANALYSIS.

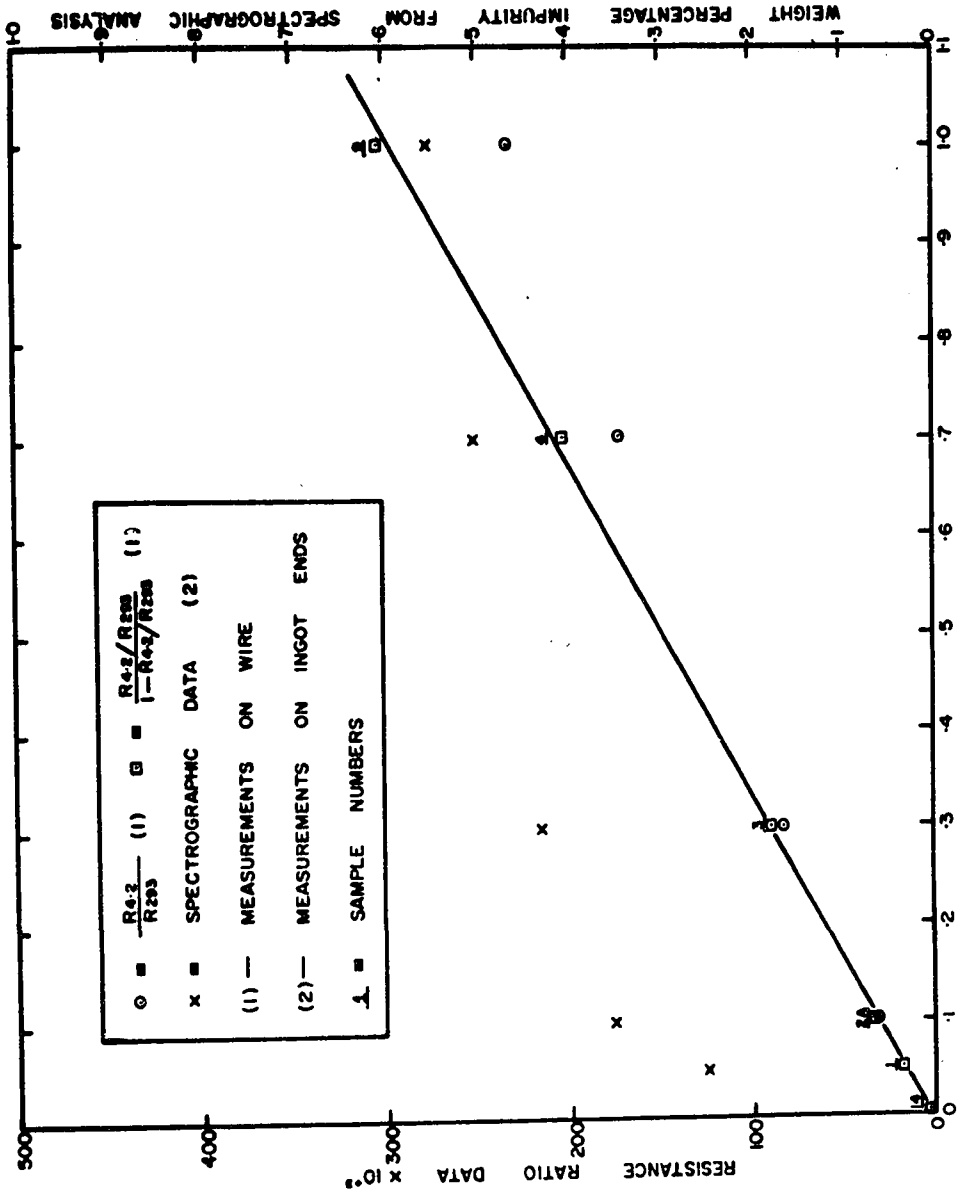

FIGURE 41 - IMPURITY CONCENTRATION FOR COPPER-GOLD ALLOYS DETERMINED FROM RESIDUAL RESISTANCE RATIO MEASUREMENTS AND SPECTROGRAPHIC ANALYSIS.

of the impurity atoms along with it, as it moves along the specimen*. Therefore the impurity concentration of the single crystal may be lower than the alloy wire from which it was grown. It was therefore considered necessary to check the impurity concentration of each single crystal. Since it would be very difficult to measure the resistance ratio on the specimen before the creep test without damaging it, the alternate procedure of measuring the residual resistance ratio after the creep test was adopted. In this case the residual resistance specimens were prepared by rolling the single crystal wires into thin tapes, after the deformation experiments had been carried out, and preparing and testing them in the same manner as the polycrystalline wire samples described earlier.

Studies made on a number of single and polycrystal specimens have shown that single crystals grown from a polycrystal alloy have an average residual resistance ratio much higher than the original, as well as a variation in this property along their length.

The residual resistance ratio values obtained for two copper-silver alloy single crystals were found to be four or five times as large as the values determined originally on the polycrystalline alloy material. The original values for polycrystal specimen 6(A)B-1 (0.1 at. % silver) and 7B+1(0.3 at. % silver) were approximately 11×10^{-3} and 20×10^{-3} whereas the values for the single crystals were approximately 65×10^{-3}

* Observed in some metals but not all.

and 94 x 10^{-3} respectively. This increase cannot be explained by an annealing or other contamination effect since differences between polycrystal and single crystal specimens of pure copper have never exceeded 10 x 10^{-3}.

The residual resistance ratio was also measured at a number of points along the length of the two alloy single crystal samples (6(A)B-1 and 7B-1). In both cases a variation was noted. Sample 6(A)B-1 showed a value of 49 x 10^{-3} at the lower end increasing continuously up to 76 x 10^{-3} at the upper end. Sample 7B-1 showed a value of 85 x 10^{-3} at the lower end increasing continuously up to 109 x 10^{-3} at the upper end.

As mentioned earlier in this section the residual resistance ratio values do not appear to represent the alloy concentration directly but are related to it in some manner. It does appear however that a very definite relationship does exist since the variation of the residual resistance ratio follows the same trend as would be expected for the variation of impurity concentration. This behaviour can not be further discussed with the small amount of data available. Unfortunately it makes it impossible to use the original residual resistance ratio versus alloy concentration curves for determining the alloy concentration of the single crystal test specimens. Instead test specimens will be referred to in terms of their nominal alloy concentration and/or their measured residual resistance ratio values.

CHAPTER IV

RESULTS AND CONCLUSIONS

1. Introduction

Tests were conducted on a number of copper and copper-silver alloy single crystal specimens using the completed apparatus. These tests were useful for two purposes, first they provided experimental data by which the actual operation of the apparatus could be judged, and secondly the data obtained enabled a preliminary determination to be made of the strain rate sensitivity factor (K_3) and the strain hardening coefficient (θ) for pure copper and some copper-silver alloys using the incremental transient creep method. Data was obtained illustrating the variation of K_3 with applied stress, temperature, and impurity concentration over a limited range of these variables.

2. Analysis of Experimental Data

The incremental loading method is illustrated in Figure 41A. The temperature of the specimen is held constant, and the applied stress on the specimen is increased until it begins to show pronounced creep (point A) and a transient creep curve (A-C) is produced. A small addition is then made to the applied load (point C(D)) which generates a new transient creep curve (D-F). At a later point (point F(G)) the same process may be repeated. The important factors involved are the following:

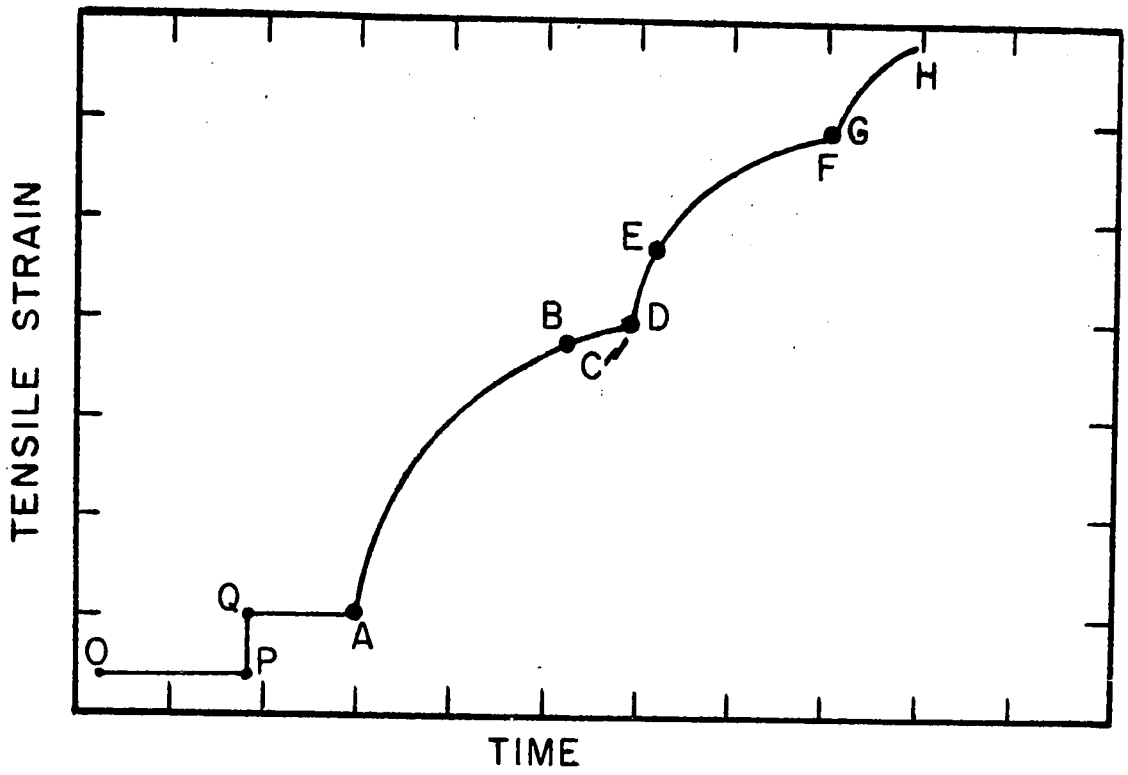

FIGURE 41A-TYPICAL TRANSIENT CREEP CURVES FOR AN INCREMENTAL LOADING EXPERIMENT.

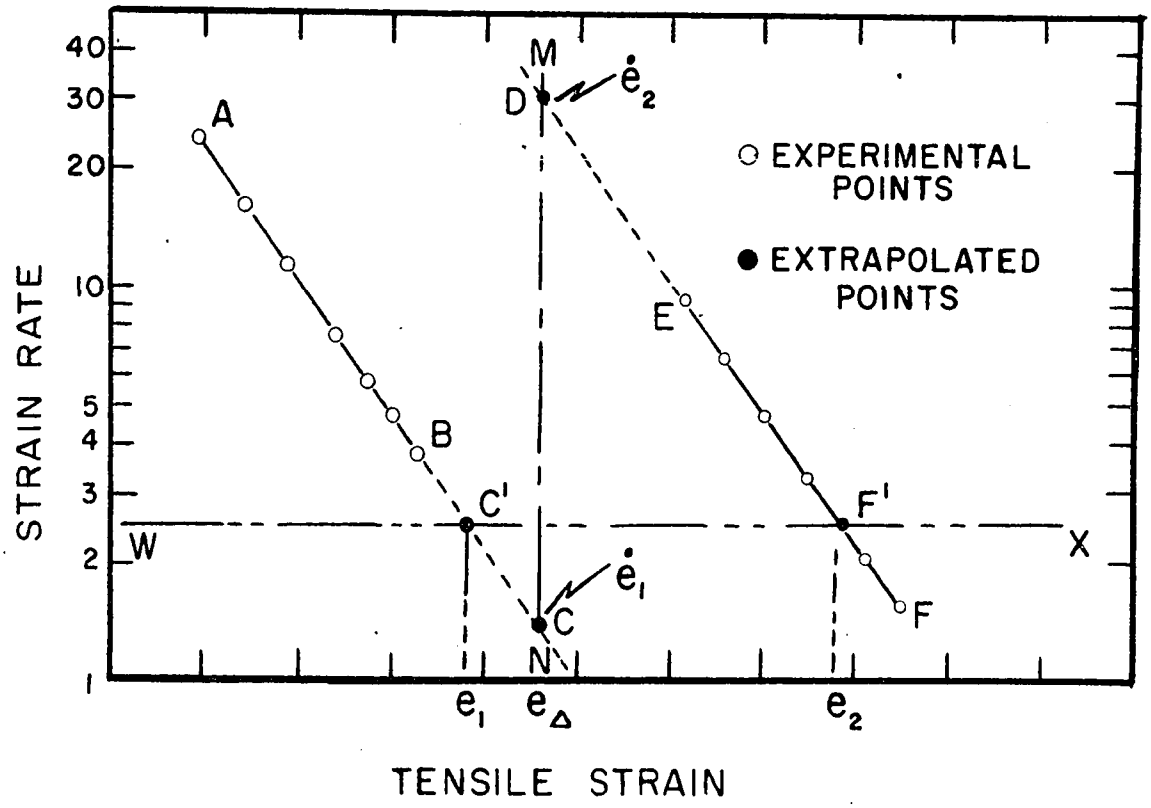

FIGURE 41B-GRAPHICAL METHOD OF OBTAINING THE REQUIRED DATA FROM THE TRANSIENT CREEP CURVES.

T - the specimen temperature,

σ - the initial applied stress,

$\Delta\sigma$ - the incremental stress (applied at the point D),

$\dot{e}_1 + \dot{e}_2$ - the strain rates (slope of the creep curve) at the point D, just before and just after the stress change. ($\dot{e}_2$ was defined as the maximum strain rate regardless of whether it was the initial or the final).

Δe - the strain which occurs between two points of equal strain rate (some convenient value $\dot{e}_a$) on the initial and final creep curves.

Similar data may be obtained by making small decreases in the applied stress. In fact a method of cyclic incremental loading, where the incremental load was alternately applied and removed, was employed with success during some of the experiments. There appeared to be some difference in the results depending on whether there was an increase or decrease in the applied load. This point will be discussed later in the thesis.

The values of $\dot{e}_1$, $\dot{e}_2$ and Δe could be determined directly from the transient creep curves, however the accuracy of the results would be extremely low. Instead the method of 'graphical differentiation' described by Sherby et al (1955) was employed. This consists of plotting the logarithm of the strain rate as a function of the specimen strain.

The resulting curve for an incremental loading experiment is shown in Figure 41B. It is made up of two straight lines, section A-B before the load change and E-F after it. The points shown were obtained by measuring the slope of the transient creep curve at the respective values of strain. The vertical line MN ($e = e_\Delta$) represents the strain at which the incremental load was applied. As it is difficult to measure the strain rate near the point of load change an extrapolation must be made. As shown (see Figure 41B) the line AB was extrapolated and intersected line MN at C, and the line EF was extrapolated and intersected line MN at D. These two intersections are the required values of strain rate $\dot{e}_1$, and $\dot{e}_2$ respectively. The value of Δe ($=e_2-e_1$) for a strain rate of $\dot{e}_a$ is found from the intersection of ABC and FED with the horizontal line WX ($\dot{e}=\dot{e}_a$).

It should be noted that the original experimental data (stresses and strains) are in tensile form. This data must be converted to its resolved form (see Appendix I), in terms of the crystal orientation, in all cases except where it appears in ratios like $\frac{\Delta\sigma}{\sigma}$, $\frac{\dot{e}_2}{\dot{e}_1}$, etc.

The strain rate sensitivity factor (K_3) was determined from the experimental values of $\tau, \sigma, \Delta\sigma, \dot{e}_1$ and $\dot{e}_2$ using the formula:

$$K_3 = \frac{1}{\tau}\left(\frac{\Delta\sigma}{\sigma}\right)\left(\frac{1}{\ln(\dot{e}_2/\dot{e}_1)}\right) \qquad (17)$$

where all factors have been defined previously.

The strain hardening coefficient θ (the slope of the stress-strain curve) was also determined from the creep data using the formula:

$$\theta = \frac{\Delta\sigma}{(e_2 - e_1)_a} \quad , \qquad (18)$$

where all the factors have been previously defined. This factor was useful as an indication of whether the specimen was deforming in the easy glide region ($\theta \lesssim 2000$ gm/ mm^2) or in the linear hardening region ($2000 \leq \theta \leq 15,000$ gm/ mm^2).

The calculated values of K_3 and θ along with other associated data were tabulated for the individual test specimens in Appendix II. Where a group of tests gave very similar results an average value and standard deviation was determined.

3. Experimental Results

Values of the strain rate sensitivity (K_3) and the strain hardening coefficient (θ) were determined (see Appendix II) for a polycrystal specimen of pure copper and for single crystals of pure copper and copper-silver alloys. These factors were determined for temperatures ranging from 300 to 78°K. and over a stress range up to approximately 2000 g/ mm^2.

3.1 Consistancy of Results

At each value of applied stress a number of incremental loadings were made, and the average value of K_3 and its standard deviation determined for this stress. It was found that the percent standard deviation varied from 5% to 20% of the mean, with increasing values of K_3. Using the constant strain rate technique (on Basinski's Apparatus at the National Research Council) percent standard deviations of 9% were observed. The larger deviations obtained using the transient creep method were thought to be due to (a) the error involved in the graphical method of reducing the creep data, (b) the difficulty in accurately applying or removing the secondary loads, and (c) the presence of electrical and mechanical noise.

3.2 Effect of the Magnitude of the Secondary Load

The magnitude of the incremental or decremental secondary loads apparently does not influence the experimentally determined values of K_3. Secondary loads ranging from approximately 4 to 17 gms appear to give very similar results. In some cases (single crystals in the easy glide region) a strain rate change of 10^5 (10^{-6} sec^{-1} to 10^{-1} sec^{-1}) produced by a 16.65 gm load change gave approximately the same result as a strain rate change of 10^2 due to a smaller load change.

3.3 Effect of the Sign of the Secondary Load

Slightly different values of K_3 were obtained, for any particular specimen, depending on whether the secondary load was added or removed. In many cases (but not always) the value was less when the load was removed. A similar situation was observed using the constant strain rate method. Lower values of K_3 being obtained when the strain rate was reduced (resulting in a decrease in flow stress).

3.4 Comparison of Results from Transient Creep, Constant Strain Rate, and Stress Relaxation Experiments

A number of workers have published experimental values of K_3 obtained from either transient creep or constant strain rate experiments. It has been assumed, but never shown, that the results obtained by the two methods were similar. Since facilities were available to carry out both types of tests as well as stress relaxation tests, it was decided to conduct a short study to compare the values of K_3 obtained by the three methods. This study consisted of a series of experiments on a copper single crystal specimen* (14H-2) in the following order: a) transient creep, b) constant strain rate, c) stress relaxation, and d) transient creep. The constant strain rate and stress relaxation experiments were

---

* High purity, oxygen free copper, for details on composition and orientation see previous chapter. This specimen apparently did not exhibit any easy glide deformation due to its particular orientation.

carried out on Basinski's apparatus at the National Research Council. Figure 42 shows the results of this series of tests (see also Table XI, Appendix II). The values of K_3 obtained were as follows: initial creep test - $K_3 \approx 1.1$, constant strain rate test - $K_3 \approx 1.14$, stress relaxation test - $K_3 = 1.47$, final creep test - $K_3 \approx 0.93$.

The constant strain rate and stress relaxation results appear consistent with the initial and final creep results, although the value obtained by the stress relaxation method appears to be on the high side. The difference between the results obtained from the initial and final creep experiments is probably due to the fact that K_3 was a decreasing function of stress in the range investigated. Therefore within the limitations of this set of experiments it appears that comparable values of K_3 may be obtained using transient creep, constant strain rate, and stress relaxation methods.

3.5. Variation of K_3 with Stress

The variation of K_3 with stress was investigated for three groups of specimens.

Group I consisted of two copper single specimens, 14H-2* and 14F-2*. The orientation of these crystals fell very near the (100) - (111) line in the orientation triangle and as expected they showed no obvious easy glide region. The values of Θ ranged from 6000-20,000 g/mm^2 in-

* High purity, oxygen free copper, for details of orientation, and residual resistance ratio see Tables IV and VIII respectively.

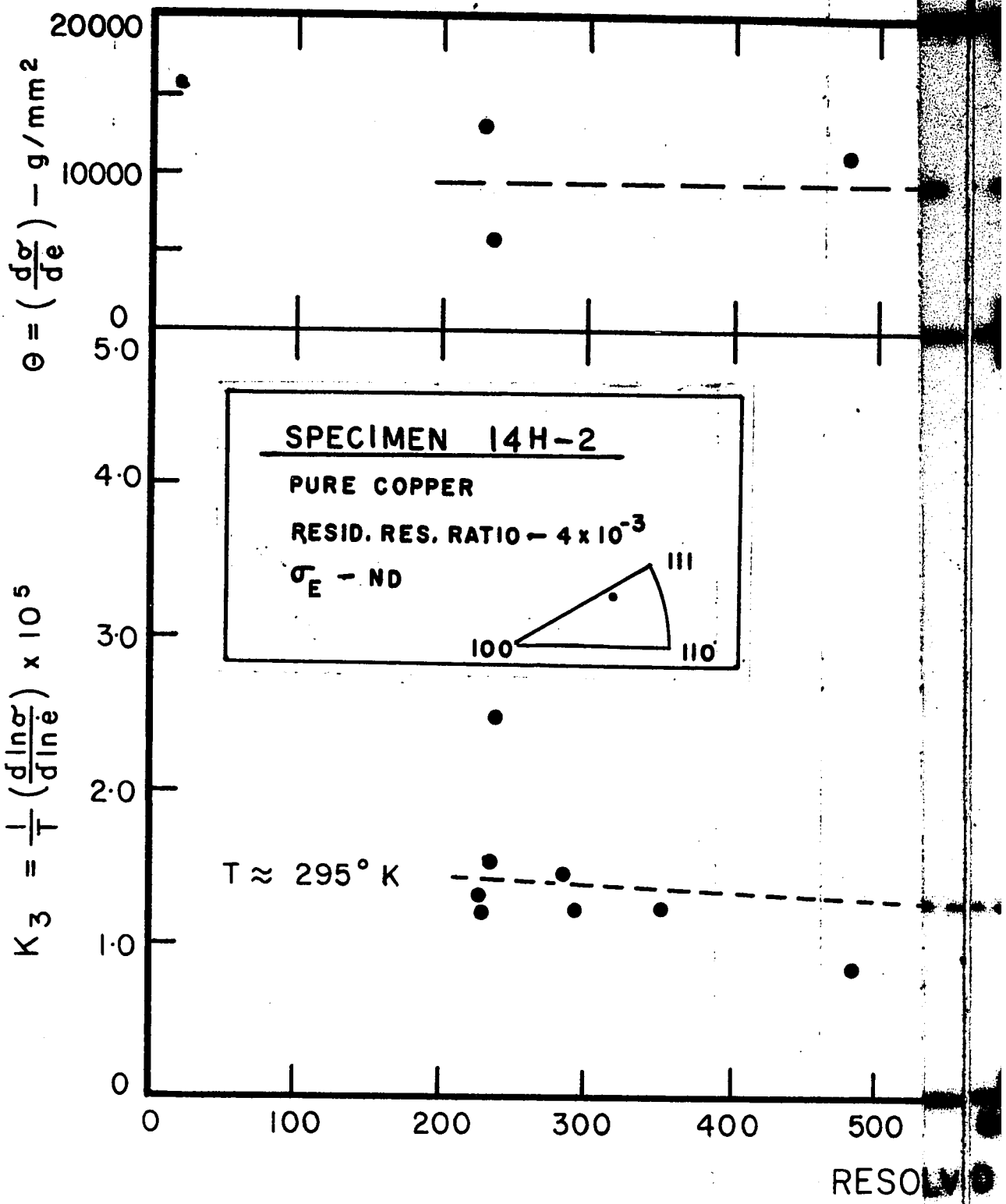

FIGURE 42 — VARIATION OF THE SENSITIVITY (K_3) WI

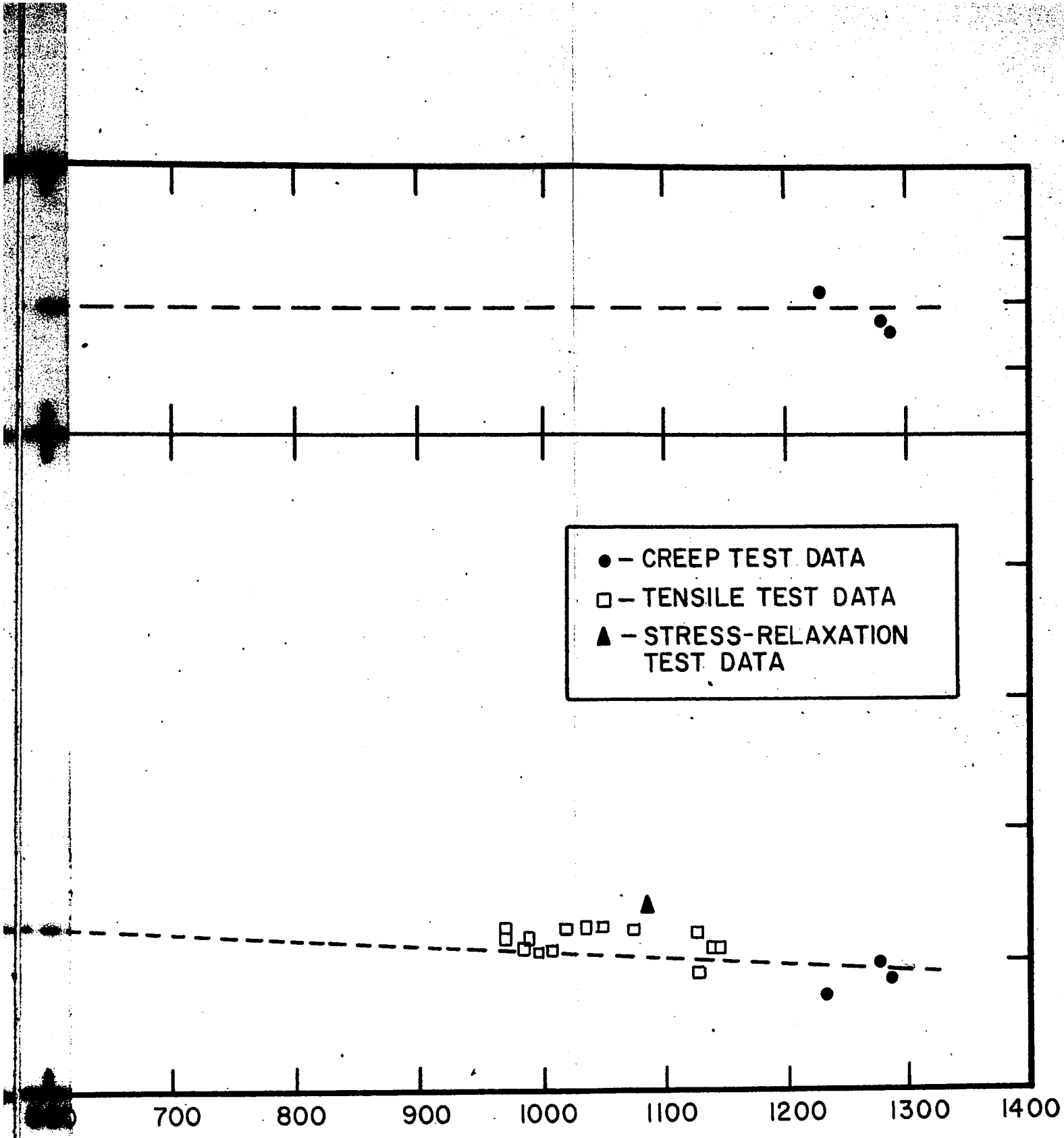

ENING COEFFICIENT (Θ), AND THE STRAIN RATE
HE RESOLVED SHEAR STRESS, FOR SPECIMEN 14H-2

dicating the specimens were in stage II deformation. Experiments conducted at 295°K (see Tables XI and XII) indicate that in the stress range of approximately 200-1300 g/ mm^2, K_3 was a decreasing function of applied stress (see Figures 42 and 43). Values of K_3 varied from 1.5 (at 200 g/ mm^2) to 0.8 (at 1300 g/ mm^2) with a percent standard deviation of 10-15%.

Group II consisted of four copper single crystals: 13C-1* 13C-2*, 14E-1* and 14G-1* whose orientations were in or very near the region of unperturbed glide. The values of Θ ranged from 1000- 2000 g/ mm^2 for specimens 14E-1 and 14G-1. Experiments conducted at temperatures from 295 - 80°K (see Tables XIII to XVI) indicated that K_3 was a decreasing function of stress over the range 200 to 1200 g/ mm^2 (see Figures 45 to 47). Values of K_3 for 295°K varied from 1.7 down to 1.3 over this stress range. At 80°K the variation was even more pronounced, K_3 varying from 5.2 down to 1.7 over approximately the same stress range. The data exhibited a percent standard deviation from 15-30%. It should be noted that the apparent increase of K_3 with stress for specimen 13C-2 (Figure 45) at 80°K is probably due to experimental error, and the fact that the behaviour was not studied over a wider range of stress.

---

* High purity, oxygen free copper, for details of orientation and residual resistance ratio see Tables IV and VIII respectively.

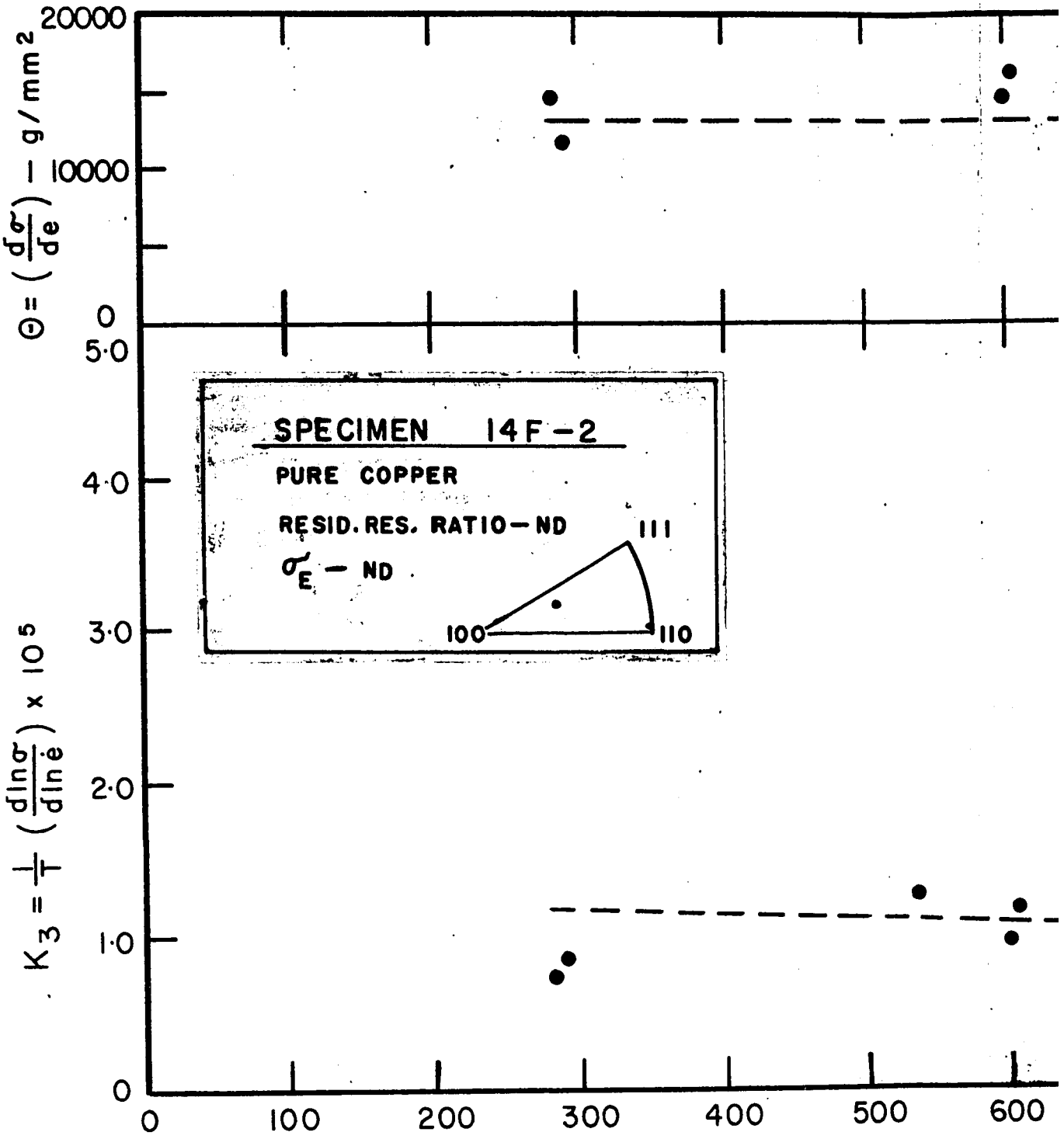

FIGURE 43 – VARIATION OF THE HARDE
SENSITIVITY (K_3) WITH RE

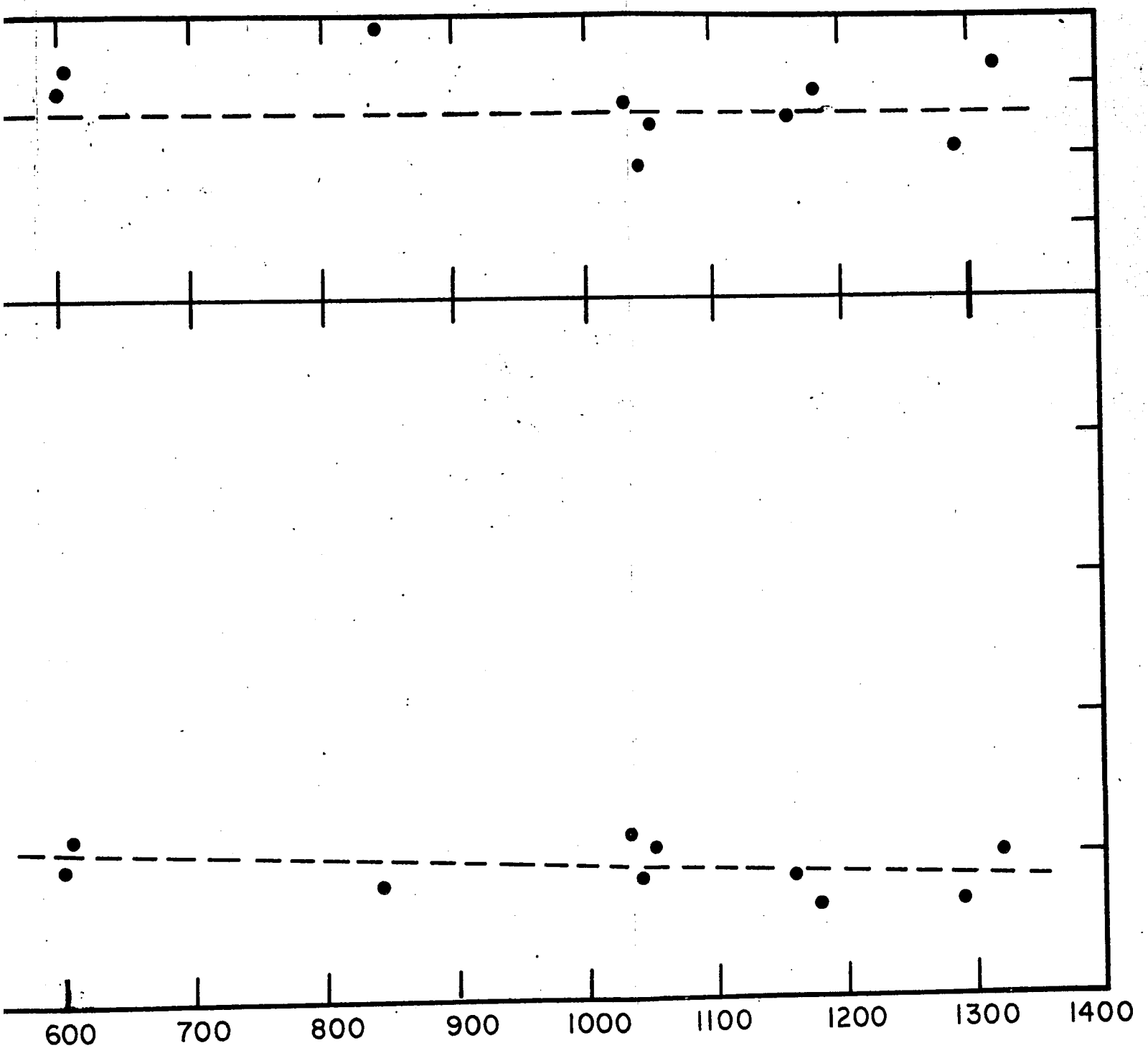

EAR STRESS — g/mm^2

HARDENING COEFFICIENT (Θ), AND STRAIN RATE

H RESOLVED SHEAR STRESS, FOR SPECIMEN 14F-2

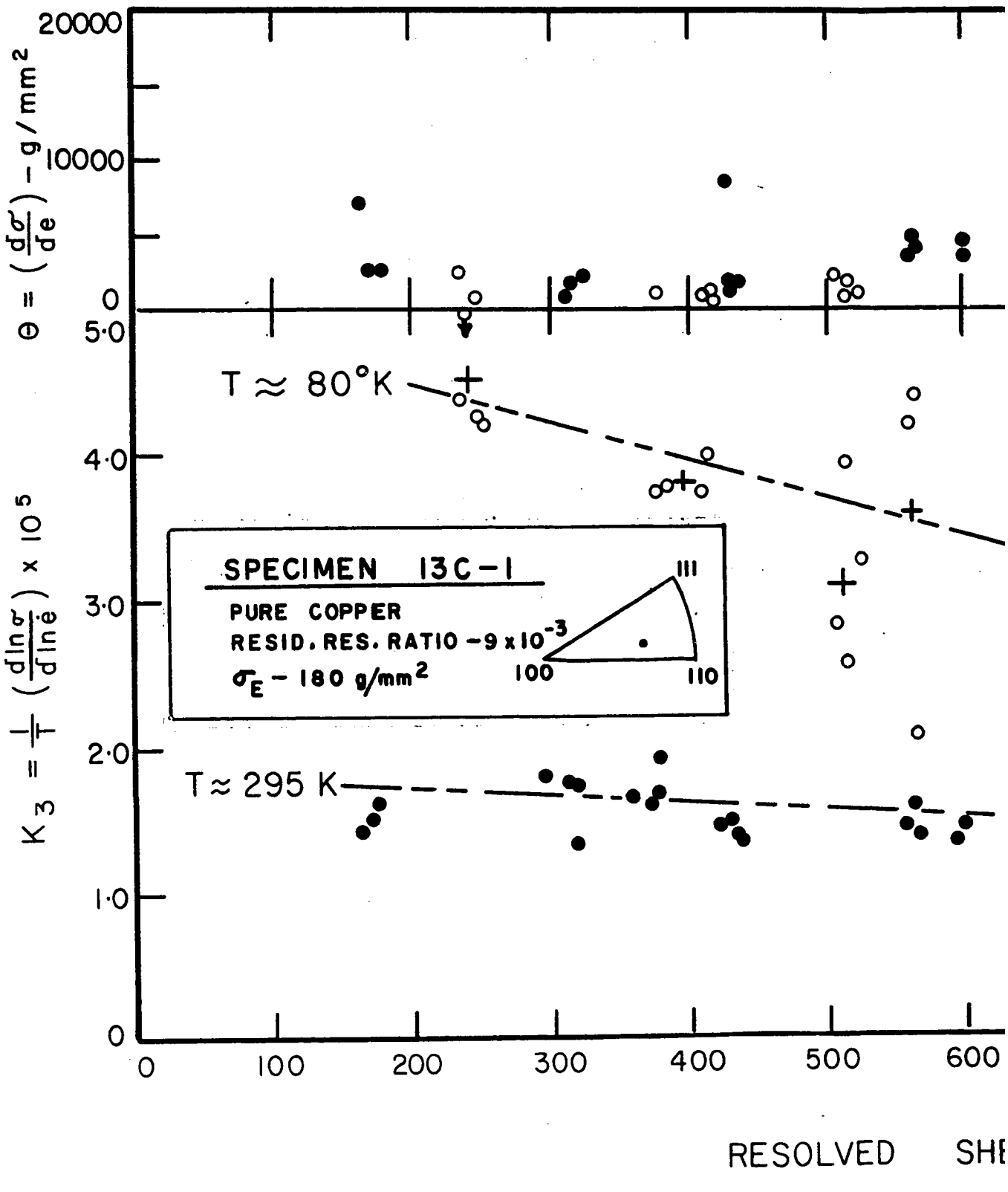

FIGURE 44 — VARIATION OF THE HARDENING
SENSITIVITY (K_3) WITH THE F

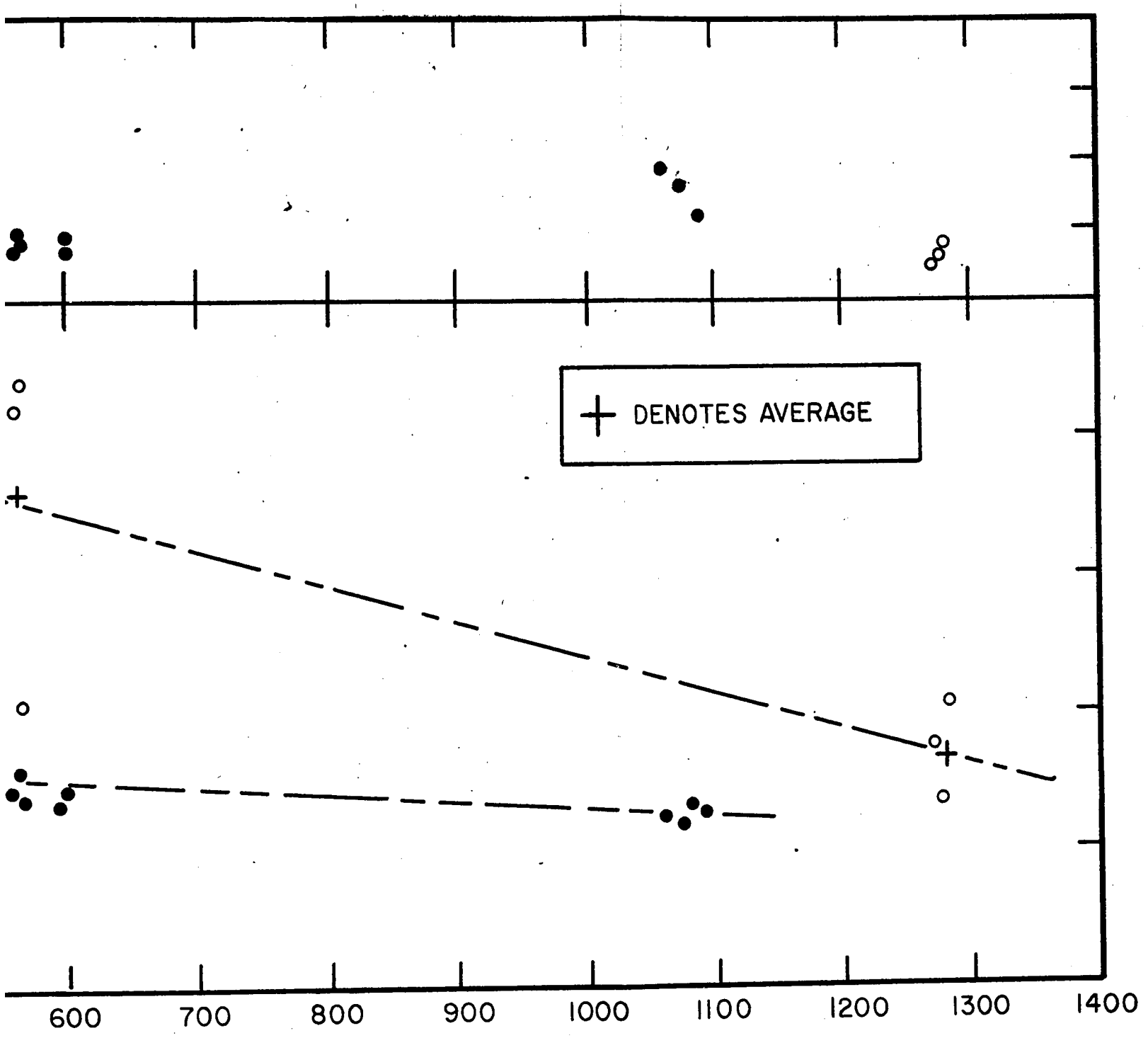

ENING COEFFICIENT (Θ), AND THE STRAIN RATE
THE RESOLVED SHEAR STRESS, FOR SPECIMEN 13C-1

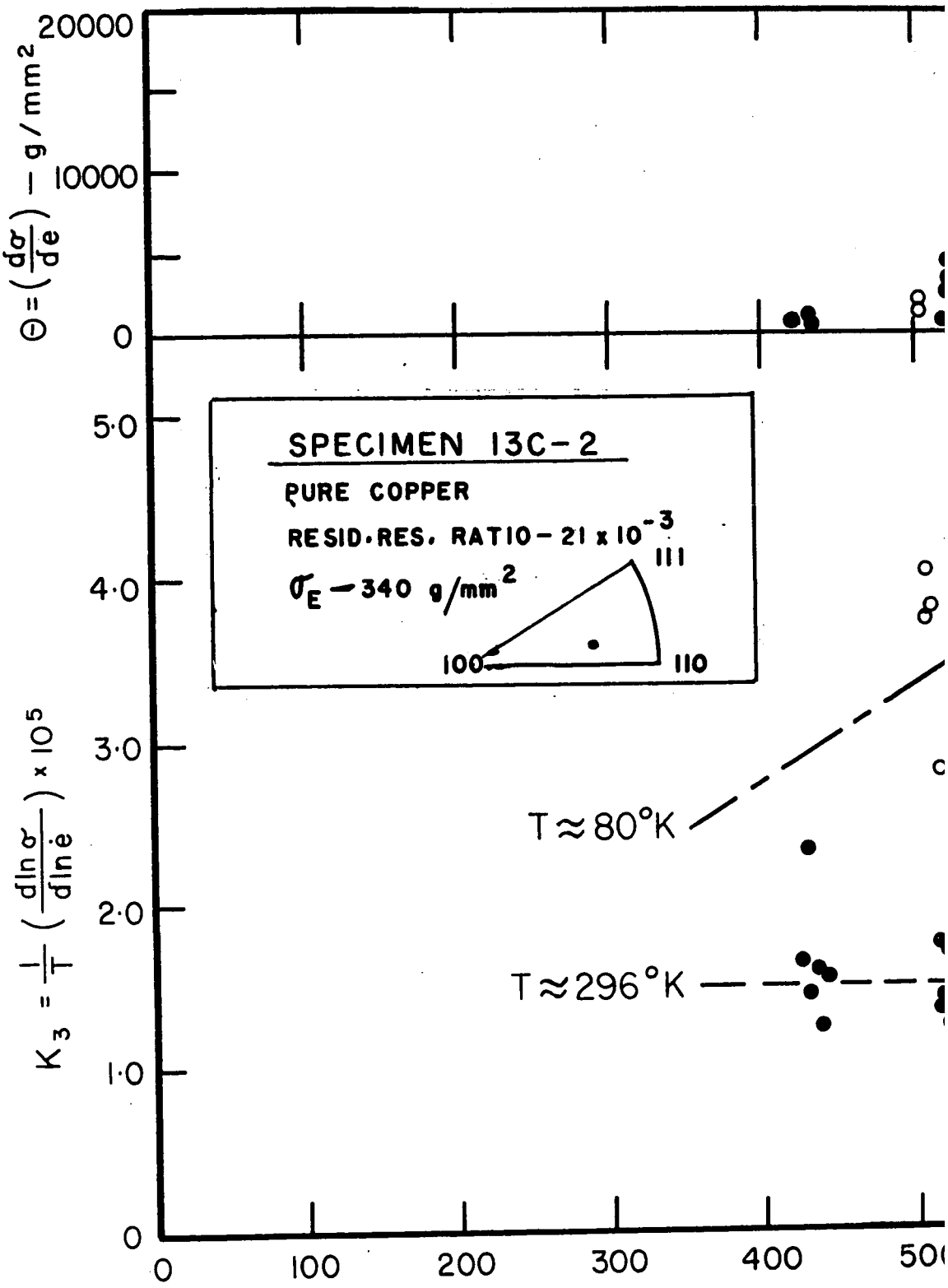

FIGURE 45 — VARIATION OF THE ST
AND THE STRAIN RATE
RESOLVED SHEAR STRES

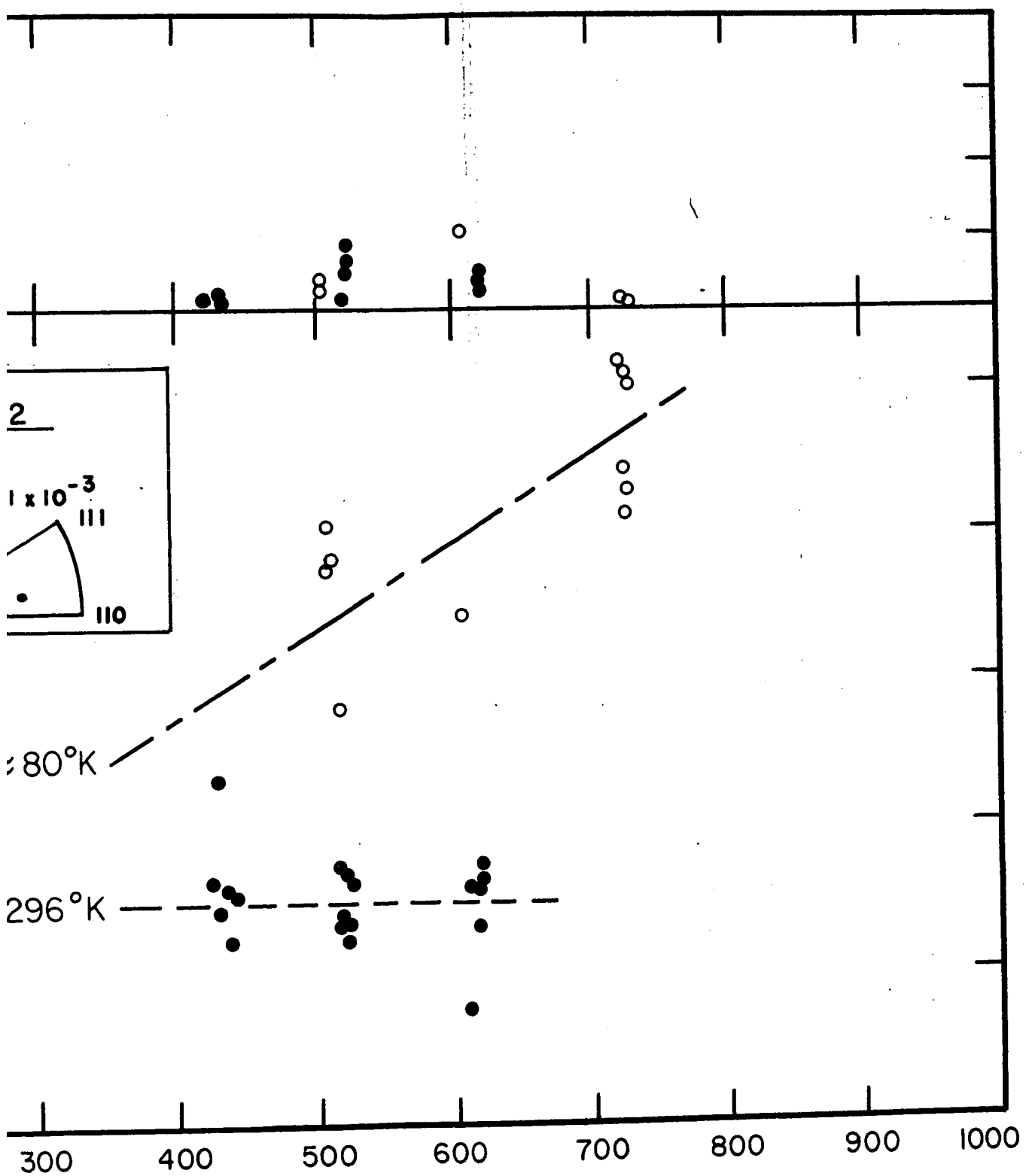

ED SHEAR STRESS – g/mm²

ION OF THE STRAIN HARDENING COEFFICIENT (Θ)
HE STRAIN RATE SENSITIVITY (K_3) WITH
VED SHEAR STRESS, FOR SPECIMEN 13C-2

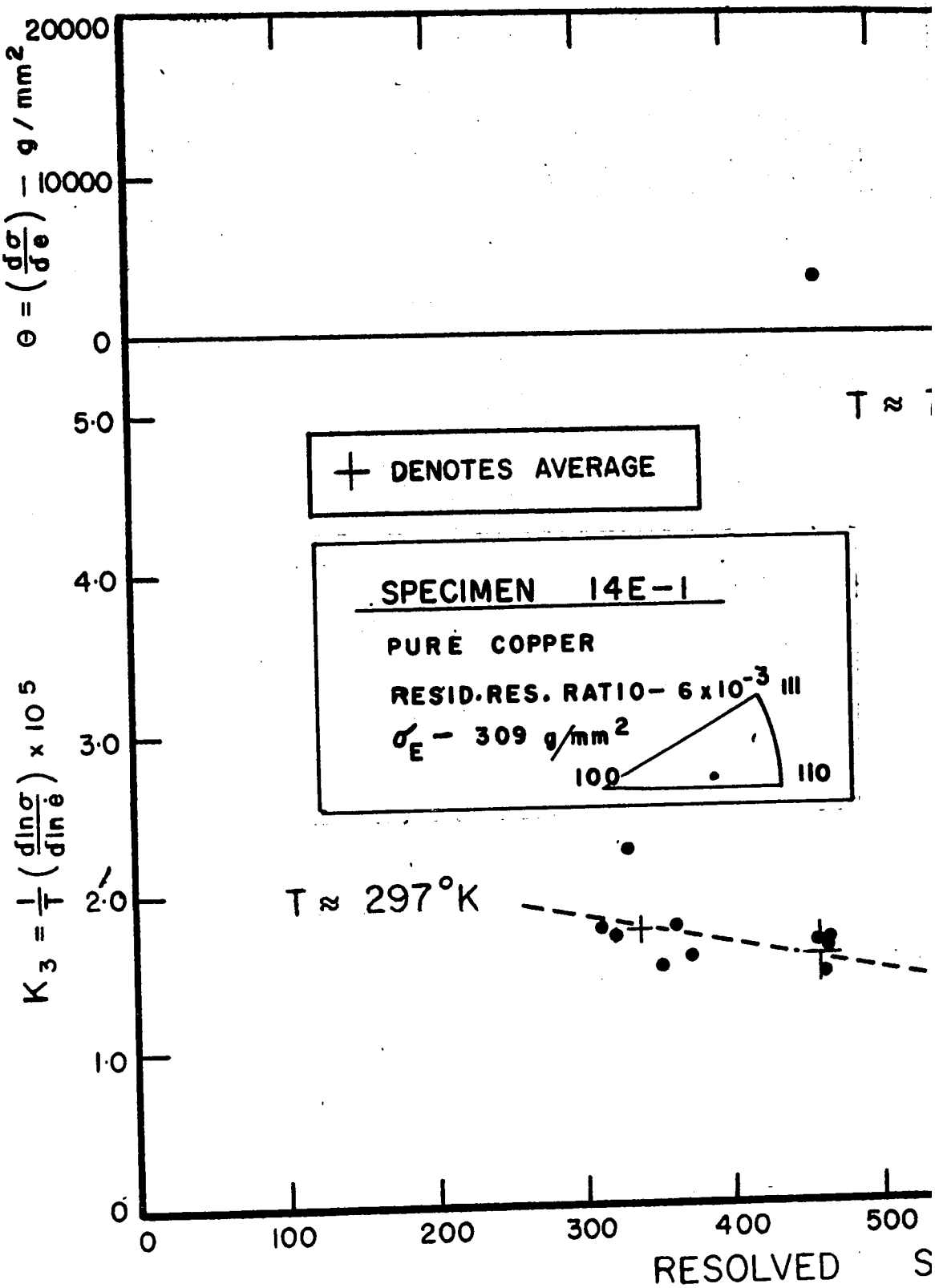

FIGURE 46 — VARIATION OF THE
STRAIN RATE SENSITIVI
FOR SPECIMEN 14E-1

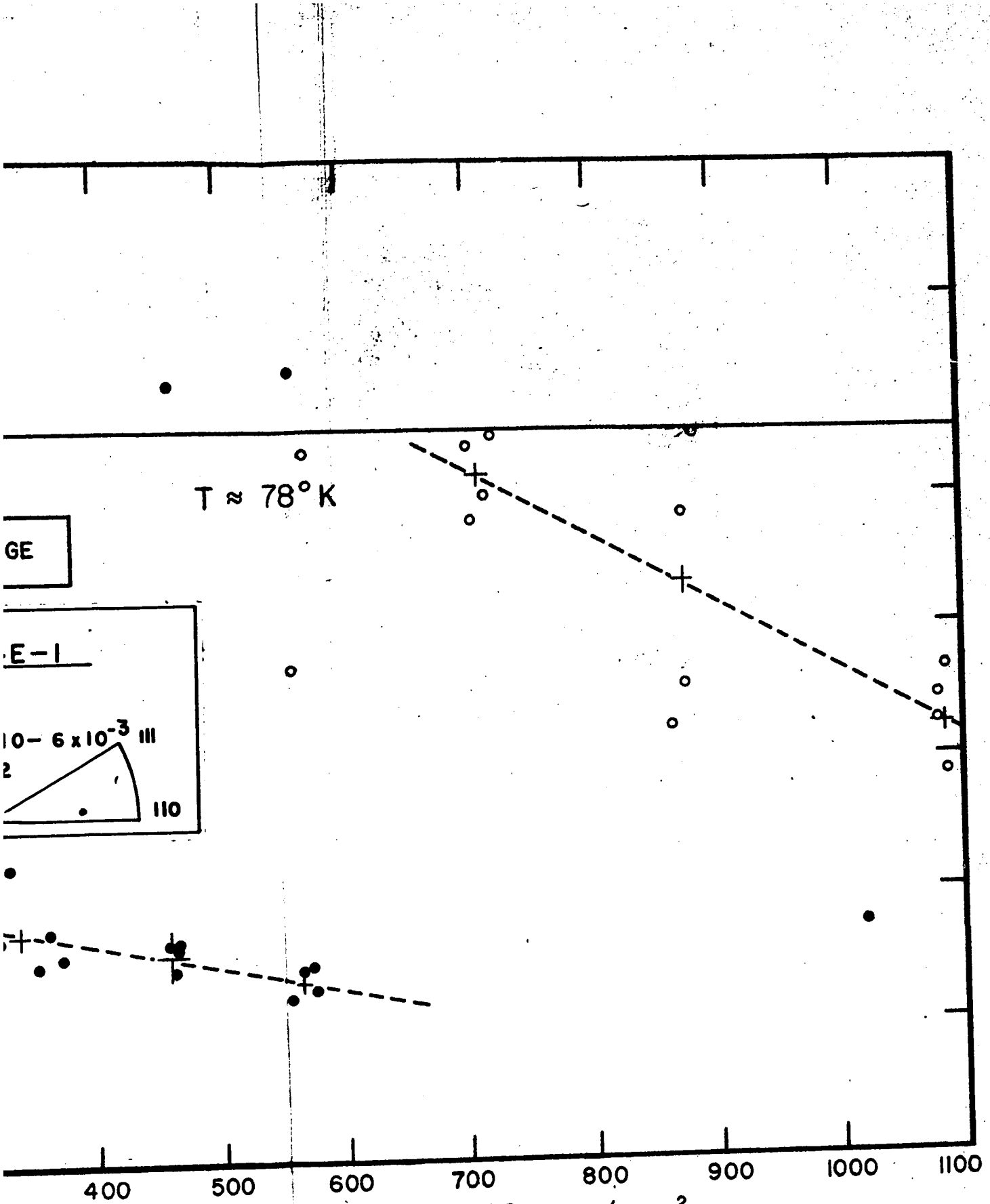

ION OF THE HARDENING COEFFICIENT (Θ), AND THE RATE SENSITIVITY (K_3) WITH RESOLVED SHEAR STRESS

PECIMEN 14E-1

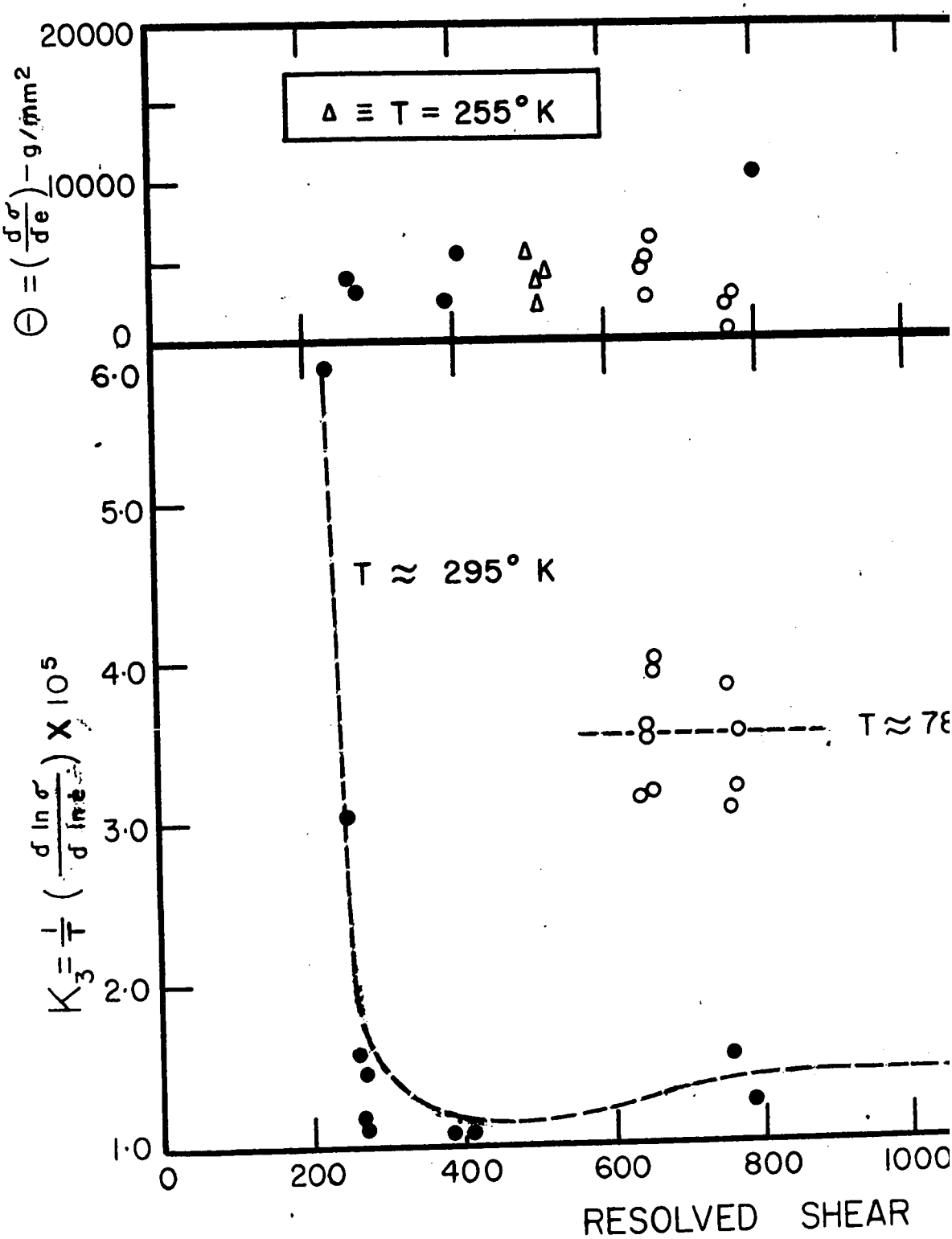

FIGURE 47 — VARIATION OF THE HAF
THE STRAIN RATE SEN
SHEAR STRESS, FOR

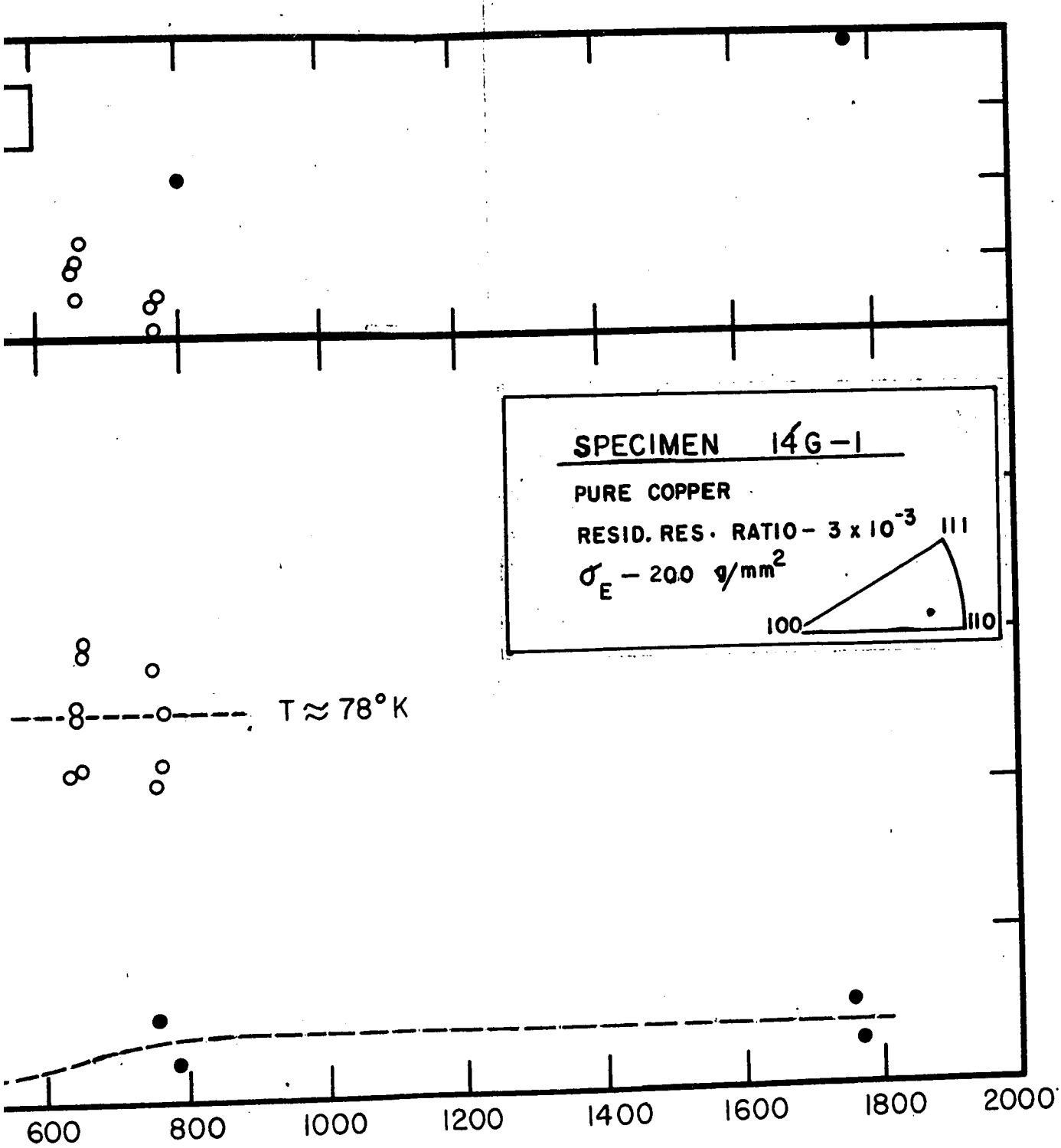

IATION OF THE HARDENING COEFFICIENT (Θ), AND
: STRAIN RATE SENSITIVITY (K_3) WITH RESOLVED
:AR STRESS, FOR SPECIMEN 14G-1

The observed values of K_3 are higher than quoted by Basinski (1959) for deformation in the linear hardening region but this would be expected since K_3 appears to be a decreasing function of stress both in the easy glide and the early stages of the linear hardening region.

The behaviour of specimen 14G-1 at 295°K is of particular interest since it exhibits a very high initial value of K_3 which decreases with stress, goes to an apparent minimum and then levels off to a relatively constant value. Similar behaviour has been observed by Basinski (1960) and he suggested that such behaviour might be associated with deformation in the knee region (transition region between elastic and plastic regions) of the stress-strain curve. An attempt to reconstruct the stress-strain curve for specimen 14G-1 was not successful but curves were available for specimens 13C-1 and 13C-2 and these are shown in Figures 48 and 49 along with the associated values of K_3. The results for specimen 13C-1 indicate that early in the transition region $K_3 = 1.5$, as the stress-strain curve bends over K_3 rises to a maximum of 1.7, and then slowly falls to an approximately constant value of 1.5 in the easy glide region. No values of K_3 in the knee-region were available for specimen 13C-2.

These results suggest that K_3 increases during the transition region, reaches a maximum as the stress-strain curve bends over, and

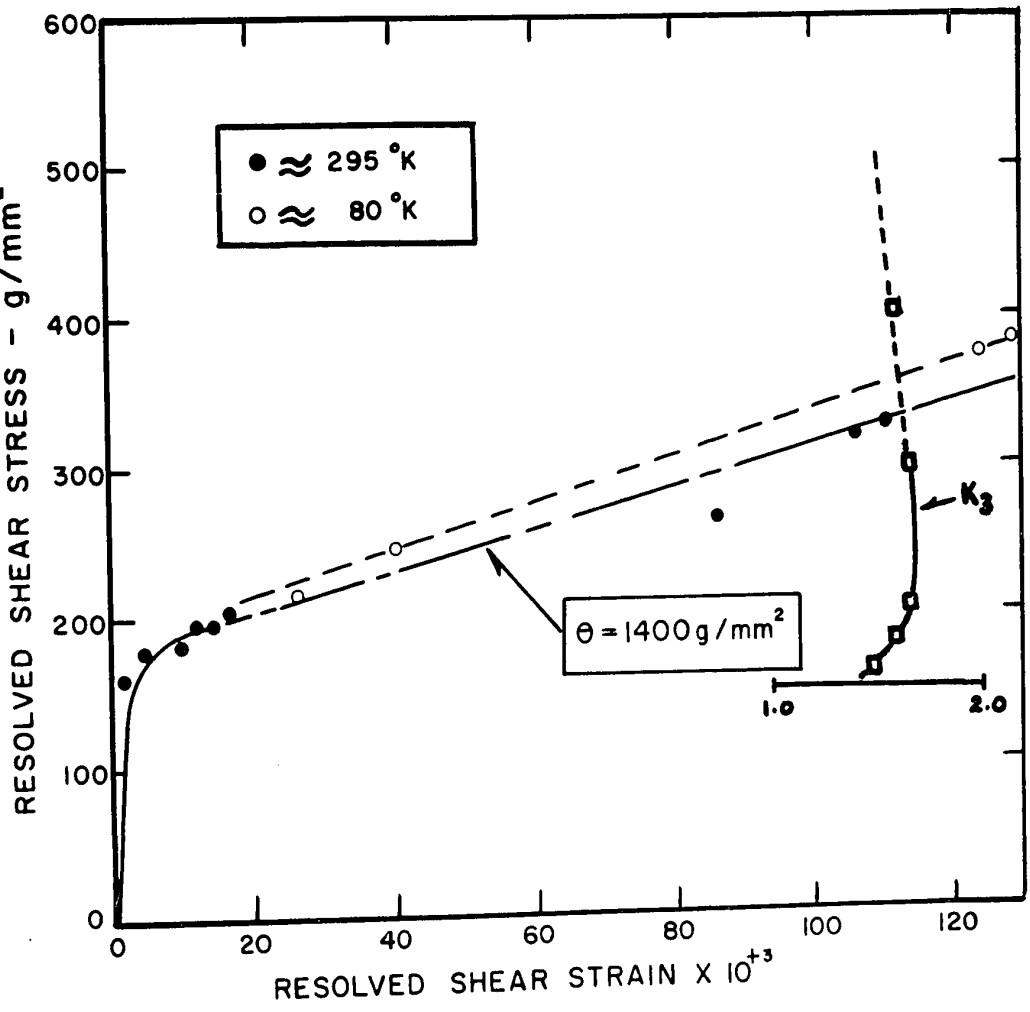

FIGURE 48 - STRESS - STRAIN CURVE FOR SPECIMEN 13 C-1 (PURE COPPER)

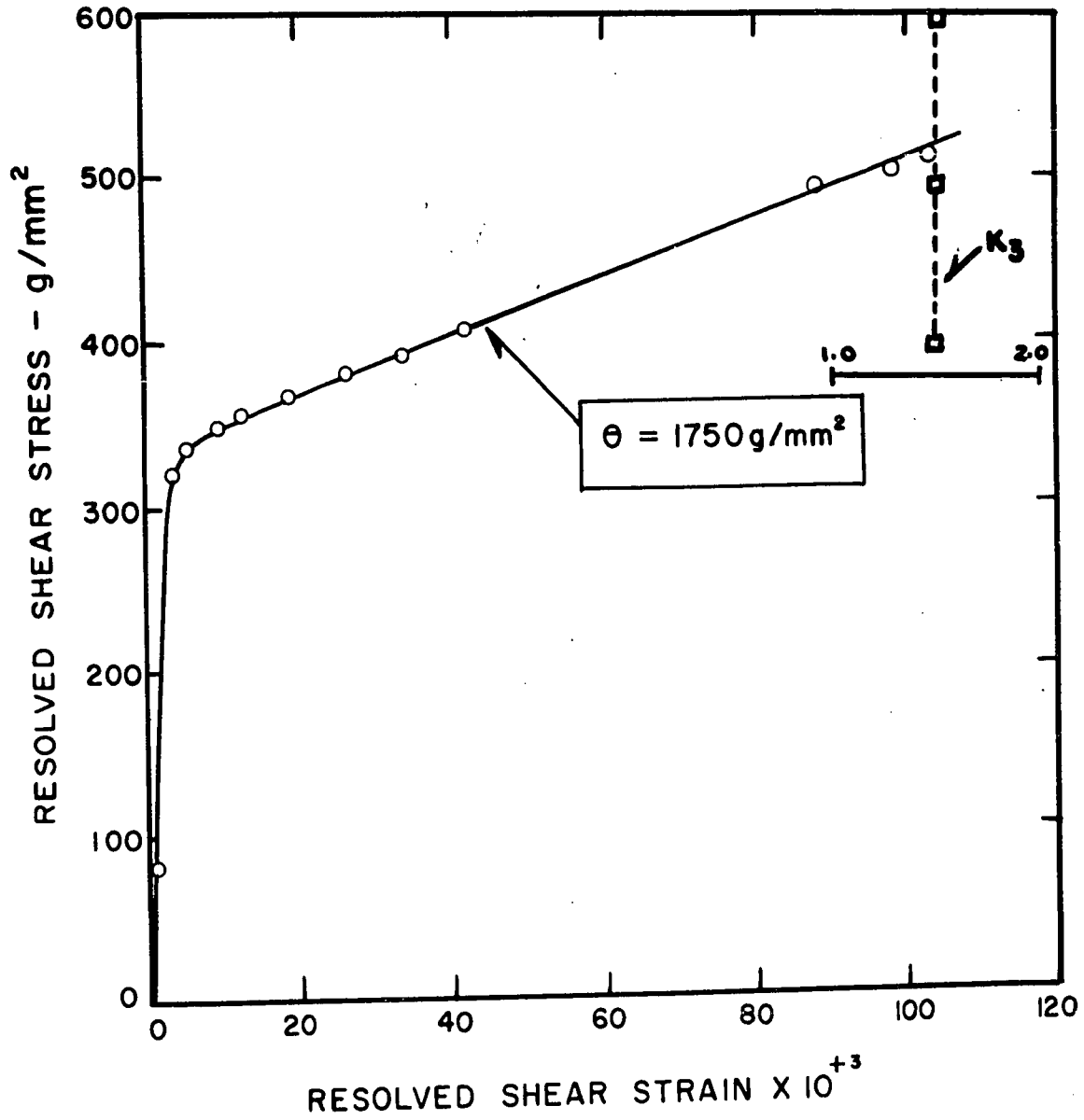

FIGURE 49 - STRESS-STRAIN CURVE FOR SPECIMEN 13C-2 (PURE COPPER)

then decreases with continued deformation through the easy glide region and into the linear hardening region.

Group III consisted of two copper-silver alloy single crystals, 6(A)B-1* and 7B-1+ whose orientations were within the region of unperturbed glide. Both specimens exhibited a very extended region of easy glide. It should be noted that the initial resolved shear stress for easy glide was considerably higher for the alloy specimens, (6(A)B-1, 725 gm/ mm^2; 7B-1, 750 gm/ mm^2) than those for pure copper studied in Group I and II. Experiments conducted at temperatures from 300 - 78°K are presented in Tables XVII and XVIII of Appendix II and the variation of K_3 with stress is shown in Figures 50 and 51.

For specimen 6(A)B-1, K_3 at room temperature (300°K) appears to be approximately independent of stress in the range 750-1350 g/ mm^2. At 78°K the data is limited but average values of K_3 appear to decrease with applied stress from 9.7 to 8.7 in the range 1150-1500 g/ mm^2.

For specimen 7B-1 at room temperature the average values of K_3 appear to decrease with applied stress from 7.3 to 4.7 in the range 750-950 g/ mm^2. This rapid initial decrease in K_3 is very similar to

---

* Nominal alloy concentration 0.1 at. % silver.
\+ Nominal alloy concentration 0.3 at. % silver.
Details of orientation and residual resistance ratio for both specimens are given in Tables IV and VIII respectively.

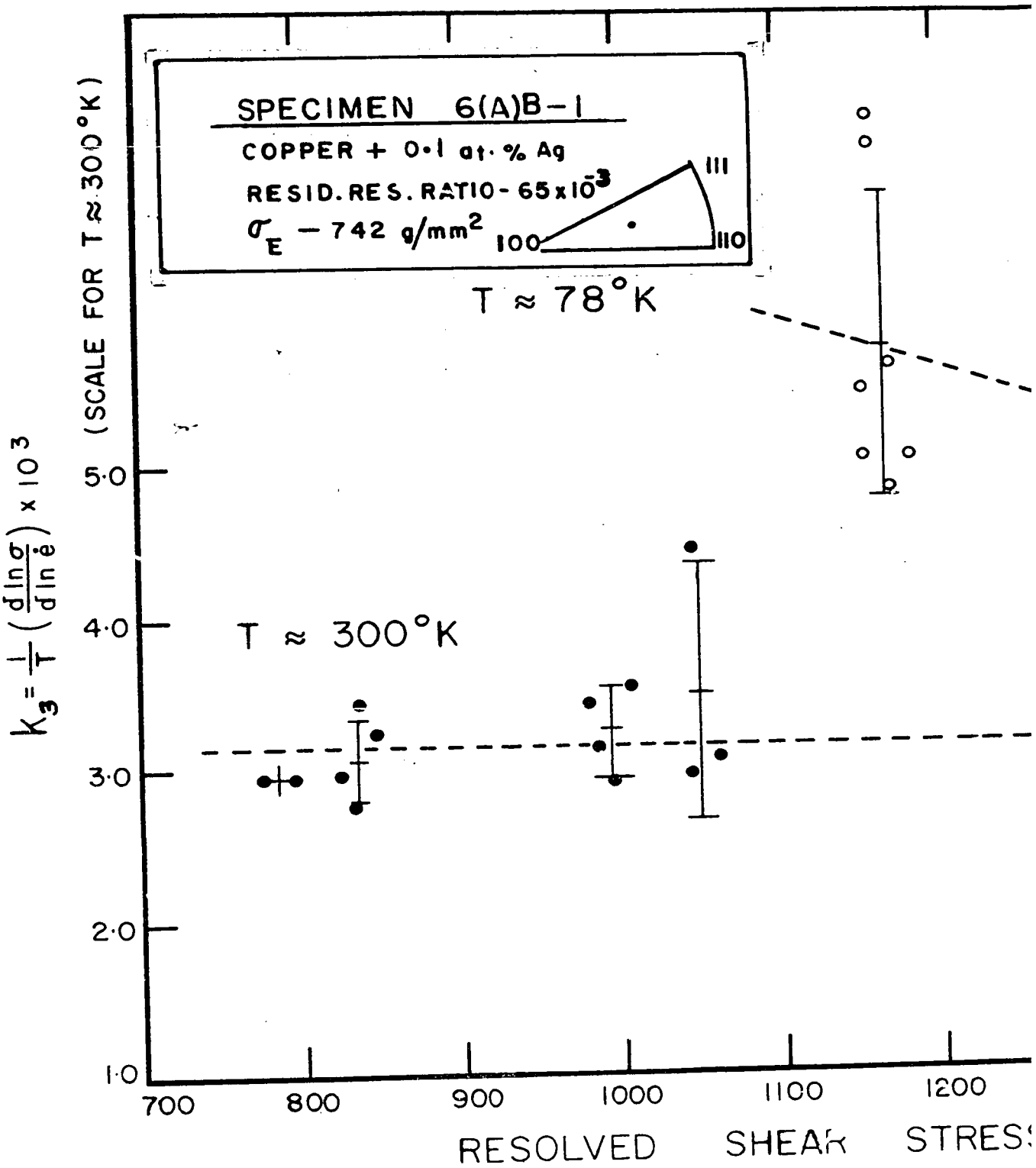

FIGURE 50 — VARIATION OF THE STR
WITH RESOLVED SHEAR

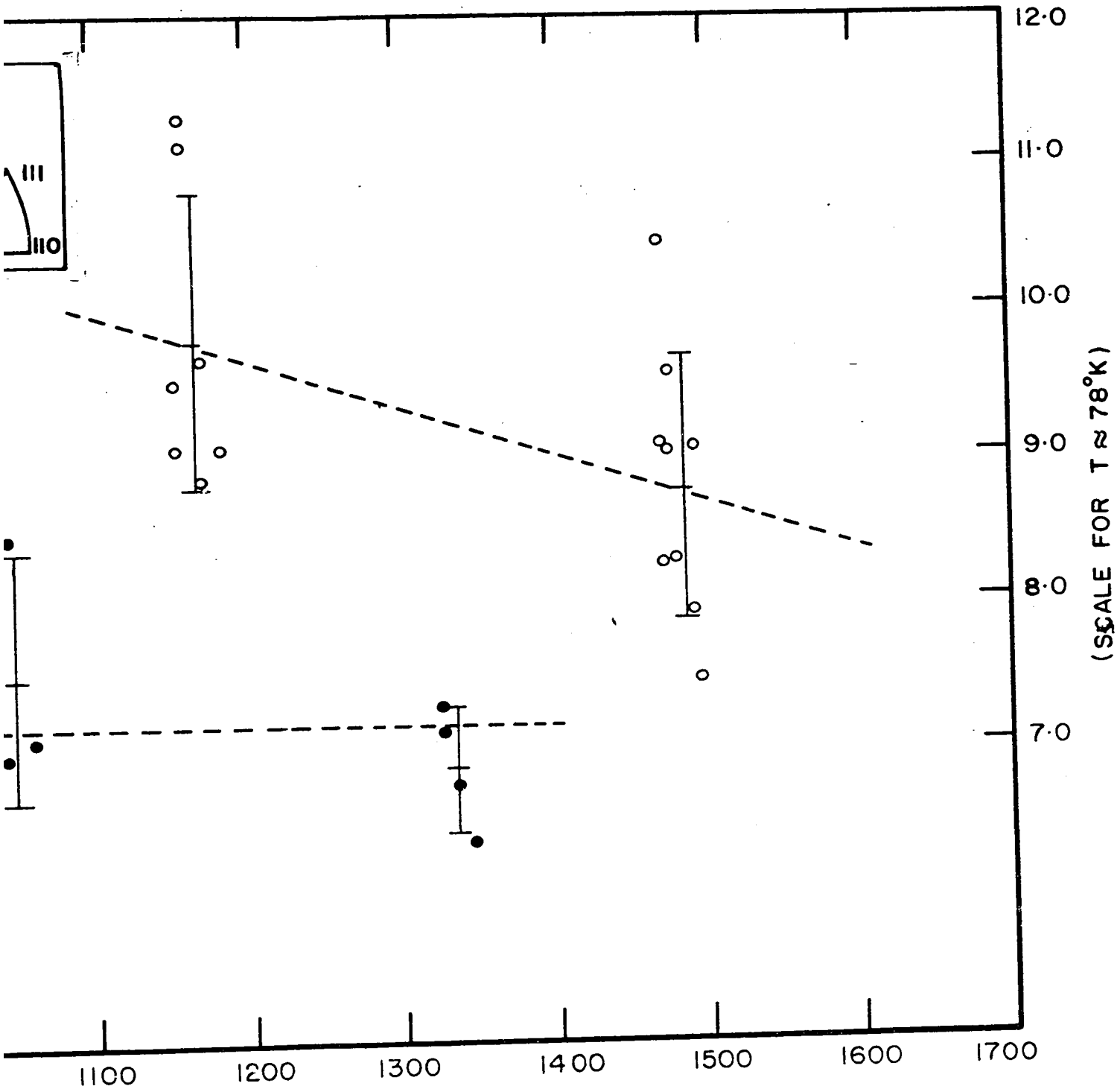

OF THE STRAIN RATE SENSITIVITY (K_3)

SOLVED SHEAR STRESS FOR SPECIMEN 6(A)B-1

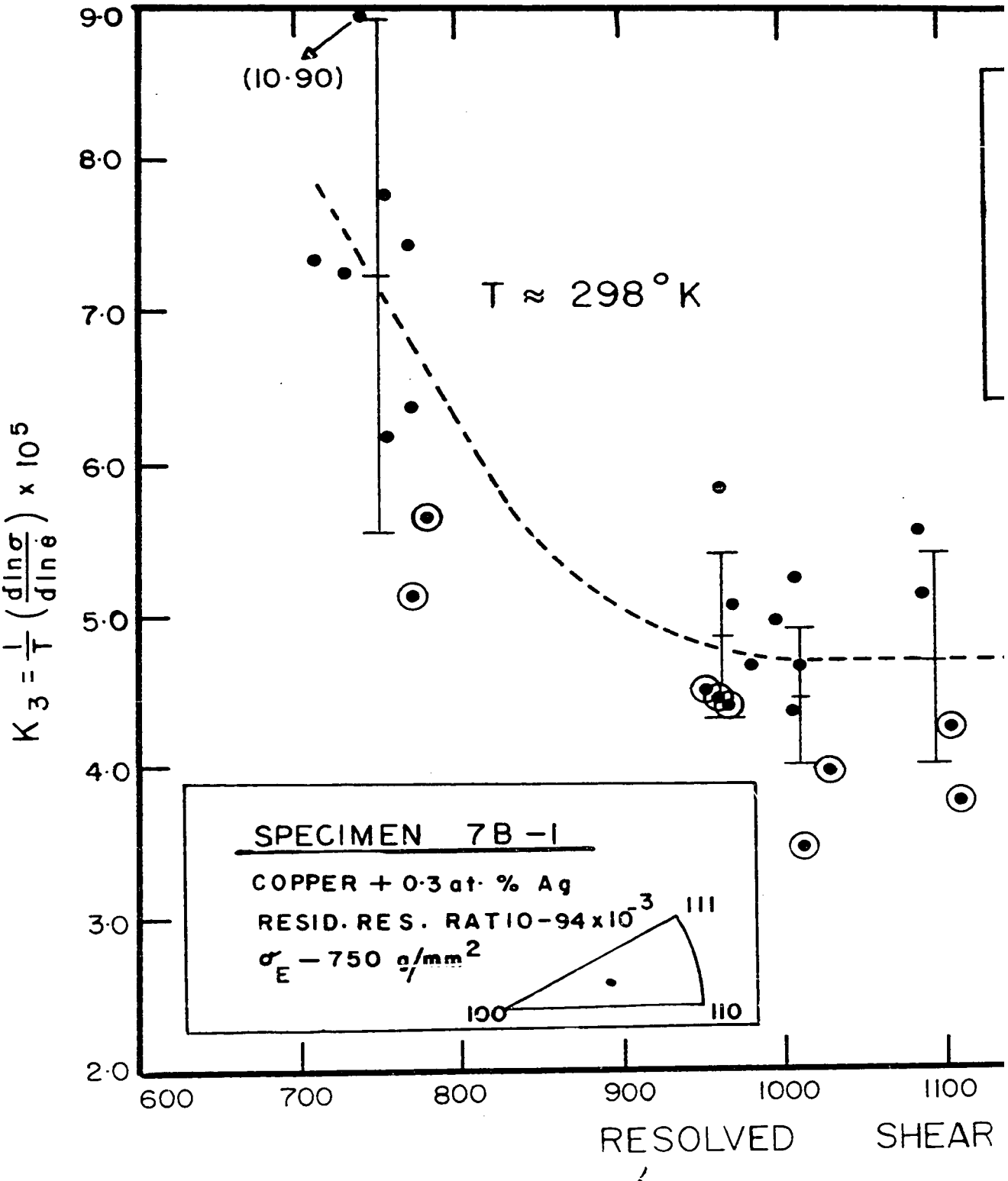

FIGURE 51 — VARIATION OF THE
STRESS FOR SPECIM

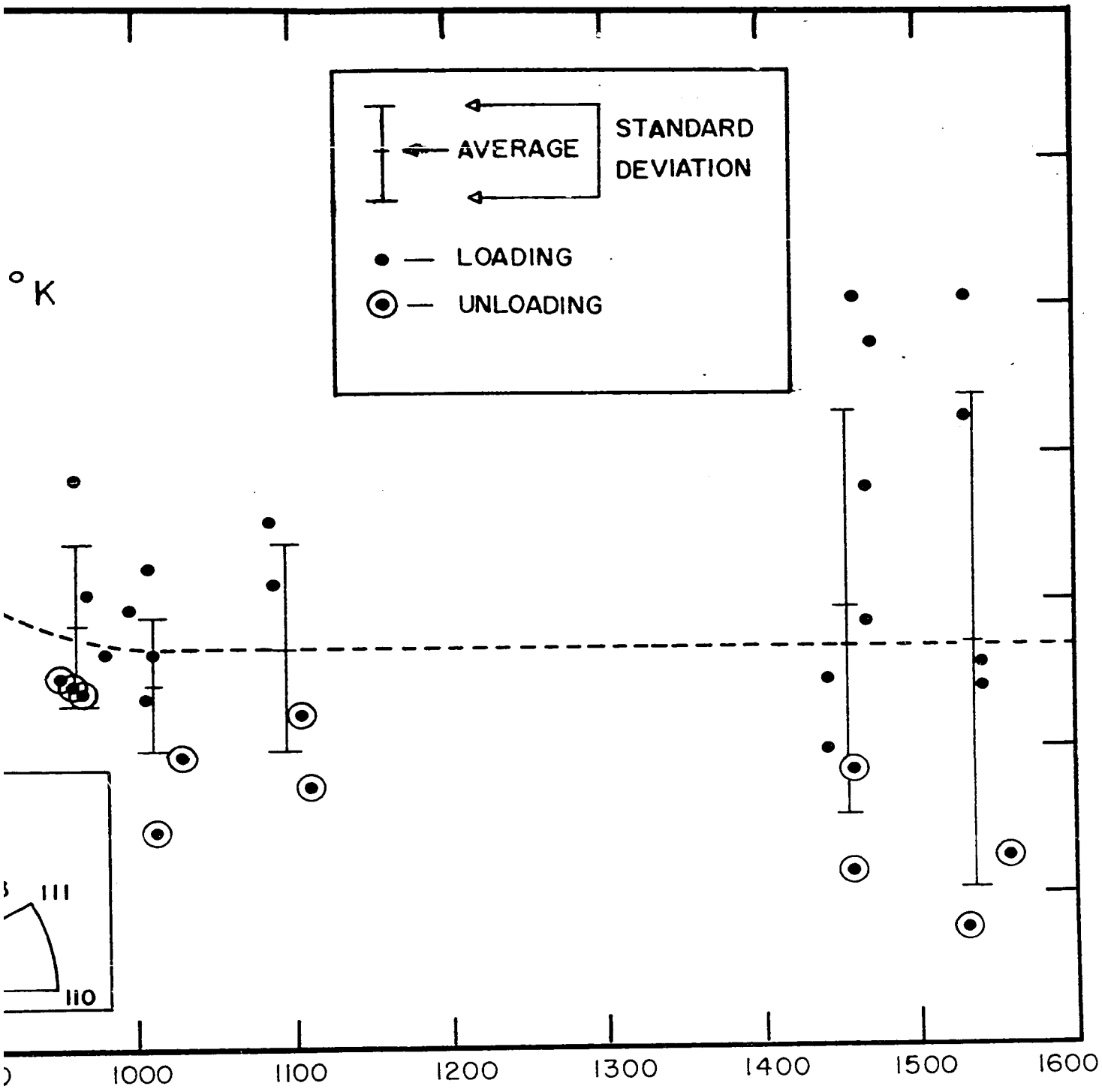

SOLVED SHEAR STRESS — g / mm²

ON OF THE STRAIN RATE SENSITIVITY (K_3)
S FOR SPECIMEN 7B-1

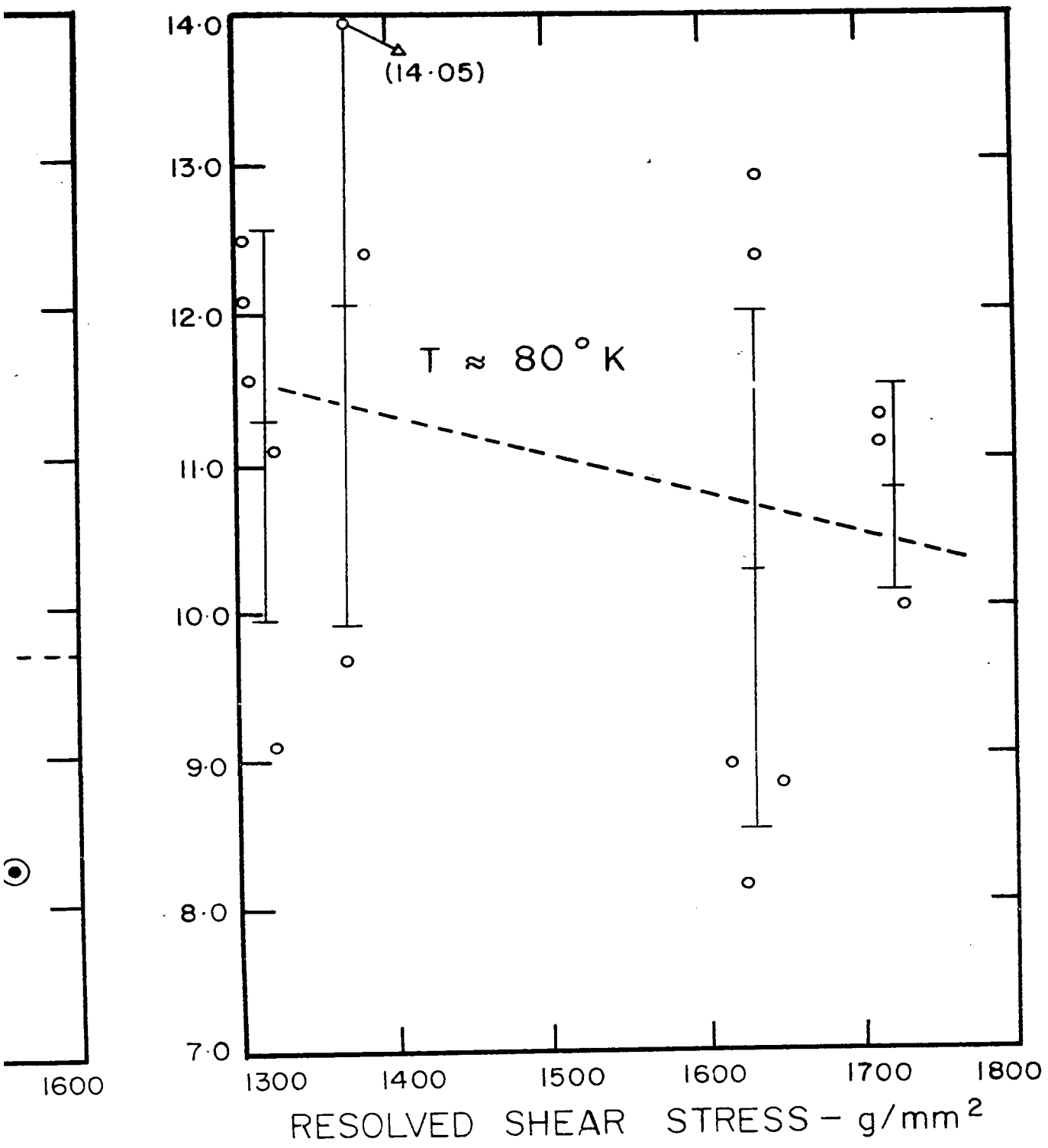

(K_3) WITH RESOLVED SHEAR

that observed in the pure copper specimen 14G-1 and is probably similarly associated with the inception of easy glide. In the range 950-1550 g/mm^2 K_3 appears to be approximately independent of stress. At 78°K, K_3 appears to be a decreasing function of stress although the large deviations in the results make an accurate determination difficult. The standard deviation in the results for the alloys vary from 15-25%. There also appears to be a more pronounced difference in the values of K_3 determined by loading and unloading experiments than was observed with the pure copper specimens.

The results for Group I, II and III indicate in general that for temperatures in the range 300 to 78°K, K_3 is a decreasing function of stress. The rate of decrease with stress appears greater for the lower temperatures. This is in agreement with the results of Basinski (1960), and Adams and Cottrell (1955) on copper using the constant strain rate method, and the work of Conrad (1958) on copper using the transient creep method.

3.6. Variation of K_3 with Temperature

Only a limited amount of data on the temperature dependence of K_3 was obtained. Figure 52 shows the variation of K_3 with temperature from room temperature (295°K) down to 78°K for a copper single crystal (14G-1) in the easy glide region. The values of K_3 used here

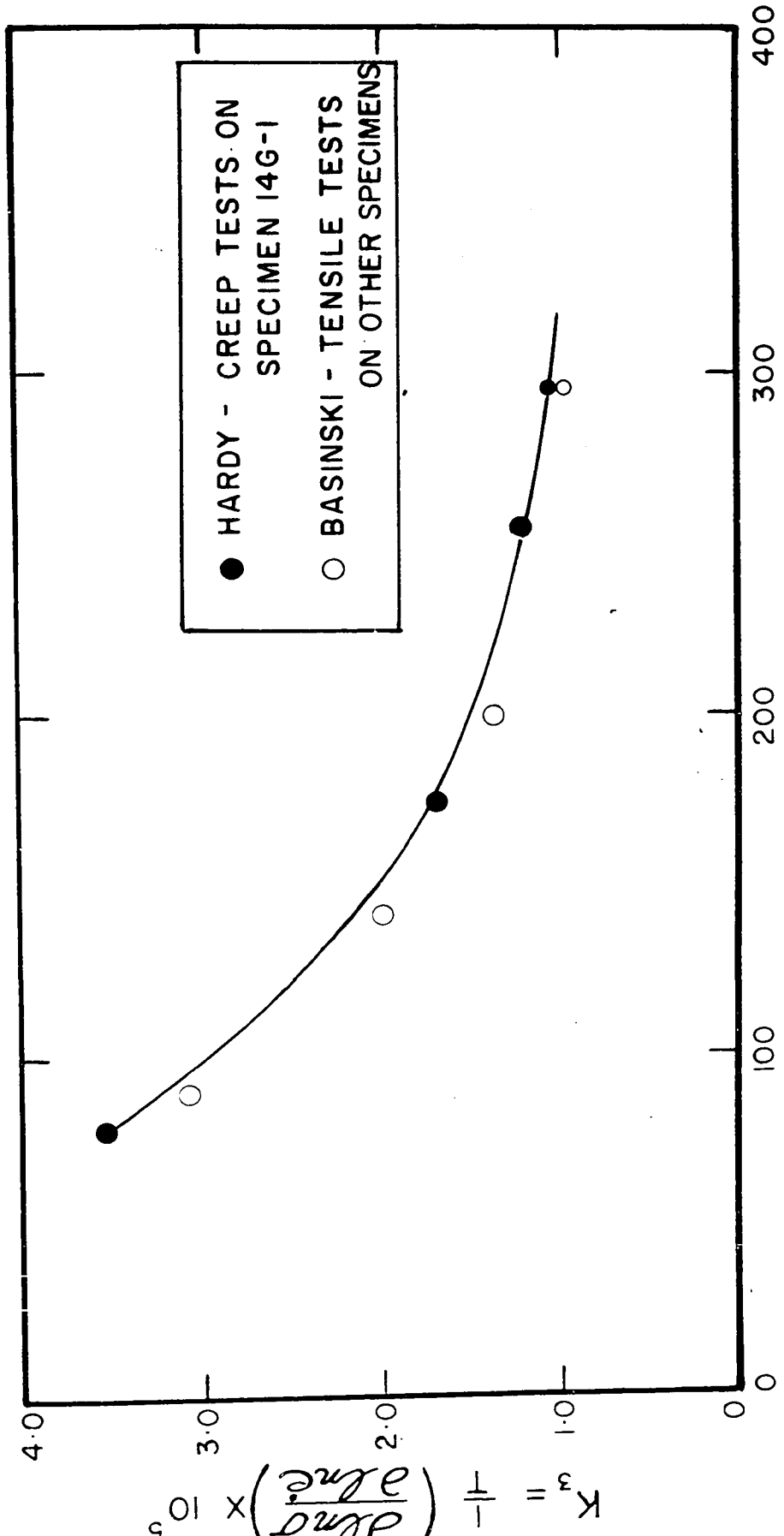

FIGURE 52 – VARIATION OF STRAIN RATE SENSITIVITY (K_3) WITH TEMPERATURE FOR SPECIMEN 14G-1

were associated with changes in strain rate in the range of 10^{-4} sec^{-1} to 10^{-1}** sec^{-1}. Also plotted on the same graph are data obtained by Basinski (1959) from a number of experiments on similar copper single crystals in the linear hardening region using the constant strain rate method. These later values of K_3 were associated with changes in strain rate in the range of 10^{-3} sec^{-1} to 10^{-5} sec^{-1}*. It is interesting to note that the results for the two cases appear to be identical although the two sets of experiments were conducted in different regions of the stress-strain curve.

3.7. Variation of K_3 with Nominal Alloy Concentration and Residual Resistance Ratio

To illustrate the variation of K_3 with impurity concentration average values of K_3, ($\overline{K_3}$) were calculated for the linear regions of the K_3 versus stress curves for room temperature (295°K) and for 80°K. These data are listed in Table VIII along with the nominal alloy concentration, the residual resistance ratio and other related factors. Figure 53 illustrates the variation of $\overline{K_3}$ with the residual resistance, and with the nominal alloy concentration. The value of $\overline{K_3}$ increases with both the residual resistance ratio and the nominal alloy concentration although

---

* Basinski (1959) has shown that K_3 is independent of the strain rate over the range 10^{-3} sec^{-1} to 10^{-5} sec^{-1} using the constant strain rate method.

** Experiments have shown that the values of K_3 are essentially independent of the associated change in strain rate in the range 10^{-1} sec^{-1} to 10^{-6} sec^{-1} using the transient creep method (see chapter IV, section 3.2.)

TABLE VIII

Relationship of the Average Strain Rate Sensitivity (K_3) and Initial Stress for Easy Glide (σ_E) to Nominal Impurity Concentration and Residual Resistance Ratio for Copper and Copper-Silver Alloy Single Crystals

Specimen Number	Nominal Impurity Concentration	Residual Resistance Ratio x 10^3	σ_{E}* g/mm^2	$\bar{K}_3$** T ≈ 295°K -	$\bar{K}_3$** T ≈ 80°K -
14P(K)-1	Pure	1.8	++	1.08±0.30 (4)	4.9 (1)
14H-1	Pure	4	+	0.80±0.12 (4)	-
14H-2	Pure	4	+	1.25±0.32 (27)	-
14F-2	Pure	-	+	0.92±0.20 (13)	-
13C-1	Pure	9	180	1.58±0.28 (31)	3.52±0.97 (23)
13C-2	Pure	21	340	1.52±0.30 (20)	4.40±0.91 (14)
14E-1	Pure	6	309	1.60±0.24 (15)	4.49±1.25 (15)
14G-1	Pure	3	200	1.29±0.21 (10)	3.51±0.10 (10)
6(A)B-1	0.1 at.% Ag.	65	742	3.13±0.46 (17)	9.22±1.02 (16)
7B-1	0.3 at.% Ag.	94	750	5.03±1.52 (40)	11.02±1.71 (16)

* σ_E — denotes the stress at which easy glide begins for T ≈ 295°K.

** $\bar{K}_3$ — denotes the average strain rate sensitivity (K_3). The data is in the form A + B (C), where A is the average value, B is the standard deviation and C is the number of tests averaged.

\+ —— specimen exhibited no easy glide region.

++ —— polycrystal specimen.

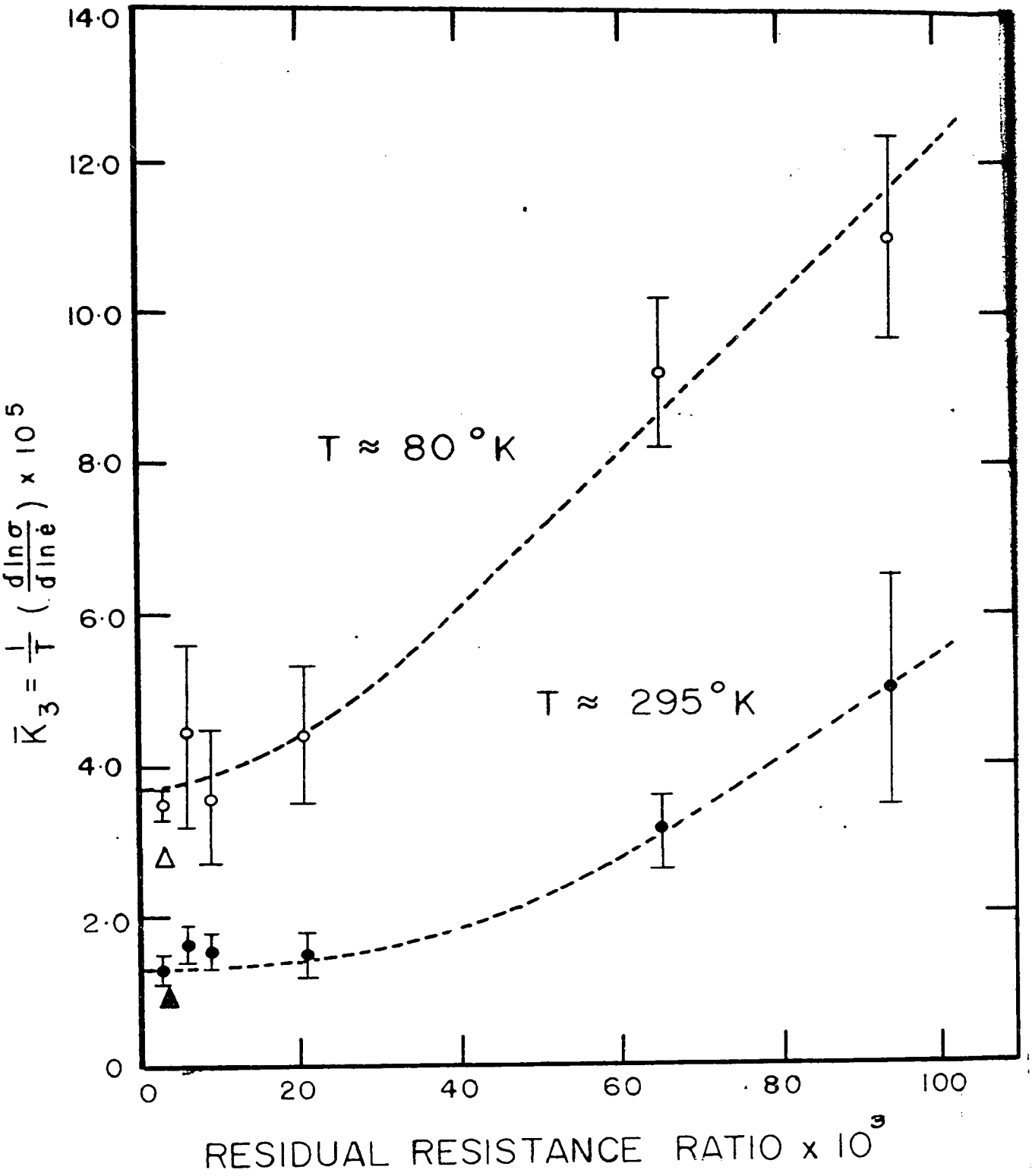

FIGURE 53 — VARIATION OF AVERAGE STR
WITH RESIDUAL RESISTANCE R
CONCENTRATION .

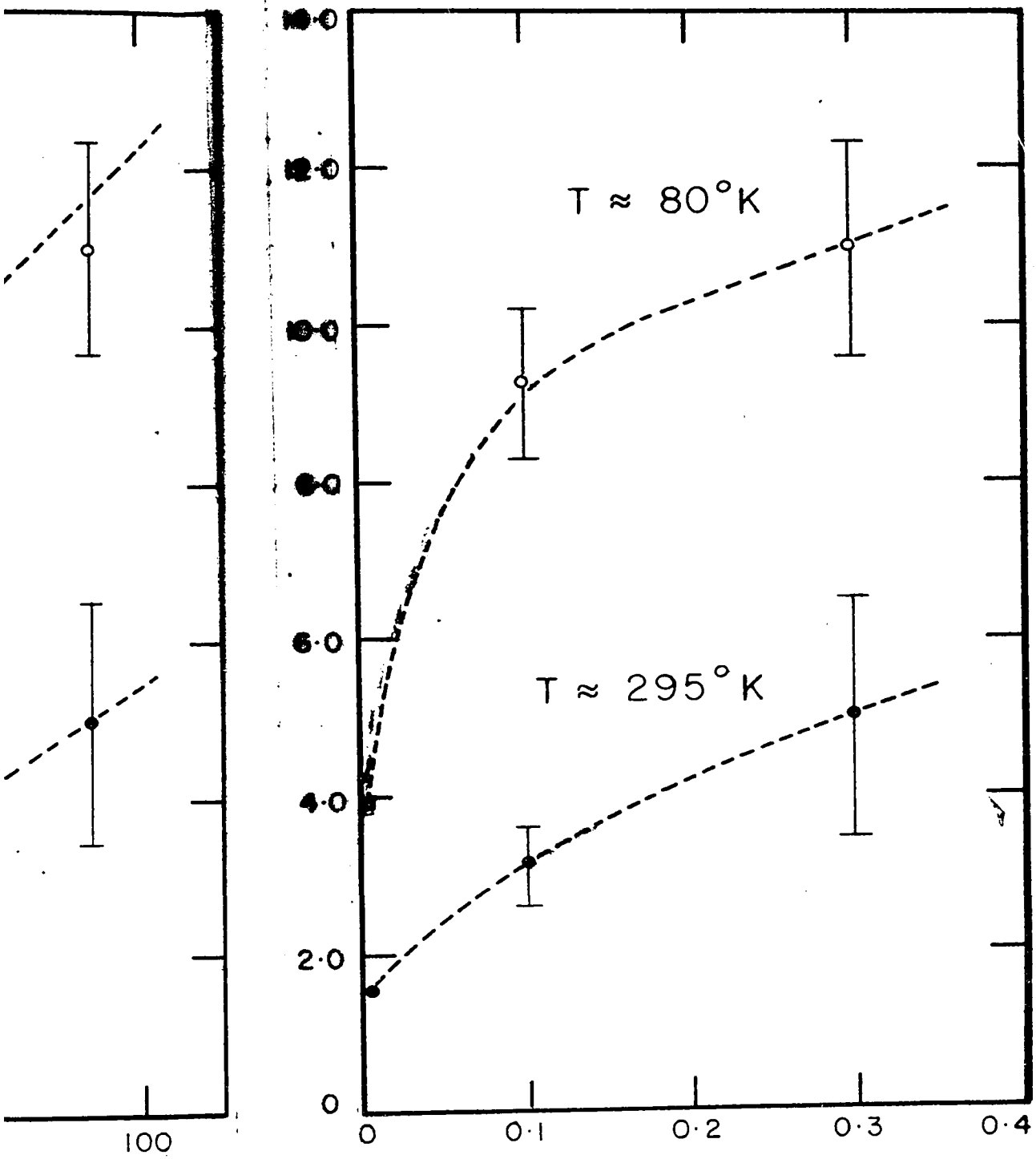

× 10^{3}

NOMINAL ALLOY CONCENTRATION At % Ag

AVERAGE STRAIN RATE SENSITIVITY ($\bar{K}_3$)

RESISTANCE RATIO AND NOMINAL ALLOY

the curves are of a different form. $\overline{K}_3$ appears to increase linearly with the residual resistance ratio after an initial curved region. The variation of $\overline{K}_3$ with nominal alloy concentration appears to be concave downward. The region studied is not large enough to make any predictions for larger alloy concentrations.

3.8. Variation of τ_E and Extent of Easy Glide Region with Resistance Ratio*

The initial stress for easy glide (τ_E) is listed in Table VIII. Figure 54 shows the variation of τ_E with residual resistance ratio*. A plot of this property (τ_E) against the nominal alloy concentration had no apparent meaning. The data is limited but it appears that τ_E is an increasing function of the residual resistance ratio*. This is in agreement with the observations of other workers, e.g. Garstone and Honeycombe (1956).

The extent of the easy glide region was also increased with alloying such that the load capacity of the machine was exceeded for the two alloy specimens without noticeable deviation from easy glide behaviour. This behaviour is in agreement with the observations of Schroder (1959) on copper-arsenic single crystals.

---

* Residual resistance ratio is being utilized here as a measure of impurity concentration.

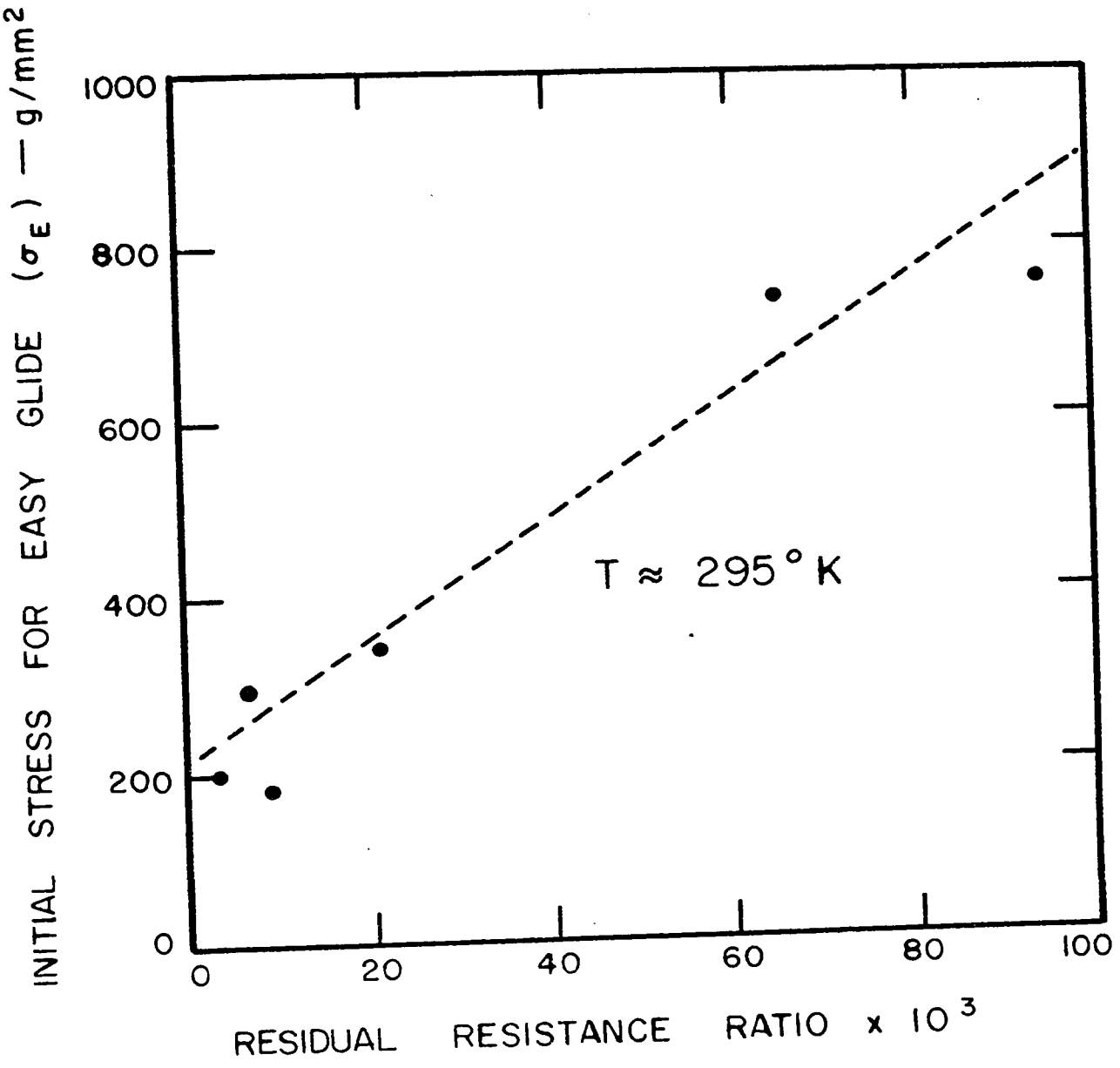

FIGURE 54 – VARIATION OF INITIAL STRESS FOR EASY GLIDE (σ_E) WITH RESIDUAL RESISTANCE RATIO

4. Conclusions

The apparatus developed for the study of the strain rate sensitivity (K_3) of single crystal wire specimens using the incremental transient creep method was found to perform in a satisfactory manner since the values determined using this apparatus compared closely with those obtained from constant strain rate and stress relaxation experiments. Although the apparatus was reasonably easy and convenient to operate it could be further improved by using an electronic strain recording system coupled to the photocell drive screw (Figure 25) rather than the mechanical one employed. This would provide a range of convenient strain sensitivities and would make it possible to examine any region of the strain-time curve at high sensitivity. The development of an improved loading device in which loading weights could be more easily handled and which allowed a greater range of loads is suggested. Finally the design of a suitable cryostat would be required if the variation of K_3 with temperature were to be studied in detail, or if temperatures below 78°K were contemplated.

Although the prime purpose of this thesis was to develop a suitable apparatus, a short series of experiments, which were carried out mainly to check the operation of the apparatus, have indicated the following: a) K_3 remains relatively constant or decreases only slightly throughout most of the easy glide region and into the early stages of the

linear hardening region; b) there is some evidence that K_3 has a relatively high value in the knee region of the stress-strain curve which decreases as easy glide is initiated; c) the variation of K_3 with temperature in the range 78-300°K appears similar in both the easy glide and linear hardening region; d) K_3 appears to increase with impurity concentration (based on residual resistance ratio values). These conclusions are based on a relatively few specimens and considerably more experiments will be required to substantiate the results. Future work should include a more detailed study of the variation of K_3 in the knee region, and the variation of K_3 with impurity concentration.

REFERENCES

Adams, M.A., and Cottrell, A.H. 1955. Phil. Mag. 46, 1187.

Andrade, da C. E.N., and Chalmers, B., 1932. Proc. Roy. Soc. 138, 348.

Andrade, da C. E.N., and Roscoe, R., 1937. Proc. Phys. Soc. 49, 152.

Barrett, C.S., 1943. Structure of Metals, McGraw-Hill Book Company, Inc. New York.

Basinski, Z.S., 1959. Private Communication.

Basinski, Z.S., 1959. Phil. Mag. 4, 393.

Basinski, Z.S., 1960. Private Communication.

Bowman, H.A., and Macurdy, L.B., 1959. Jour. Research Nat. Bur. of Standards, 63C, 91.

Buerger, M.J., 1942, X-ray Crystallography, John Wiley and Sons, Inc. New York.

Conrad, H., 1958. Acta. Met. 6, 339.

Cottrell, A.H., 1953. Dislocations and Plastic Flow in Crystals. Oxford Press, Clarendon, U.K.

Cottrell, A.H., and Stokes, R.J., 1955, Proc. Roy. Soc. A., 233, 17.

Craw, D.A., and Henry, W.G., 1956. Jour. Sci. Inst. 33, 22.

Foreman, A.J.E., 1955. Acta. Met. 3, 322.

Friedel, J., 1955. Phil. Mag. 46, 1169.

Garstone, J., Honeycombe, R.W.K., and Greetham, G., 1956. Acta. Met. 4, 485.

REFERENCES (Cont'd)

Garstone, J., and Honeycombe, R.W.K., 1956. Dislocations and Mechanical Properties of Crystals. John Wiley and Sons, Inc. New York.

Goss, A.J., 1953. Proc. Phys. Soc. 66, 525.

Henry, W.G., 1959. Private Communication.

Laws, F.A., 1938. Electrical Measurement, McGraw-Hill Book Company, Inc. New York.

Mott, N.F., 1952. Phil. Mag. 43, 1151.

Mott, N.F., 1953. Phil. Mag. 44, 742.

Overton, W.C., and Gaffney, J., 1955. Phys. Rev. 98, 969.

Owen, D., 1950. Alternating Current Measurement. Methuem and Co. Ltd. London.

Porter, A., 1950. An Introduction to Servomechanisms, Methuem and Co. Ltd. London.

Read, W.T., 1953. Dislocations in Crystals, McGraw-Hill, New York.

Schmid, E., and Boas, W., 1950. Plasticity of Crystals, F.A. Hughes and Co. Ltd., London.

Schroder, K., 1959. Proc. Phy. Soc. 73, 674.

Seeger, A., 1956. Dislocations and Mechanical Properties of Crystals. John Wiley and Sons, Inc. New York.

Sherby, O.D., Lytton, J.L., and Dorn, J.E., 1957, Acta. Met. 5, 219.

REFERENCES (Cont'd)

Taylor, G.I., 1934. Proc. Roy. Soc. A 145, 362.

Thaler, J., and Brown, R.G., 1953. Servomechanism Analysis, McGraw-Hill Book Company, Inc. New York.

Wolff, H.H., 1959. Rev. Sci. Inst. 30, 1116.

Wyatt, O.H., 1953. Proc. Phy. Soc. B 66, 459.

VITA

NAME: HENRY REGINALD HARDY JR.

BORN: 19th August, 1931, Ottawa, Canada.

EDUCATED:

Ottawa Technical High School, Ottawa (1944-1949).
McGill University, Montreal, B.Sc. (1949-1953).

APPOINTMENTS:

Scientific Officer, Mines Branch, Canadian Department of Mines and Technical Surveys from May 1953 to present.

PUBLICATIONS:

Rock Pressure Studies in the Mines of Springhill, N.S. III - Determination of Rock Strength Characteristics: Trans. Mining Soc. Nova Scotia, 59, 250 (1956).

Time-Dependent Deformation and Failure of Geological Materials: Colorado School of Mines Quarterly 54, 135 (1959).

Standardized Procedures for the Determination of the Physical Properties of Mine Rock under Short-Period Uniaxial Compression: Department of Mines and Technical Surveys, Ottawa, Mines Branch Technical Bulletin, TB 8 (1959).

Design of Instrumentation for the Measurement of Time-Dependent Strain in Stressed Rock Specimens: Inst. Soc. America, Winter Instrument-Automation Conference, 1960, Preprint No. 1-H60 (1960).

APPENDIX I

Mechanics of Crystal Deformation

Following Schmid and Boas (1935) the relationship which exists between the axial extension of a single crystal specimen and its orientation is as follows:

$$\frac{l_1}{l_0} = \frac{\sin\lambda_0}{\sin\lambda_1} = \frac{\sin\chi_0}{\sin\chi_1} \quad , \qquad (19)$$

and $$\bar{e} = \frac{l_1}{l_0} - 1 = d - 1 \quad ,$$

where l_0 and l_1 are the length of the specimen before and after extension, $\bar{e}$ is the axial strain, and λ_0 and χ_0 and λ_1 and χ_1 are the orientation angles* before and after extension.

When dealing with single crystals the axial stress and the axial strain are no longer basic quantities and these must be replaced by the resolved shear stress and the resolved shear strain. The value of resolved shear strain e corresponding to an axial strain $\bar{e}$ is given as follows:

$$e = \frac{1}{\sin\chi_0}\left\{\sqrt{d^2 - \sin^2\lambda_0} - \cos\lambda_0\right\} \quad , \qquad (20)$$

where $d = 1 + \bar{e}$ and all other factors have been defined previously. For all positions of the glide elements a small change in the axial strain $\Delta\bar{e}$ will result in a change Δe in the resolved shear strain

---

* λ is the angle between the tensile (wire) axis and the glide direction, χ is the angle between the tensile (wire) axis and the glide plane.

given by the following equation (determined by differentiation of equation (20) ;

$$\Delta e = \frac{\Delta \bar{e}}{\sin \chi_o \cos \lambda_1} \quad . \qquad (21)$$

The resolved shear stress σ_1 is defined as the component of the shear stress on the slip plane which lies in the glide direction. The equation relating the resolved shear stress to the applied axial load is as follows:

$$\sigma_1 = L\left(\frac{\sin \chi_o}{A}\right) \cos \lambda_1 \, , \qquad (22)$$

where σ_1 is the resolved shear stress, L is the applied axial load, A is the original cross-sectional area of the specimen, and χ_o and λ_1 were defined previously. It is important to note that for a fixed applied load L the resolved shear stress varies with cos λ_1 (since χ_o and A are constant) which itself varies with extension.

The experiments described in this thesis were carried out on an apparatus in which the resolved shear stress was held constant over a wide range of specimen extension at a value given by:

$$\sigma_o = L\left(\frac{\sin \chi_o \cos \lambda_o}{A}\right) \, , \qquad (23)$$

where all factors have been defined previously.

APPENDIX II

Tables of Experimental Data

This appendix consists of a series of Tables listing the experimental results for individual test specimens. Values of the strain rate sensitivity (K_3), and the strain hardening coefficient (θ) are given along with other experimental parameters.

TABLE IX

Experimental Data for Specimen 14P(1)-1
(Pure Copper Polycrystal)

Sheet	Event	L*	σ_R	ΔL	T	K_3	$\bar{K}_3$	θ
		gms	g/mm^2	gms	°K	-	-	g/mm^2
A	1	688	3340	+8.6	299	(0.74)		-
	2	676.7	3384	+16.7	299	1.19	1.32±0.18	-
	3	693.4	3467	+28.5	299	1.45		-
B	1	728	3640	+8.7	299	0.93	-	-
C	2	880.6	4403	+8.7	81	4.92	-	-

* Symbols used in all tables are as follows:

L is total applied load, σ_R is the corresponding resolved shear stress, ΔL is the incremental or decremental load, T is the specimen temperature, K_3 is the strain rate sensitivity and $\bar{K}_3$ is the average values for a particular stress or temperature range, and θ is the strain hardening coefficient.

TABLE X

Experimental Data for Specimen 14H-1

(Pure Copper Single Crystal)

Sheet	Event	L	τ_R	ΔL	T	K_3	$\bar{K}_3$	θ
		gms	g/mm^2	gms	°K	-	-	g/mm^2
A	1	458	294	+8.6	294	0.68	0.71±0.06	7,550
	2	466.6	289	+8.55	294	0.71		8,150
	3	475.2	295	+8.57	294	0.79		8,550
	4	483.7	300	+16.65	294	0.64		7,000
B	1	531.8	330	+8.6	294	0.89	-	8,450

* Symbols used in all tables are as follows:

L is total applied load, τ_R is the corresponding resolved shear stress, ΔL is the incremental or decremental load, T is the specimen temperature, K_3 is the strain rate sensitivity and $\bar{K}_3$ is the average value for a particular stress or temperature range, and θ is the strain hardening coefficient.

TABLE X

Experimental Data for Specimen 14H-1

(Pure Copper Single Crystal)

Sheet	Event	L	τ_R	ΔL	T	K_3	$\overline{K}_3$	θ
		gms	g/mm^2	gms	°K	-	-	g/mm^2
A	1	458	284	+8.6	294	0.68		7,550
	2	466.6	289	+8.55	294	0.71	0.71±0.06	8,150
	3	475.2	295	+8.57	294	0.79		8,550
	4	483.7	300	+16.65	294	0.64		7,000
B	1	531.8	330	+8.6	294	0.89	-	8,450

* Symbols used in all tables are as follows:

L is total applied load, τ_R is the corresponding resolved shear stress, ΔL is the incremental or decremental load, T is the specimen temperature, K_3 is the strain rate sensitivity and $\overline{K}_3$ is the average value for a particular stress or temperature range, and θ is the strain hardening coefficient.

TABLE XI

Experimental Data for Specimen 14H-2

(Pure Copper Sincle Crystal)

Sheet	Event	L	σ_R	ΔL	T	K_3	$\overline{K_3}$	θ
		gms	g/mm^2	gms	°K	-	-	g/mm^2
	1	366.6	277	+ 8.55	298	1.37	1.40±0.17	-
	2	370.3	230	+ 8.57	298	1.24		13,000
	3	378.8	235	+ 3.70	298	1.58		-
	4	382.5	237	+ 3.70	298	(2.50)		5,450
B	L	458	284	+ 8.57	299	1.45	1.33±0.17	-
	N	470.3	292	+ 3.72	299	1.21		-
	EE	566.6	351	+ 8.55	299	1.25	-	-
C	4	778.8	483	+16.65	298	0.85	-	11,800
NRC*	T-1	1560	967	-13	295	1.21	1.16±0.05	-
	T-2	1560	967	+11	295	1.18		-
	T-3	1585	983	- 7.3	295	1.12		-
	T-4	1594	988	- 5	295	1.14		-
	T-5	1603	994	+ 4.8	295	1.08		-
NRC	T-6	1617	1002	+ 7	295	1.05	1.18±0.10	-
	T-7	1640	1016	-13.5	295	1.23		-
	T-8	1665	1032	-14.5	295	1.26		-
	T-9	1661	1030	+12	295	1.05		-
	T-10	1688	1047	-14.9	295	1.25		-
	T-11	1730	1073	-14.8	295	1.24		-
NRC	SR-1 †	1750	1085	-35.5	295	1.47	-	-
NRC	T-12	1806	1120	-15	295	1.21	1.08±0.11	-
	T-13	1811	1123	+11.5	295	0.92		-
	T-14	1836	1138	- 8.5	295	1.10		-
	T-15	1846	1145	- 5.5	295	1.10		-

TABLE XI (Cont'd)

Experimental Data for Specimen 14H-2 (Cont'd)

(Pure Copper Single Crystal)

Sheet	Event	L	σ_R	ΔL	T	K_3	$\overline{K}_3$	θ
		gms	g/mm^2	gms	°K	-	-	g/mm^2
D	3	1983	1239	+16.65	300	0.72	-	10,800
E	2	2058	1276	+ 8.6	298	0.99	0.93±0.09	8,800
	3	2067	1282	+16.65	298	0.87		7,800

* Tests conducted at National Research Council, June 7, 1960.

** T-1 denotes tensile test No. 1.

+ SR-1 denotes stress relaxation test No. 1.

TABLE XII

Experimental Data for Specimen 14F-2

(Pure Copper Single Crystal)

Sheet	Event	L	σ_R	ΔL	T	K_3	$\overline{K}_3$	θ
		gms	g/mm^2	gms	°K	-	-	g/mm^2
A	1	458	284	+ 8.57	296	0.77	0.83±0.09	14,900
	2	466.6	289	+ 8.55	296	0.89		11,200
B	1	858	533	+16.65	296	1.22	1.11±0.14	29,000
	2	958	598	+16.65	296	0.94		14,500
	3	974.7	605	+ 8.60	296	1.16		16,000
	4	1358	840	+16.65	296	0.78	-	19,200
C	2	1667	1030	+16.65	296	1.16	1.02±0.16	13,400
	3	1683	1040	+ 8.57	296	0.84		8,900
	4	1691	1050	+ 8.55	296	1.05		12,000
	6	1867	1160	+16.65	296	0.83	0.73±0.11	12,950
	7	1892	1180	+ 8.57	296	0.62		16,500
D	1	2083	1290	+ 8.57	296	0.64	-	10,200
	3	2120	1320	+ 8.55	296	1.00	-	16,500

TABLE XIII

Experimental Data for Specimen 13C-1
(Pure Copper Single Crystal)

Sheet	Event	L	σ_R	ΔL	T	K_3	$\bar{K}_3$	θ
		μms	g/mm²	μms	°K	-	-	g/mm²
A	D	250	162.5	+ 8.60	295	1.41	1.51±0.11	7,110
	E	258.6	168	+ 8.57	295	1.49		2,590
	F	266.2	173	+ 8.55	295	1.62		2,595
B	J	280	182	+ 8.55	253	(2.18)	1.31±0.14	-
	K	288.6	188	+ 8.57	253	1.15		1,930
	L	297.1	193	+ 8.60	253	1.43		1,562
	M	305.7	198	+ 3.72	253	1.35		1,452
C	V	360	234	+ 8.60	79	4.36	4.45±0.35	2,360
	X	368.6	239	+ 8.57	79	4.97		-
	Y	377.2	245	+ 3.72	79	4.26		249
D	Ā	380.8	248	+ 3.70	79	4.20	-	120
E	K	460	299	+20.0	292	1.80	1.65±0.21	-
	L	480	312	+ 3.70	292	1.73		525
	M	483.7	314	+ 3.70	293	1.73		1,330
	N	487.4	317	+ 8.57	293	1.33		1,790
F	U	580	377	+ 3.72	77	(1.90)	3.77±0.12	791
	V	583.7	379	+ 3.70	78	3.73		-
	W	587.4	382	+ 3.70	78	3.74		-
	X	583.7	379	+ 3.70	78	3.84		-

TABLE XIII (Cont'd)

Experimental Data for Specimen 13C-1 (Cont'd)
(Pure Copper Single Crystal)

Sheet	Event	L	τ_R	ΔL	T	K_3	$\bar{K}_3$	θ
		gms	g/mm^2	gms	°K	-	-	g/mm^2
G	C*	630	409	+ 3.70	81	3.74		478
	D*	633.7	412	+ 3.72	82	4.05		123
	E*	637.4	414	− 3.72	83	3.86	3.93±0.12	112
	F*	633.7	412	+ 3.72	83	3.84		521
	G*	637.4	414	− 3.72	83	4.05		429
	H*	633.7	412	+ 3.72	83	4.04		-
H	J*	550	358	+20.00	296	1.64		-
	K*	570	371	+ 3.72	296	1.70		749
	L*	573.7	373	- 3.72	296	(2.45)		614
	M*	570.0	371	+ 3.72	296	1.50		1,065
	N*	573.7	373	+ 8.57	296	1.58	1.69±0.15	-
	O*	582.3	378	- 8.57	296	1.88		-
	P*	573.7	373	+ 8.57	296	1.68		670
	Q*	582.3	378	- 8.57	296	1.97		824
	R*	573.7	373	+ 8.57	296	1.68		1,270
	Total Tensile Strain at this point ≈ 12% Specimen cut and remounted to a 10 cm. gauge length.							
I	2	650	423	+ 8.57	296	1.47		8,900
	3	6586	427	+ 3.72	296	1.62		1,315
	4	662.3	431	- 3.72	296	(2.25)	1.41±0.08	966
	5	658.6	427	+ 3.72	296	1.30		1,488

TABLE XIII (Cont'd)

Experimental Data for Specimen 13C-1 (Cont'd)
(Pure Copper Single Crystal)

Sheet	Event	L	σ_R	ΔL	T	K_3	$\bar{K}_3$	θ
		gms	g/mm^2	gms	°K	-	-	g/mm^2
I	6	662.3	431	+ 8.60	296	1.39	-	1,860
	7	670.9	436	+ 3.70	296	1.37	-	1,756
J	14	780	506	+ 8.60	79	2.80	3.14±0.61	2,380
	15	788.6	512	+ 3.72	79	3.93		616
	16	792.3	515	+ 8.57	80	2.56		1,760
	17	800.9	525	+ 3.70	80	3.27		920
K	24	860	559	+ 8.60	78	4.20	4.32±0.17	-
	25	868.6	564	+ 8.57	78	4.44		-
L	31	860	560	+ 3.72	297	1.45	1.45±0.09	3,200
	32	863.7	561	+ 3.70	297	1.57		3,[illegible]
	33	867.4	562	+ 8.60	297	1.37		4,210
	37	910	592	+ 8.60	297	1.36		4,345
	38	918.6	597	+ 8.57	297	1.49		3,[illegible]0
M	5	1630	1060	+20	297	1.23	1.26±0.06	[illegible]5
	6	1650	1074	+16.65	297	1.19		8,040
	7	1666.7	1080	+ 8.57	297	1.32		5,450
	8	1675.2	1090	+ 8.60	297	1.30		-
N	27	1950	1270	+ 8.60	79	1.74	1.72±0.36	2,465
	28	1958.6	1273	+ 8.57	79	1.34		2,840
	29	1967.2	1280	+16.7	79	2.08		3,985

TABLE XIV

Experimental Data for Specimen 13C-2

(Pure Copper Single Crystal)

Sheet	Event	L	σ_R	ΔL	T	K_3	$\overline{K}_3$	θ
		gms	g/mm^2	gms	°K	-	-	g/.mm^2
B	46	650	423	8.60	298	1.65		-
	47	658.6	428	3.72	298	(2.34)		507
	48	662.3	430	3.70	298	1.48		817
	49	666.0	433	8.57	298	1.59	1.50±0.17	-
	50	674.6	438	8.57	298	1.57		-
	51	666.0	433	8.57	298	1.22		943
C	64	770	501	3.72	79	3.71		1,160
	65	773.7	503	3.70	79	4.04	3.59±0.54	2,240
	66	777.4	505	16.65	79	3.80		-
	69	794.1	516	8.60	79	2.81		-
D	84	790	514	+ 8.55	296	1.37		-
	85	798.6	519	- 8.55	296	1.70		-
	86	790	514	+ 8.55	296	1.39		-
	87	797.6	519	+ 3.72	296	1.27	1.50±0.19	[illegible]
	88	802.3	521	- 3.72	296	1.65		2,690
	89	798.6	519	+ 3.72	296	1.72		4,460
	90	802.3	521	+ 3.70	296	1.37		3,120
E	97	930	605	+10.0	78	3.44	-	5,140
F	104	940	611	+ 3.72	297	0.76		1,849
	105	943.7	613	+ 8.60	297	1.34		-
	107	952.3	619	- 8.60	297	1.66		-
	108	943.7	613	+ 8.60	297	1.33	1.43±0.34	1,394

TABLE XIV (Cont'd)

Experimental Data for Specimen 13C-2 (Cont'd)
(Pure Copper Single Crystal)

Sheet	Event	L	σ_R	ΔL	T	K_3	$\bar{K}_3$	θ
		gms	g/mm^2	gms	°K	-	-	g/mm^2
F	109	952.3	619	- 8.60	297	1.60		2,085
	110	943.7	613	+ 8.60	297	1.60	1.43 ± 0.34	2,495
	111	952.3	619	+ 8.60	297	1.75		2,620
G	128	1110	722	+ 3.72	78	5.41		-
	129	1114	724	- 3.72	78	5.09		-
	130	1110	722	+ 3.72	78	4.45		825
	131	1114	724	- 3.72	78	4.10		-
	132	1110	722	+ 3.72	78	5.14	4.84 ± 0.80	-
	133	1114	724	+ 3.70	78	3.94		-
	134	1117	726	- 3.70	78	4.96		-
	135	1114	724	+ 3.70	78	6.33		665
	136	1117	726	- 3.70	78	4.34		-

TABLE XV

Experimental Data for Specimen 14E-1
(Pure Copper Single Crystal)

Sheet	Event	L	σ_R	ΔL	T	K_3	$\bar{K}_3$	θ
		gms	g/mm^2	gms	°K	-	-	g/mm^2
	19	300	309	+10	297	1.74		-
	20	310	319	+10	297	1.71		-
	21	320	330	+20	297	2.24	1.74±0.27	-
	22	340	350	+ 8.60	297	1.50		-
	25	348.6	359	+ 8.55	297	1.74		-
	26	357.2	368	+ 3.70	297	1.53		-
B	41	443.7	457	+ 3.72	297	1.66		-
	42	447.4	461	- 3.72	297	1.62	1.60±0.10	3.300*
	43	443.7	457	+ 3.72	297	1.65		-
	44	447.4	461	+ 8.60	297	1.45		-
C	55	542.3	559	+ 3.70	78	3.71		-
	58	546.0	562	+ 8.55	78	(7.23)	4.53±1.17	-
	59	554.6	571	- 8.55	78	5.34		-
D	69	540	556	+ 8.55	299	1.21		-
	70	548.6	565	+ 3.72	299	1.45	1.36±0.13	4,700*
	71	552.3	569	+ 3.70	299	1.48		-
	74	556	573	+ 8.60	299	1.30		-
E	86	680	700	+ 3.72	78	5.39		-
	87	683.7	704	+ 8.60	78	4.69	5.15±0.37	-
	88	692.3	713	+ 8.55	78	5.01		-
	89	700.9	722	+ 3.70	78	5.51		-

* Values θ were determined from an approximate stress-strain curve.

TABLE XV (Cont'd)

Experimental Data for Specimen 14E-1 (Cont'd)

(Pure Copper Single Crystal)

Sheet	Event	L	σ_R	ΔL	T	K_3	$\overline{K_3}$	θ
		gms	g/mm^2	gms	°K	-	-	g/mm^2
E	101	840	865	+ 8.55	78	3.24		-
	102	848.6	874	+ 8.60	78	3.53	4.32±1.13	-
	103	857.2	883	- 8.60	78	5.65		-
	104	848.6	874	+ 8.60	78	4.84		-
F	117	1049	1080	+ 8.60	78	3.26		-
	118	1057	1089	- 8.60	78	3.66	3.30±0.35	-
	119	1049	1080	+ 8.55	78	3.44		-
	120	1057	1089	+ 8.57	78	2.84		-
	127	988.6	1018	+ 8.57	297	1.71	-	-

TABLE XVI

Experimental Data for Specimen 14G-1
(Pure Copper Single Crystal)

Sheet	Event	L	σ_R	ΔL	T	K_3	$\overline{K_3}$	θ
		gms	g/mm^2	gms	°K	-	-	g/mm^2
A	4	180	225	+20.0	295	5.85	-	-
	5	200	250	+ 8.55	295	3.03	-	-
	6	208.6	261	+ 3.70	295	1.15		3,945
	7	212.3	265	- 3.70	295	1.46	1.31±0.22	-
	8	208.6	261	+ 3.70	295	1.53		-
	9	212.3	265	- 3.70	295	1.10		3.050
	21	310.6	388	+ 3.72	295	1.02	1.04±0.03	2,910
	22	322.3	403	+ 3.70	295	1.06		5,785
B	33	400	500	+ 8.55	256	1.17		5,785
	34	408.6	511	+ 3.72	255	1.29	1.22±0.31	2,515
	35	412.3	515	+ 3.70	254	1.58		4,050
	36	416	520	+ 8.60	254	0.83		4,190
C	40	450	563	+ 8.60	175	1.69	-	-
	46	520	650	+ 3.72	78	3.60		-
	47	523.7	655	- 3.72	78	3.94		4,835
	48	520	650	+ 3.72	78	3.54	3.57±0.34	2,275
	49	523.7	655	- 3.72	78	3.20		5,310
	50	527.4	659	+ 3.70	78	3.96		6.070
	51	523.7	655	- 3.70	78	3.19		3,450

TABLE XVI (Cont'd)

Experimental Data for Specimen 14G-1 (Cont'd)

(Pure Copper Single Crystal)

Sheet	Event	L	σ_R	ΔL	T	K_3	$\overline{K_3}$	θ
		gms	g/mm^2	gms	°K	-	-	g/mm^2
D	58	610	763	+ 3.70	78	3.07	3.43±0.36	2,815
	59	612.7	767	+ 3.72	78	3.22		846
	60	617.4	772	+ 3.70	78	3.59		936
	61	613.7	767	+ 3.70	78	3.84		2,780
E	71	610	762	+ 8.60	297	1.53	1.38±0.23	-
	74	630.9	789	+10.0	297	1.22		10,440
	89	1410	1763	+ 8.55	297	1.56	1.41±0.21	63,600
	90	1419	1774	+16.65	297	1.25		20,350

TABLE XVII

Experimental Data for Specimen 6(A)B-1

(Copper Alloy Single Crystal, 0.1 at. % Ag.)

Sheet	Event	L	σ_R	ΔL	T	K_3	$\bar{K}_3$	θ
		gms	g/mm^2	gms	°K	-	-	g/mm^2
	33	900	786	+ 8.60	299	2.96		-
	34	908.6	793	+ 8.57	299	2.95	2.96±0.01	-
B	43	940	821	+ 8.57	298	2.90		-
	44	948.6	828	+ 8.55	298	2.75	3.08±0.32	-
	45	957.1	836	+ 8.60	298	3.47		-
	46	965.7	843	+16.65	298	3.23		-
C	62	1320	1152	+ 8.57	78	9.05		-
	63	1329	1160	- 8.57	78	11.30		-
	66	1320	1152	+ 8.57	78	9.50		-
	67	1329	1160	+ 8.55	78	11.10	9.78±1.01	-
	68	1338	1168	+16.65	78	8.81		-
	69	1354	1182	-16.65	78	9.05		-
	70	1338	1168	+16.65	78	9.66		-
D	74	1120	978	+ 8.57	302	3.42		-
	77	1129	986	- 8.57	302	3.11	3.25±0.29	-
	80	1137	993	- 8.55	302	2.91		-
	83	1154	1007	-16.65	302	3.54		-
	91	1199	1047	- 8.85	302	2.98		-
	96	1224	1069	-16.65	302	3.06	3.50±0.84	-
	97	1207	1054	+16.65	302	4.48		-

TABLE XVII

Experimental Data for Specimen 6(A)B-1

(Copper Alloy Single Crystal, 0.1 at. % Ag.)

Sheet	Event	L	σ_R	ΔL	T	K_3	$\bar{K}_3$	α
		gms	g/mm^2	gms	°K	-	-	g/mm^2
	33	900	786	+ 8.60	299	2.96		-
	34	908.6	793	+ 8.57	299	2.95	2.96±0.01	-
B	43	940	821	+ 8.57	298	2.90		-
	44	948.6	828	+ 8.55	298	2.75	3.08±0.32	-
	45	957.1	836	+ 8.60	298	3.47		-
	46	965.7	843	+16.65	298	3.23		-
C	62	1320	1152	+ 8.57	78	9.05		-
	63	1329	1160	- 8.57	78	11.30		-
	66	1320	1152	+ 8.57	78	9.50		-
	67	1329	1160	+ 8.55	78	11.10	9.78±1.01	-
	68	1338	1168	+16.65	78	8.81		-
	69	1354	1182	-16.65	78	9.05		-
	70	1338	1168	+16.65	78	9.66		-
D	74	1120	978	+ 8.57	302	3.42		-
	77	1129	986	- 8.57	302	3.11	3.25±0.29	-
	80	1137	993	- 8.55	302	2.91		-
	83	1154	1007	-16.65	302	3.54		-
	91	1199	1047	- 8.85	302	2.98		-
	96	1224	1069	-16.65	302	3.06	3.50±0.84	-
	97	1207	1054	+16.65	302	4.48		-

TABLE XVII (Cont'd)

Experimental Data for Specimen 6(..)B-1 (Cont'd)
(Copper Alloy Single Crystal, 0.1 at. % Ag.)

Sheet	Event	L	σ_R	ΔL	T	K_3	$\bar{K}_3$	θ
		gms	g/mm^2	gms	°K	-	-	g/mm^2
E	113	1680	1467	+ 8.57	78	9.06		-
	114	1687	1473	+ 8.57	78	9.55		-
	115	1680	1467	+ 8.57	78	10.45		-
	116	1687	1473	+16.65	78	9.01		-
F	119	1687	1473	+16.65	78	8.25	8.78±0.91	-
	120	1704	1488	+16.65	78	7.95		-
	121	1687	1473	+16.65	78	8.29		-
	122	1704	1488	+ 8.55	78	9.01		-
	123	1712	1495	- 8.55	78	7.45		-
	132	1520	1326	+ 8.60	302	3.10		-
	133	1529	1335	- 8.60	302	2.74	2.87±0.43	-
	134	1520	1326	+ 8.60	302	3.30		-
	138	1538	1343	- 8.57	302	2.32		-

TABLE XVIII

Experimental Data for Specimen 7B-1

(Copper Alloy Single Crystal, 0.3 at. % Ag.)

Sheet	Event	L	σ_R	ΔL	T	K_3	$\overline{K}_3$	θ
		gms	g/mm^2	gms	°K	-	-	g/mm^2
A	11	800	711	+20	297	7.33	7.11±1.69	-
	12	820	729	+20	297	7.26		-
	13	840	747	+ 8.57	297	(10.90)		-
	14	848.6	754	+16.65	297	7.79		-
	15	865.2	769	-16.65	297	5.08		-
	16	848.6	754	+16.65	297	6.17		-
	17	865.2	769	+ 8.55	297	7.48		-
	18	873.8	777	- 8.55	297	5.60		-
	19	865.2	769	+ 8.55	297	6.34		-
B	42	1470	1307	+16.65	80	12.10	11.28±1.34	-
	43	1487	1322	-16.65	80	11.10		-
	44	1470	1307	+ 8.57	80	12.50		-
	45	1487	1322	- 8.57	80	9.10		-
	46	1470	1307	+ 8.57	80	11.6		-
	51	1539	1368	+16.65	80	14.05	12.06±2.17	-
	52	1555	1382	-16.65	80	12.40		-
	53	1539	1368	+16.65	80	9.75		-
C	60	1079	959	- 8.57	299	4.41	4.85±0.53	-
	61	1070	951	+ 8.57	299	4.79		-
	63	1087	966	- 8.55	297	4.43		-
	64	1079	959	+ 8.55	298	5.81		-
	66	1104	981	-16.65	298	4.59		-

TABLE XVIII (Cont'd)

Experimental Data for Specimen 7B-1 (Cont'd)
(Copper Alloy Single Crystal, 0.3 at. % Ag.)

Sheet	Event	L	σ_R	ΔL	T	K_3	$\bar{K}_3$	θ
		gms	g/mm^2	gms	°K	-	-	g/mm^2
C	67	1087	966	+16.65	298	5.08		-
	72	1129	1004	- 8.57	298	4.36		-
	73	1120	996	+ 8.57	298	4.95		-
	75	1138	1012	- 8.55	297	3.41	4.42±0.45	-
	76	1129	1004	+ [illegible]	297	5.24		-
	78	1154	1026	-16.65	297	3.92		-
	79	1137	1011	+16.65	297	4.64		-
D	87	1220	1085	+16.65	297	5.11		-
	88	1237	1100	-16.65	297	4.24		-
	89	1220	1085	+16.65	[illegible]	5.56	4.67±0.70	-
	91	1245	1107	- 8.57	297	3.77		-
	92	1237	1100	+ 8.57	297	[illegible]		-
E	108	1829	1626	- 8.57	80	8.14		-
	109	1820	1618	+ 8.57	80	8.96		-
	111	1837	1633	+16.65	80	12.40	10.24±1.82	-
	112	1854	1648	-16.65	80	8.81		-
	113	1837	1633	+16.65	80	12.90		-
	119	1920	1707	+16.65	80	11.10		-
	120	1937	1722	-16.65	80	10.00	10.80±0.70	-
	121	1920	1707	+16.65	80	11.30		-
F	126	1620	1440	+16.65	296	3.98		-
	127	1637	1455	-16.65	296	3.83		-

Experimental Data for Specimen 7B-1 (Cont'd)
(Copper Alloy Single Crystal, 0.3 at. % Ag.)

Sheet	[illegible]nt	L	σ_R	ΔL	T	K_3	$\overline{K}_3$	θ
		gms	g/mm^2	gms	°K	-	-	g/mm^2
F	128	1620	1440	+16.65	296	4.46		-
	[illegible]29	1637	1455	+ 8.57	296	7.02	4.98±1.41	-
	[illegible]30	1645	1464	+ 8.55	296	4.85		-
	131	1654	1470	- 8.55	296	3.19		-
	132	1645	1464	+ 8.55	296	5.77		-
	133	1654	1470	+ 8.60	296	6.77		-
	138	1720	1529	+ 8.60	296	7.04		-
	139	1729	1537	- 8.60	296	2.74		-
	140	1720	1529	+ 8.60	296	6.23	4.71±1.67	-
	141	1729	1537	+16.65	[illegible]	4.51		-
	142	1745	1551	-16.65	296	3.24		-
	143	1729	1537	+16.65	296	4.47		-